# Hydrogen Bonding Phase-Transfer Catalysis with Sodium Azide and Potassium Cyanide


**Jimmy Wang**

Lady Margaret Hall

*Submitted in partial fulfilment of the requirements for the degree of*

**Doctor of Philosophy**

Summer 2021

## Contents

Contents ..... ii

Declaration of Authorship ..... vii

Acknowledgements ..... viii

Abstract ..... x

Abbreviations and Acronyms ..... xi

1 Introduction ..... 1

1.1 Phase-transfer catalysis ..... 1

1.2 Chiral cation phase transfer catalysis ..... 2

1.3 Chiral anion phase-transfer catalysis ..... 3

1.4 Hydrogen bonding phase-transfer catalysis ..... 4

1.4.1 Inspiration from fluorinase ..... 4

1.4.2 Catalysis with nucleophilic hydrogen bonded anions ..... 5

1.4.3 Structure and reactivity of hydrogen bonded fluoride ..... 14

1.4.4 Discovery, scope, and mechanism ..... 17

1.5 Research proposal ..... 22

1.6 References ..... 23

2 Hydrogen Bonding Phase-Transfer Catalysis with Sodium Azide ..... 27

2.1 Introduction ..... 27

2.1.1 Organoazides ..... 27

2.1.2 Enzyme-azide structure and reactivity ..... 30

2.1.3 Structure of hydrogen bonded azide complexes ..... 32

2.1.4 Enantioselective azidation ..... 36

2.1.5 Initial results for HB-PTC with sodium azide ..... 39

2.1.6 Aims ..... 40

2.2 Achiral hydrogen bonded azide complexes ..... 41

2.2.1 Solid state studies ..... 41

2.2.2 Solution studies ..... 49

2.3 Chiral urea bound azide ..... 54

2.3.1 Establishing association in solution ..... 54

2.3.2 Investigating structure in solution ..... 60

2.3.3 Solid state studies ..... 73

2.4 Reaction development and scope ..... 76

2.4.1 Synthesis of β-thioazides ..... 76

2.4.2 Racemic synthesis of β-aminoazides ..... 76

2.4.3 Enantioselective synthesis of β-aminoazides ..... 79

2.5 Mechanistic studies ..... 84

2.5.1 Achiral HB-PTC with Schreiner's urea ..... 84

2.5.2 Uncatalysed azidation with sodium azide ..... 89

2.5.3 Understanding enantioselective HB-PTC with sodium azide ..... 91

2.6 Conclusions and outlook ..... 98

2.7 References ..... 99

3 Hydrogen Bonding Phase-Transfer Catalysis with Potassium Cyanide ..... 105

3.1 Introduction ..... 105

3.1.1 Organonitriles ..... 105

3.1.2 Enzyme-cyanide structure and reactivity ..... 107

3.1.3 Structure of hydrogen bonded cyanide complexes ..... 109

3.1.4 Enantioselective cyanation ..... 110

3.1.5 Aims ..... 114

3.2 Structure and coordination in urea-cyanide complexes ..... 114

3.2.1 Solid state studies ..... 114

3.2.2 Solution studies ..... 116

3.3 Enantioenriched γ-aminonitriles under HB-PTC ..... 128

3.3.1 Reaction discovery and optimisation ..... 128

3.3.2 Reaction scope ..... 135

3.4 Conclusions and outlook ..... 136

3.5 References ..... 137

4 Supporting Information ..... 145

4.1 General Considerations ..... 145

4.1.1 Reagents and solvents ..... 145

4.1.2 Equipment and analysis ..... 145

4.1.3 Azide quench ..... 146

4.1.4 Cyanide quench ..... 146

4.2 General procedure for $^{1}$H NMR titrations ..... 147

4.2.1 Titration procedure ..... 147

4.2.2 Data analysis & model fitting ..... 147

4.3 Supporting Information for Chapter 2 ..... 149

4.3.1 General procedures ..... 149

4.3.2 Synthesis of hydrogen bond donors ..... 151

4.3.3 Synthesis and crystallisation of hydrogen bonded azide complexes ..... 152

4.3.4 Evaluation of achiral hydrogen bond donor solubility ..... 159

4.3.5 $^{1}$H NMR titrations of achiral HBDs and tetrabutylammonium azide ..... 160

4.3.6 Chiral urea bound azide - solution studies – establishing association ..... 172

4.3.7 Chiral urea bound azide - solution studies – understanding structure ..... 175

4.3.8 Chiral urea bound azide - solid state studies ..... 180

4.4.3 Synthesis of β-thioazides under HB-PTC ..... 180

4.4.4 Synthesis of β-aminoazides under HB-PTC ..... 181

4.4.5 Mechanistic studies of HB-PTC with sodium azide ..... 213

4.4 Supporting Information for Chapter 3 ..... 218

4.4.1 General procedures ..... 218

4.4.2 Solid state studies of a urea-cyanide complex ..... 219

4.4.3 Solution studies of urea-cyanide complexes ..... 221

4.4.4 Synthesis of chiral catalysts ..... 226

4.4.5 Additional reaction optimisation data ..... 238

4.4.6 Synthesis of substrates and products.....238

4.5 References.....241

Appendix.....244

Additional crystal structures.....244

## Declaration of Authorship

This course of study was pursued in the University of Oxford under the supervision of Prof. Véronique Gouverneur in accordance with the provisions for students for the Degree of Doctor of Philosophy. This thesis has not already been accepted and is not concurrently being submitted for any degree or diploma or certificate or other qualification in this University or elsewhere. The thesis I am submitting is my own work except where otherwise indicated.

## Acknowledgements

I am very grateful to my supervisor Prof. Véronique Gouverneur for the opportunity to join her research group. I have undoubtedly learnt a great deal during my time at the University of Oxford and it was great to meet Billy!

I am also very thankful to my industrial mentor Dr. Tejas Pathak for his positive energy, scientific input, and supervision during my DPhil, as well as all his efforts into arranging a placement (that was sadly cancelled last-minute due to COVID-19) at Novartis in Massachusetts.

I am especially grateful to many colleagues and collaborators who helped with several key aspects of my DPhil. The NMR studies were helped enormously by Prof. Timothy D. W. Claridge, as well as Dr. Nader Amin, Dr. Francesco Ibba, Maria Marshall, and Noelle Goodyear. It was a pleasure to collaborate with Dr. Francesco Ibba, Yuan Gao, Prof. Guy C. Lloyd-Jones during the kinetic studies. The X-ray crystallography studies were kindly supported by Dr. Kirsten E. Christensen, Dr. Amber L. Thompson, and Dr. Gabriele Pupo. Prof. Robert Paton's input and insight as an expert in computational chemistry was highly valuable. It was great to have worked with Dr. Matthew A. Horwitz during the azide project and experience his pragmatism. I am particularly appreciative to Giulia Roagna for our close teamwork during the cyanide project. During the writing of this thesis, various sections were kindly proofread by Dr. Tim Möllner, Dr. Alexandru Grozavu, Dr. Emy Andre-Joyaux, Dr. Gabriele Pupo, Dr. Anna C. Vicini, Dr. Francesco Ibba, and Dr. Jeroen B. I. Sap.

I am grateful to the many members of the Gouverneur group I have worked alongside in F11 and F12 over the last few years for the many interesting and helpful discussions. It was a great experience to have worked alongside so many talented DPhil students including David Ascough, Jeroen Sap, Francesco Ibba, Osman Tack, Anna Chiara Vicini, Sandrine Hell, Claudio

Meyer, Tim Möllner, Tobi Arisa, Robert Szpera, Giulia Roagna, Konstantinos Afratis, and Zijun Chen.

It was a pleasure to be invited to join the 2016 cohort of SBM-CDT students. I am grateful to the EPSRC Centre for Doctoral Training in Synthesis for Biology and Medicine (EP/L015838/1) for a studentship, generously supported by AstraZeneca, Diamond Light Source, Defence Science and Technology Laboratory, Evotec, GlaxoSmithKline, Janssen, Novartis, Pfizer, Syngenta, Takeda, UCB, and Vertex.

Finally, I am very thankful and appreciative of all my many wonderful friends and family members outside of the CRL who have supported me throughout this DPhil.

## Abstract

Hydrogen Bonding-Phase Transfer Catalysis (HB-PTC) enables use of alkali metal fluoride salts as reactive reagents in enantioselective catalysis and this platform has been successfully applied towards enantioselective fluorination. This thesis details a study into the structure and reactivity of hydrogen bonded azide and cyanide anions and the development of enantioselective reactions using sodium azide and potassium cyanide under HB-PTC for the synthesis of enantioenriched organoazide and organonitriles.

The first chapter introduces phase-transfer catalysis and discusses the advantages of HB-PTC. The second chapter presents a detailed study into the structure and coordination of hydrogen bonded azide complexes in both solid state and solution, and discusses the development and mechanistic study of an enantioselective azidation reaction with sodium azide under HB-PTC. The third chapter describes the structure and coordination of hydrogen bonded cyanide complexes in both solid state and solution and details the development of an enantioselective cyanation reaction with potassium cyanide under HB-PTC. The final chapter contains supporting information including experimental procedures and characterisation data. An appendix with additional crystal structures is also included.

## Abbreviations and Acronyms

| | |
|---|---|
| 1,2-DFB | 1,2-difluorobenzene |
| 2OG | 2-oxoglutarate |
| 5'-FDA | 5'-fluoro-5'-deoxyadenosine |
| 15-crown-5 | 1,4,7,10,13-pentaoxacyclopentadecane |
| BIMP | bifunctional iminophosphorane |
| BINAM | 2,2'-diamino-1,1'-binaphthalene |
| CAPT | chiral-anion phase-transfer |
| CHP | cumene hydroperoxide |
| COSY | Correlation Spectroscopy |
| $(DHQD)_2AQN$ | hydroquinidine (anthraquinone-1,4-diyl) diether |
| $(DHQD)_2Pyr$ | hydroquinidine-2,5-diphenyl-4,6-pyrimidinediyl diether |
| DIBAL-H | diisobutylaluminium hydride |
| DMAP | 4-dimethylaminopyridine |
| E2 | bimolecular elimination |
| e.r. | enantiomeric ratio |
| ee | enantiomeric excess |
| HB-PTC | Hydrogen Bonding Phase-Transfer Catalysis |
| HBD | hydrogen bond donor |
| HMBC | Heteronuclear Multiple Bond Correlation |
| HSQC | Heteronuclear Single Quantum Coherence |
| IPD | intraparticle diffusion |
| IR | infrared |
| nd | not determined |
| LUMO | lowest unoccupied molecular orbital |
| NMR | nuclear magnetic resonance |
| NMRy | NMR yield |
| NOESY | Nuclear Overhauser Effect Spectroscopy |
| SAM | *S*-adenosyl methionine |
| Selectfluor | 1-chloromethyl-4-fluoro-1,4-diazoniabicyclo[2.2.2]octane bis(tetrafluoroborate) |
| $S_N2$ | bimolecular nucleophilic substitution |
| TMG | 1,1,3,3-tetramethylguanidine |
| VAPOL | 2,2'-diphenyl-3,3'-(4-biphenanthrol) |
| Zhdankin reagent | 1-azido-1,2-benziodoxol-3(1H)-one |

# 1 Introduction

## 1.1 Phase-transfer catalysis

Chemical reactions between reagents in separate phases (e.g. solid and solution, or immiscible solutions) are hindered by the inherent difficulty for the reactants to interact.[1] A phase-transfer catalyst accelerates the rate of a reaction between reagents in different phases by transporting a reactant across the interface so they are in the same phase, enabling the desired reaction to proceed.[2]

The concept of phase-transfer catalysis was first described by Starks in 1971.[1] Stirring a mixture of 1-bromooctane **1.1** with aqueous sodium cyanide produced no desired nitrile product **1.2**, even after heating the mixture at 100 °C for 2 weeks (**Scheme 1.1A**). Addition of hexadecyltributylphosphonium bromide (0.01 equiv) as a phase-transfer catalyst enabled the reaction to proceed, leading to high conversion of **1.2** after only 90 min (**Scheme 1.1B**). Quaternary ammonium salts were also examined and found catalytically active, however phosphonium salts were reported to be stable up to 200 °C whilst the corresponding tetraalkylammonium salts only appeared stable up to 100 °C.[1] Starks proposed an extractive mechanism for the phase-transfer process, with the quaternary ammonium or phosphonium cation shifting wth a counter anion between the organic and aqueous phases (**Scheme 1.1C**).[1]

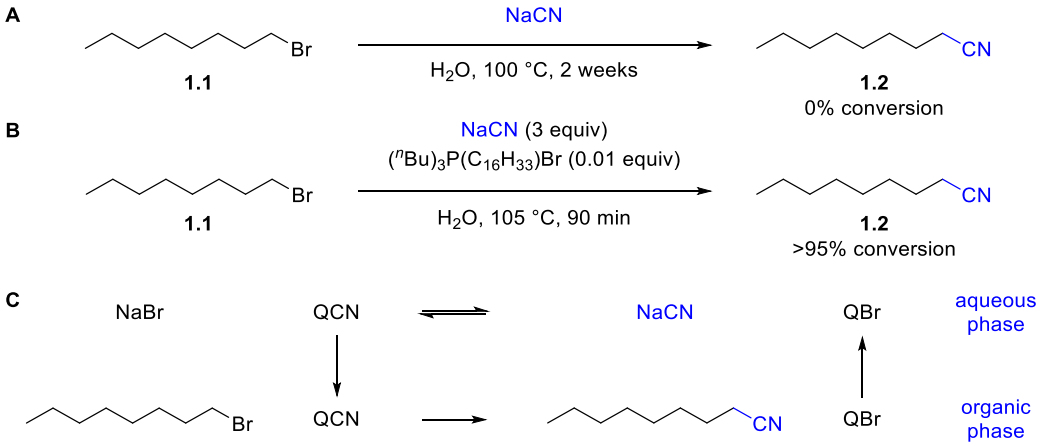


**Scheme 1.1** (A) Reaction of 1-bromooctane with sodium cyanide. (B) Reaction of 1-bromooctane with sodium cyanide and a tetraalkylphosphonium salt as phase-transfer catalyst. (C) Proposed extractive phase-transfer mechanism. Q = quaternary ammonium or phosphonium cation.

Since Stark's seminal publication, further developments in phase-transfer catalysis have realised multiple advantages of this catalytic platform, including mild reaction conditions, operational simplicity, reduced waste, lower costs, higher yields, and higher purity of products compared to conventional methods.[3] In addition, phase-transfer catalysis has developed into a widely used platform for enantioselective synthesis,[4,5] with large scale applications in industry.[6]

## 1.2 Chiral cation phase transfer catalysis

The first efficient and practical example of enantioselective phase-transfer catalysis was reported by Dolling *et al*. in 1984.[7] A chiral quaternary ammonium salt **1.5** acts as both the phase-transfer catalyst and source of enantiocontrol (**Scheme 1.2A**). Mąkosza proposed an interfacial mechanism for this process, where deprotonation of a pro-nucleophile (in this case (±)-**1.3**) by aqueous base occurs at the interface of the organic and aqueous phases (**Scheme 1.2B**).[8] The resultant enolate and quaternary ammonium cation form a reactive chiral ion pair. The enolate undergoes an enantioselective alkylation directed by the quaternary ammonium cation to afford the desired product. A broad range of enantioselective transformations under phase-transfer catalysis with a chiral onium salt have since been developed.[4,5]

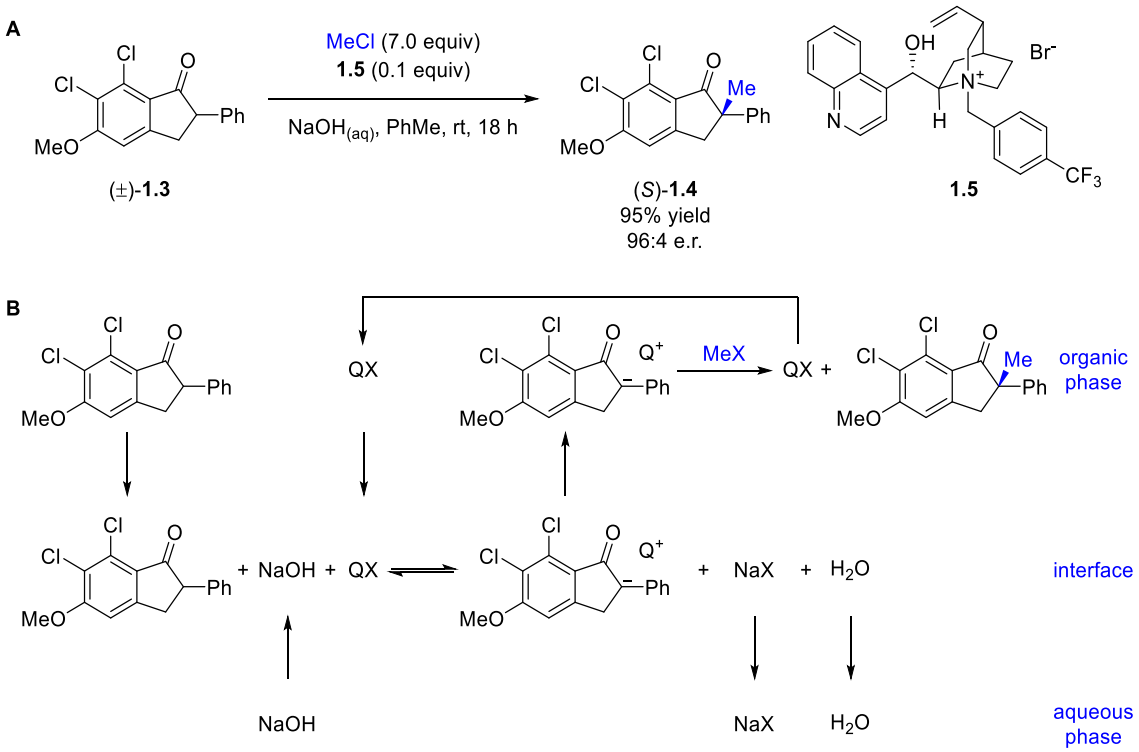


**Scheme 1.2** (A) Enantioselective alkylation under phase-transfer catalysis. (B) Proposed interfacial phase-transfer mechanism. Q = chiral quaternary ammonium cation, X = Cl or Br.

## 1.3 Chiral anion phase-transfer catalysis

Chiral anion phase-transfer (CAPT) catalysis was introduced by the Toste group in 2011.[9] A chiral anionic catalyst mediates the phase-transfer process, a distinct change in mechanism from chiral cation directed processes. The chiral anionic catalyst solubilises an otherwise insoluble cationic reagent and provides enantiocontrol in a subsequent reaction.

The fluorocyclisation of benzothiophene **1.6** with Selectfluor highlights the advantages of CAPT catalysis. Attempted fluorocyclisation of **1.6** in MeCN, which solubilises all components in this reaction, produces a complex mixture of products (**Scheme 1.3A**). Under CAPT conditions, fluorocyclisation of **1.6** proceeds cleanly with a good yield of 69%, high diasteroselectivity of >20:1 d.r., and high enantiomeric ratio of 95:5 (**Scheme 1.3B**).[9]

The proposed mechanism involves the *in situ* generation of the chiral phosphate anion of (*R*)-**1.8** which transports Selectfluor into solution (**Scheme 1.3C**). This ensures both the starting material and Selectfluor only interact in solution in the presence of a chiral anion, providing high levels of enantiocontrol, whilst avoiding undesired side reactions and degradation

pathways. The enantioselective fluorination is directed by the chiral anionic catalyst, generating the fluorinated product with enantiocontrol. The scope of enantioselective reactions under CAPT has since been expanded significantly.[10,11,20,12–19]

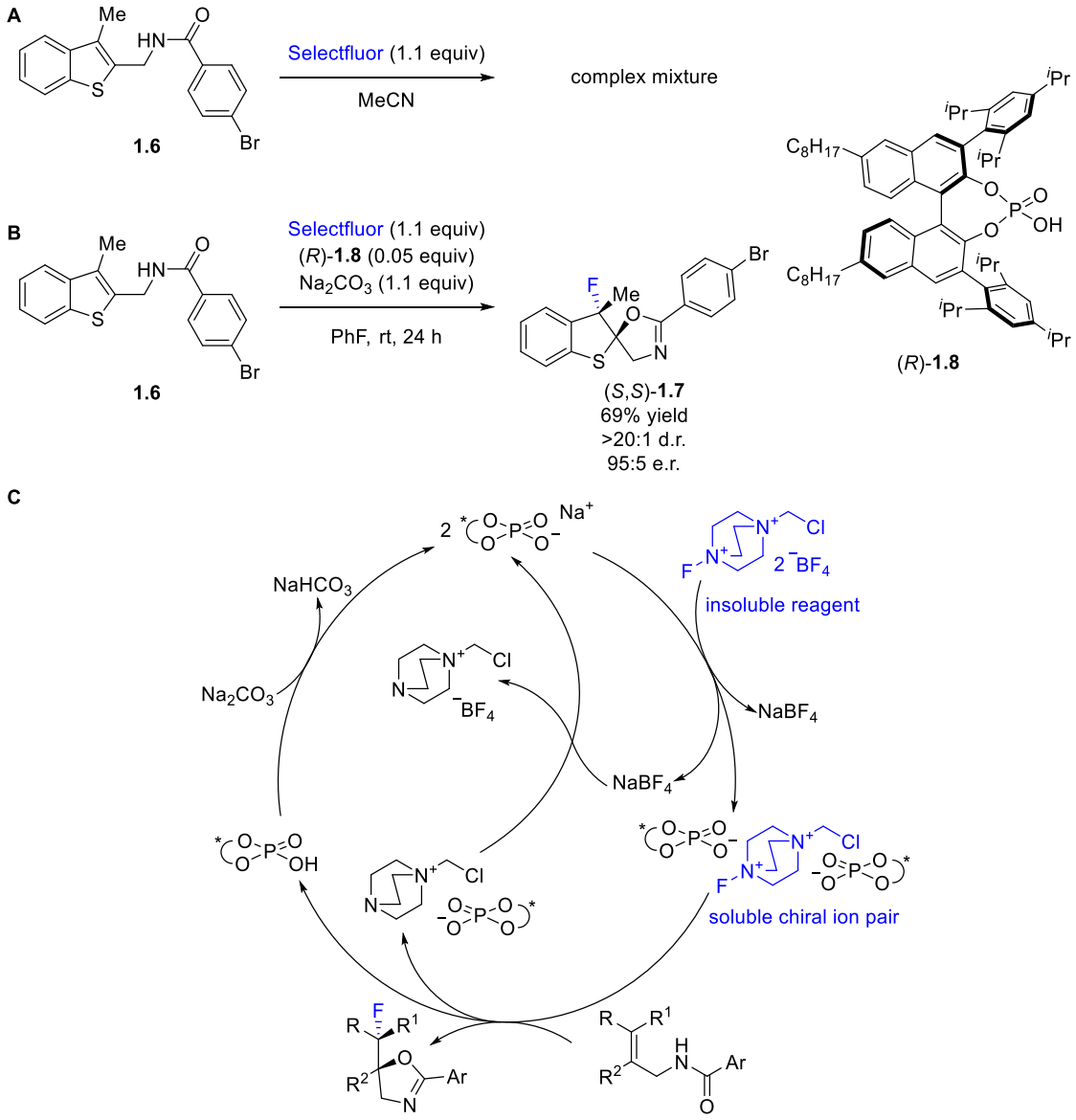


**Scheme 1.3** (A) Attempted fluorocyclisation under homogenous conditions. (B) Enantioselective fluorocyclisation under CAPT. (C) Proposed catalytic cycle for CAPT catalysis. Selectfluor = 1-chloromethyl-4-fluoro-1,4-diazoniabicyclo[2.2.2]octane bis(tetrafluoroborate)

## 1.4 Hydrogen bonding phase-transfer catalysis

### 1.4.1 Inspiration from fluorinase

The inspiration for hydrogen bonding phase-transfer catalysis (HB-PTC) stems from the mechanism of the fluorinase enzyme.[21] In 2002, O'Hagan and co-workers reported an enzymatic transformation occurring in the bacterium *Streptomyces cattleya* involving the

reaction of *S*-adenosyl-L-methionine (SAM) **1.9** with fluoride to form 5'-fluoro-5'-deoxyadenosine (5'-FDA) **1.10** (**Scheme 1.4A**).[22] This seminal publication represented the first identification of a fluorinase enzyme. The proposed mechanism involves initial coordination of fluoride within the fluorinase active through three hydrogen bond donors, followed by coordination of SAM to this enzyme-fluoride complex (**Scheme 1.4B**). Subsequent nucleophilic displacement of methionine by the hydrogen bonded fluoride anion occurs with inversion to afford the 5'-FDA product.[23]

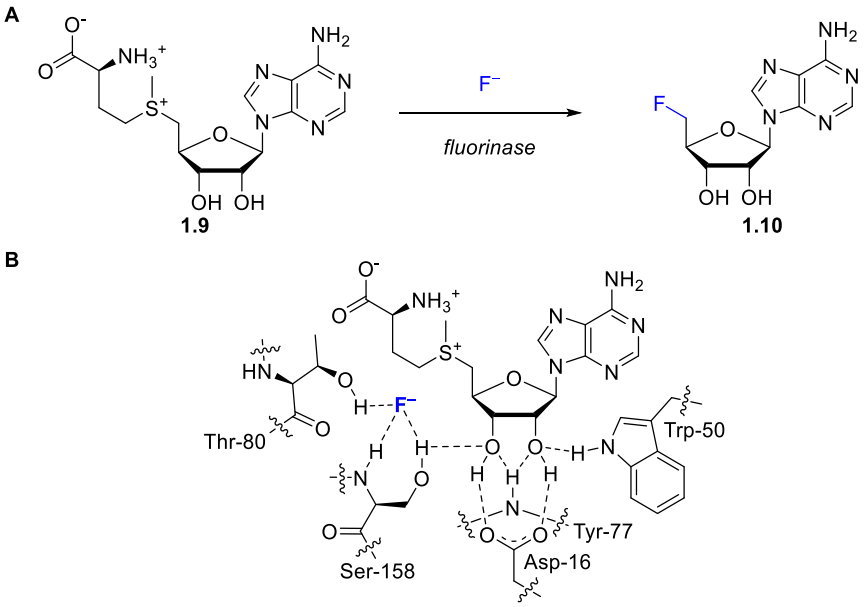


**Scheme 1.4** (A) Transformation of *S*-adenosyl-L-methionine (SAM) to 5'-fluoro-5'-deoxyadenosine (5'-FDA) catalysed by fluorinase. (B) Key interactions in the fluorinase active site with SAM and fluoride.

### 1.4.2 Catalysis with nucleophilic hydrogen bonded anions

#### Challenges

Enantioselective organocatalysis often involves dual hydrogen bond donor catalysts that increase the reactivity of an electrophile by lowering its LUMO. This is through direct coordination, abstracting an anion, or binding the anion from a suitable Lewis or Brønsted acid co-catalyst (**Figure 1.1**).[24–26] An external nucleophile can subsequently react with the activated electrophile to afford the desired product.

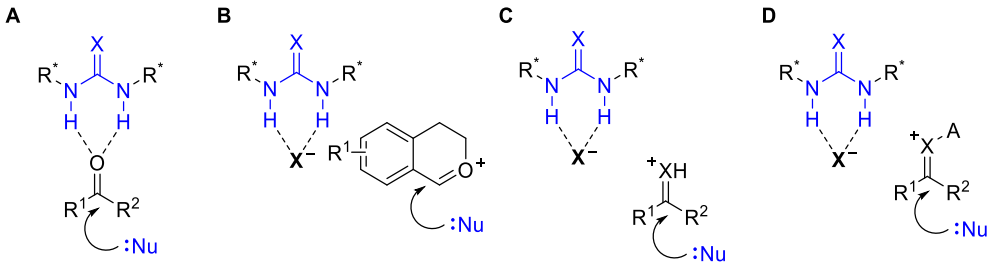


**Figure 1.1** Typical strategies for electrophile activation with dual hydrogen bond donor catalysts include (A) direct coordination, (B) anion abstraction, (C) Brønsted acid co-catalysis, and (D) Lewis acid co-catalysis.

A hydrogen bonded anion is expected to be less charge dense, less nucleophilic, and less reactive than the corresponding unbound anion, counterproductive if a reaction with the hydrogen bonded anion is desired (**Figure 1.2**). Limited examples of enantioselective organocatalytic transformations where a hydrogen bonded anion is also suggested to behave as the nucleophile are reported,[27–33] and are rare compared to those involving electrophile activation.[24–26]


**Figure 1.2** Expected difference in reactivity between a hydrogen bonded anionic nucleophile and the corresponding unbound nucleophile.

**Protonated pro-anionic nucleophiles**

One strategy to access a hydrogen bonded nucleophilic anion whilst supressing formation of the unbound species is to utilise a system where the hydrogen bond donor catalyst also enables the deprotonation of an acidic pro-nucleophile. The p$K_a$ of the conjugate acid of the desired anion is limited to a range compatible with the catalyst used. This mechanism is often proposed as a potential pathway in reactions using a bifunctional catalyst containing an additional Lewis basic functional group. Bifunctional catalysis encompasses a broad field within organic chemistry, and reactions within this platform typically involve an acidic pro-nucleophile that undergoes deprotonation by a catalyst containing both hydrogen bond donor and Lewis basic groups.

The conjugate addition of acetylacetone to *trans*-β-nitrostyrene **1.11** catalysed by (*R*,*R*)-**1.13** represents the prototypical type of transformation enabled under bifunctional catalysis (**Scheme 1.5A**). Acetylacetone, an acidic pro-nucleophile undergoes deprotonation by the catalyst and a network of hydrogen bond interactions control the enantioselectivity of its subsequent conjugate addition. Two alternative pathways may be considered plausible as both are expected to yield product with the same absolute configuration. One proposed pathway involves an initial deprotonation of acetylacetone by the diamine of (*R*,*R*)-**1.13**, resulting in coordination of acetylacetonate with the thiourea hydrogen bond donors of (*R*,*R*)-**1.13**.[34] The resultant hydrogen bonded anion remains nucleophilic at the central carbon and can undergo a catalyst controlled enantioselective addition to *trans*-β-nitrostyrene to form the desired product in a 80% yield and 94.5:5.5 e.r. (**Scheme 1.5B**). The alternative proposed pathway is more representative of hydrogen bond donor catalysed reactions and involves the thiourea of (*R*,*R*)-**1.13** directly interacting with the *trans*-β-nitrostyrene electrophile (**Scheme 1.5C**).

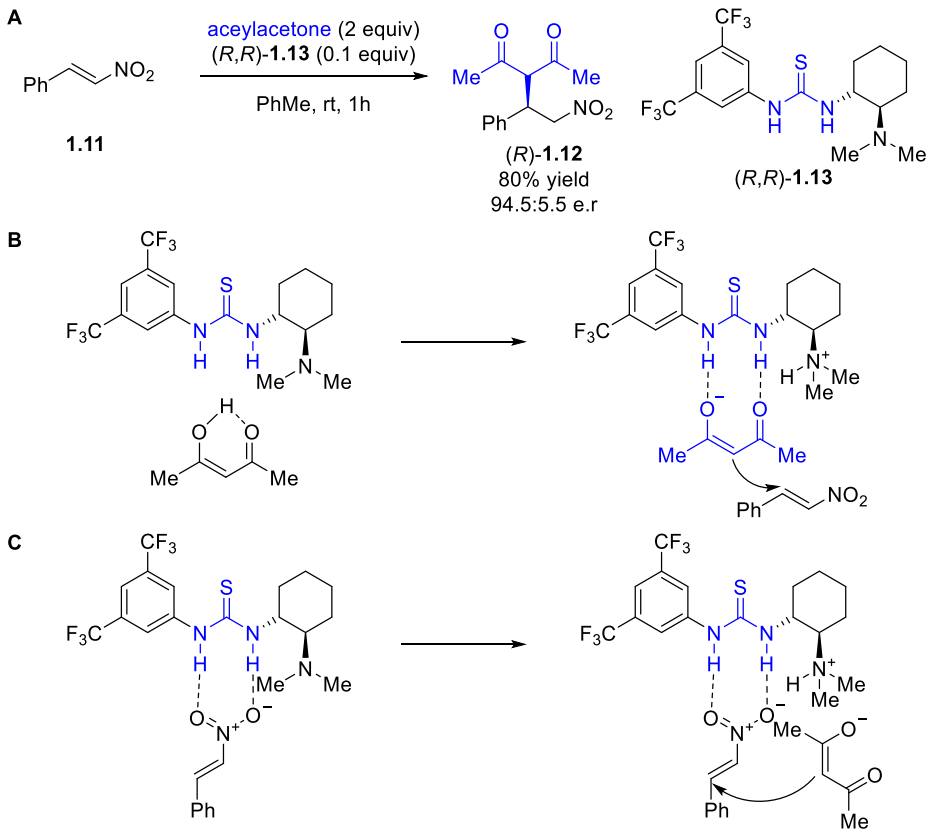


**Scheme 1.5** (A) Conjugate addition of acetylacetone to nitrostyrene **1.11**. (B) Plausible mechanism involving a nucleophilic hydrogen bonded acetylacetonate. (C) Plausible mechanism involving direct electrophile activation.

In contrast, reactions involving an acidic pro-nucleophile but where the catalyst does not contain a Lewis basic functional group to facilitate the deprotonation are proposed to proceed by a hydrogen bonded nucleophilic anion.

The Jacobsen group published comprehensive experimental and computational mechanistic studies of an enantioselective imine hydrocyanation (**Scheme 1.6A**).[29,30] Thiourea catalyst (*S*)-**1.14** is proposed to coordinate with hydrogen isocyanide and decrease its p$K_a$, enabling deprotonation by the imine substrate. The resultant hydrogen bonded cyanide anion undergoes a nucleophilic addition from its carbon terminus to the iminium electrophile, affording enantioenriched α-aminonitriles in excellent yields and enantiomeric ratios. (**Scheme 1.6B**). As cyanide is the anion of interest in this transformation, there is the inherent need for the generation of highly toxic and potentially explosive hydrogen cyanide.

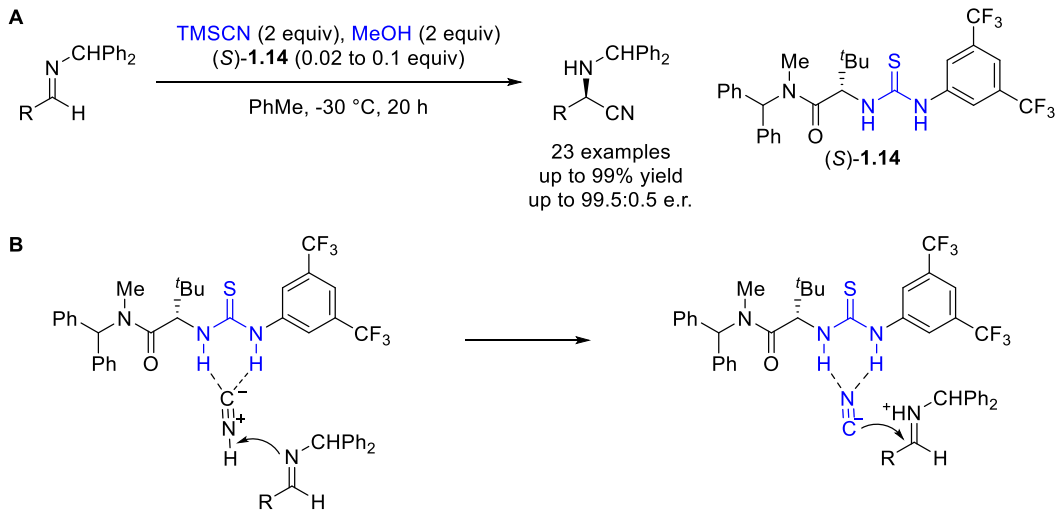


**Scheme 1.6** (A) Enantioselective imine hydrocyanation. (B) Formation and reactivity of hydrogen bonded cyanide.

The Seidel group published an enantioselective synthesis of substituted lactams by a Mannich reaction with homophthalic anhydride, followed by a subsequent transamidification (**Scheme 1.7A**).[27] Coordination of homophthalic anhydride with thiourea catalyst (*R*,*R*)-**1.15** enabled its deprotonation by the imine electrophile, generating a hydrogen bonded isochromenolate species. The coordinated anion undergoes addition to the iminium, forming a new carbon-carbon bond in a stereodetermining Mannich addition (**Scheme 1.7B**).

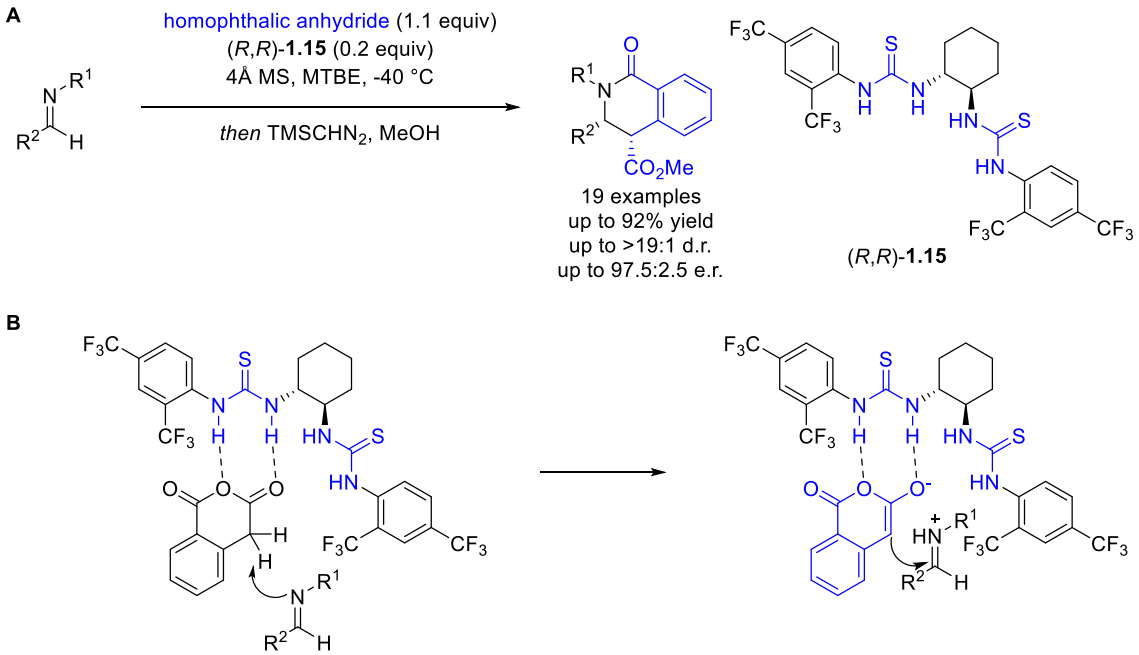


**Scheme 1.7** (A) Mannich reaction and transamidification to afford enantioenriched lactams. (B) Generation and reactivity of hydrogen bonded isochromenolate.

The generation of hydrogen bonded anions by a catalyst mediated deprotonation represents a valuable strategy in the synthesis of enantioenriched organic compounds. Using a neutral catalyst, hydrogen bonded cyanide and isochromenolate have explored for enantioselectve carbon-carbon bond formation. The broader scope of this mode of activation to install simple functional groups may become limited by the toxicity and reactivity of the necessary conjugate acid; if groups such as fluoride, azide, and cyanide are desired, hydrofluoric acid, hydrazoic acid, and hydrogen cyanide would be necessary.

**Acyl(oxy) bound pro-anionic nucleophiles**

Acyl(oxy) groups release an anionic leaving group upon displacement with a nucleophilic co-catalyst and examples of this anion becoming hydrogen bonded and remaining nucleophilic have been described.

The Jacobsen group developed an enantioselective acylation of silyl ketene acetyls with acyl fluorides for the synthesis of enantioenriched α,α-disubstituted butyrolactones (**Scheme 1.8A**).[28] Two unique anion bound intermediates were proposed as parts of the catalytic cycle. Coordination of thiourea catalyst (*S*,*R*)-**1.16** to an acyl fluoride enables the 4-(pyrrolindin-1-yl)pyridine co-catalyst to displace a fluoride leaving group, which is subsequently coordinated by (*S*,*R*)-**1.16**. This hydrogen bonded fluoride is nucleophilic and is used to release an enolate from a silyl ketene acetal (**Scheme 1.8B**). Subsequent steps of this transformation are discussed in *vida infra*.

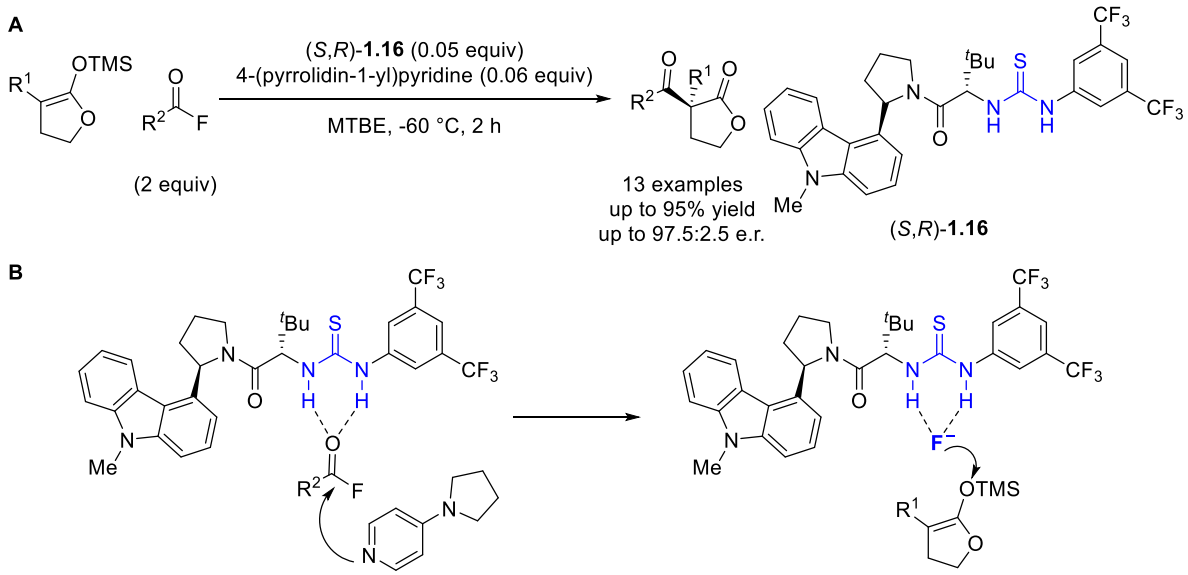


**Scheme 1.8** (A) Synthesis of enantioenriched α,α-disubstituted butyrolactones. (B) Generation and reactivity of hydrogen bonded fluoride from an acyl fluoride.

The Seidel group proposed the generation of a hydrogen bonded enolate from an *O*-acyloxy substrate, enabling the synthesis of enantioenriched azalactones (**Scheme 1.9A**).[31] Thiourea catalyst (*S*)-**1.17** and DMAP co-catalyst release an oxazol-5-olate anion from the substrate. The oxazol-5-olate is hydrogen bonded by (*S*)-**1.17** and reacts with the activated acyloxy species to form the desired product (**Scheme 1.9B**).

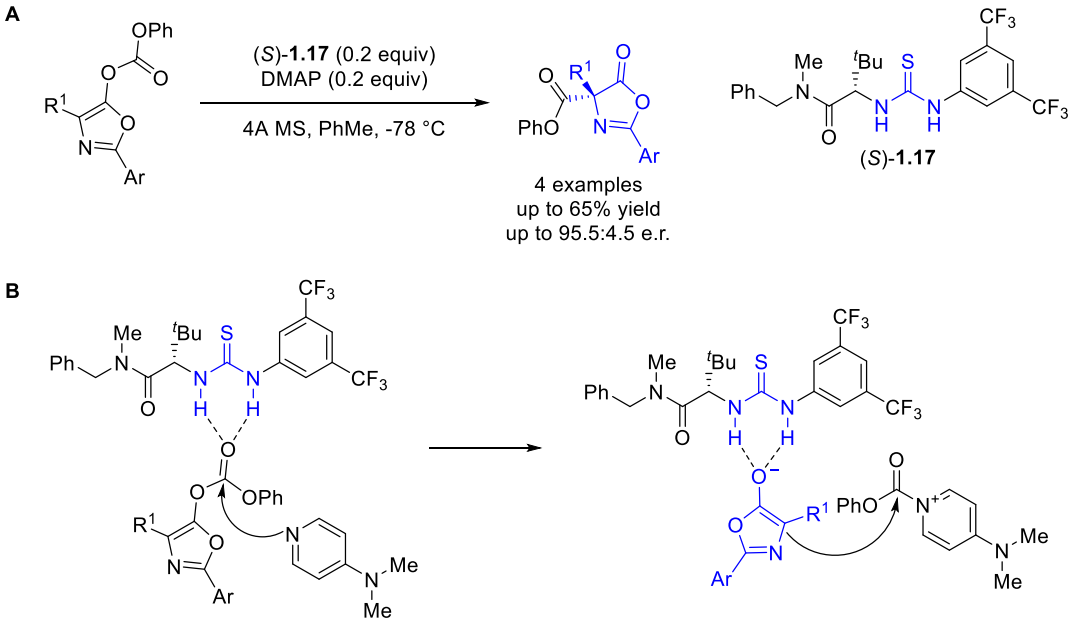


**Scheme 1.9** (A) Synthesis of α,α-disubstituted amino acid derivatives. (B) Proposed formation and reactivity of hydrogen bonded oxazol-5-olate anion. Ar = 3,5-bis(methoxy)phenyl.

The Seidel group also demonstrated that *O*-acyloxy compound could generate a nucleophilic hydrogen bonded oxazol-5-olate anion with a range of isoquinolines (**Scheme 1.10A**).[31] In

these examples, the anion remains nucleophilic at the same position, but the electrophile reacts to form highly functionalized α,β-diamino acid derivatives (**Scheme 1.10B**).

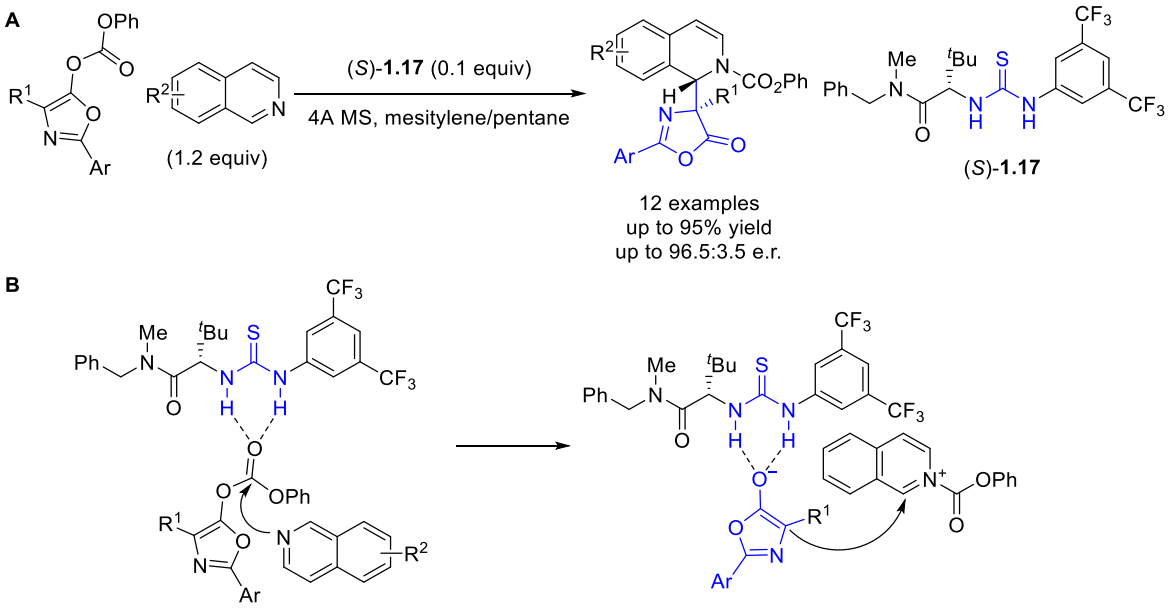


**Scheme 1.10** (A) Synthesis of α,β-diamino acid derivatives. (B) Proposed formation and reactivity of hydrogen bonded oxazol-5-olate anion. Ar = 3,5-bis(methoxy)phenyl.

Acyl(oxy) groups and a nucleophilic co-catalyst provide an alternative to deprotonation for the generation of anions. Notably, the use of an acyl fluoride notably enabled the first catalytic generation of a nucleophilic hydrogen bonded fluoride. This strategy may find broader applicability for enantioselective synthesis where the conjugate acid of a desired anion is unwanted.

**Trimethylsilyl bound pro-anionic nucleophiles**

Trimethylsilyl bound anions are typically used to generate the free acid by *in situ* hydrolysis or alcoholysis. However examples of their direct involvement within the catalytic cycle to generate a hydrogen bonded anion have been published.

An enantioselective synthesis of enantioenriched α,α-disubstituted butyrolactones from the Jacobsen group was previously introduced, which involved the generation of a hydrogen bonded fluoride from an acyl fluoride (**Scheme 1.8A**).[28] This fluoride coordinated to **1.16** was proposed to release an enolate upon reaction with a silyl ketene acetal. This subsequently generates an enolate hydrogen bonded to **1.16** that reacts with the previously formed *N*-acyl

pyridinium, resulting in the desired α,α-disubstituted butyrolactones products (**Scheme 1.11B**). The involvement of two catalyst bound nucleophilic anions in the proposed mechanism is noteworthy and highlights the potential for a hydrogen bond donor catalyst to coordinate to more than one specific nucleophilic anion.

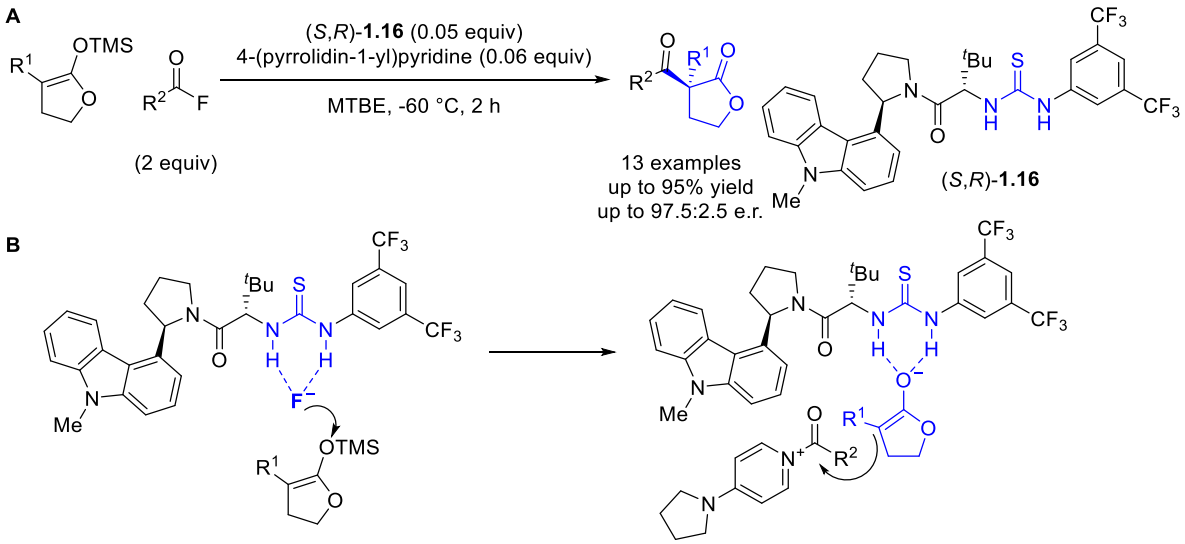


**Scheme 1.11** (A) Enantioenriched α,α-disubstituted butyrolactones. (B) Formation and reactivity of hydrogen bonded enolates.

The Jacobsen group also demonstrated an enantioselective addition of trimethylsilyl bromide to oxetanes proceeding through a hydrogen bonded bromide (**Scheme 1.12**).[33] Trimethylsilyl bromide ionises the oxetane substrate in the presence of catalyst **1.18**, resulting in a bromide anion coordinated by the squaramide of **1.18**. The coordinated bromide anion undergoes a stereoselective addition to the activated oxetane, causing it to open and form enantioenriched 1,3-bromohydrins. This represents the first example of squaramides acting as hydrogen bond donors with nucleophilic anions, and the first example of a nucleophilic hydrogen bonded bromide used in enantioselective catalysis. The unique size and shape of the bromide anion may have led to the necessity of the squaramide functional group, highlighting the unique challenges involved in developing these systems.[32]

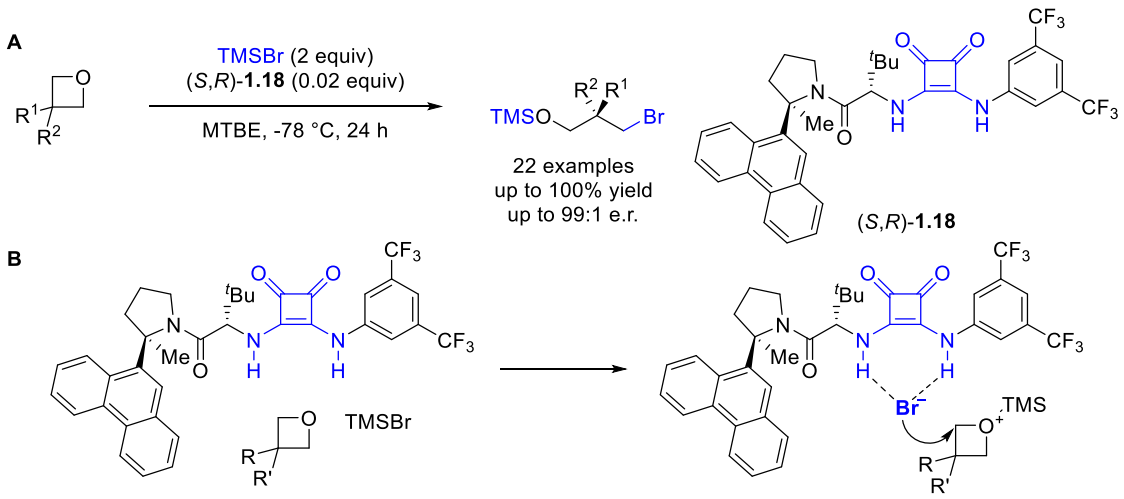


**Scheme 1.12** (A) Enantioselective addition of trimethylsilyl bromide to oxetanes. (B) Proposed mechanism with a nucleophilic hydrogen bonded bromide.

Trimethylsilyl reagents can be simple to handle although are often hydroscopic or moisture sensitive and can require additional synthetic steps to prepare. They remain a potentially convenient source of simple anions primed for nucleophilic addition without necessitating the corresponding acid but has only been applied to the generation of hydrogen bonded nucleophilic enolates and bromide.

### 1.4.3 Structure and reactivity of hydrogen bonded fluoride

The mechanism of the fluorinase enzyme involving a hydrogen bonded fluoride and the lack of knowledge regarding the impact of hydrogen bonding on the behaviour of fluoride initiated a series of systematic investigations into the structure and reactivity of hydrogen bonded fluoride complexes in the Gouverneur group.[35,36] A variety of techniques were used, notably X-ray crystallography, which provided direct insight into structure and connectivity of single crystal of hydrogen bonded fluoride complexes.

Initial studies evaluated the impact of hydrogen bonding on the structure and reactivity of alcohol-fluoride complexes.[35] A diverse set of fourteen alcohol-fluoride complexes were synthesised, isolated, and characterised. Crystallisation led to a wide range of structures characterised by X-ray crystallography, revealing coordination numbers ranging from two to four depending on the steric environment of the alcohol.

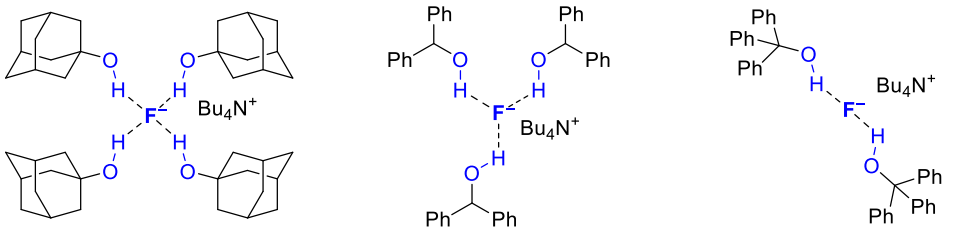


**Figure 1.3** Structure of selected alcohol-fluoride complexes.

Investigations into the reactivity of these complexes with alkyl bromide substrate **1.19** enabled comparison of the nucleophilicity and basicity of the hydrogen bonded fluoride anion. Fluoride can act as either a nucleophile or base, resulting in fluorinated product **1.20** by $S_N2$ or alkene **1.21** by E2 elimination. The results suggested fluoride complexed by fewer alcohol hydrogen bond donors were more reactive, albeit less selective for $S_N2$ compared to E2 (**Table 1.1**).

**Table 1.1** Reactivity of selected alcohol-fluoride complexes.[36]

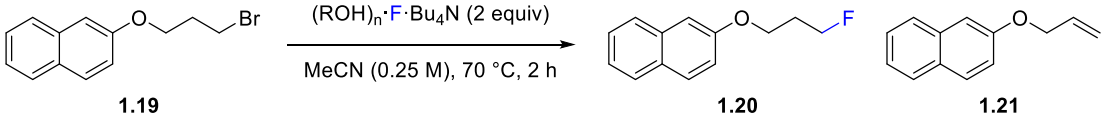


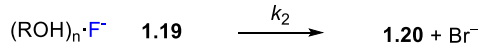


| entry | $(ROH)_n·F·Bu_4N$ | coordination number | $k_2$ ($\times10^{-3}$ $M^{-1}$ $s^{-1}$) | [**1.20**]/[**1.21**] |
|---|---|---|---|---|
| 1 | $(pinacol)_2·F·Bu_4N$ | 4 | 2.1 | 2.8 |
| 2 | $(H_2O)_3·F·Bu_4N$ | 3 | 6.1 | 1.6 |
| 3 | (tri-*p*-tolyl-methanol)$_4$·F·$Bu_4N$ | 2 | 25.1 | 2.1 |

1,3-Diarylureas are widespread in anion recognition and catalysis, and a subsequent study from the Gouverneur group focused on the structure and reactivity of 1,3-diarylurea-fluoride complexes.[36] A set of 1,3-diarylurea-fluoride complexes derived from tetrabutylammonium fluoride were synthesised, isolated, and characterised. These urea-fluoride structures were categorised into three distinct types: type 1.1A structures with a unit cell containing a fluoride anion coordinated by two urea molecules; type 1.1B structures with a unit cell containing two fluoride anions coordinated by four urea molecules; type 1.1C structures consisting of two fluoride anions coordinated by two urea molecules and two molecules of water. A fourth type

1.1D structure was also observed with tetramethylammonium or tetraethylammonium fluoride, with a unit cell containing a fluoride anion coordinated by six hydrogen bonding interactions from three urea molecules (**Figure 1.4**).[36]

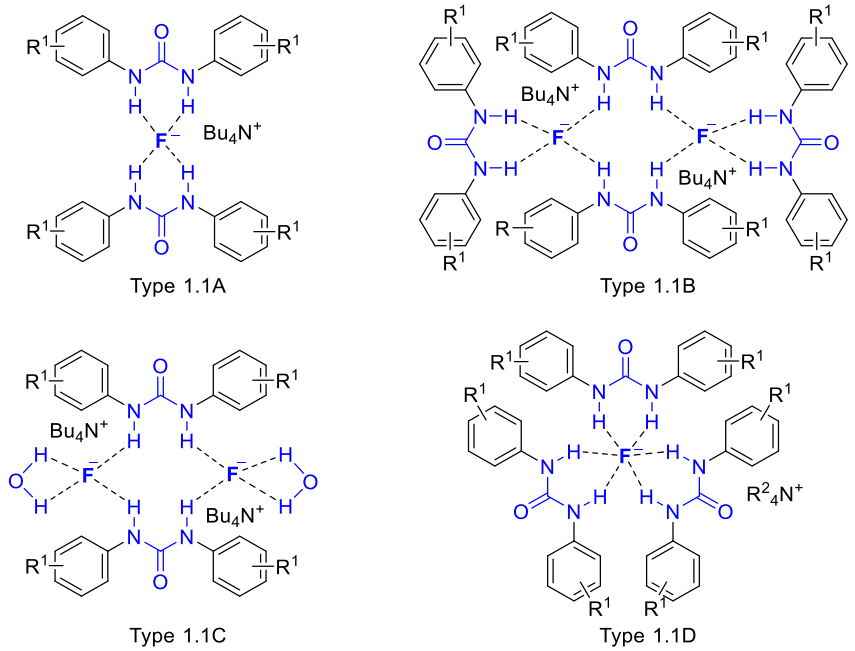


**Figure 1.4** Four structure classes of urea-fluoride complexes.

The reactivity of these urea-fluoride complexes with alkyl bromide substrate **1.19** was evaluated, enabling comparison between the nucleophilicity and basicity of the hydrogen bonded fluoride anion (**Table 1.2**). The proposed mechanism involved the initial 2:1 urea-fluoride complex dissociating to form a 1:1 urea-fluoride complex. This 1:1 urea-fluoride complex can act as either a nucleophile or a base, leading to **1.20** and **1.21** respectively. Importantly, the ratio between $S_N2$ and E2 could be fine-tuned by variation of the urea electronics. The complexes produced from the more electronic deficient ureas resulted in more product derived from an $S_N2$ reaction, although they exhibited a slower overall reactivity than the complexes produced from the more electronic rich ureas. The reaction with tetrabutylammonium fluoride trihydrate without any urea hydrogen bond donors was significantly faster and less selective, highlighting the challenge of catalysis with a hydrogen bonded nucleophilic anion, where the uncoordinated anion reacts faster than the coordinated anion.

**Table 1.2** Mechanism and reactivity of selected urea-fluoride complexes.[36]

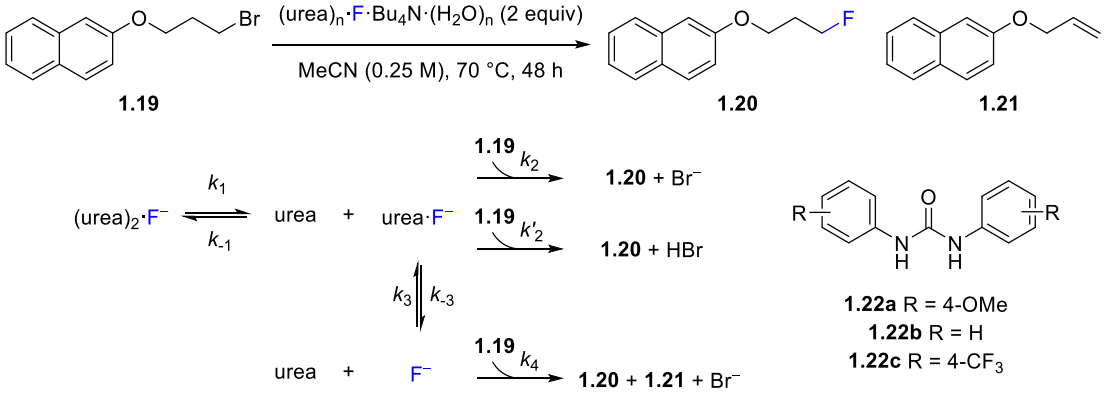


| entry | complex | $k_2$ (×$10^{-5}$ $M^{-1}$ $s^{-1}$) | $k_2(S_N2)/k'_2(E2)$ |
|---|---|---|---|
| 1 | (**1.22a**)$_2$·F·$Bu_4N$ | 12.7 | 5.2 |
| 2 | (**1.22b**)$_2$·F·$Bu_4N$ | 5.76 | 6.8 |
| 3 | (**1.22c**)$_2$·F·$Bu_4N$ | 1.65 | 8.7 |
| 4 | $Bu_4N$·F·$(H_2O)_3$ | 375 | 1.6 |

### 1.4.4 Discovery, scope, and mechanism

These studies led to the development of Hydrogen Bonding Phase-Transfer Catalysis (HB-PTC),[21] an novel phase-transfer platform enabling enantioselective fluorination utilising a hydrogen bonded fluoride anion.[21] This platform merges hydrogen bonding to control the reactivity of a fluoride anion with a phase-transfer process to supress quantities of soluble uncoordinated fluoride.

Initial studies highlighted neutral and achiral Schreiner's urea **1.22d** as a uniquely competent catalyst for HB-PTC, enabling both phase-transfer and fluorination (**Scheme 1.13**). Stirring *meso*-episulfonium precursor (±)-**1.23** with caesium fluoride in $CH_2Cl_2$ resulted in no reaction, presumably due to the insolubility of caesium fluoride. However, the addition of **1.22d** resulted in successful formation of desired fluorinated product (±)-**1.24** in a high yield.[21] The significantly reduced background reaction by retaining fluoride in a separate phase provided a strong foundation for the development of an enantioselective variation of this transformation.

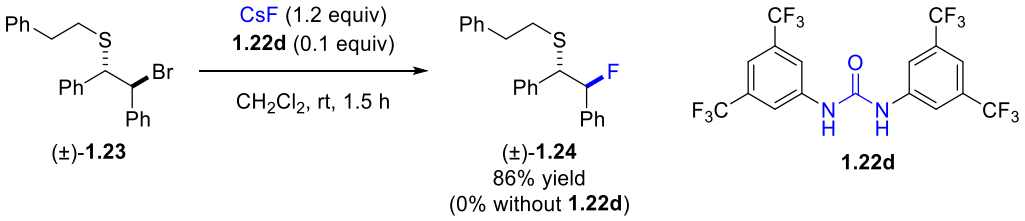


**Scheme 1.13** Initial results of hydrogen bonding phase transfer catalysis with an achiral urea catalyst.

The enantioselective desymmetrisation of *meso*-episulfonium ions formed *in situ* from β-bromosulfides with caesium fluoride was successfully achieved under HB-PTC (**Scheme 1.14**). Use of the chiral (*S*)-(−)-1,1′-dinaphthyl-2,2′-diamine ((*S*)-BINAM) derived bis-urea catalyst (*S*)-**1.17a** enabled formation of (*S*,*S*)-**1.16** with good enantioselectivity. A single *N*-alkylation of this tetradentate hydrogen bond donor catalyst to produce (*S*)-**1.17b**, a tridentate hydrogen bond donor, led to an improvement in enantiomeric ratio of (*S*,*S*)-**1.16** whilst maintaining high yields.[21]

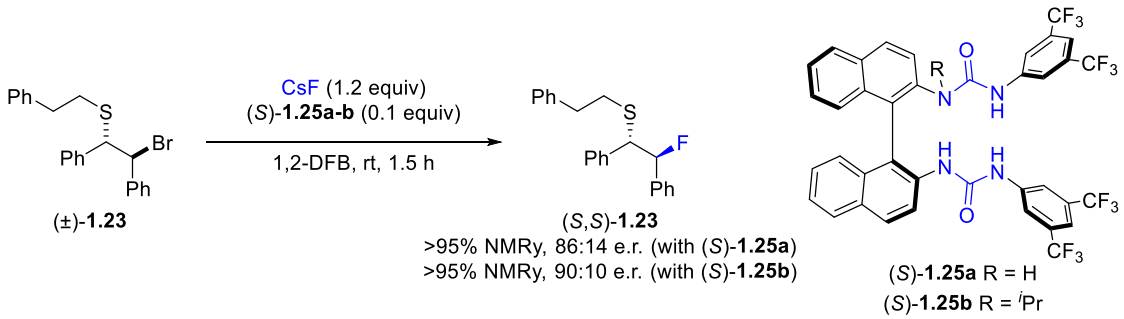


**Scheme 1.14** Discovery of an enantioselective desymmetrisation of *meso*-episulfonium precursor (±)-**1.23** with (*S*)-**1.25a** and improvement provided by (*S*)-**1.25b**. NMRy determined with 4-fluoroanisole internal standard. 1,2-DFB = 1,2-difluorobenzene.

Further optimisation of this reaction involved a reduction in temperature and an increased two equivalents of caesium fluoride. A reaction scope with (*S*)-**1.25b** demonstrated high yields and enantiomeric ratios up to 97:3 across twelve examples (**Scheme 1.15**). These reactions represented the first published examples of an organocatalytic enantioselective nucleophilic fluorination, utilising an alkali metal fluoride salt, caesium fluoride.

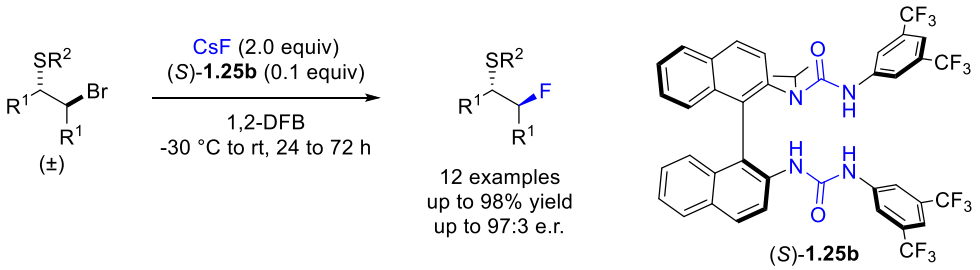


**Scheme 1.15** Enantioselective fluorination of *meso*-episulfonium precursors with caesium fluoride under HB-PTC. 1,2-DFB = 1,2-difluorobenzene.

The proposed mechanism involves a phase transfer mediated by the neutral urea catalyst modelled as an ion metathesis between the bromide bound catalyst and the fluoride salt. The resultant nucleophilic hydrogen bonded fluoride complex reacts with the *meso*-episulfonium ion to form the desired fluorinated product, with enantiocontrol provided by the chiral hydrogen bond donor (**Figure 1.5**).[21]

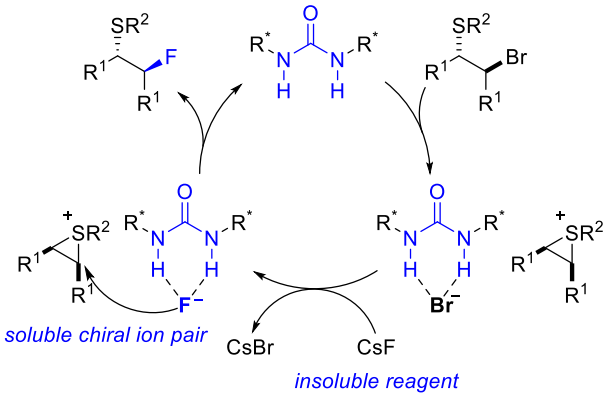


**Figure 1.5** Proposed catalytic cycle for the desymmetrisation of *meso*-episulfonium ions under HB-PTC.

Structural and mechanistic studies provided further insight into the nature of the urea-fluoride complex. Titration of (*S*)-**1.25b** with fluoride revealed formation of both 1:1 and 2:1 urea-fluoride species in solution (**Figure 1.6A**).[21,37] A $K_{a(1:1)}$ of 1.43 ± 0.04 × $10^6$ $M^{-1}$ and smaller $K_{a(2:1)}$ of 3.1 ± 0.9 × $10^3$ $M^{-1}$ suggested a strong preference for the formation of the 1:1 urea-fluoride complex in solutions containing excess fluoride, but also the ability to form a 2:1 urea-fluoride species. $^1H$-$^{19}F$ NMR experiments revealed scalar couplings between the hydrogen bonded fluoride anion and the urea hydrogen bond donors, with coupling constants of 34 Hz, 51 Hz, and 61 Hz (**Figure 1.6B**).[37] The unique structure of (*S*)-**1.25b** complexed to fluoride was also demonstrated in the solid state by the synthesis and crystallisation of (*S*)-**1.25b**·F·$Bu_4N$ and

displayed three different hydrogen bond lengths to fluoride at 2.662(2) Å, 2.690(2) Å, and 2.667(2) Å (**Figure 1.6C**).

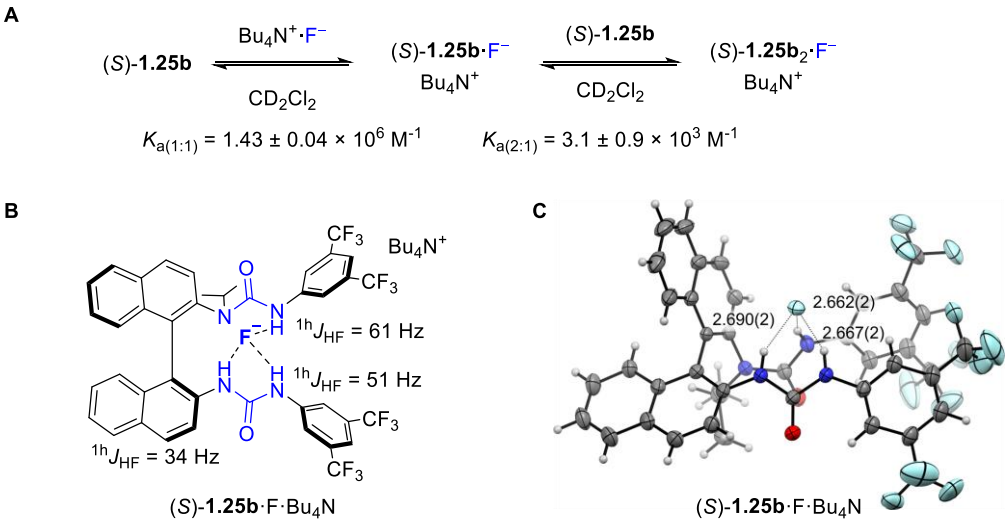


**Figure 1.6** (A) Association constants of (*S*)-**1.25b** with tetrabutylammonium fluoride (3 mM (*S*)-**1.25b**, $CD_2Cl_2$, 298 K). (B) Coupling constants between three urea hydrogen bond donors of (*S*)-**1.25b** and fluoride (3 mM (*S*)-**1.25b**, $CD_2Cl_2$, 298 K). (C) Crystal structure of (*S*)-**1.25b**·F·$Bu_4N$ (CCDC 1812188).[21] Distances provided in Ångstroms, tetrabutylammonium cation omitted for clarity, displacement ellipsoids drawn at 50% probability level.

An important development into the range of reactions under HB-PTC was demonstrated in the synthesis of enantioenriched β-aminofluorides from caesium or potassium fluoride (**Scheme 1.16A**).[38] The optimised catalyst (*S*)-**1.18** paralleled (*S*)-**1.25b**, consisting of an *N*-alkyl-bis-urea scaffold derived from (*S*)-BINAM. The use of *meso*-aziridinium precursors resulted in highly valuable β-aminofluoride products, and the ability to use potassium fluoride represented the first expansion of the alkali metal fluoride salt and suggested a broader range of nucleophilic reagents derived from alkali metal salts may be applicable to HB-PTC. Additional optimisation enabled the scale-up of this procedure to a 200 g scale using a mechanically stirred reactor (**Scheme 1.16B**).[39]

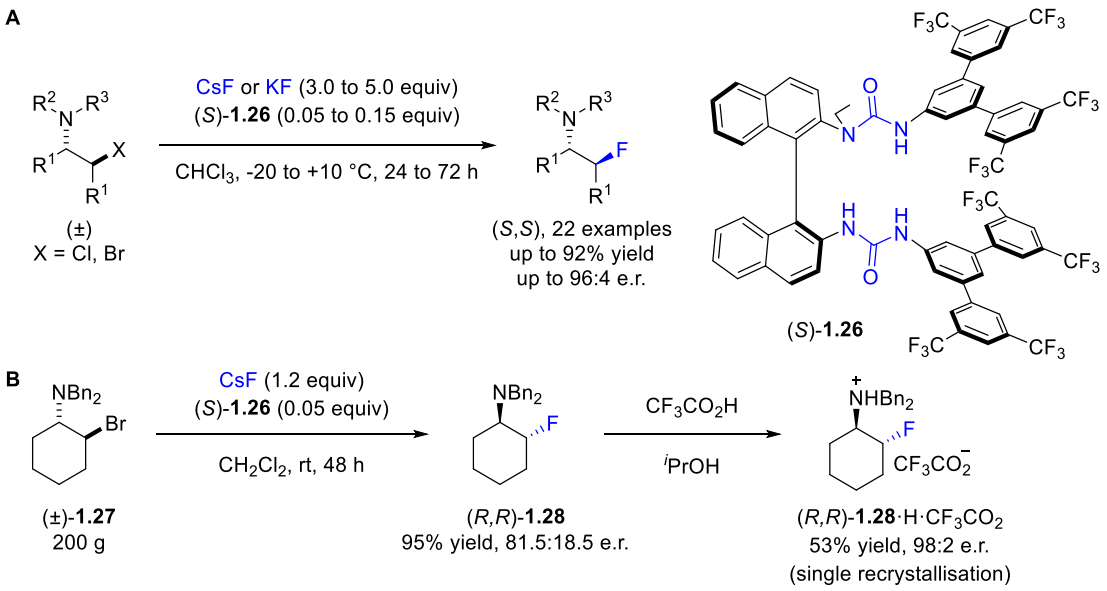


**Scheme 1.16** (A) HB-PTC for enantioselective synthesis of β-fluoroamines with caesium fluoride or potassium fluoride. (B) Scale-up of HB-PTC protocol to 200 g.

Whilst conducting the investigations described in this thesis, it was realised preformed azetidinium salts were also competent substrates for enantioselective fluorination with caesium fluoride (**Scheme 1.17**).[40,41] Despite the possibility for the salt itself to be a phase-transfer agent, use of catalyst (*S*)-**1.25b** with caesium fluoride successfully provided enantioenriched γ-fluoroamines in up to 99% yield and enantiomeric ratios up to 97:3 under HB-PTC by asymmetric ring opening of the azetidinium salt with fluoride.

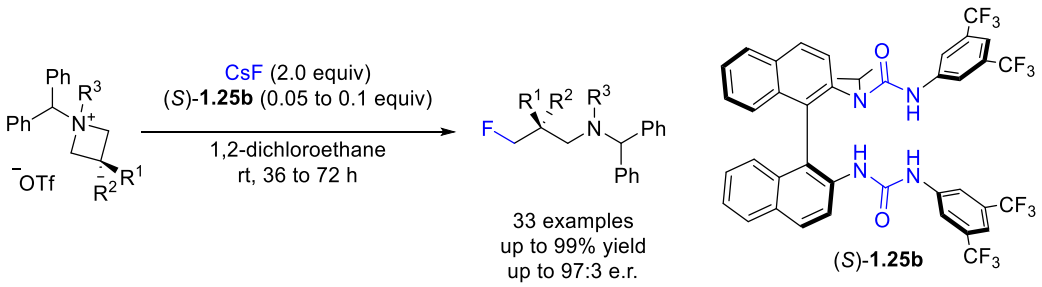


**Scheme 1.17** HB-PTC for enantioselective synthesis of γ-fluoroamines from azetidinium salts.[40]

The predominant advantage of HB-PTC is the ability to use alkali metal fluoride salts as reagents for enantioselective organic synthesis, which typically represent the most cost effective fluoride sources.[42] In addition, the practical protocol is facile, not requiring stringent drying of solvents or an inert atmosphere. Hitherto, HB-PTC has seen exclusive application in the delivery of fluoride for the synthesis of enantioenriched organofluorines, although it was

hypothesised this platform could be applied towards enantioselective synthesis with other salts and nucleophiles that are poorly soluble in organic solvents.[21]

## 1.5 Research proposal

HB-PTC has been demonstrated to be a powerful platform for the synthesis of enantioenriched organofluorides directly from the caesium and potassium salts of fluoride by generate a nucleophilic hydrogen bonded fluoride anion capable of enantioselective fluorination. Azide and cyanide both provide valuable functionality to organic molecules in both their native motif and upon further functionalisation. Recognisable advantages exist if their alkali metal salts could be utilised in enantioselective organocatalytic synthesis. In addition, nitrogen and carbon are both far more abundant in medicinal chemistry than fluorine.[43] Hence studies into applying HB-PTC to sodium azide and potassium cyanide are proposed.

The many inherent differences between fluoride, azide and cyanide anions may present challenges when attempting to translate the HB-PTC platform from fluoride to azide or cyanide (**Table 1.3**). Structural and symmetrical variations may result in significant differences in their interaction with urea due to geometry.[44] Their electronic differences result in different charge densities and basicities, potentially impacting their hydrogen bond acceptor abilities. Comparison of the p$K_a$ of their respective conjugate acids in water and DMSO suggest that these three anions are influenced very differently by their hydrogen bonding environment; the conjugate acid of fluoride is the most acidic in $H_2O$, and the least acidic in DMSO.[45] Comparison of Mayr's nucleophilicity parameter in acetonitrile solvent mixtures suggested the cyanide anion was most reactive, followed by azide, followed by fluoride.[46–48] Cyanide is also ambident, with potential to form nitrile or isonitrile products depending which termini acts as the nucleophilic site.[48]

**Table 1.3** Comparison of selected properties of fluoride, azide, and cyanide.

| property | fluoride | azide | cyanide |
|---|---|---|---|
| constitution | 1 atom | 3 atoms | 2 atoms |
| shape | spherical | linear | linear |
| point group | $K$ | $D_{\infty h}$ | $C_{\infty v}$ |
| valence electrons | 8 | 16 | 10 |
| charge density (C $mm^{-3}$) | 24 | 6 | 7 |
| p$K_a$ (conjugate acid, $H_2O$) | 3.2 | 4.7 | 9.1 |
| p$K_a$ (conjugate acid, DMSO) | 15 ± 2 | 7.9 | 12.9 |
| Mayr's nucleophilicity parameter | 10.88 (2% $H_2O$ in MeCN) | 15.01 (45% MeOH in MeCN) | 16.27 (MeCN) |

Initial studies focused on the azide anion and investigated its structure and coordination with urea HB-PTC catalysts in both the solution and solid state. These studied provided a robust platform the development of an enantioselective azidation reaction for the synthesis of β-aminoazides, and mechanistic insights provided further details into the applicability of HB-PTC to azide. Subsequent studies focused on the cyanide anion and investigated its hydrogen bonding interaction with urea HB-PTC catalysts in solution whilst developing a robust protocol for the enantioselective synthesis of β-chiral nitriles from potassium cyanide. This research aims to introduce novel methodologies for enantioselective synthesis and provide new insights into structure and reactivity of hydrogen bonded azide and cyanide.

## 1.6 References


1 C. M. Starks, *J. Am. Chem. Soc.*, 1971, **93**, 195–199.

2 P. Muller, *Pure Appl. Chem.*, 1994, **66**, 1077–1184.

3 M. Makosza, *Pure Appl. Chem.*, 2000, **72**, 1399–1403.

4 T. Ooi and K. Maruoka, *Angew. Chem. Int. Ed.*, 2007, **46**, 4222–4266.

5 S. Shirakawa and K. Maruoka, *Angew. Chem. Int. Ed.*, 2013, **52**, 4312–4348.

6 J. Tan and N. Yasuda, *Org. Process Res. Dev.*, 2015, **19**, 1731–1746.

7 U. H. Dolling, P. Davis and E. J. J. Grabowski, *J. Am. Chem. Soc.*, 1984, **106**, 446–447.

8 M. Makosza, *Pure Appl. Chem.*, 1975, **43**, 439–462.

9 V. Rauniyar, A. D. Lackner, G. L. Hamilton and F. D. Toste, *Science*, 2011, **334**, 1681–1684.

10 H. P. Shunatona, N. Früh, Y.-M. Wang, V. Rauniyar and F. D. Toste, *Angew. Chem. Int. Ed.*, 2013, **52**, 7724–7727.

11 R. J. Phipps and F. D. Toste, *J. Am. Chem. Soc.*, 2013, **135**, 1268–1271.

12 J. Wu, Y.-M. Wang, A. Drljevic, V. Rauniyar, R. J. Phipps and F. D. Toste, *Proc. Natl. Acad. Sci.*, 2013, **110**, 13729–13733.

13 X. Yang, R. J. Phipps and F. D. Toste, *J. Am. Chem. Soc.*, 2014, **136**, 5225–5228.

14 W. Zi, Y.-M. Wang and F. D. Toste, *J. Am. Chem. Soc.*, 2014, **136**, 12864–12867.

15 H. M. Nelson, J. S. Patel, H. P. Shunatona and F. D. Toste, *Chem. Sci.*, 2015, **6**, 170–173.

16 C. M. Avila, J. S. Patel, Y. Reddi, M. Saito, H. M. Nelson, H. P. Shunatona, M. S. Sigman, R. B. Sunoj and F. D. Toste, *Angew. Chem. Int. Ed.*, 2017, **56**, 5806–5811.

17 S. Biswas, K. Kubota, M. Orlandi, M. Turberg, D. H. Miles, M. S. Sigman and F. D. Toste, *Angew. Chem. Int. Ed.*, 2018, **57**, 589–593.

18 R. J. Phipps, K. Hiramatsu and F. D. Toste, *J. Am. Chem. Soc.*, 2012, **134**, 8376–8379.

19 Y. Wang, C. Hoong, V. Rauniyar and F. D. Toste, *J. Am. Chem. Soc.*, 2012, **134**, 12928–12931.

20 E. Miller, S. Kim, K. Gibson, J. S. Derrick and F. D. Toste, *J. Am. Chem. Soc.*, 2020, **142**, 8946–8952.

21 G. Pupo, F. Ibba, D. M. H. Ascough, A. C. Vicini, P. Ricci, K. E. Christensen, L. Pfeifer, J. R. Morphy, J. M. Brown, R. S. Paton and V. Gouverneur, *Science*, 2018, **360**, 638–642.

22 D. O'Hagan, C. Schaffrath, S. L. Cobb, J. T. G. Hamilton and C. D. Murphy, *Nature*, 2002, **416**, 279–279.

23 D. O'Hagan and H. Deng, *Chem. Rev.*, 2015, **115**, 634–649.

24 K. Brak and E. N. Jacobsen, *Angew. Chem. Int. Ed.*, 2013, **52**, 534–561.

25 A. G. Doyle and E. N. Jacobsen, *Chem. Rev.*, 2007, **107**, 5713–5743.

26 S. M. Banik, A. Levina, A. M. Hyde and E. N. Jacobsen, *Science*, 2017, **358**, 761–764.

27 C. L. Jarvis, J. S. Hirschi, M. J. Vetticatt and D. Seidel, *Angew. Chem. Int. Ed.*, 2017, **56**, 2670–2674.

28 J. A. Birrell, J. N. Desrosiers and E. N. Jacobsen, *J. Am. Chem. Soc.*, 2011, **133**, 13872–13875.

29 S. J. Zuend and E. N. Jacobsen, *J. Am. Chem. Soc.*, 2009, **131**, 15358–15374.

30 S. J. Zuend, M. P. Coughlin, M. P. Lalonde and E. N. Jacobsen, *Nature*, 2009, **461**, 968–970.

31 C. K. De, N. Mittal and D. Seidel, *J. Am. Chem. Soc.*, 2011, **133**, 16802–16805.

32 D. A. Strassfeld, R. F. Algera, Z. K. Wickens and E. N. Jacobsen, *J. Am. Chem. Soc.*, 2021, **143**, 9585–9594.

33 D. A. Strassfeld, Z. K. Wickens, E. Picazo and E. N. Jacobsen, *J. Am. Chem. Soc.*, 2020, **142**, 9175–9180.

34 A. Hamza, G. Schubert, T. Soós and I. Pápai, *J. Am. Chem. Soc.*, 2006, **128**, 13151–13160.

35 K. M. Engle, L. Pfeifer, G. W. Pidgeon, G. T. Giuffredi, A. L. Thompson, R. S. Paton, J. M. Brown and V. Gouverneur, *Chem. Sci.*, 2015, **6**, 5293–5302.

36 L. Pfeifer, K. M. Engle, G. W. Pidgeon, H. A. Sparkes, A. L. Thompson, J. M. Brown and V. Gouverneur, *J. Am. Chem. Soc.*, 2016, **138**, 13314–13325.

37 F. Ibba, G. Pupo, A. L. Thompson, J. M. Brown, T. D. W. Claridge and V. Gouverneur, *J. Am. Chem. Soc.*, 2020, **142**, 19731–19744.

38 G. Pupo, A. C. Vicini, D. M. H. Ascough, F. Ibba, K. E. Christensen, A. L. Thompson, J. M. Brown, R. S. Paton and V. Gouverneur, *J. Am. Chem. Soc.*, 2019, **141**, 2878–2883.

39 A. C. Vicini, PhD thesis, University of Oxford, 2020.

40 G. Roagna, D. M. H. Ascough, F. Ibba, A. C. Vicini, A. Fontana, K. E. Christensen, A.

Peschiulli, D. Oehlrich, A. Misale, A. A. Trabanco, R. S. Paton, G. Pupo and V. Gouverneur, *J. Am. Chem. Soc.*, 2020, **142**, 14045–14051.

41 G. Roagna, PhD thesis, University of Oxford, 2021.

42 G. Villalba, R. U. Ayres and H. Schroder, *J. Ind. Ecol.*, 2008, **11**, 85–101.

43 V. N. Charushin, Y. A. Titova and E. R. Milaeva, *Her. Russ. Acad. Sci.*, 2020, **90**, 229–238.

44 G. Rayner-Canham and T. Overton, *Descriptive Inorganic Chemistry*, W. H. FREEMAN AND COMPANY, New York, 5th edn., 2010.

45 F. G. Bordwell, *Acc. Chem. Res.*, 1988, **21**, 456–463.

46 C. Nolte, J. Ammer and H. Mayr, *J. Org. Chem.*, 2012, **77**, 3325–3335.

47 T. B. Phan and H. Mayr, *J. Phys. Org. Chem.*, 2006, **19**, 706–713.

48 A. A. Tishkov and H. Mayr, *Angew. Chem. Int. Ed.*, 2005, **44**, 142–145.

# 2 Hydrogen Bonding Phase-Transfer Catalysis with Sodium Azide

X-ray crystallography data collection and analysis was performed by Dr. G. Pupo and Dr. K. E. Christensen. $^{1}H$-$^{15}N$ NMR experiments were conducted with Prof. T. D. W. Claridge. Reaction scope and non-linear effect investigation were conducted with Dr. M. A. Horwitz. Initial analysis of kinetic data was conducted with Dr. F. Ibba. Analysis and modelling of kinetic data were performed by Y. Gao and Prof. G. C. Lloyd-Jones.

## 2.1 Introduction

### 2.1.1 Organoazides

The first synthesis of an organoazide was the preparation of phenyl azide from benzendiazonium tribromide and ammonia by Grieß in 1864.[1] In 1890, Curtius reported the synthesis of the conjugate acid and sodium salt of the azide anion, hydrazoic acid and sodium azide respectively.[2] Since these discoveries, organoazides have developed considerable attention in organic chemistry.[3,4] Organic compounds featuring an α-chiral β-aminoazide motif are of particular interest due to their presence in bioactive molecules including antiretrovirals, antibiotics, and proteasome inhibitors (**Figure 2.1**).[5–9]

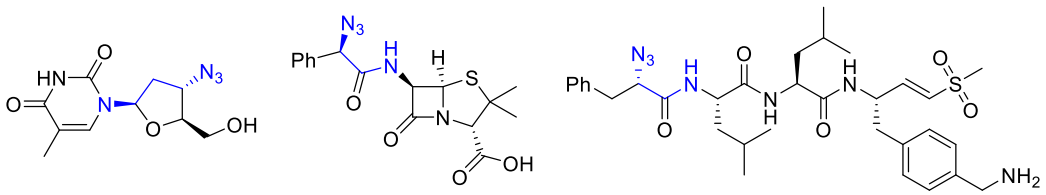


**2.1**, azidothymidine *antiretroviral*

**2.2**, azidocillin *antibiotic*

**2.3**, LU-102 *proteasome inhibitor*

**Figure 2.1** Selected examples of bioactive α-chiral β-aminoazides.

Chiral organoazides are also versatile intermediates towards many nitrogen containing functional groups and heterocycles. Several examples of these transformations feature compounds with an α-chiral-β-aminoazide group (**Scheme 2.1**).[3,4] Further reaction of the azide group by reduction affords primary amines, utilised in the synthesis of oseltamivir phosphate (*R*,*R*,*S*)-**2.5**.[10] Intramolecular cycloaddition with an appropriate partner can afford triazole **2.7** or tetrazole (*S*,*R*)-**2.9** products.[11,12] Condensation with a phosphine results in the synthesis of

iminophosphoranes, a process used in the preparation of bifunctional iminophosphorane (BIMP) organocatalysts such as (*S*)-**2.11**.[13]

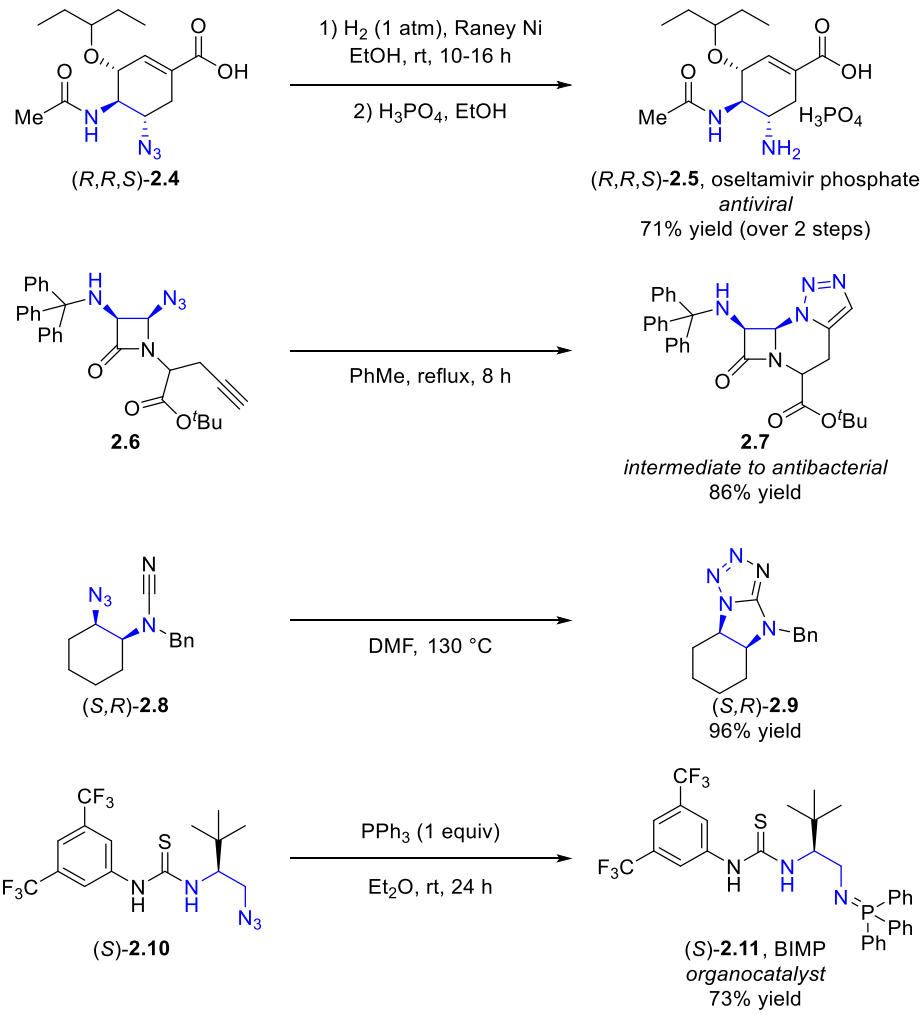


**Scheme 2.1** Selected synthetic transformations of α-chiral-β-aminoazides. BIMP = bifunctional iminophosphorane.

Organoazides are also highly relevant in the field of bioconjugation (**Scheme 2.2**). Staudinger ligation involves trapping an iminiphosporane formed between an azide and phosphine with a suitable electrophile, producing an amide bond when trapped with a methyl ester. This was demonstrated in the selective functionalisation of a cell surface prepared with azido sialic acid with a custom phosphine reagent.[14] Bioconjugation can also be achieved upon the reaction of a preinstalled azide with a cyclooctyne reagent in a strain promoted cycloaddition.[15] In addition, aryl azides have notable applications in photoaffinity labelling, covalently binding a compound to the active site of proteins.[16]

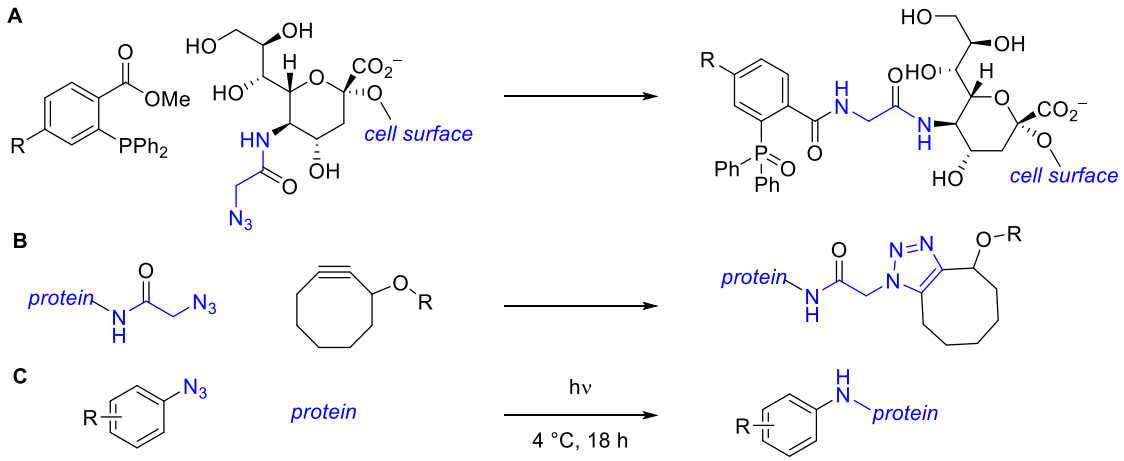


**Scheme 2.2** (A) Representative example of bioconjugation by Staudinger ligation. (B) Representative example of bioconjugation by strain promoted azide-alkyne cycloaddition. (C) Representative example of photoaffinity labelling.

Sources of azide used in organic synthesis are either commercially available or generated *in situ* from a commercially available source (**Figure 2.2**). Sodium azide is produced on the kilotonne scale from sodium amide and nitrous oxide, resulting in its high abundance and low cost.[17,18] Trimethylsilylazide and the Zhdankin reagent (1-azido-1,2-benziodoxol-3(1H)-one) are also commercially available although less cost effective and less convenient to handle than sodium azide. In addition, explosions from the preparation of these reagents are reported, and highlight an additional risk involved when the use of these reagents is necessary.[3,19,20] Hydrazoic acid and bromine azide are not commercially available due to their instability and require *in situ* synthesis.

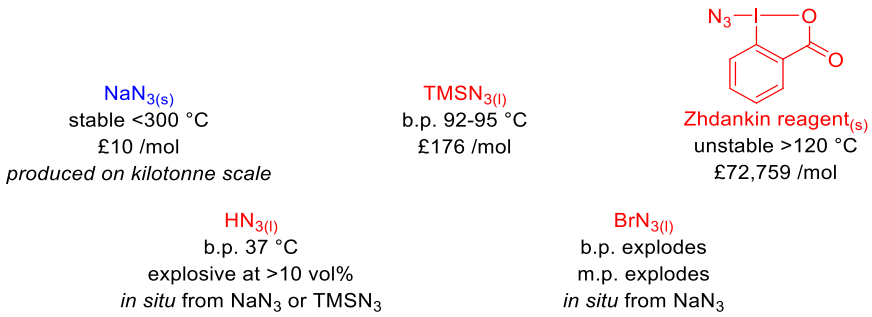


**Figure 2.2** Sources of azide used in organocatalytic enantioselective azidation.

Despite the advantages of sodium azide, it is rarely directly utilised in enantioselective organocatalytic reactions. This may be due to its poor solubility in many organic solvents (**Table 2.1**). Hansen solubility parameters provide a quantitative comparison of a solvent's

dispersion cohesion ($\delta_D$), polar cohesion ($\delta_P$), and hydrogen bonding cohesion ($\delta_H$).[21] Sodium azide possesses good solubility in protic solvents such as water at 43.60 g/ 100mL, and methanol at 2.48 g/ 100 mL. However its solubility is severely reduced in aprotic solvents, falling below 0.005 g/ 100 mL in both polar aprotic solvents such as ethyl acetate and acetone, and apolar aprotic solvents such as cyclohexane and hexane.

**Table 2.1** Solubility of sodium azide in selected solvents.

| entry | solvent | Hansen solubility parameters | | | sodium azide solubility |
|---|---|---|---|---|---|
| | | $\delta_D$ | $\delta_P$ | $\delta_H$ | (g /100 mL) |
| 1 | water | 15.5 | 16.0 | 42.3 | 43.60 |
| 2 | methanol | 15.1 | 12.3 | 22.3 | 2.48 |
| 3 | ethyl acetate | 15.8 | 5.3 | 7.2 | <0.005 |
| 4 | acetone | 15.5 | 10.4 | 7.0 | <0.005 |
| 5 | chloroform | 17.8 | 3.1 | 5.7 | <0.005 |
| 6 | carbon tetrachloride | 17.8 | 0.0 | 0.6 | <0.005 |
| 7 | cyclohexane | 16.8 | 0.0 | 0.2 | <0.005 |
| 8 | hexane | 14.9 | 0.0 | 0.0 | <0.005 |

$NaN_3$ solubility measured at 25 °C

### 2.1.2 Enzyme-azide structure and reactivity

The azide anion is known to impact the activity of enzymes by acting as an inhibitor through direct coordination with metal cofactors in the active site or by hydrogen bonding interactions in the active site of an enzyme. Enzymatic azidation reactions with the azide anion are also reported, forming organoazide products with both regiocontrol and enantiocontrol.

Cytochrome c oxidase (CcO) is the final enzyme in the respiratory electron transport chain, located in the mitochondrial membrane. CcO catalyses the oxidation of an iron(II) bound cytochrome c to an iron(III) bound cytochrome c (**Scheme 2.3A**). Yoshikawa *et al.* reported a crystal structure of azide-bound bovine heart CcO at 2.9 Å resolution.[22–24] This structure contains an azide anion forming a bridge between the heme iron(III) and copper(II) within the active site (**Scheme 2.3B**).

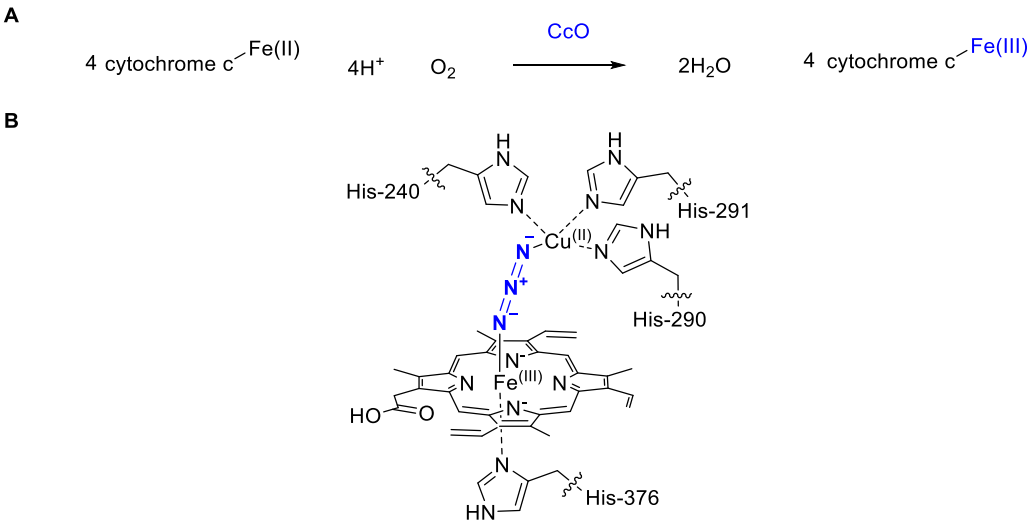


**Scheme 2.3** (A) Oxidation of cytochrome c catalysed by CcO. (B) Azide coordination to iron(III) and copper(II) in the CcO active site (PDB 1OCZ).[22,23] CcO = cytochrome c oxidase.

Formate dehydrogenases catalyse the oxidation of formate to carbon dioxide (**Scheme 2.4A**). A crystal structure where azide mimics carbon dioxide in a transition state analogue was obtained by Cheatum and co-workers.[25,26] Five hydrogen bonding interactions with azide arise from Ile-122, Asp-146, Arg-284, and His-332 residues in the active site (**Scheme 2.4B**).

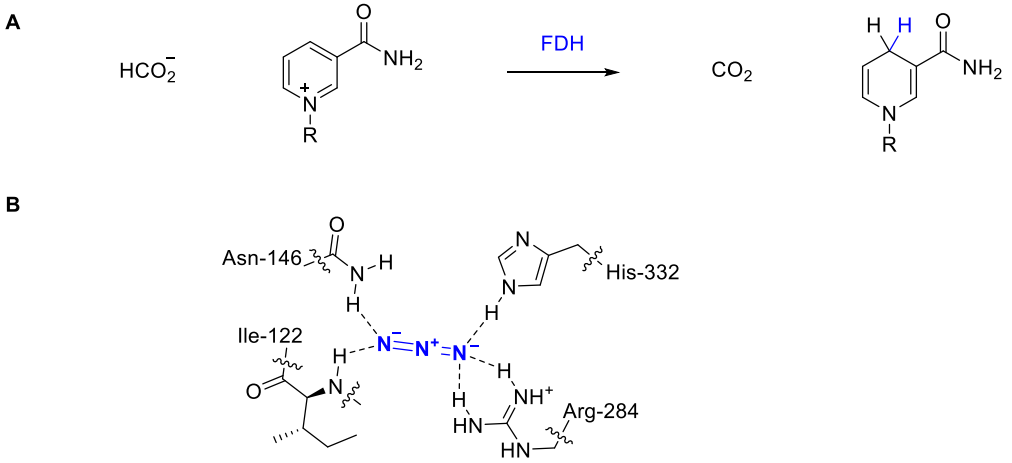


**Scheme 2.4** (A) Oxidation of formate catalysed by FDH. (B) Hydrogen bonded azide in the FDH active site (PDB 2NAD).[25] FDH = formate dehydrogenase.

Promiscuous wild type halogenase enzymes can utilise azide in place of their native halide anions for synthetic transformations (**Scheme 2.5**). SyrB2 from the syringomycin biosynthetic pathway of *Pseudomonas syringae* B301D is a member of the non-heme iron(II) 2-oxoglutarate (2OG) dependent enzyme superfamily and is capable of transforming an aliphatic carbon-hydrogen bond to an aliphatic carbon-azide bond. The A118G mutant of SyrB2 provided increased reactivity in this transformation, producing a 13% yield of azide product

(*S*)-**2.13**. Additionally, halohydrin dehalogenases A (HheA), B (HheB), and C (HheC) are involved in the degradation of 1,2-halohydrins, and reports have demonstrated the ability of HheA and HheC to enable the regioselective and enantioselective ring opening of racemic chiral epoxides with azide to afford enantioenriched 1,2-azidoalcohols in high yields and enantioselectivities.[27–29] These halohydrin dehalogenases are proposed to control reaction selectivity through hydrogen bonding interactions from the enzyme to both substrate and azide anion.

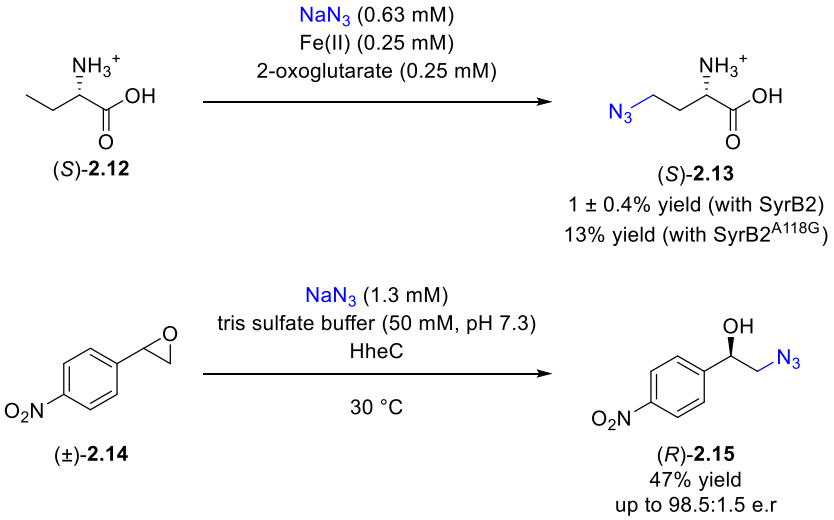


**Scheme 2.5** Selected examples of enzyme catalysed azidation reactions. HheC = Halohydrin dehalogenases C; tris = tris(hydroxymethyl)aminomethane.

### 2.1.3 Structure of hydrogen bonded azide complexes

X-ray crystallography is a powerful technique able to provide direct insight into structure and connectivity of atoms in a single crystal. Several crystal structures involving an anion receptor hydrogen bonded to azide with a polar NH hydrogen bond donor are published.

The mode of coordination can be categorised into eight generic types depending on the number and arrangement of hydrogen bond donors: Type 2.1A and 2.1B with azide coordinated to two hydrogen bond donors, Type 2.1C with azide coordinated to three hydrogen bond donors, Type 2.1D and 2.1E with azide coordinated to four hydrogen bond donors, Type 2.1F with azide coordinated to five hydrogen bond donors, and Type 2.1G and 2.1H with azide coordinated to six hydrogen bond donors (**Figure 2.3**). Investigations into the

structure and connectivity of these crystal structures typically focused on the shape and geometry of the anion receptor.

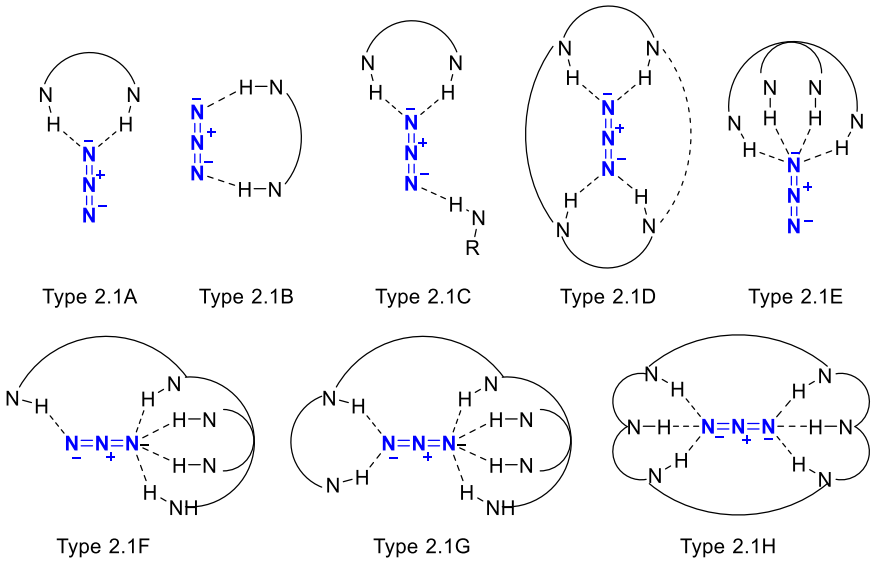


**Figure 2.3** General structure types of published crystal structures with a hydrogen bonded azide anion.

A diverse array of hydrogen bond donors highlighted the versatile nature of azide as a hydrogen bond acceptor (**Figure 2.4-5**). Pyrrole based hydrogen bond donors appear prominently and receptors **2.16**, **2.21**, **2.22**, and **2.23** form two to six hydrogen bonds with azide described by Type 2.1A, Type 2.1D, Type 2.1E, Type 2.1F, and Type 2.1G.[30,31] Protonated macrocyclic cryptands **2.17** and **2.24** encapsulate azide at both termini through two (Type 2.1B) or six (Type 2.1H) hydrogen bond donors.[32,33] **2.18** and **2.20** possessing amide hydrogen bond donors coordinate to azide with three or four hydrogen bond donors described by Type 2.1C and Type 2.1D.[34,35] Similarly, tetraurea **2.19** coordinates to two azide anions in both Type 2.1C and 2.1D structures.[36] This was the only urea-azide crystal structure reported in the literature, and although NMR studies and UV-vis titrations corroborated the binding mode and stoichiometry in solution, no association constants were quantified. A nickel(II) metallamacrocycle (±)-**2.25** featuring multiple metal-azide bonds containing an additional cavity with six hydrogen bond donors was also demonstrated to coordinate azide as described by Type 2.1H.[37,38]

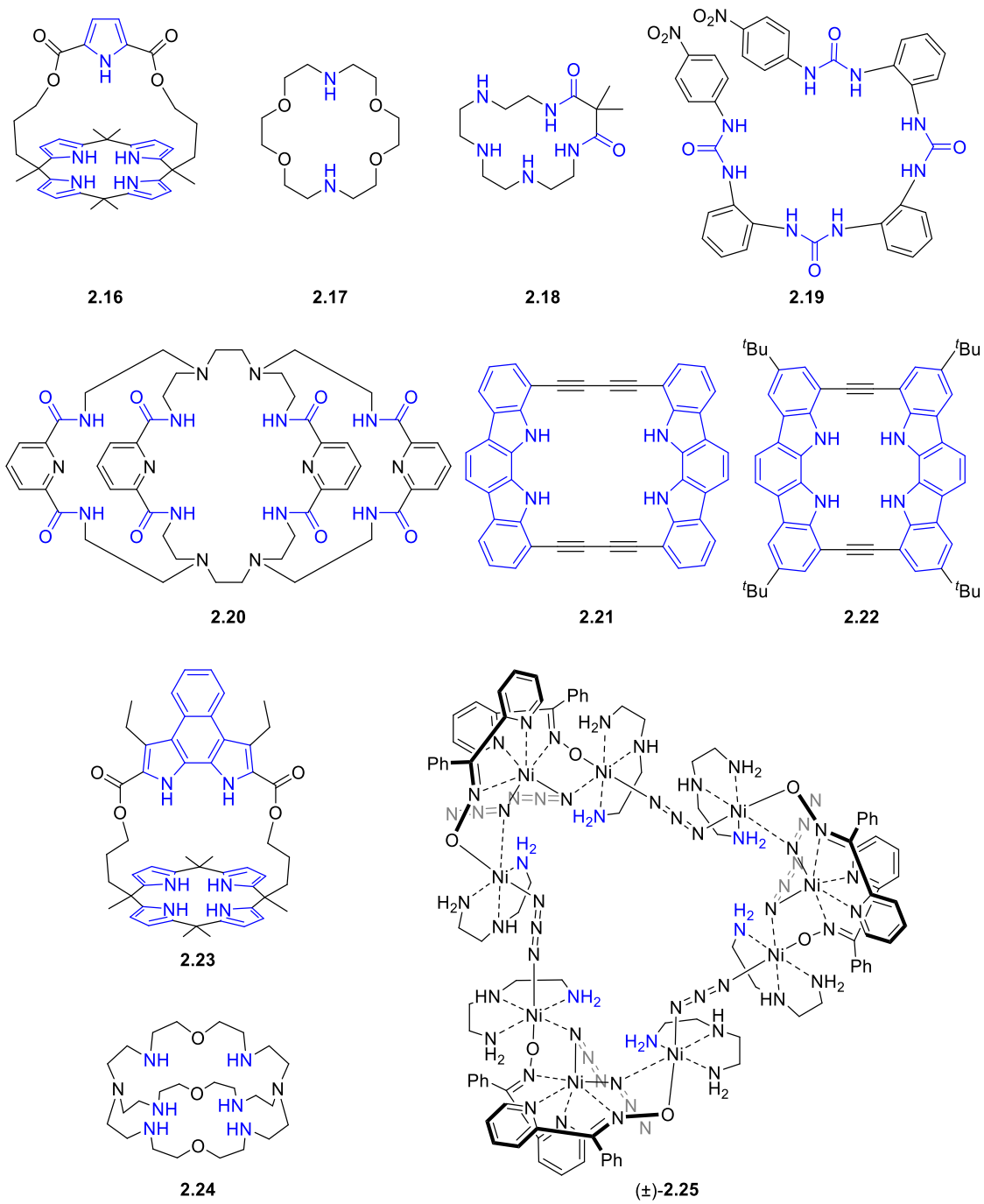


**Figure 2.4** Selected examples of azide anion receptors.

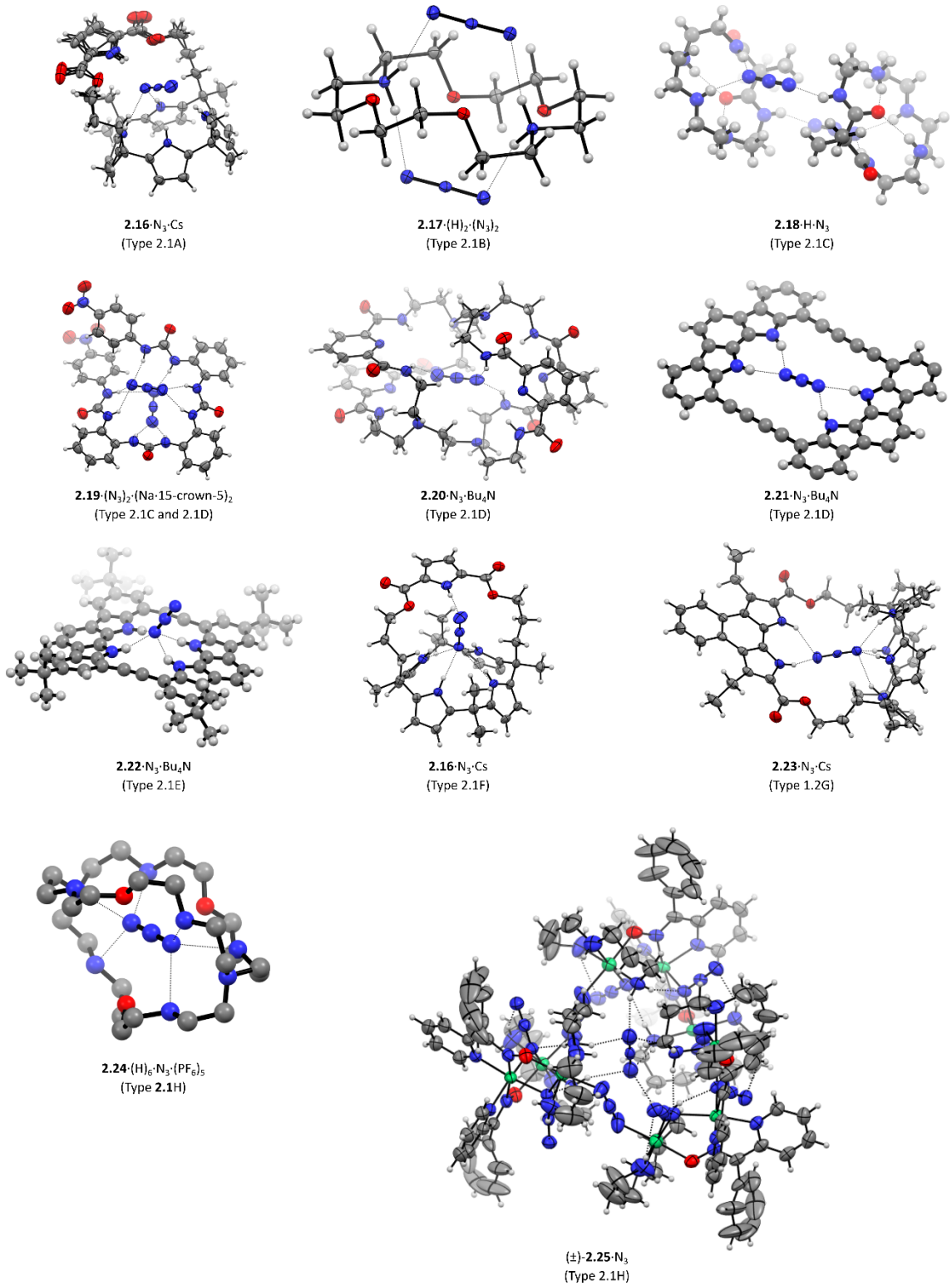


**Figure 2.5** Crystal structures of azide complexed by selected hydrogen bond donors. Caesium, tetrabutylammonium, and hexafluorophosphate ions omitted for clarity, displacement ellipsoids (if available) drawn at 50% probability level (CCDC 1586343, 801422, 1192816, 827002, 647369, 643422, 643421, 1586342 1586344, 1124895, 876039).

### 2.1.4 Enantioselective azidation

Transition metal catalysis for enantioselective azidation has witnessed considerable success but also risks formation of explosive heavy metal-azido complexes.[5,39] The enantioselective ring opening of *meso*-aziridines with azide represents an efficient strategy to access enantioenriched β-aminoazides.[40] Several examples of this transformation have been achieved utilising a range of metal catalysts including chromium(III),[41] yttrium(III),[42,43] and magnesium(II)[44] (**Scheme 2.6**). Whilst the mechanisms for the chromium(III) and yttrium(III) catalysed reactions were proposed to involve both azide and substrate bonding to a metal centre, the magnesium(II) catalyst was proposed to only coordinate to substrate, with attack from an external azide nucleophile.

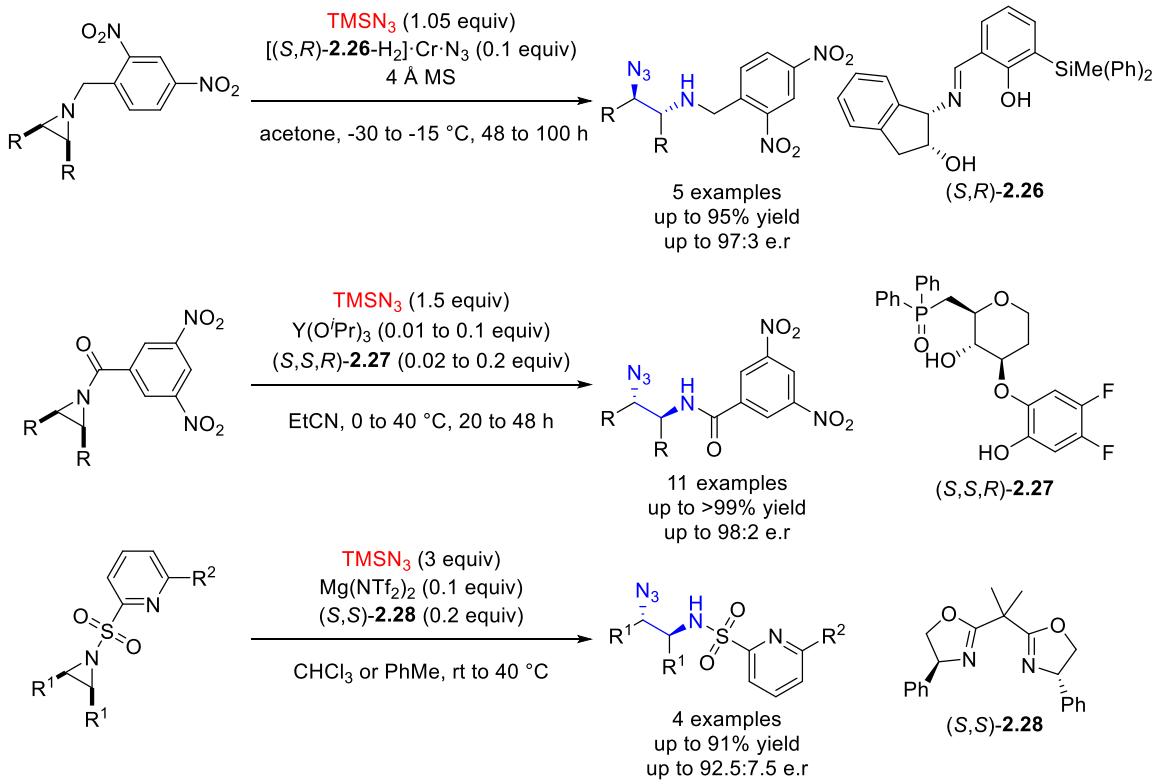


**Scheme 2.6** Selected examples of enantioselective metal catalysed azidation for the synthesis of enantioenriched β-aminoazides.

Examples of organocatalytic enantioselective azidation reactions to generate enantioenriched β-aminoazides motif have been published, although these rely on *in situ* generation of hydrazoic acid from trimethylsilyl azide (**Scheme 2.7**).[45–47] These involve the conjugate

addition or hydrazoic acid to prochiral nitroalkenes, or a chiral Brønsted acid catalysed ring opening of a *meso*-aziridine.

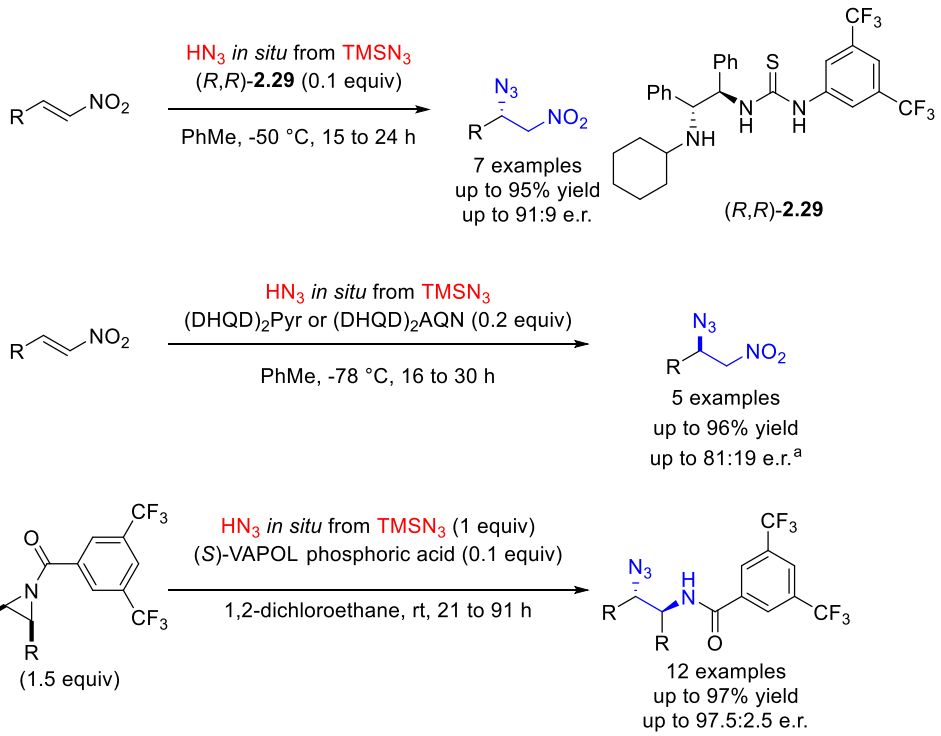


**Scheme 2.7** Organocatalytic enantioselective synthesis of β-aminoazides require *in situ* generation of hydrazoic acid from trimethylsilyl azide. [a]Absolute configuration not determined. $(DHQD)_2Pyr$ = hydroquinidine-2,5-diphenyl-4,6-pyrimidinediyl diether, $(DHQD)_2AQN$ = hydroquinidine (anthraquinone-1,4-diyl) diether, VAPOL = 2,2′-diphenyl-3,3′-(4-biphenanthrol).

Recently, examples of organocatalytic enantioselective azidation with sodium azide have been disclosed (**Scheme 2.8**). These examples are conducted under chiral cationic phase-transfer catalysis in two phase water-organic solvent mixtures, with catalysts consisting of a chiral lipophilic cation and a spectator counter anion. In 2018, the Tan group published an enantioconvergent halogenophilic nucleophilic substitution reaction, where a chiral pentanidium catalyst (*S*,*S*,*S*,*S*)-**2.30** facilitates a prochiral nucleophile to reacts with *in situ* generated bromine azide.[48] In 2019, da Silva Gomes and Corey published a synthesis of chiral α-azido ketones via a planar nitroso-ene intermediate utilising a cinchona alkaloid derived catalyst **2.31**.[49] In 2020, Ishihara and co-workers reported an oxidative α-azidation of carbonyl compounds with cumene hydroperoxide oxidant and a binapthylene derived chiral ammonium salt catalyst (*R*,*R*)-**2.32**. Procedures directly utilising sodium azide for

enantioselective organocatalytic azidation provide both practical and economic advantages to traditional methods that generate *in situ* hydrazoic acid. Hence, enantioselective organocatalytic methods to synthesise the β-aminoazide motif from sodium azide are highly desirable.

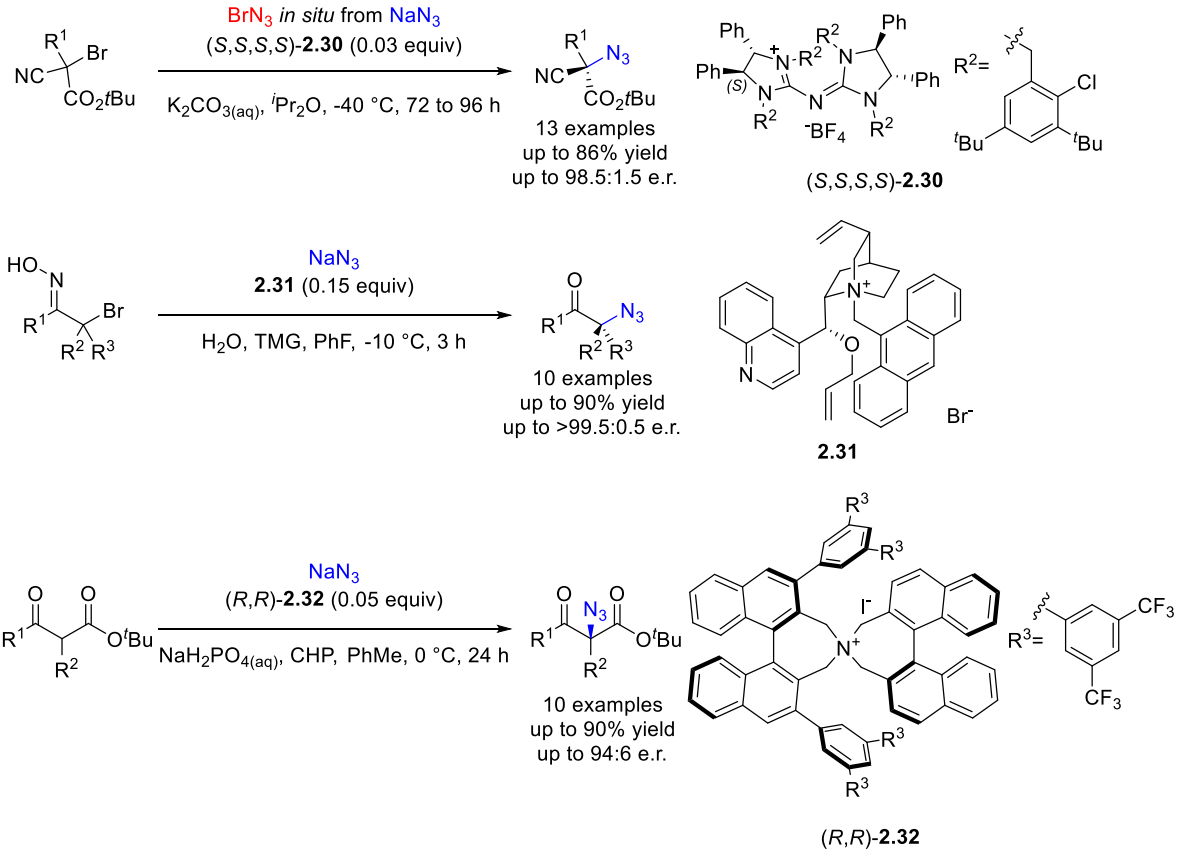


**Scheme 2.8** Organocatalytic enantioselective azidation using sodium azide. TMG = tetramethylguanidine, CHP = cumene hydroperoxide.

Whilst a range of catalyst structures for enantioselective azidation are published, limited examples of urea based organocatalysts are available. The results with these catalysts remain within optimisation tables and demonstrate the ability of urea based organocatalysts to promote azidation in good yields, albeit with negligible enantioselectivities (**Scheme 2.9**).[50,51] None of the final optimised catalysts continued to possess the urea moiety and the interaction with these urea based catalysts and azide remain unknown.

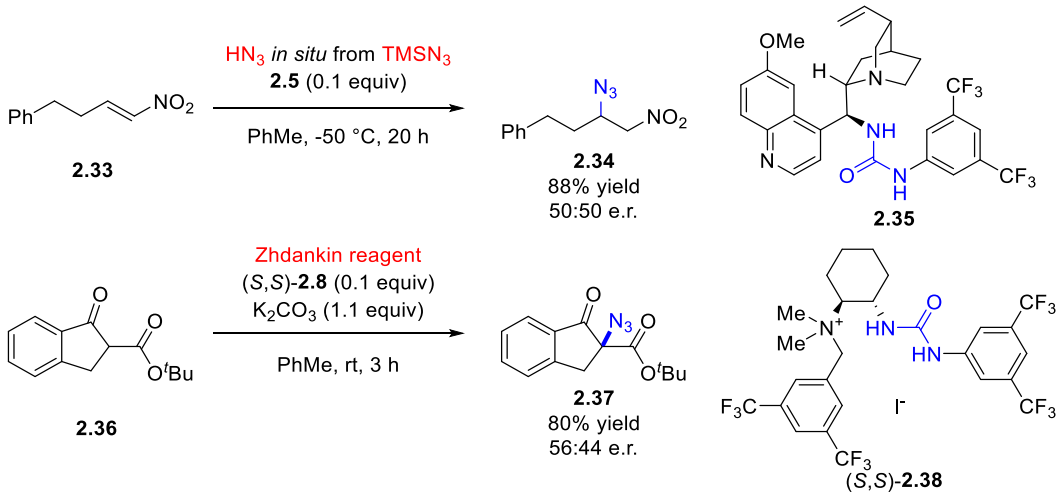


**Scheme 2.9** Organocatalytic azidation with urea based organocatalysts. Zhdankin reagent = 1-azido-1,2-benziodoxol-3(1H)-one.

### 2.1.5 Initial results for HB-PTC with sodium azide

Initial investigations within the Gouverneur group demonstrated that sodium azide was a suitable reagent for HB-PTC with *meso*-episulfonium substrate (±)-**2.39a** (**Table 2.1**).[52] Stirring sodium azide with a *meso*-episulfonium precursor in $CH_2Cl_2$ resulted in no reaction, but addition of urea **2.41a** (0.1 equiv) as catalyst afforded an 80% NMRy of the desired β-thioazide product (±)-**2.40a**. Thiourea **2.42** was a less effective catalyst and produced (±)-**2.40a** in 49% NMRy.

**Table 2.1** Initial investigations into using sodium azide under HB-PTC.

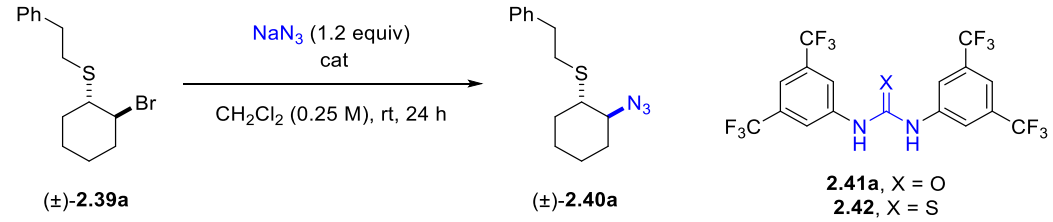


| entry | cat | NMRy |
|---|---|---|
| 1 | **2.41a** (0.1 equiv) | 80% |
| 2 | **2.42** (0.1 equiv) | 49% |
| 3 | none | 0% |

NMRy determined with internal standard.

An enantioselective variant was explored utilising (*S*)-2,2'-diamino-1,1'-binaphthalene ((*S*)-BINAM) derived catalyst (*S*)-**2.41a** (**Table 2.2**). Substrate (±)-**2.39a** produced β-thioazide **2.40a** in 99% NMRy, although no enantioselectivity was observed. In contrast, use of stilbene derived substrate (±)-**2.39b** with (*S*)-**2.41a** produced enantioenriched **2.40b** in 26% NMRy and

66:34 e.r., demonstrating the successful application of HB-PTC to sodium azide for the synthesis of enantioenriched β-thioazides.[52]

**Table 2.2** Key initial results into enantioselective synthesis with sodium azide under HB-PTC.

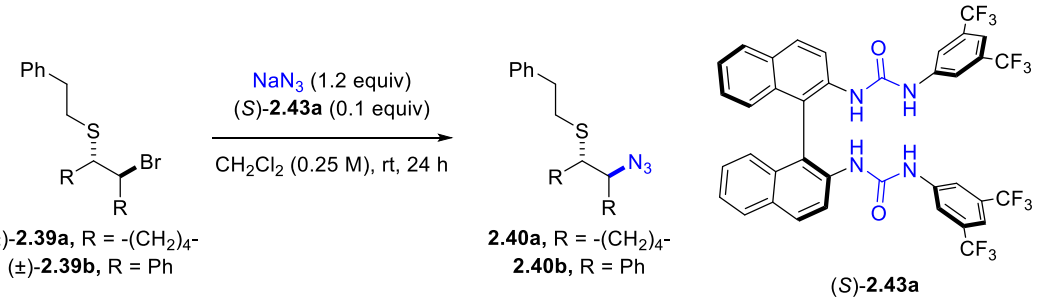


(±)-**2.39a**, R = -$(CH_2)_4$-
(±)-**2.39b**, R = Ph

**2.40a**, R = -$(CH_2)_4$-
**2.40b**, R = Ph

(*S*)-**2.43a**

| entry | substrate | product | NMRy | e.r. |
|---|---|---|---|---|
| 1 | (±)-**2.39a** | **2.40a** | 99% | 50:50 |
| 2 | (±)-**2.39b** | **2.40b** | 26% | 66:34 |

NMRy determined with internal standard. Absolute configuration of **2.40a-b** not determined.

### 2.1.6 Aims

Urea-based catalysts are highly effective for HB-PTC with fluoride[53,54] and urea-azide coordination represents an important interaction in organic chemistry that has received little attention in the context of catalysis. Investigations into the structure, stoichiometry, and association strength of urea-azide complexes in solid state and solution are aimed to provide new insights into this relationship. Study of azide complexed with a series of achiral 1,3-diarylureas would improve the understanding of the influence of steric and electronic effects on the urea-azide interaction (**Scheme 2.10A**). Additional investigations into azide complexed with a chiral *N*-alkyl (*S*)-BINAM derived bis-urea to characterise its structure and association strength in solution and solid-state would provide a robust foundation for further research into an enantioselective azidation with a hydrogen bonded azide anion (**Scheme 2.10B**).

In addition, further optimisation into the reaction of *meso*-episulfonium precursors and sodium azide under HB-PTC may provide a useful method for the enantioselective synthesis of β-thioazides from sodium azide. An additional valuable transformation may involve the reaction of *meso*-aziridinium precursors with sodium azide under HB-PTC, as this would provide access enantioenriched β-aminoazides with applications in medicinal chemistry

(**Scheme 2.10C**). Further study of this system to elucidate its mechanism and role of catalyst would provide new insights into a novel enantioselective azidation reaction under HB-PTC.

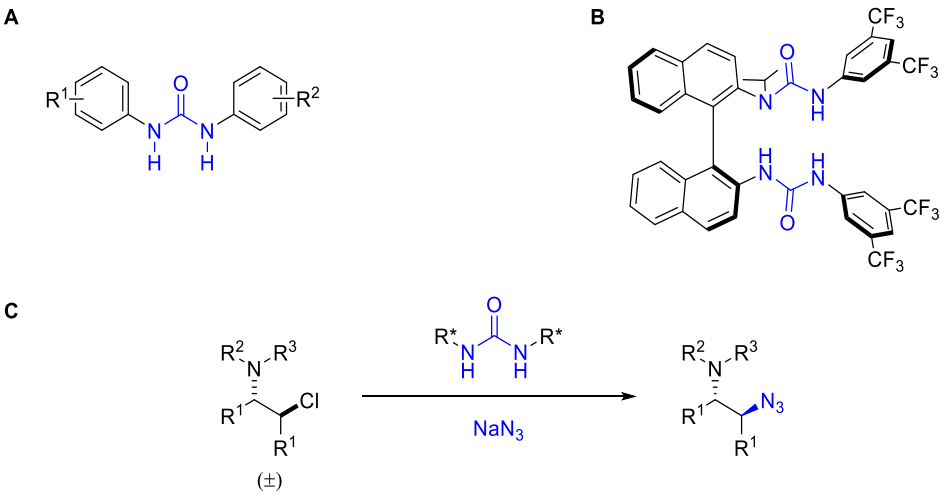


**Scheme 2.10** (A) Achiral urea-azide complexes studied. (B) Chiral *N*-alkyl (*S*)-BINAM derived bis-urea-azide complex studied. (C) Proposed synthesis of β-aminoazides under HB-PTC.

## 2.2 Achiral hydrogen bonded azide complexes

### 2.2.1 Solid state studies

Studies to probe the structure of the urea-azide interaction in the solid state commenced with the synthesis and isolation of twelve complexes of azide associated with eleven dual hydrogen bond donors, including nine 1,3-diarylureas (**Table 2.3**). These complexes were prepared by stirring an equimolar mixture of the desired hydrogen bond donor and hygroscopic tetrabutylammonium azide in acetonitrile (0.1 M) for 24 h. Evaporation of these mixture to dryness afforded non-hygroscopic solids with an amorphous appearance in excellent yields. Use of sodium azide and 15-crown-5 (1,4,7,10,13-pentaoxacyclopentadecane) in place of tetrabutylammonium azide afforded the sodium·15-crown-5 complex.

The resultant products were characterised by $^{1}$H NMR, $^{13}$C NMR, $^{19}$F NMR (when applicable), and IR spectroscopy. A single set of signals shifted from the spectra of the individual components were observed by NMR, consistent with an interaction between these species in solution. IR spectroscopy of the neat solids revealed characteristic absorbances of the azide asymmetric stretch ranging from 2004 cm$^{-1}$ to 2068 cm$^{-1}$, a noticeable shift from the

corresponding signal in tetrabutylammonium azide (1992 $cm^{-1}$) and hydrazoic acid gas (2140 $cm^{-1}$),[55] and suggesting the presence of a hydrogen bonded azide in the solid products. The signal from the sample prepared with **2.41a** (**Figure 2.6A**) exhibited a clear single peak at 2004 $cm^{-1}$, and similar spectra were obtained with **2.41a-h**, **2.42**, and **2.45**. The sample prepared from thiourea **2.42** possessed two signals in the region characteristic of the azide asymmetric stretch at 2058 $cm^{-1}$ and 2027 $cm^{-1}$, which suggests a complex mixture of species in the solid state may be present (**Figure 2.6B**).

Single crystals of these complexes suitable for X-ray diffraction analysis were obtained by crystallisation of the amorphous solid by either layering, slow diffusion, or slow evaporation. All complexes were prepared with equimolar hydrogen bond donor and azide salt, yet a diverse set of crystal structures were obtained (**Table 2.4, Figure 2.7**). The urea-azide bond lengths measured from the urea nitrogen atom to the azide nitrogen atoms ranged from 2.780(9) Å to 3.332(9) Å, longer than those observed in analogous urea-fluoride complexes,[56] which ranged from 2.648(4) Å to 2.807(8) Å when measured by neutron diffraction. The coordination modes and stoichiometries could be categorised into four distinct types: Type 2.2A structures with an azide anion bound side-on to the urea; Type 2.2B structures with an azide anion bound end-on to the urea and stabilised at the opposing terminus by the counter-cation; Type 2.2C structures possessing an azide anion bound end-on to the urea and one terminus, and bridging to an additional urea molecule at the opposing terminus; and Type 2.2D structures with a 2:1 urea-azide complex with the azide anion bound end-on and bridging two separate urea molecules. The angle between the N-N urea vector and the vector defined by the terminal nitrogen atoms of the azide for Type 2.2A complexes, and the angle between the vector defined by the carbonyl of the urea and the vector defined by the terminal nitrogen atoms of the azide for Type 2.2B-C ranged from 1.15(14)° up to 62.40(30)°.

**Table 2.3** Synthesis and azide IR stretch of hydrogen bonded azide complexes.

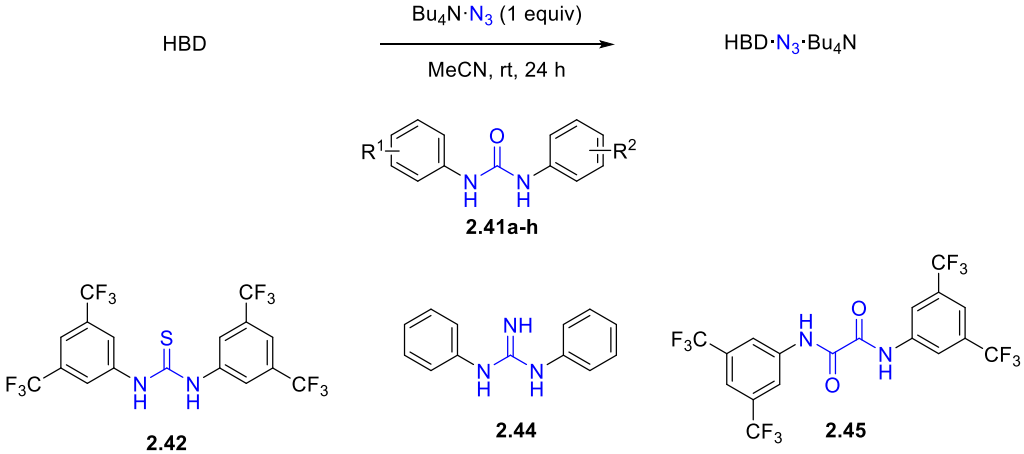


| entry | hydrogen bond donor | yield | $N_3^-$ IR stretch (neat) ($cm^{-1}$) |
|---|---|---|---|
| 1 | **2.41a**, $R^1 = R^2 = 3,5\text{-}CF_3$ | 95% | 2004 |
| 2[a] | **2.41a**, $R^1 = R^2 = 3,5\text{-}CF_3$ | *quant*. | 2068 |
| 3 | **2.41b**, $R^1 = R^2 = 3\text{-}Cl$ | *quant*. | 2015 |
| 4 | **2.41c**, $R^1 = 3,5\text{-}CF_3$; $R^2 = H$ | *quant*. | 2023 |
| 5 | **2.41d**, $R^1 = R^2 = 4\text{-}CF_3$ | 99% | 2006 |
| 6 | **2.41e**, $R^1 = R^2 = H$ | *quant*. | 2022 |
| 7 | **2.41f**, $R^1 = R^2 = 4\text{-}Br$ | *quant*. | 2020 |
| 8 | **2.41g**, $R^1 = R^2 = 4\text{-}F$ | 95% | 2021 |
| 9 | **2.41h**, $R^1 = R^2 = 4\text{-}CN$ | *quant*. | 2014 |
| 10 | **2.42** | 98% | 2058, 2027 |
| 11 | **2.44** | *quant*. | 2011 |
| 12 | **2.45** | *quant*. | 2011 |

[a]using sodium azide (1 equiv) and 15-crown-5 (1 equiv) instead of tetrabutylammonium azide. HBD = hydrogen bond donor.

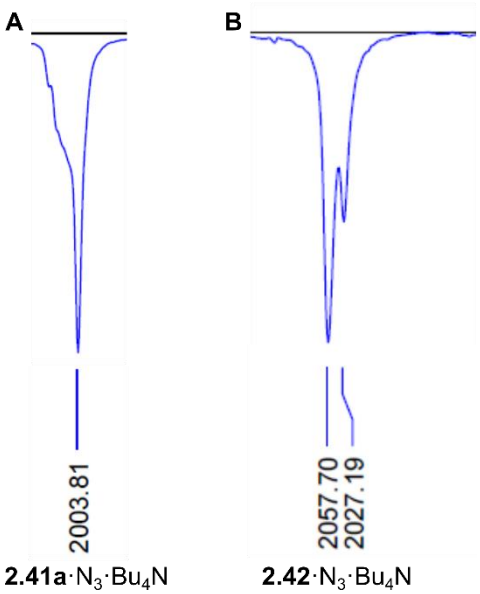


**Figure 2.6** IR spectra of (A) **2.41a**·$N_3$·$Bu_4N$ and (B) **2.42**·$N_3$·$Bu_4N$.

**Table 2.4** Comparison of structure types, bond lengths, and bond angles in azide complexes.[a]

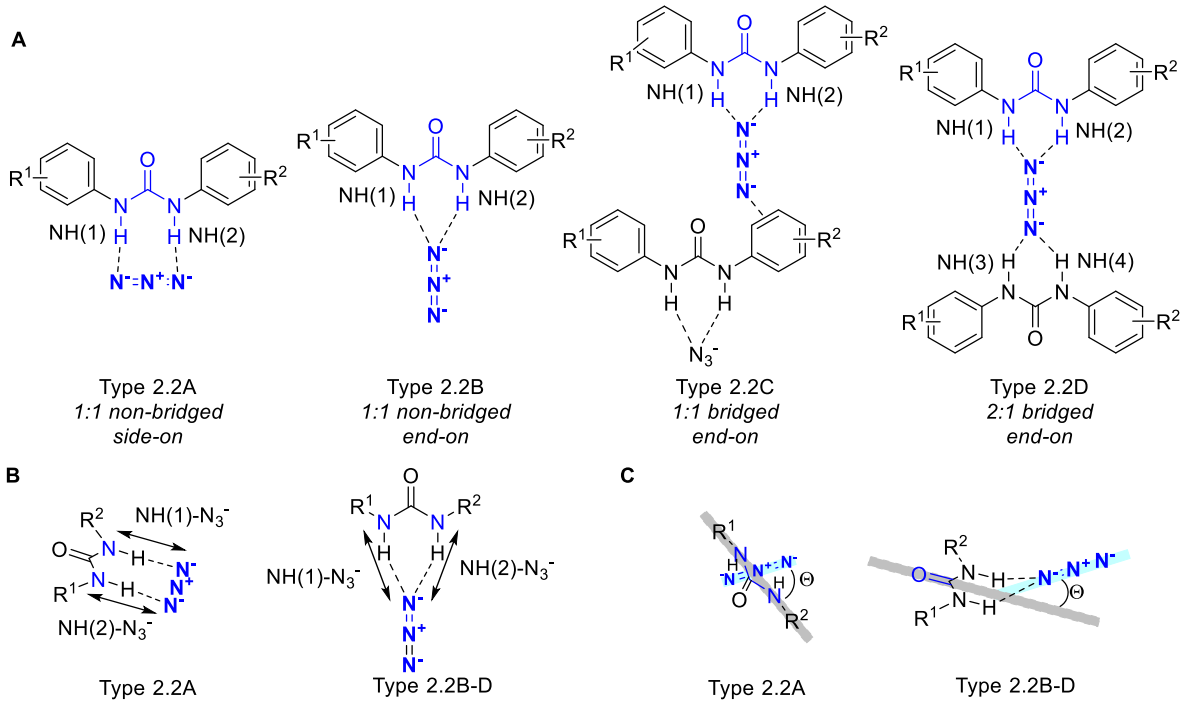


| entry | crystal complex | type | NH(1)-$N_3^-$ length (Å) | NH(2)-$N_3^-$ length (Å) | Θ[b] |
|---|---|---|---|---|---|
| 1[b] | **2.41a**·$N_3$·$Bu_4N$ | 2.2A | 2.966(4)<br>2.962(4) | 2.974(4)<br>3.069(4) | 1.15(14)<br>15.79(7) |
| 2 | **2.41a**·$N_3$·Na·15-crown-5 | 2.2B | 2.780(9) | 3.332(9) | 62.40(30) |
| 3 | **2.41b**·$N_3^-$·$Bu_4N^+$ | 2.2B | 2.876(4) | 3.000(4) | 51.90(14) |
| 4[b] | **2.41c**·$N_3$·$Bu_4N$ | 2.2B | 2.852(9)<br>2.834(9) | 2.946(9)<br>2.940(9) | 27.60(19)<br>34.21(12) |
| 5 | **2.41d**·$N_3$·$Bu_4N$ | 2.2C | 2.838(5) | 2.905(5) | 46.53(8) |
| 6 | **2.41e**·$N_3$·$Bu_4N$ | 2.2C | 2.870(2) | 2.996(2) | 7.43(14) |
| 7 | **2.41f**·$N_3$·$Bu_4N$ | 2.2C | 2.909(8) | 2.923(8) | 24.90(3) |
| 8 | **2.41g**·$N_3$·$Bu_4N$ | 2.2C | 2.833(3) | 2.912(3) | 37.13(6) |
| 9[c] | **2.41h**$_2$·$N_3$·$Bu_4N$·$(H_2O)_2$ | 2.2D | 2.860(2) | 2.976(2) | nd |
| 10 | **2.41a**$_2$·$N_3$·Na·15-crown-5 | 2.2D | nd | nd | nd |
| 11 | **2.44**·$N_3$·$Bu_4N$ | 2.2C | 2.842(2) | 3.202(2) | nd |
| 12 | **2.45**·$N_3$·$Bu_4N$ | 2.2C | 2.923(3) | | nd |

[a](A) Description of complex types. (B) Description of bond lengths measured. (C) Description of bond angles measured. Θ for Type 2.2A complexes is the angle between the N-N urea vector and the vector defined by the terminal nitrogen atoms of the azide. Θ for Type 2.2B-C complexes is defined as the angle between the vector defined by the carbonyl of the urea and the vector defined by the terminal nitrogen atoms of the azide. Angles were calculated using PLATON.[57] [b]Calculated for the two crystallographically distinct motifs. [c]The second molecule of **2.41h** involves one hydrogen bonded NH at 2.144(2) Å. Data collection and analysis by Dr. G. Pupo and Dr. K. E. Christensen.

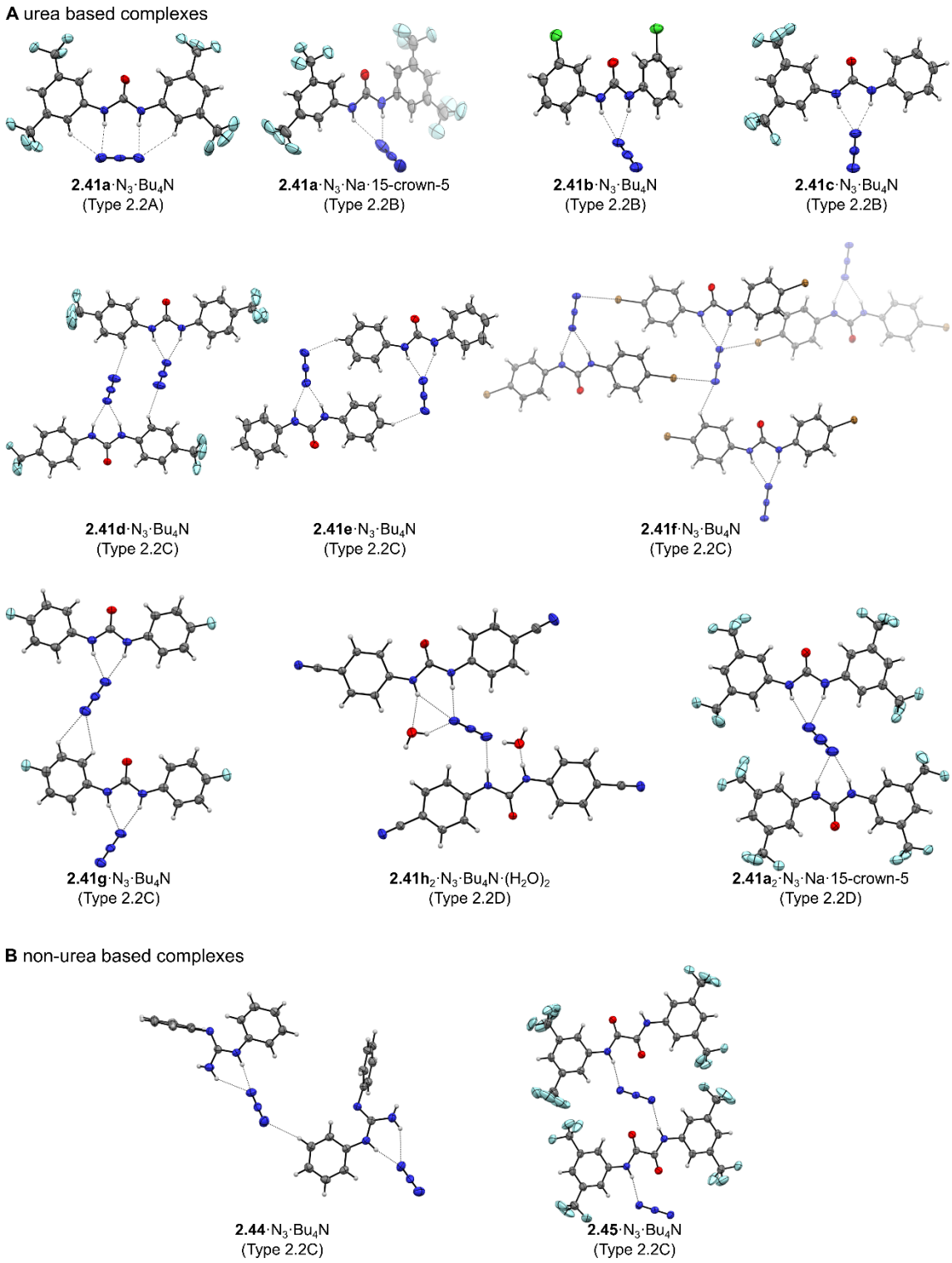


**Figure 2.7** (A) Diversity of hydrogen bonded 1,3-diarylurea-azide complexes. (B) Non-urea based dual hydrogen bonded azide complexes. Tetrabutylammonium and sodium·15-crown-5 cations omitted for clarity, displacement ellipsoids drawn at 50% probability level. Data collection and analysis by Dr. G. Pupo and Dr. K. E. Christensen.

Schreiner's urea **2.41a** was identified as a uniquely effective catalyst for HB-PTC with fluoride, and three distinct crystal structures were obtained from the two amorphous solids of **2.41a** and azide prepared, depending on the counterion and crystallisation conditions (**Figure 2.8**). These possessed Type 2.2A, Type 2.2B, and Type 2.2D structures.

The crystals grown from **2.41a**·$N_3^-$·$Bu_4N^+$ contained urea and azide in a 1:1 stoichiometry. The azide anion was bound at each terminus in a novel side-on fashion across a single urea molecule. This Type 2.2A side-on urea-azide interaction was not observed in any subsequent crystal structures. This may be attributed to the trifluoromethyl groups of **2.41a** increasing the acidity and hydrogen bond donor capability of the remaining *ortho*-aromatic protons.

The 1:1 complex of **2.41a** and sodium·15-crown-5 azide produced two different crystal structures depending on the crystallisation conditions. A structure consisting of **2.41a** and sodium·15-crown-5 in a 1:1 ratio was obtained by layering cyclohexane onto a saturated solution of the solid in tetrahydrofuran. This Type 2.2B structure possessed an azide anion coordinated by a urea hydrogen bond donor with the largest deviation from the urea plane at 62.40(30)°, as well as both the shortest and longest urea-azide bond lengths at 2.780(9) Å and 3.332(9) Å respectively. An additional Type 2.2D structure was obtained upon crystallisation from toluene and acetonitrile consisting of **2.41a** and sodium·15-crown-5 in a 2:1 ratio. This 2:1 complex contained an azide anion hydrogen bonded at both termini by individual units of **2.41a**, with the sodium·15-crown-5 cation effectively separate from the urea-azide interaction.

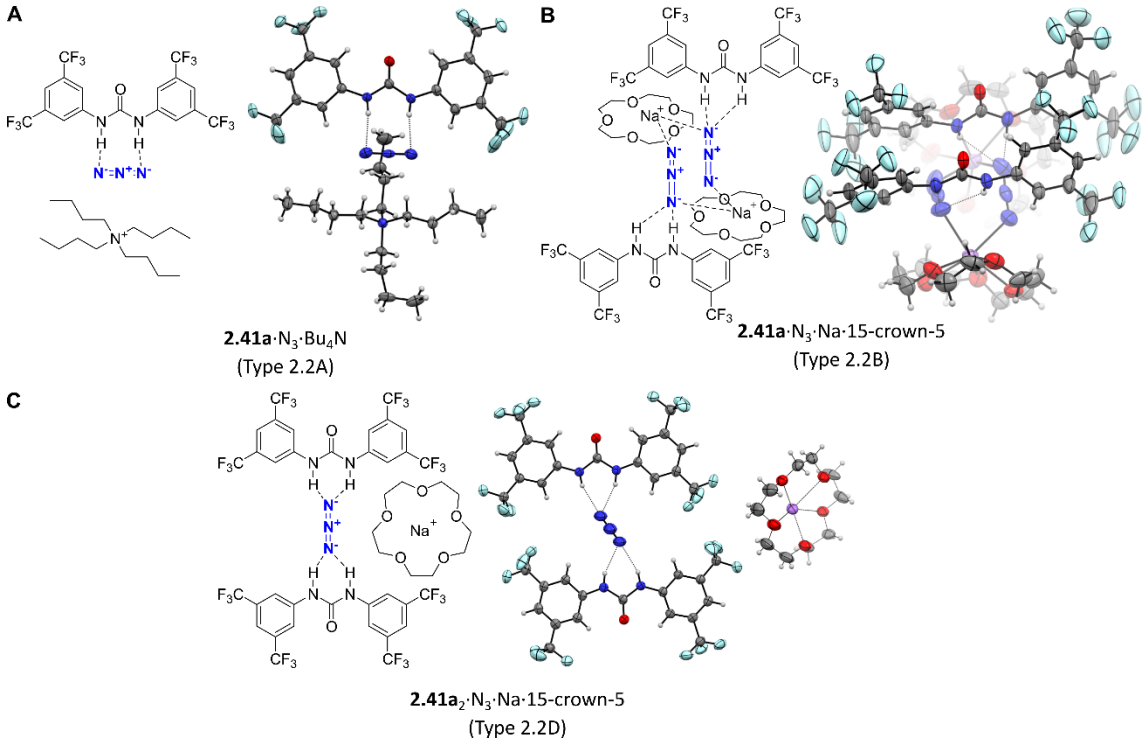


**Figure 2.8** (A) Crystal structure of **2.41a** complexed to tetrabutylammonium azide. (B) Crystal structure of a 1:1 complex of **2.41a** and sodium·15-crown-5. (C) Crystal structure of a 2:1 complex of **2.41a** and sodium·15-crown-5. Displacement ellipsoid plots drawn at 50% probability level. Data collection and analysis by Dr. G. Pupo and Dr. K. E. Christensen.

Previous studies have demonstrated halogen bonded azide anions,[58,59] with bond lengths from 2.806(3) Å to 3.216(4) Å reported between an azide and carbon tetrabromide.[59] The complex obtained from urea **2.41f** containing two aryl bromide substituents was a Type 2.2C structure that displayed both hydrogen bonding and halogen bonding. Two halogen bonds from two additional units of urea interact with the azide anion at each terminus, resulting in an interlocking of the urea-azide ribbon (**Figure 2.9**). These halogen bonds have distances of 3.140(2) Å and 3.131(2) Å, and are within the higher end of the range of reported azide halogen bond lengths.

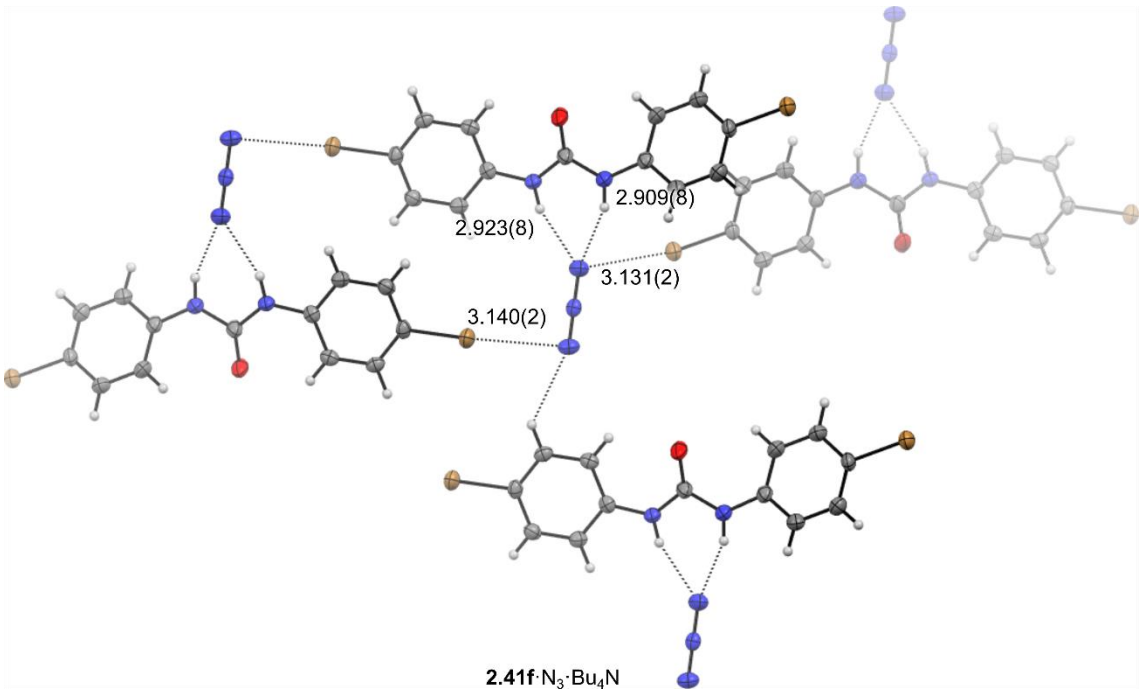


**Figure 2.9** Crystal structure of **2.41f** complexed to tetrabutylammonium azide. Distances in Å, tetrabutylammonium cations omitted for clarity, displacement ellipsoids drawn at 50% probability level. Data collection and analysis by Dr. G. Pupo and Dr. K. E. Christensen.

In addition to the urea motif, complexes of azide with diphenylguanidine **2.44**, a dioxalylamide **2.45**, and Schreiner's thiourea **2.42** were also synthesised, with crystal structures of **2.44** and **2.45** complexed with azide successfully obtained. The structure of guanidine **2.44** complexed to azide consisted of the 1,3-diarylguanidine present as its amine form, resulting in distinct orientation from the structures of 1,3-diarylureas complexed to azide (**Figure 2.10A**). The hydrogen bond donors of oxalylamide of **2.45** arrange *anti* to each other, forming a repeating pattern of azide coordinated by only one hydrogen bond donor from alternative molecules of **2.45** (**Figure 2.10B**). Attempts to crystalise thiourea **2.42** complexed to azide resulted in the *in situ* deprotonation of **2.42**, likely due to its increased acidity[60] and is consistent with the poor performance of **2.42** as a catalyst for HB-PTC (**Figure 2.10C**).[53,60] Both complexes containing an azide were similar to Type 2.2C urea-azide structures, where the azide bridges two molecules of hydrogen bond donor in a 1:1 stoichiometry. These crystal structures highlight the variety of dual hydrogen bond donors able to interact with azide.

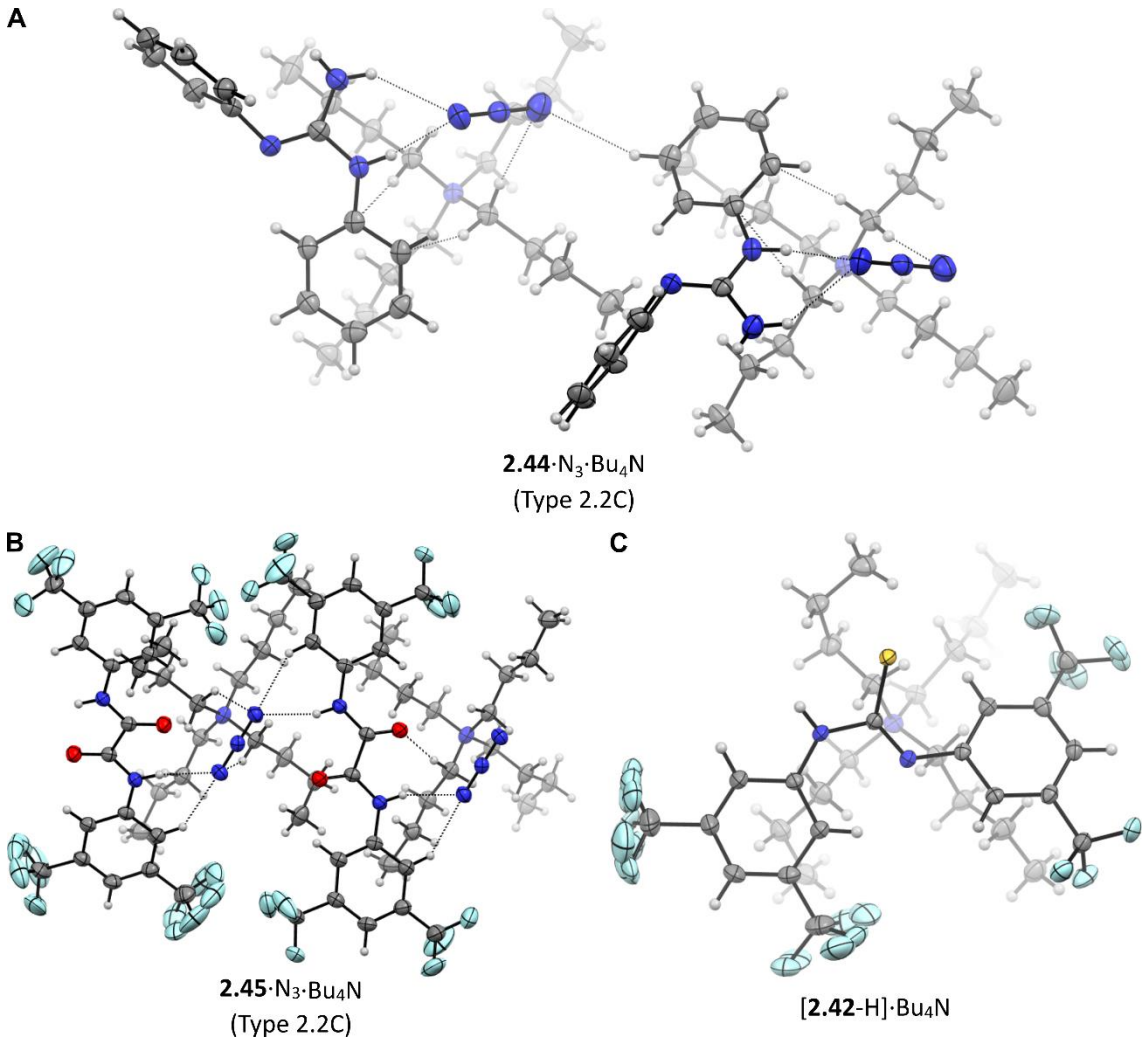


**Figure 2.10** (A) Crystal structure of **2.44** complexed to tetrabutylammonium azide. (B) Crystal structure of **2.45** complexed to tetrabutylammonium azide. (C) Crystal structure of [**2.42**-H]·$Bu_4N$ obtained upon crystallisation of **2.42**·$N_3$·$Bu_4N$. Displacement ellipsoid plots drawn at 50% probability level. Data collection and analysis by Dr. G. Pupo and Dr. K. E. Christensen.

### 2.2.2 Solution studies

NMR titrations were conducted to probe the binding strength and stoichiometry of selected hydrogen bond donors studied by X-ray crystallography with azide in solution. Acetonitrile was used for solvent since it solubilised several hydrogen bond donors of interest, is itself a poor hydrogen bond acceptor and donor,[61] and is widely available as the deuterated isotopologue. Azide was added as the tetrabutylammonium salt due to the cation's non-coordinating nature and desirable solubility profile.[62]

The principles of host-guest chemistry can be applied to these hydrogen bond donor-azide systems in solution, with the hydrogen bond donor as 'host' and azide as 'guest'. Upon

addition of tetrabutylammonium azide, the chemical shifts and line widths of resonances corresponding to host changed, but the number of peaks remained constant. These observations are consistent with a dynamic system in solution where components consisting of both coordinated and uncoordinated species exist in equilibrium. Two models for this behaviour may be envisaged,[56] a 1:1 equilibrium, or 'full'[63] 2:1 system where the 1:1 complex is coordinated by an additional molecule of host (**Scheme 2.11**).

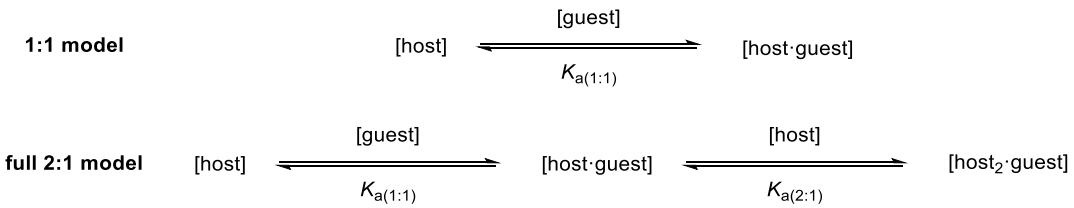


**Scheme 2.11** Equilibria for 1:1 and full 2:1 binding models.

Tracking the change in chemical shift of signals corresponding to the host across sequential addition of titrant allowed for determination of association constants and binding model. Use of BindFit software enabled a global analysis approach to data fitting, with fits determined by nonlinear regression.[64,65]

The appropriate binding model was determined by attempting to fit the data to both 1:1 and full 2:1 models then comparing the quality of the two fits.[63] As the full 2:1 model included additional parameters, it was important to ensure any improvement to the fit was not due to the increased number of parameters. In statistics, covariance provides a measure for the strength of the correlation between two variables. The covariance of fit ($cov_{fit}$) provides a quantitative measure of the quality of fit independent of the number of parameters and is calculated by dividing the covariance of the residual with the covariance of the experimental data. A lower $cov_{fit}$ indicates an improved fit to the selected model. The $cov_{fit}$ factor, determined by dividing the $cov_{fit}$ for the 1:1 model by the $cov_{fit}$ for the binding model under study, can be used to evaluate the scale of improvement, with a value $\gg 3$ typically sufficient to consider the more complex 2:1 model as appropriate.[63]

A representative example of a full 2:1 model is illustrated by Schreiner's urea **2.41a** and tetrabutylammonium azide (**Table 2.5**). The $cov_{fit}$ for the 1:1 model was $2.04 \times 10^{-3}$ whereas the $cov_{fit}$ for the 2:1 model was $0.095 \times 10^{-3}$. This results in a $cov_{fit}$ factor of 23.3, hence the improved fit is likely indicative of the presence of an additional 2:1 equilibrium, with both 1:1 and 2:1 complexes formed in solution.

A representative example of a 1:1 binding model can be found with 1,3-diphenylurea **2.41e** and tetrabutylammonium azide (**Table 2.5**). The $cov_{fit}$ for the 1:1 model was $3.41 \times 10^{-3}$ whereas the $cov_{fit}$ for the 2:1 model was $1.68 \times 10^{-3}$. This results in a $cov_{fit}$ factor of 2.0, hence the improved fit was likely predominantly due to the increased number of parameters, and not indicative of the presence of an additional 2:1 equilibrium, with **2.41e** forming only a 1:1 complex with azide in solution.

**Table 2.5** Titration data and association constants of **2.8a** and **2.8e** with tetrabutylammonium azide.

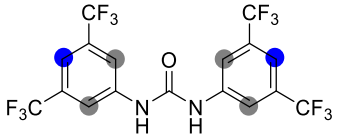


**2.41a**

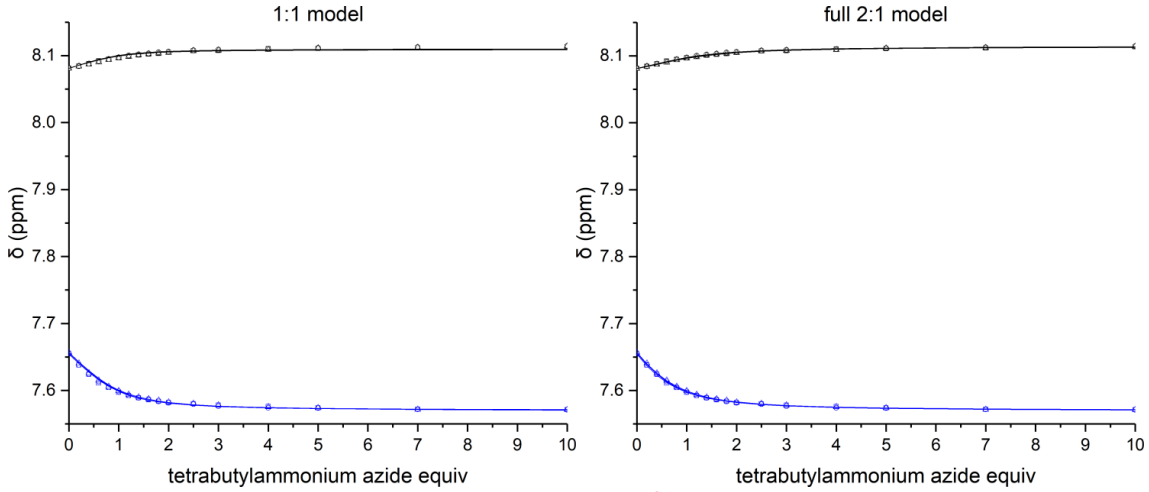


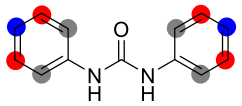


**2.41e**

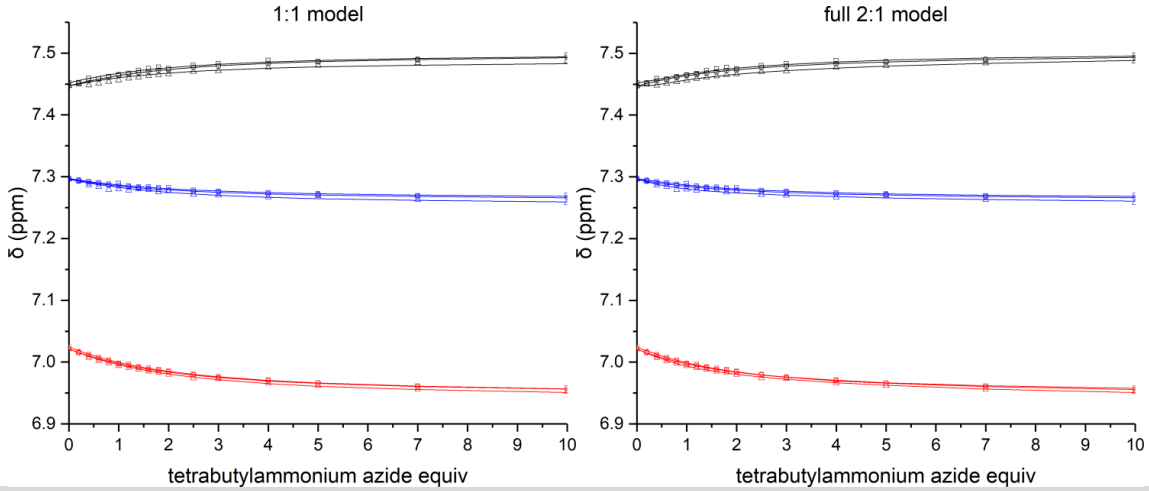


| entry | host | model | $cov_{fit}$ ($10^{-3}$) | $cov_{fit}$ factor | $K_{a(1:1)}$ ($M^{-1}$) | $K_{a(2:1)}$ ($M^{-1}$) |
|---|---|---|---|---|---|---|
| 1 | **2.41a** | 1:1 | 2.04 | 1 | $2.66 \pm 0.18 \times 10^3$ | - |
| **2** | | **full 2:1** | **0.095** | **23.3** | $\mathbf{1.57 \pm 0.06 \times 10^3}$ | $\mathbf{7 \pm 3 \times 10^1}$ |
| **3** | **2.41e** | **1:1** | **3.41** | **1** | $\mathbf{3.14 \pm 0.03 \times 10^2}$ | - |
| 4 | | full 2:1 | 1.68 | 2.0 | $6 \pm 2 \times 10^2$ | $7 \pm 7 \times 10^2$ |

One set of symbols (□, ○, △) refers to experimental data from one set of measurements (2 mM, $CH_3CN/CD_3CN$ 8:2, 500 MHz, 298 K). Lines are the calculated isotherms of the described model. $cov_{fit}$ factor is $cov_{fit}$ for the 1:1 model divided by the $cov_{fit}$ for the binding model under study.[63] Values are the mean of 3 independent replicas calculated with BindFit v0.5,[64] error is the standard deviation.

Six hydrogen bond donors studied by X-ray crystallography possessed a suitable solubility profile in acetonitrile for titration (**Table 2.6**). Four of the hydrogen bond donors studied formed 1:1 hydrogen bond donor-azide complexes in solution, and two are proposed to form both 1:1 and 2:1 complexes. More acidic hydrogen bond donors typically possessed higher association constants with azide in solution. The systems best described by the full 2:1 binding model had a lower $K_{a(2:1)}$ than $K_{a(1:1)}$, suggesting solutions of excess azide would favour formation of the 1:1 complex, with predominant formation of the 2:1 complexes occurring in solutions containing excess urea.

**Table 2.6** Proposed models and association constants of selected hydrogen bond donors with azide.

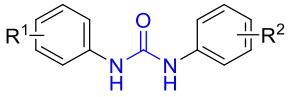

**2.41a**, $R^1 = R^2 =$ 3,5-$CF_3$ **2.41e**, $R^1 = R^2 =$ H
**2.41c**, $R^1 =$ 3,5-$CF_3$; $R^2 =$ H **2.41g**, $R^1 = R^2 =$ 4-F
**2.41d**, $R^1 = R^2 =$ 4-$CF_3$

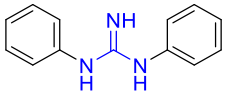

**2.44**

| entry | model | host | p$K_a$ in DMSO[60] | $K_{a(1:1)}$ ($M^{-1}$) | $K_{a(2:1)}$ ($M^{-1}$) |
|---|---|---|---|---|---|
| 1 | full 2:1 | **2.41a** | 13.8 ± 0.2 | $1.57 \pm 0.06 \times 10^3$ | $7 \pm 3 \times 10^1$ |
| 2 | 1:1 | **2.41c** | 16.1 ± 0.1 | $9.4 \pm 1.7 \times 10^2$ | - |
| 3 | full 2:1 | **2.41d** | - | $1.25 \pm 0.12 \times 10^3$ | $1.3 \pm 0.5 \times 10^2$ |
| 4 | 1:1 | **2.41e** | 18.7 ± 0.1 | $3.14 \pm 0.03 \times 10^2$ | - |
| 5 | 1:1 | **2.41g** | - | $4.82 \pm 0.05 \times 10^2$ | - |
| 6 | 1:1 | **2.44** | - | $1.4 \pm 0.3 \times 10^2$ | - |

Titrations conducted at 2 mM, $CH_3CN/CD_3CN$ 8:2, 500 MHz, 298 K. Values are the mean of 3 independent replicas calculated with BindFit v0.5,[64] error is the standard deviation.

The solution studies confirmed the ability for azide to be coordinated by a range of hydrogen bond donors, including Schreiner's urea **2.41a** in solution. This data highlights the impact of the urea electronics and p$K_a$ on hydrogen bond strength and the dynamic nature of these systems in solution. As with X-ray crystallography, both 1:1 and 2:1 species were observed. In combination with the solid-state studies, these results provide strong evidence for the ability of azide to be coordinated by 1,3-diarylurea hydrogen bond donors both in solution and solid state.

## 2.3 Chiral urea bound azide

### 2.3.1 Establishing association in solution

With an improved understanding of the properties of azide with achiral hydrogen bond donors, attention was turned towards a chiral system. (*S*)-**2.43b** was extensively studied with fluoride,[53,66] and is representative of the *N*-alkyl BINAM derived bis-urea class of catalysts successful with HB-PTC. Initial NMR studies aimed to establish firm evidence of association between azide and (*S*)-**2.43b** in solution. $CDCl_3$ was preferred for solvent as it is unreactive towards nucleophiles,[67,68] has a wide operational temperature range, and is in a class of polar non-coordinating solvents typically used in HB-PTC.[53,54,66,69]

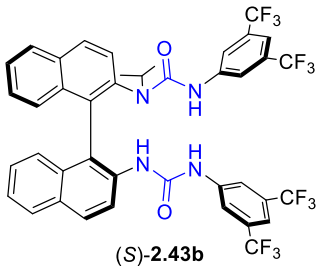

(*S*)-**2.43b**

**Figure 2.11** Structure of *N*-alkyl BINAM derived bis-urea (*S*)-**2.43b** selected for study.

A full assignment of the $^1H$ NMR signals of (*S*)-**2.43b** in $CDCl_3$ was achieved by collection of additional $^1H$-$^1H$ COSY, $^1H$-$^1H$ NOESY, and $^1H$-$^{15}N$ HMBC NMR spectra, and suggested the presence of a secondary structure as previously described in $CD_2Cl_2$ (**Figure 2.12**).[66]

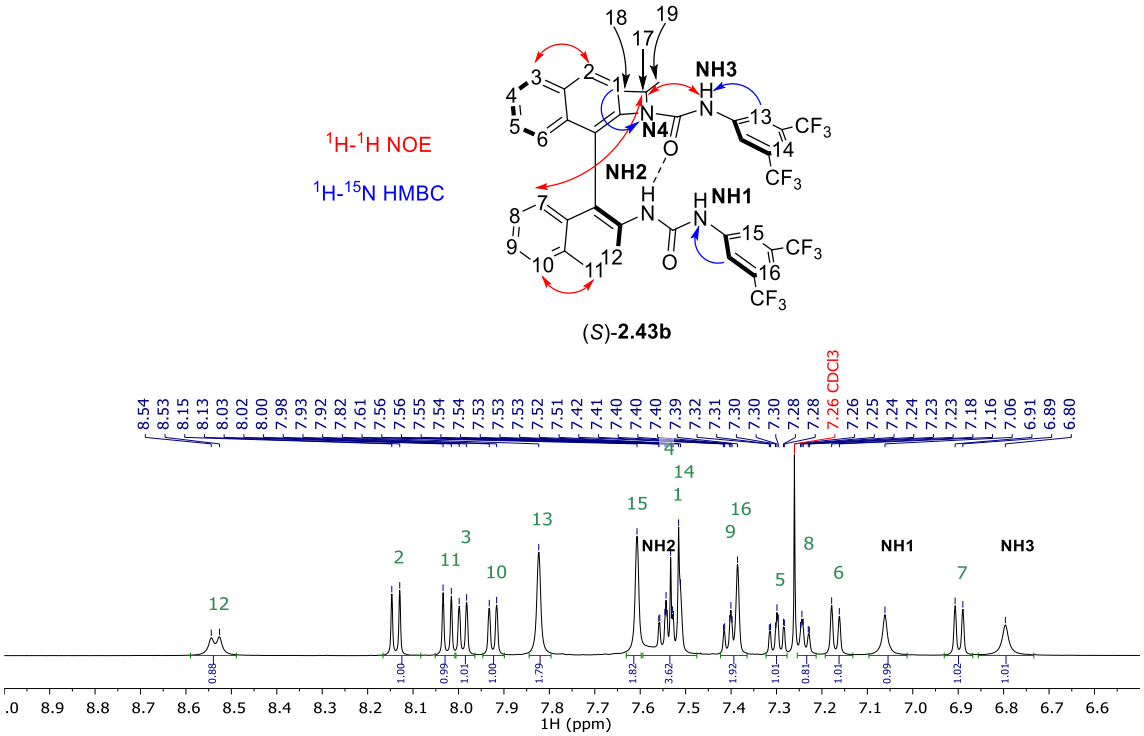


**Figure 2.12** Proposed assignment and secondary structure of (*S*)-**2.43b** in $CDCl_3$ and $^1$H NMR spectrum highlighting NH signals and key correlations. (25 mM (*S*)-**2.43b**, $CDCl_3$, 500 MHz, 298 K).

The $^1$H-$^{15}$N HSQC spectra displayed two correlations with NH signals corresponding to the NHs distal to the (*S*)-BINAM backbone, with the third NH signal represented within the multiplet from 7.56 – 7.51 ppm too broad to exhibit any correlations. The $^1$H-$^{15}$N HMBC spectra displayed correlations from the tertiary nitrogen with a $^{15}$N NMR shift of 120 ppm to both the $^i$Pr group and a doublet at 7.52 ppm, leading to the assignment of this doublet to H1 (**Figure 2.13**).

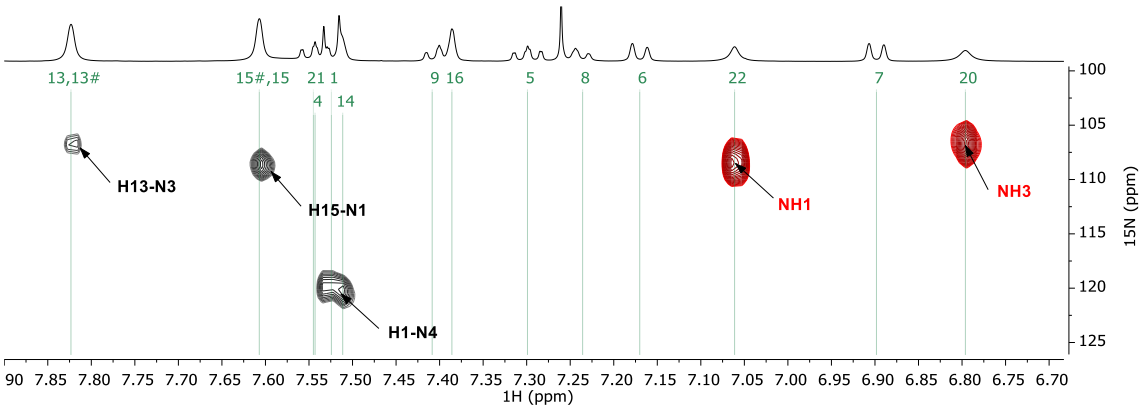


**Figure 2.13** Superimposed $^{1}$H-$^{15}$N HSQC (red) and $^{1}$H-$^{15}$N HMBC (black) NMR spectra of (*S*)-**2.43b** in $CDCl_3$ (25 mM (*S*)-**2.43b**, $CDCl_3$, 500 MHz, 298 K).

NOE interactions from H17 with the singlet at 6.80 ppm resulted in its designation as NH3, leaving the singlet at 7.06 ppm to be assigned as NH1, and the remaining broad NH as NH2 (**Figure 2.14**). These were in line with the assignment of (*S*)-**2.43b** in $CD_2Cl_2$.[53,66]

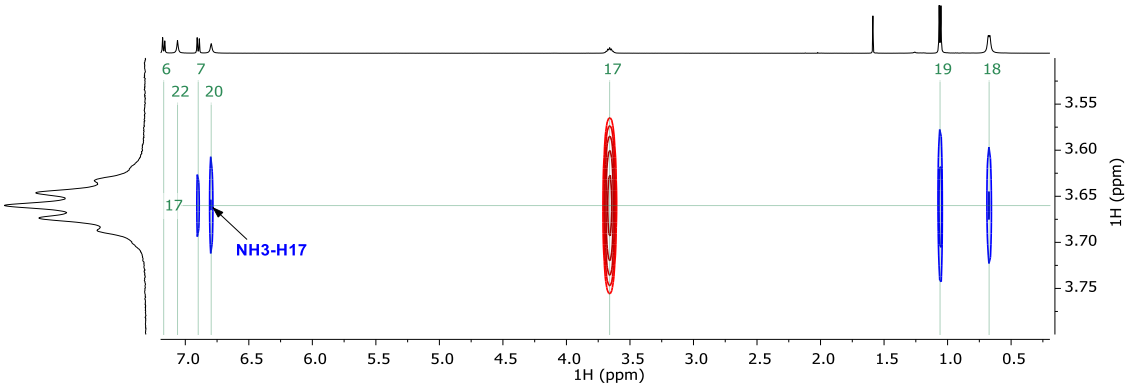


**Figure 2.14** Expanded $^{1}$H-$^{1}$H NOESY NMR spectrum of (*S*)-**2.43b** in $CDCl_3$ (25 mM (*S*)-**2.43b**, $CDCl_3$, 500 MHz, 298 K).

The remainder of the (*S*)-BINAM backbone was assigned by following crosspeaks through the $^{1}$H-$^{1}$H COSY NMR spectra. NOE relationships were necessary to link H2 to H3 and H10 to H11 (**Figure 2.15**).

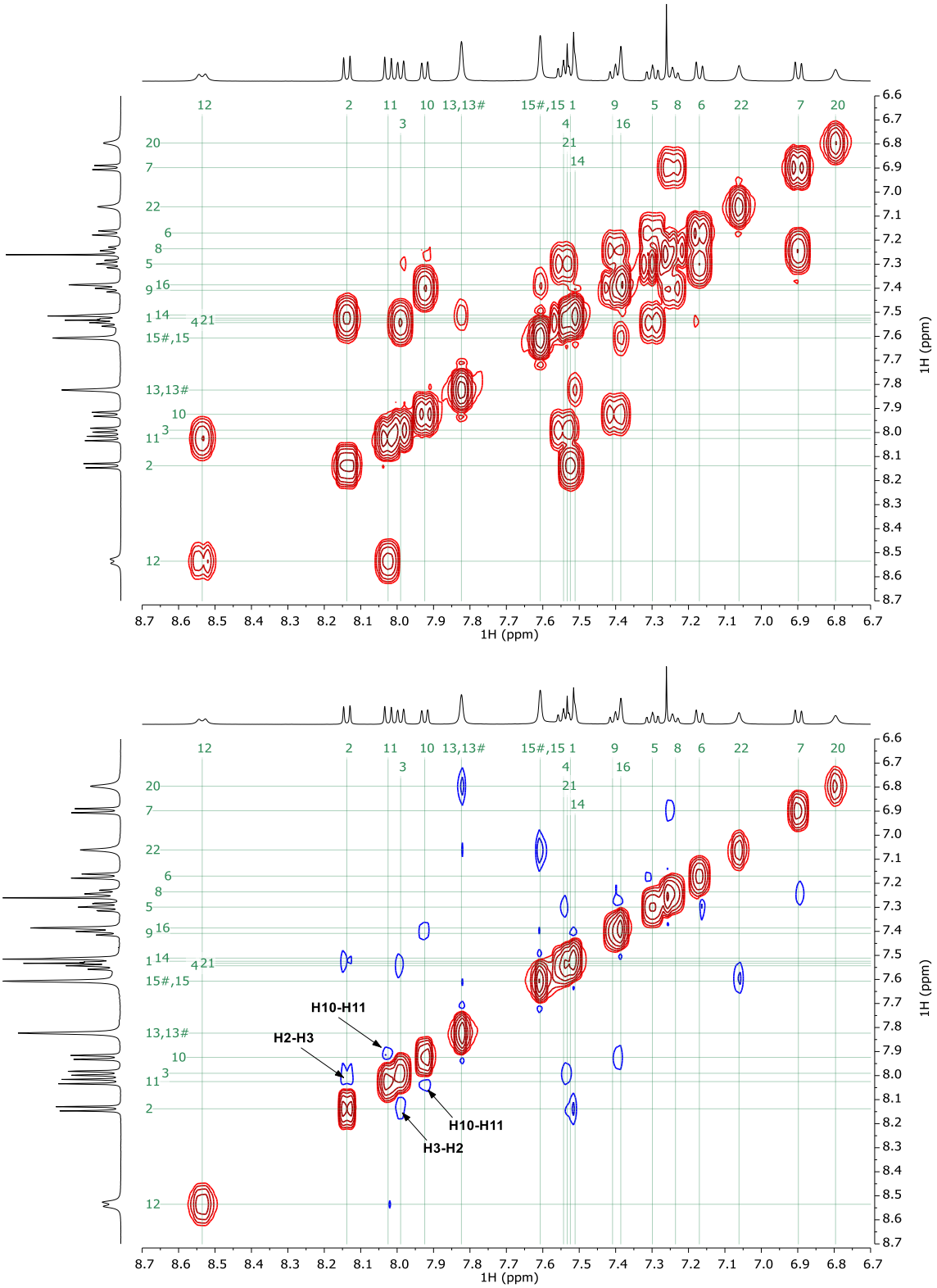


**Figure 2.15** $^{1}$H-$^{1}$H COSY (red) and $^{1}$H-$^{1}$H NOESY (blue and red) NMR spectra of (*S*)-**2.43b** in $CDCl_3$ (25 mM (*S*)-**2.43b**, $CDCl_3$, 500 MHz, 298 K).

Investigations into the association of azide with (*S*)-**2.43b** in solution commenced with $^{1}$H NMR titrations. As with the achiral systems, addition of tetrabutylammonium azide to a solution of (*S*)-**2.43b** in $CDCl_3$ resulted in a movement of its $^{1}$H chemical shifts, indicative of an interaction

in solution. The shift of three protons at 8.41 ppm, 7.82 ppm, and 7.61 ppm were tracked at each addition from the beginning of the titration and were used to determine the association constants and binding model (**Figure 2.16**).

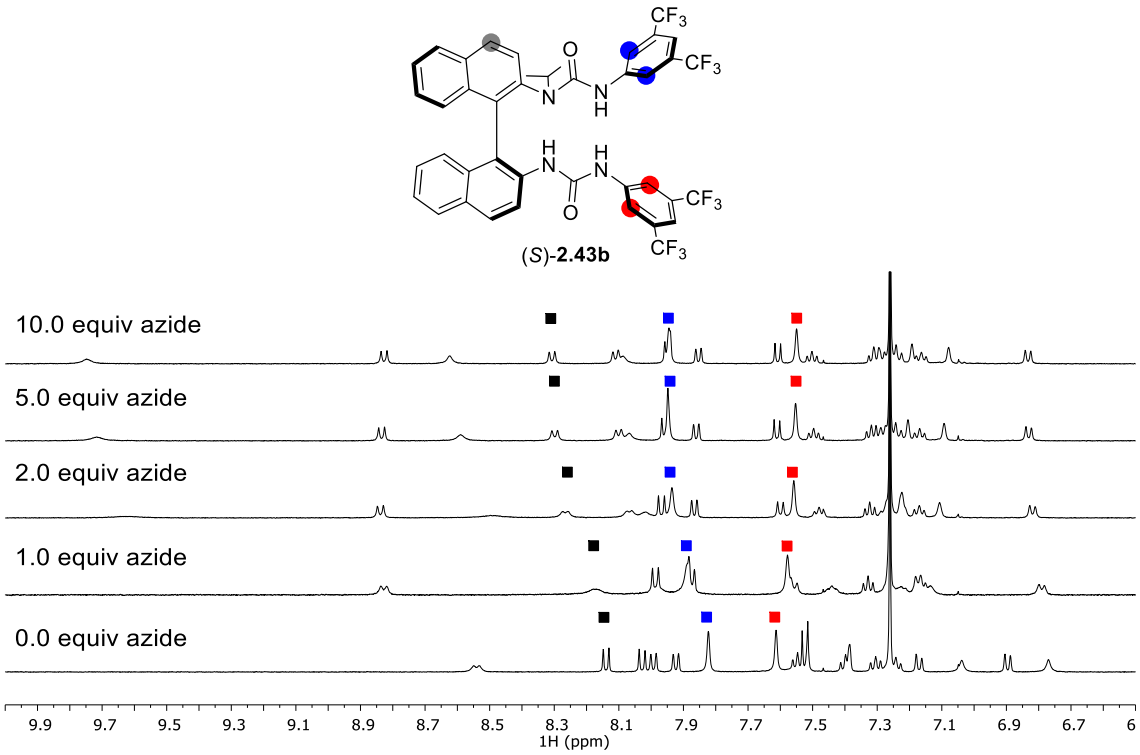


**Figure 2.16** Representative $^{1}$H NMR spectra from the titration of (*S*)-**2.43b** with tetrabutylammonium azide with aromatic proton shifts monitored highlighted in black, blue and red. (2 mM (*S*)-**2.43b**, $CDCl_3$, 500 MHz, 298 K).

Visual analysis and comparison of $cov_{fit}$ factors showed a clear improvement when the association was modelled as the full 2:1 model (**Table 2.7**). As with the achiral hydrogen bond donors studied, the $K_{a(1:1)}$ at 9.1 ± 0.9 × $10^3$ was higher than the $K_{a(2:1)}$ at 1.0 ± 0.6 × $10^2$, suggesting the major species in solutions containing excess azide is the 1:1 complex, but formation of the 2:1 species is favoured in solutions containing excess (*S*)-**2.43b**. The second association of a urea with the 1:1 urea-azide complex is likely to involve the additional urea coordinating to the azide anion, as observed in the Type 2.2D 2:1 hydrogen bond donor-azide structures.

**Table 2.7** Titration modelling, and association constants of (*S*)-**2.43b** and azide.

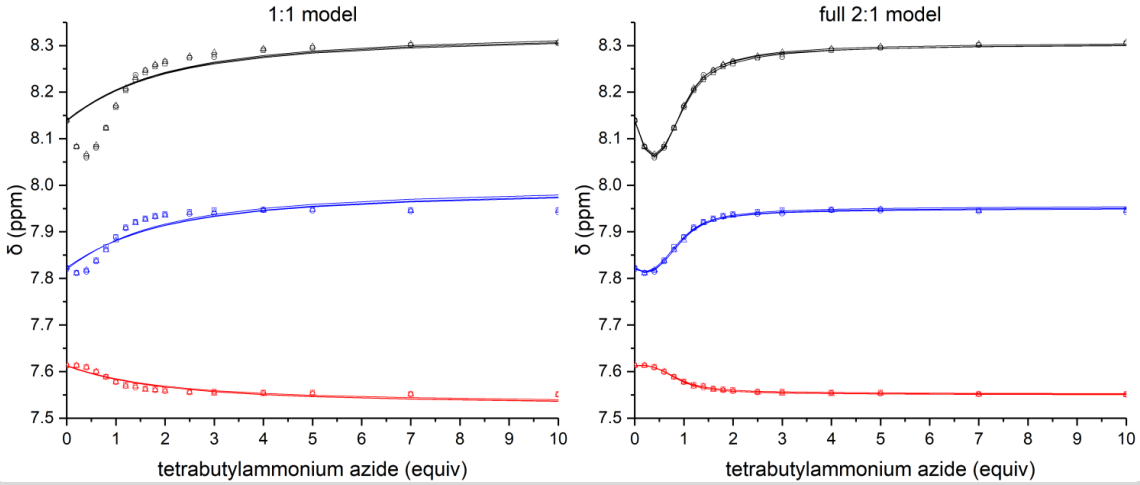


| entry | model | $cov_{fit}$ ($10^{-3}$) | $cov_{fit}$ factor | $K_{a(1:1)}$ ($M^{-1}$) | $K_{a(2:1)}$ ($M^{-1}$) |
|---|---|---|---|---|---|
| 1 | 1:1 | 130.67 | 1 | $3.68 \pm 0.08 \times 10^2$ | - |
| **2** | **full 2:1** | **0.72** | **191.0** | **$9.1 \pm 0.9 \times 10^3$** | **$1.0 \pm 0.6 \times 10^2$** |

One set of symbols (□, ○, △) refers to experimental data from one set of measurements (2 mM, $CDCl_3$, 500 MHz, 298 K). Lines are the calculated isotherms of the described model. $cov_{fit}$ factor is $cov_{fit}$ for the 1:1 model divided by the $cov_{fit}$ for the binding model under study.[63] Values are the mean of 3 independent replicas calculated with BindFit v0.5,[64] error is the standard deviation.

Natural abundance azide consists primarily of nitrogen-14, a quadrupolar nuclei with spin 1. $^{14}N$ NMR enabled direct observation of the azide anion solution and provided additional data consistent of its interaction with (*S*)-**2.43b**. All three nitrogen signals are visible in the $^{14}N$ NMR spectra of free tetrabutylammonium azide albeit with different peak widths due to the symmetry of their environments (**Figure 2.17A**). The tetrabutylammonium cation is in the most symmetrical environment and exhibits the sharpest peak at 67.2 ppm with a width at half-height of 55 Hz, the azide centre at 251.8 ppm possesses the next most symmetric environment and is slightly broadened with a width at half-height of 95 Hz, and the azide termini at 103.0 ppm are in the least symmetrical environment and produce the broadest signals with a width at half-height of 220 Hz. In contrast, pure (*S*)-**2.43b** contains four nitrogen atoms in highly asymmetric environments and a significant broadening of the $^{14}N$ signals are observed to the extent that no signals above the noise appear (**Figure 2.17B**). In a mixture of (*S*)-**2.43b** and tetrabutylammonium azide, the peaks corresponding to the azide anion centre becomes significantly broadened from 95 Hz to *ca*. 800 Hz and the signal corresponding to the azide anion termini are broadened beyond detection, whereas the tetrabutylammonium

cation remains unchanged at 55 Hz (**Figure 2.17C**). The direct insight into the azide anion provided by $^{14}$N NMR supported the interaction of azide with (*S*)-**2.43b** in solution and the spectator nature of the tetrabutylammonium cation.

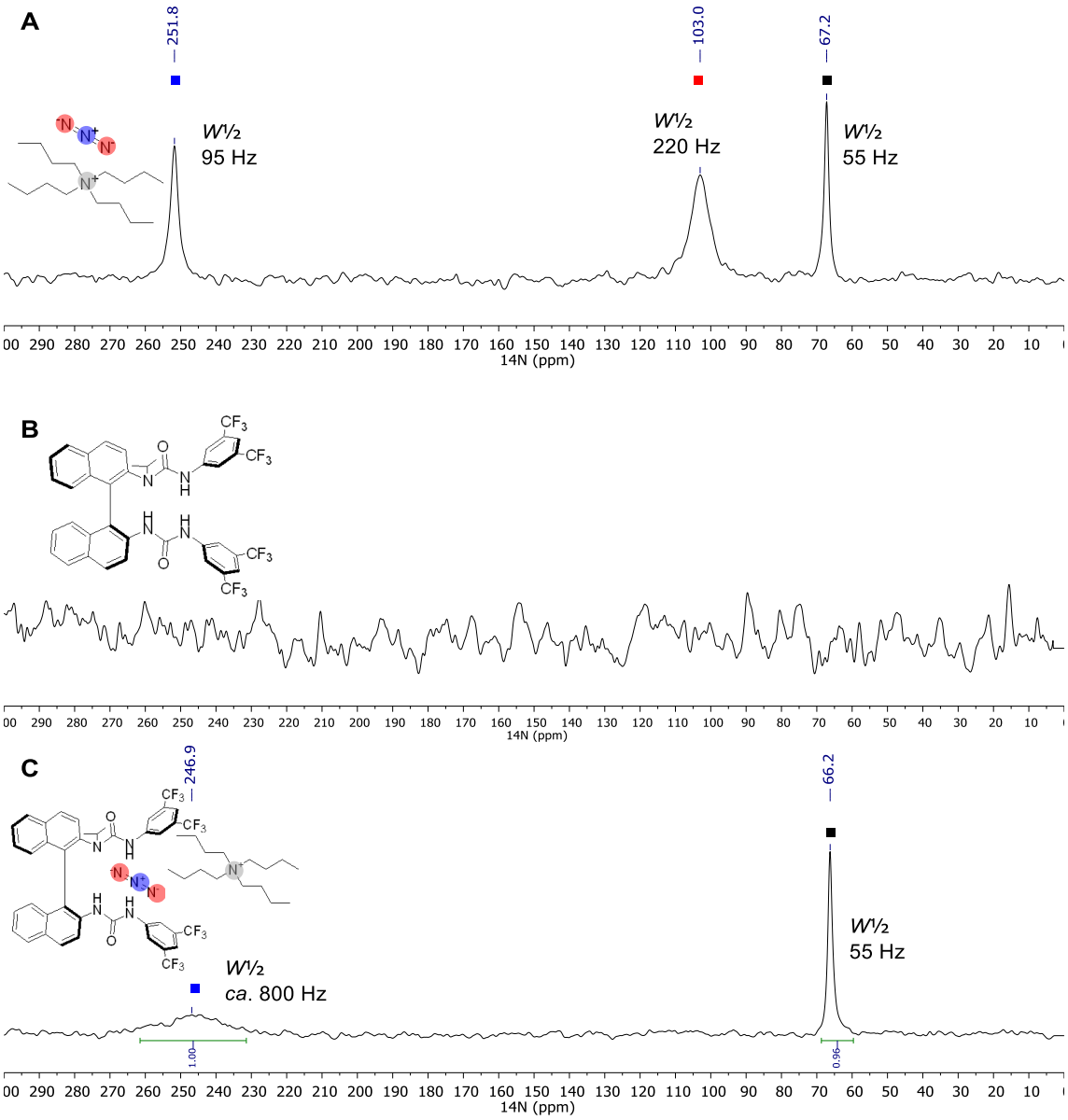


**Figure 2.17** (A) $^{14}$N NMR spectra of tetrabutylammonium azide. (B) $^{14}$N NMR spectra of (*S*)-**2.43b**. (C) $^{14}$N NMR spectra of a 1:1 mixture of (*S*)-**2.43b** and tetrabutylammonium azide. (25 mM, $CDCl_3$, 500 MHz, 298 K).

### 2.3.2 Investigating structure in solution

Further details into the structure of (*S*)-**2.43b** complexed to azide in solution by NMR utilised nitrogen-15. Although only 0.4% of nitrogen at natural abundance consists of nitrogen-15, this nucleus possesses a spin of one-half, and isotopic enrichment of tetrabutylammonium azide facilitated the study of heteronuclear $^{1}$H-$^{15}$N couplings by NMR. Tetrabutylammonium [1-

$^{15}$N]azide containing azide enriched with a single $^{15}$N at one terminus was prepared from commercial sodium [1-$^{15}$N]azide and provided a valuable additional spectroscopic handle. Studying a system with (*S*)-**2.43b** and tetrabutylammonium [1-$^{15}$N]azide in $CDCl_3$ provided the opportunity to understand the structure of the binding between the (*S*)-**2.43b** and azide in solution by NOE interactions and scalar couplings.

It was essential to understand the composition of samples prepared from (*S*)-**2.43b** and tetrabutylammonium [1-$^{15}$N]azide since combining (*S*)-**2.43b** and tetrabutylammonium [1-$^{15}$N]azide in solution produces a mixture containing a dynamic equilibrium of unbound (*S*)-**2.43b**, unbound [1-$^{15}$N]azide, the 1:1 species, and the 2:1 species. BindSim enabled simulation of the composition of these components at equilibrium from the initial concentrations of components added and the association constants determined by titration with tetrabutylammonium azide (**Table 2.8**). A sample prepared with 25 mM (*S*)-**2.43b** and 25 mM tetrabutylammonium azide would contain predominantly the 1:1 complex, with 1.8 mM of the 2:1 complex. Preparing a sample containing 50 mM of azide increases the concentration of the 1:1 complex to 24.4 mM and reduces the concentration of the 2:1 complex to 0.3 mM, but results in a much higher quantity of free tetrabutylammonium [1-$^{15}$N]azide.

**Table 2.8** Calculated concentration of species at equilibrium in solutions prepared from (*S*)-**2.43b** and tetrabutylammonium azide.

| | initial concentration | | calculated concentration at equilibrium | | | |
|---|---|---|---|---|---|---|
| entry | (*S*)-**2.43b** (mM) | $N_3^-$ (mM) | (*S*)-**2.43b** (mM) | (*S*)-**2.43b**·$N_3^-$ (mM) | (*S*)-**2.43b**$_2$·$N_3^-$ (mM) | $N_3^-$ (mM) |
| 1 | 0 | 25 | 0 | 0 | 0 | 25 |
| 2 | 25 | 0 | 25 | 0 | 0 | 0 |
| 3 | 25 | 25 | 0.9 | 20.6 | 1.8 | 2.6 |
| 4 | 25 | 50 | 0.1 | 24.4 | 0.3 | 25.4 |

BindSim used to simulate sample compositions with a $K_{a(1:1)}$ of $9.1 \times 10^3$ $M^{-1}$ and $K_{a(2:1)}$ of $1.0 \times 10^2$ $M^{-1}$.[64]

The $^1$H spectra of mixtures containing 25 mM (*S*)-**2.43b** with either 25 or 50 mM tetrabutylammonium [1-$^{15}$N]azide reflected the calculated distribution of species in solution (**Figure 2.18**). Solutions containing excess azide displayed sharper peaks, indicative of the

reduced exchange between the 1:1 and 2:2 urea-azide complexes. One remarkable difference between free (*S*)-**2.43b** and samples of (*S*)-**2.43b** coordinated to azide is the relatively small change in NH2, which changed from being the previously most deshielded NH in (*S*)-**2.43b** at 7.56 – 7.51 ppm to the most shielded NH in the azide bound system at 7.93 – 7.87 ppm in the 1:1 mixture, and 8.08 ppm in the mixture with excess [1-$^{15}$N]azide. This change was also observed with fluoride and is consistent a loss of the internal hydrogen bond and interaction of all three NH groups with a coordinated anion.

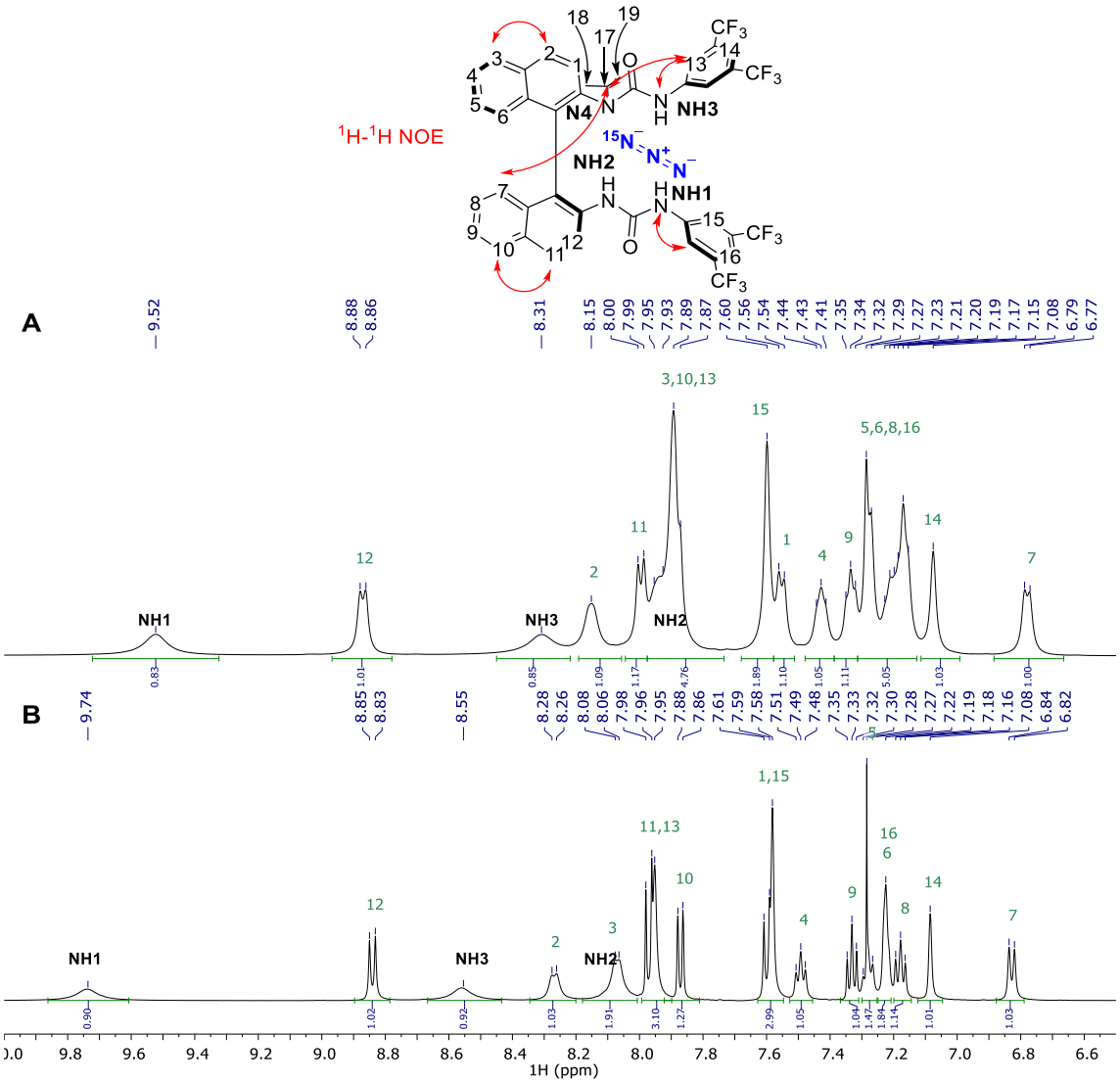


**Figure 2.18** Comparison and assignment of $^1$H NMR spectra of (*S*)-**2.43b** and tetrabutylammonium [1-$^{15}$N]azide in (A) 1:1 (B) 2:1 ratio. (25 mM (*S*)-**2.43b**, $CDCl_3$, 500 MHz, 298 K).

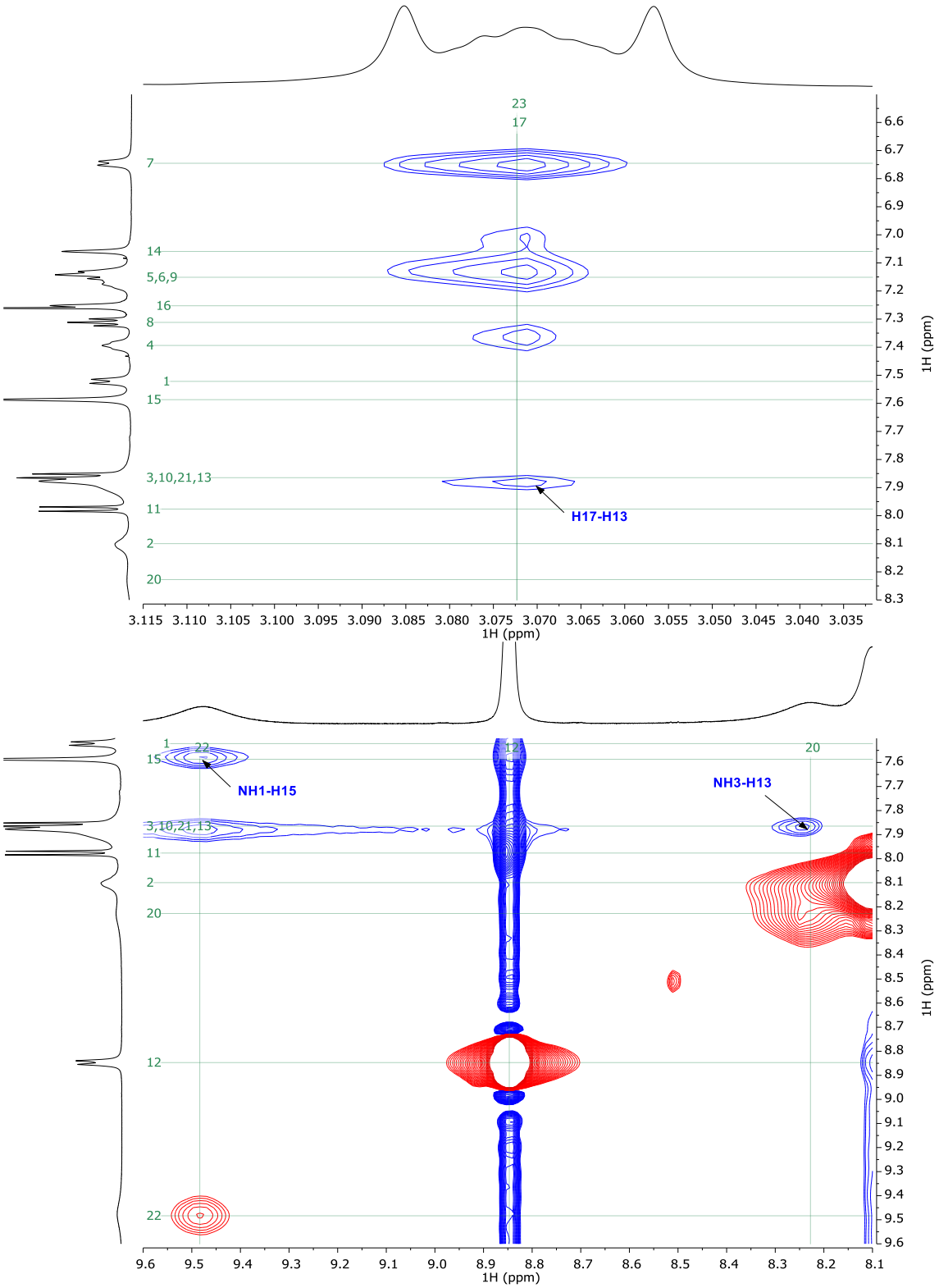


**Figure 2.19** Expansions of $^{1}$H-$^{1}$H NOESY NMR spectra of (*S*)-**2.43b** and tetrabutylammonium [1-$^{15}$N]azide in 1:1 ratio. (25 mM (*S*)-**2.43b**, $CDCl_3$, 500 MHz, 298 K). (25 mM (*S*)-**2.43b**, $CDCl_3$, 500 MHz, 298 K).

Assignment of the proton signals could be achieved by tracking shifts of (*S*)-**2.43b,** including those corresponding to H12, H2, H13, H15, and H6, along the titration, with additional support from $^{1}$H-$^{1}$H COSY and $^{1}$H-$^{1}$H NOESY NMR spectra (**Figure 2.19**). Key correlations between H17 and H13, supported the assignment of the fluorinated aromatic rings, with NOE relationships between NH1 and H15, as well as NH3 and H13 used to assign the urea NH signals.

Study of 1:1 mixtures of (*S*)-**2.43b** and tetrabutylammonium [1-$^{15}$N]azide with components at 100 mM, 25 mM, and 2.5 mM revealed minor but non-negligible changes (**Figure 2.20**). These observations are consistent with the expected concentration dependence of host-guest systems in solution. A consistent concentration of (*S*)-**2.43b** at 25 mM was utilised throughout the subsequent solution studies to avoid effects from changing the concentration influencing the distribution of components and resultant spectra. This concentration was selected since it provided a good signal-to-noise ratio and reflected the catalyst concentrations in HB-PTC reactions with fluoride.[53,66]

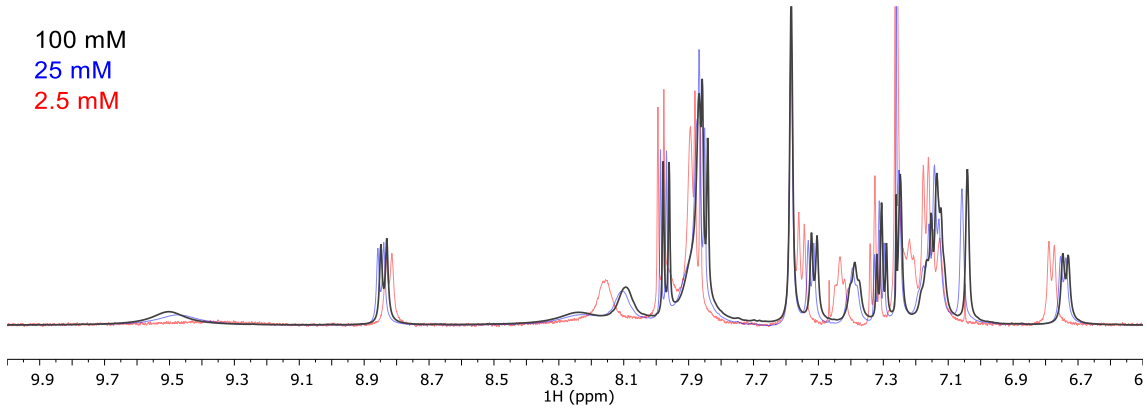


**Figure 2.20** Superimposed $^{1}$H NMR spectra of 1:1 mixtures of (*S*)-**2.43b** and tetrabutylammonium [1-$^{15}$N]azide at 100 mM, 25 mM, and 2.5 mM ($CDCl_3$, 500 MHz, 298 K).

Additional knowledge of properties of the $^{15}$N in the [1-$^{15}$N]azide complexes provided added assistance in ensuring optimal experiments when searching for NOE relationships. Comparison of the $^{15}$N NMR spectra of solutions containing pure tetrabutylammonium [1-$^{15}$N]$N_3$ and 25 mM (*S*)-**2.43b** mixed with 25 or 50 mM tetrabutylammonium [1-$^{15}$N]azide were conducted. Direct observation of $^{15}$N revealed only one signal corresponding an equilibrium

of all the species of the artificially introduced $^{15}N$ label, with all other nitrogen signals within the noise due to the poor natural abundance of $^{15}N$ (**Table 2.6**).

An inversion recovery experiment enabled quantification of the $^{15}N$ $T_1$ constant in these solutions (**Table 2.6**). The uncoordinated azide possessed the highest $T_1$ constant at 39 s, reflecting a lack of interactions with other components in solution to assist relaxation. A 1:1 mixture of (*S*)-**2.43b** and tetrabutylammonium [1-$^{15}N$]azide possessed a much shorter $T_1$ at 3.5 s, with the presence of (*S*)-**2.43b** appearing to reduce the $T_1$. The [1-$^{15}N$]azide in a solution of (*S*)-**2.43b** containing two equivalents of tetrabutylammonium [1-$^{15}N$]azide had a $T_1$ of 8 s, consistent with the expected exchange process between the multiple azide environments and reflective of the dynamic nature of azide in these systems.

**Table 2.6** $T_1$ measurements of the [1-$^{15}N$]$N_3$ in solutions of tetrabutylammonium [1-$^{15}N$]azide and (*S*)-**2.43b**.

| entry | initial concentrations (*S*)-**2.43b** (mM) | [1-$^{15}N$]$N_3$ (mM) | partial $^{15}N$ Spectra | $T_1$ (s) |
|---|---|---|---|---|
| 1 | 0 | 25 | 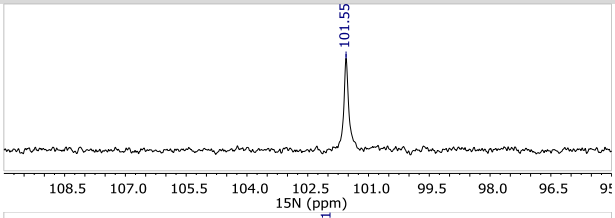 | 39 |
| 2 | 25 | 25 | 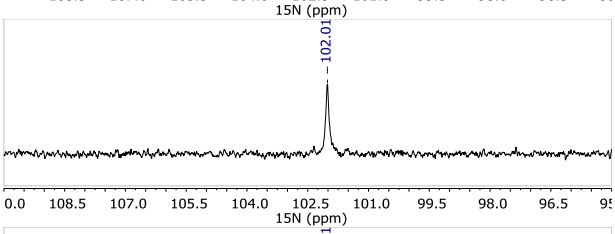 | 3.5 |
| 3 | 25 | 50 | 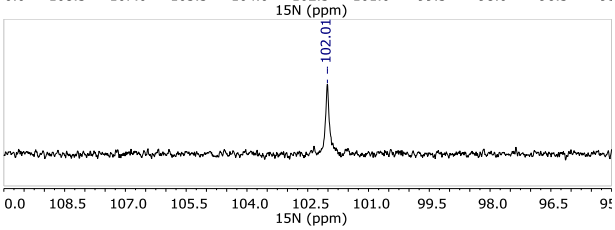 | 8 |



($CDCl_3$, 500 MHz, 298 K). Data collected in collaboration with Prof. T. D. W. Claridge.

With firm knowledge of $^{1}H$ and $^{15}N$ signals in samples of (*S*)-**2.43b** complexed to [1-$^{15}N$]azide, experiments to probe the relationship between these two components were initiated. $^{1}H$-$^{15}N$ NOE experiments aimed to link the bound [1-$^{15}N$]azide to a specific site on (*S*)-**2.43b**. A sample containing equimolar (*S*)-**2.43b** and tetrabutylammonium [1-$^{15}N$]azide at 25 mM was

preferred to avoid interference from excess unbound azide. Optimisation of presaturation and observation of the $^{1}H$ spectra ensured the selectivity of irradiation used (**Figure 2.21A**). Subsequently, generation of steady-state $^{1}H$ to $^{15}N$ NOEs under identical irradiation conditions followed by acquisition of the $^{15}N$ 1D spectrum enabled observation of any NOE effects (**Figure 2.21B**).

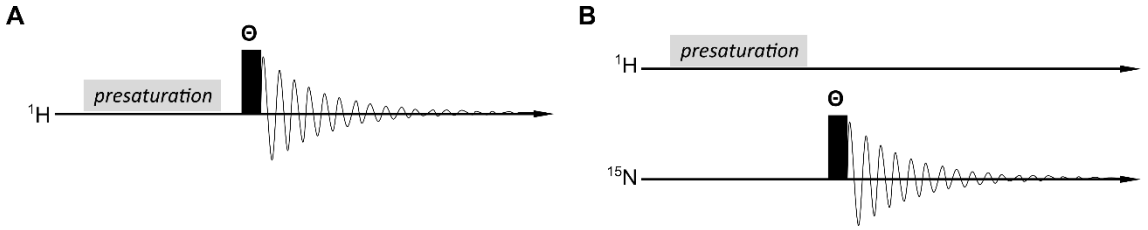


**Figure 2.21** (A) Schematic NMR sequences for optimisation of $^{1}H$ presaturation conditions. (B) Schematic NMR sequences for $^{1}H$-$^{15}N$ steady state NOE observations. Grey box indicates presaturation of a $^{1}H$ resonance during relaxation delay and black rectangle indicates excitation pulse for acquisition (θ = 30° or 90°).

Benchmarks for comparison were obtained by off-resonance irradiation at ±20 ppm of the $^{1}H$ spectra. Irradiation at a selected chemical shift with *rf* field strengths of 25 Hz and 5 Hz resulted in suppression of the corresponding signal, although spill over of saturation was observed at 25 Hz (**Figure 2.22**).

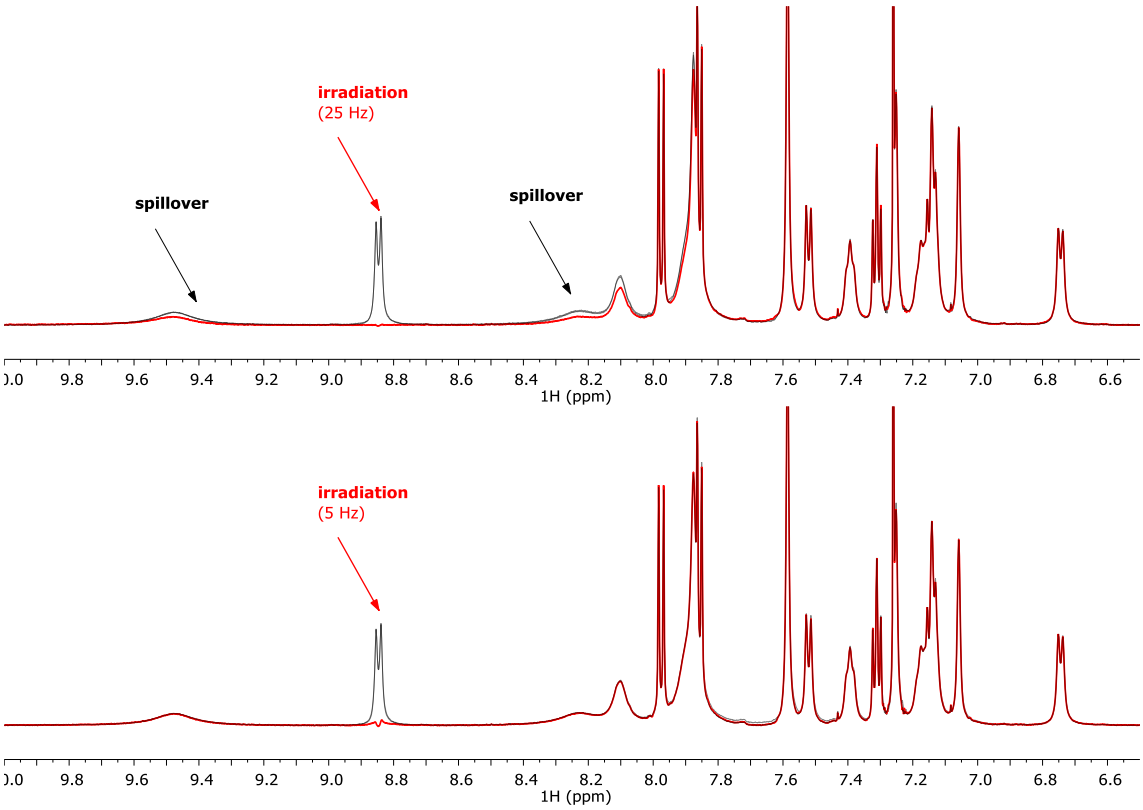


**Figure 2.22** Representative $^{1}$H NMR spectra comparing selectivity of irradiation at 8.85 ppm (red) at 25 Hz and 5 Hz, overlayed with control at 20 ppm (25 mM (*S*)-**2.43b**, $CDCl_3$, 500 MHz, 298 K). Data collected with Prof. T. D. W. Claridge.

NOE effects in small molecules are expected to lead to a reduction in the $^{15}$N resonance intensity due to the negative magnetogyric ratio of $^{15}$N. The exchange between the multiple species in the samples of (*S*)-**2.43b** and [1-$^{15}$N]azide, as well as the single label at only one azide terminus are likely to attenuate any NOE effects between the 1:1 (*S*)-**2.43b**·[1-$^{15}$N]azide complex. NOE intensity changes by direct comparison of irradiated spectra against the control spectra were observed, and resulted in intensity changes of up to -14% at 25 Hz irradiation, and -7% at 5 Hz irradiation (**Table 2.7**). Although stronger NOE effects were observed at 25 Hz irradiation, the reduced selectivity and spillover cause apparent effects with targeted $^{1}$H resonances with no real NOE interaction with azide. The data using the more selective irradiation at 5 Hz clearly show NOE effects with resonances associated with the catalyst NH protons, reflecting the predicted structure of azide association to all three urea NHs. Attempts to examine this with a sample containing excess azide to force equilibrium to more 1:1

resulted in consistent NOEs, although they were weaker due to the increased level of unbound [1-$^{15}$N]azide present.

**Table 2.7** Change in $^{15}$N signal intensity caused by irradiation of selected signal(s).

$^{1}$H-$^{15}$N NOE

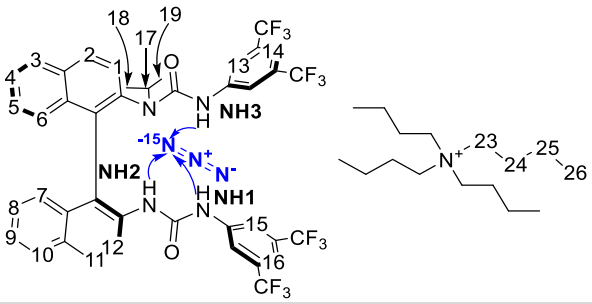


| irradiated signal(s) | change in [1-$^{15}$N]$N_3$ intensity (25 Hz irradiation) | change in [1-$^{15}$N]$N_3$ intensity (5 Hz irradiation) |
|---|---|---|
| **NH1** | **-12%** | **-7%** |
| H12 | -8% | 0% |
| **NH3** | **-13%** | **-6%** |
| **NH2, H10, H3, H13** | **-14%** | **-7%** |
| H7 | -3% | 0% |
| H17, H20 | 3% | 0% |
| H23 | 0% | 0% |
| H19 | -2% | 0% |
| H18 | -3% | 0% |

(*S*)-**2.43b** and tetrabutylammonium [1-$^{15}$N]azide in 1:1 ratio (25 mM (*S*)-**2.43b**, $CDCl_3$, 500 MHz, 298 K). Data collected with Prof. T. D. W. Claridge.

Variable temperature NMR can alter the rate of exchange, and a reduction in the rate of exchange was achieved upon reducing the temperature to 213 K (**Figure 2.23**). The NH signals of the major species appeared significantly sharper, although a complex spectra with decoalescence of a minor species designated as a 2:1 (*S*)-**2.43b**$_2$·[1-$^{15}$N]$N_3^-$ complex was also observed. Further analysis of this sample at 213 K was challenging due to the complex nature signals. Nonetheless, this data highlighted the ability to reduce exchange by a significant reduction in temperature and reflected previous calculations and predictions regarding the 2:1 species.

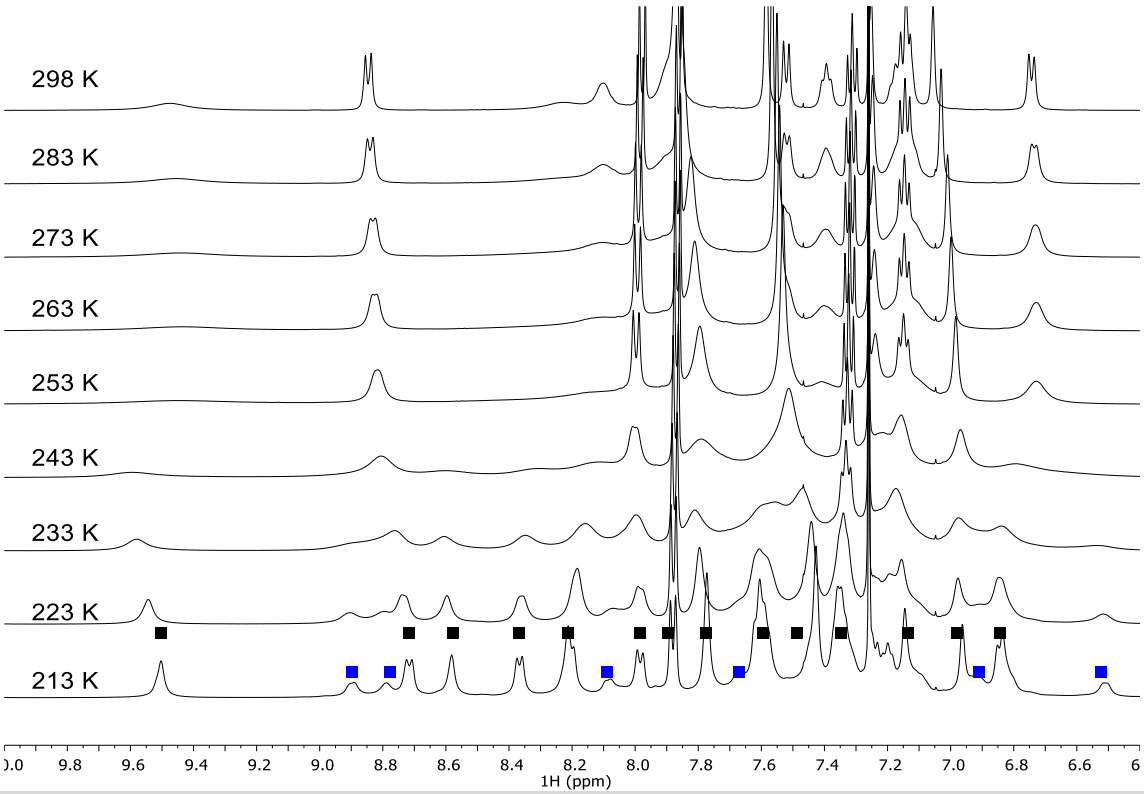


| calculated sample components concentrations at 298 K (mM) | | | |
|---|---|---|---|
| (*S*)-**2.43b** | (*S*)-**2.43b**·$N_3^-$ | (*S*)-**2.43b**$_2$·$N_3^-$ | $N_3^-$ |
| 0.9 | 20.6 | 1.8 | 2.6 |

**Figure 2.23** Variable temperature $^1$H NMR spectra of (*S*)-**2.43b** and tetrabutylammonium [1-$^{15}$N]azide (1 equiv) (25 mM (*S*)-**2.43b**, $CDCl_3$, 500 MHz). Major species highlighted in black, minor species highlighted in blue. BindSim used to simulate sample compositions with a $K_{a(1:1)}$ of $9.1 \times 10^3$ $M^{-1}$ and $K_{a(2:1)}$ of $1.0 \times 10^2$ $M^{-1}$.[64]

The quantity of the 2:1 species can be reduced in the presence of excess azide, and it was hypothesised a variable temperature NMR of a sample prepared with 25 mM (*S*)-**2.43b** with 50 mM azide would result in spectra containing predominantly the 1:1 species. Cooling this solution to 213 K revealed 1 major set of sharp peaks and negligible quantities of the minor species, supporting the hypothesis that those signals corresponded to the 2:1 (*S*)-**2.43b**$_2$·[1-$^{15}$N]$N_3^-$ complex (**Figure 2.24**).

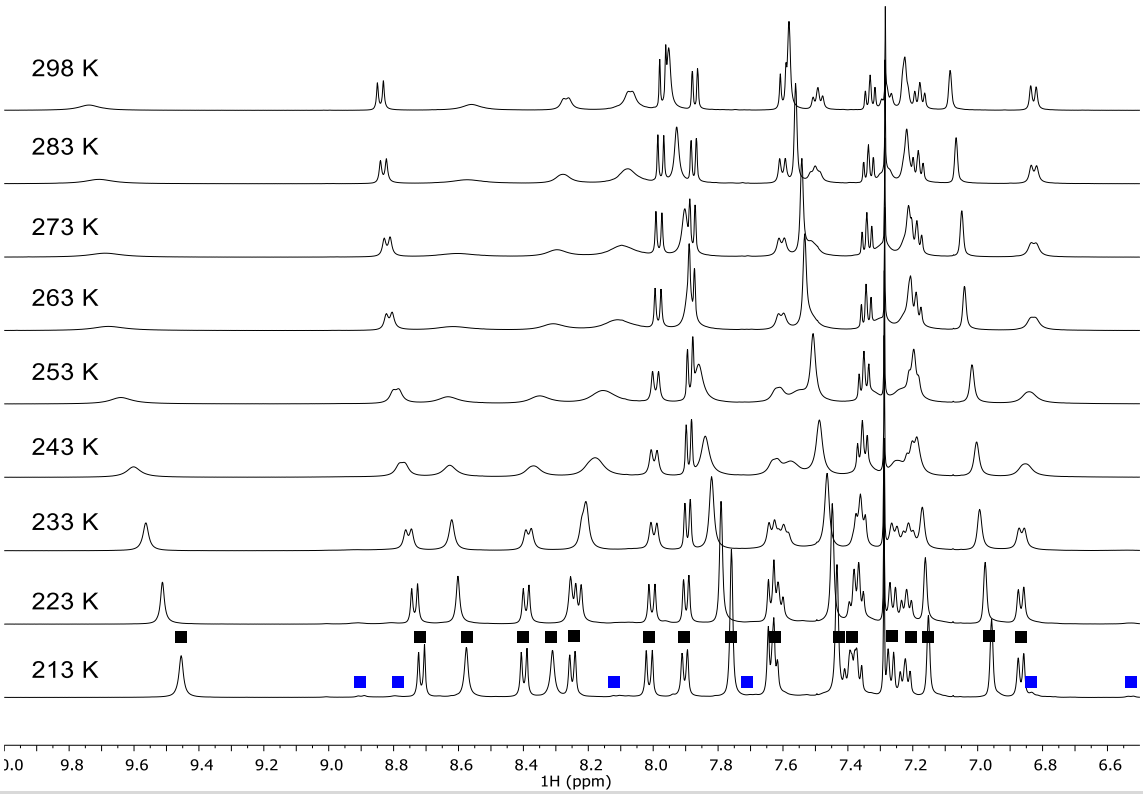


| calculated sample components concentrations at 298 K (mM) | | | |
|---|---|---|---|
| (*S*)-**2.43b** | (*S*)-**2.43b**·$N_3^-$ | (*S*)-**2.43b**$_2$·$N_3^-$ | $N_3^-$ |
| 0.1 | 24.4 | 0.3 | 25.4 |

**Figure 2.24** Variable temperature $^1$H NMR spectra of (*S*)-**2.43b** and tetrabutylammonium [1-$^{15}$N]azide (2 equiv) (25 mM (*S*)-**2.43b**, $CDCl_3$, 500 MHz). Major species highlighted in black, minor species highlighted in blue. BindSim used to simulate sample compositions with a $K_{a(1:1)}$ of $9.1 \times 10^3$ $M^{-1}$ and $K_{a(2:1)}$ of $1.0 \times 10^2$ $M^{-1}$.[64]

The assignment of the $^1$H shifts of (*S*)-**2.43b**·[1-$^{15}$N]$N_3$ in $CDCl_3$ at 213 K could be achieved by tracking the assigned $^1$H signals along the temperature change, with additional confirmation from 2D $^1$H-$^1$H COSY and $^1$H-$^1$H NOESY, $^1$H-$^{15}$N HSQC and $^1$H-$^{15}$N HMBC spectra. The sharper signals allowed for unambiguous assignment of all $^1$H signals, including the three NH protons (**Figure 2.25**). The chemical shifts corresponding to the three NH signals represent the largest change in chemical shifts observed compared to free (*S*)-**2.43b**. The change in relative shifts, whereby the previously most deshielded NH becomes the most shielded NH was observed in the fluoride complex and may suggest a similar conformer in solution.

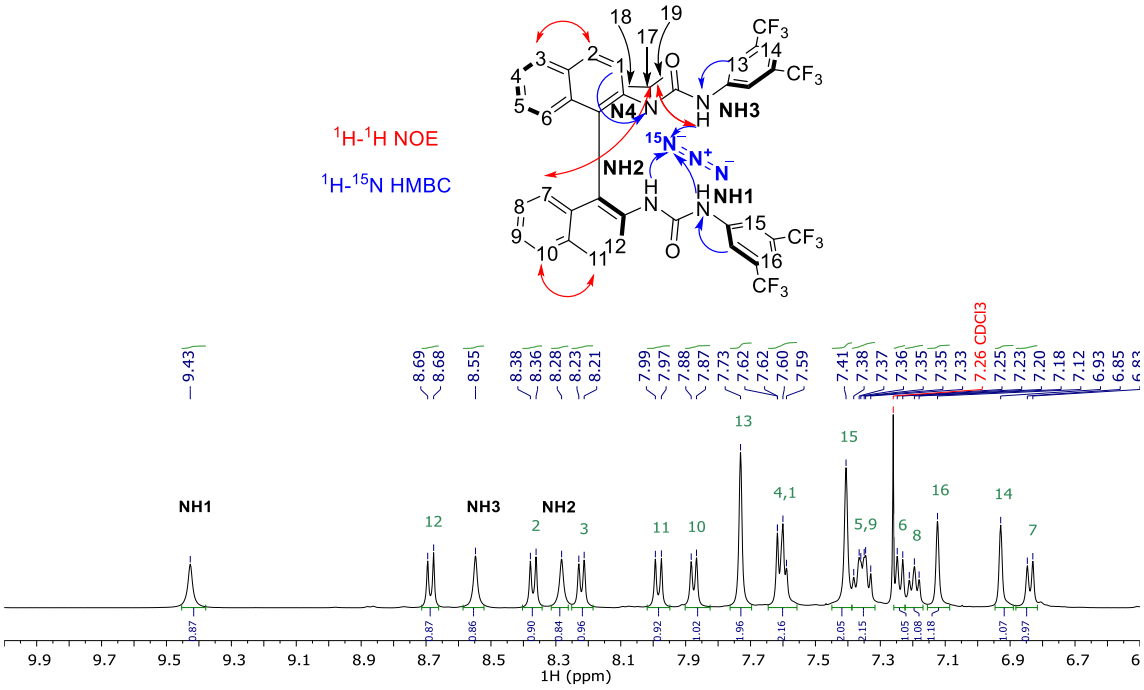


**Figure 2.25** Proposed assignment and secondary structure of (*S*)-**2.43b**·$N_3^-$ from (*S*)-**2.43b** and tetrabutylammonium [1-$^{15}$N]azide (2 equiv) in $CDCl_3$ and $^1$H NMR spectrum highlighting NH signals and key correlations. (25 mM (*S*)-**2.43b**, $CDCl_3$, 500 MHz, 213 K).

As before, a $^1$H-$^{15}$N HMBC correlation between H1 and the tertiary nitrogen was used to differentiate the two ring systems (**Figure 2.26**). $^1$H-$^{15}$N HMBC correlations were also used to unambiguously link H13 to N3 and H15 to N1 and paired each fluorinated aromatic ring with a respective NH.

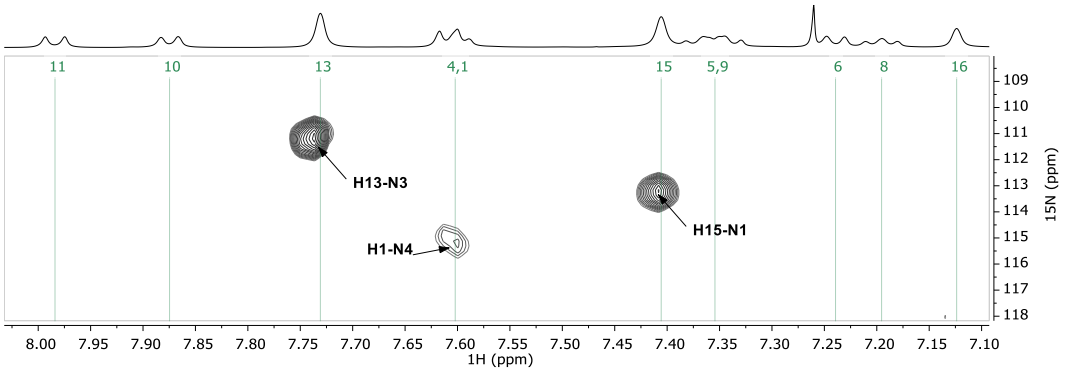


**Figure 2.26** Expanded view of $^1$H-$^{15}$N HMBC NMR spectra of (*S*)-**2.43b**·$N_3^-$ from (*S*)-**2.43b** and tetrabutylammonium [1-$^{15}$N]azide (2 equiv) (25 mM (*S*)-**2.43b**, $CDCl_3$, 500 MHz, 298 K).

$^1$H-$^1$H COSY and $^1$H-$^1$H NOESY NMR experiments were used to complete the assignment of the backbone. A $^1$H-$^1$H NOE relationship between NH3 and H17 was key to differentiating the fluorinated aromatic rings and provided further support of the individual NH assignments (**Figure 2.27**).

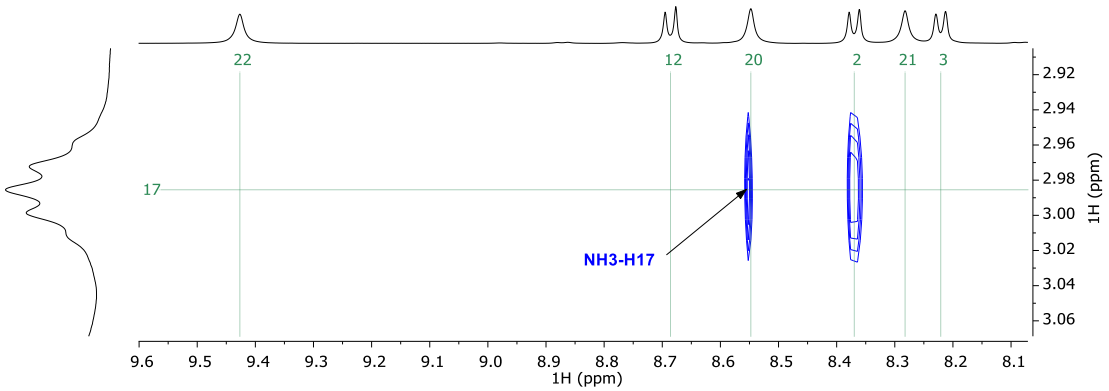


**Figure 2.27** $^{1}$H-$^{1}$H NOESY (blue) NMR spectra of (*S*)-**2.43b**·$N_3^-$ from (*S*)-**2.43b** and tetrabutylammonium [1-$^{15}$N]azide (2 equiv) (25 mM (*S*)-**2.43b**, $CDCl_3$, 500 MHz, 298 K).

The full view of the $^{1}$H-$^{15}$N HMBC NMR spectra displayed additional signals of interest (**Figure 2.28A**). Correlations were observed between each NH and a nitrogen signal at 100 ppm, the characteristic chemical shift of [1-$^{15}$N]azide.[70] This was attributed to the presence of scalar couplings through a hydrogen bond from the three NH protons of (*S*)-**2.43b** to the bound [1-$^{15}$N]azide (**Figure 2.28A**). These signals represented the first observed $^{1}$H to $^{15}$N scalar couplings from a hydrogen bond donor to an azide, an interaction unreported in the literature. Conducting 1D $^{1}$H-$^{15}$N HMBC spectra with removal of the phase modulator provided a method to measure the respective coupling constants (**Figure 2.28B**). Three antiphase doublets corresponding to each NH coupling to the [1-$^{15}$N]azide were observed. The $^{1h}J_{HN}$ coupling constants were determined to be in the range of 5 Hz but further precision could not be obtained due to limitations of line widths.

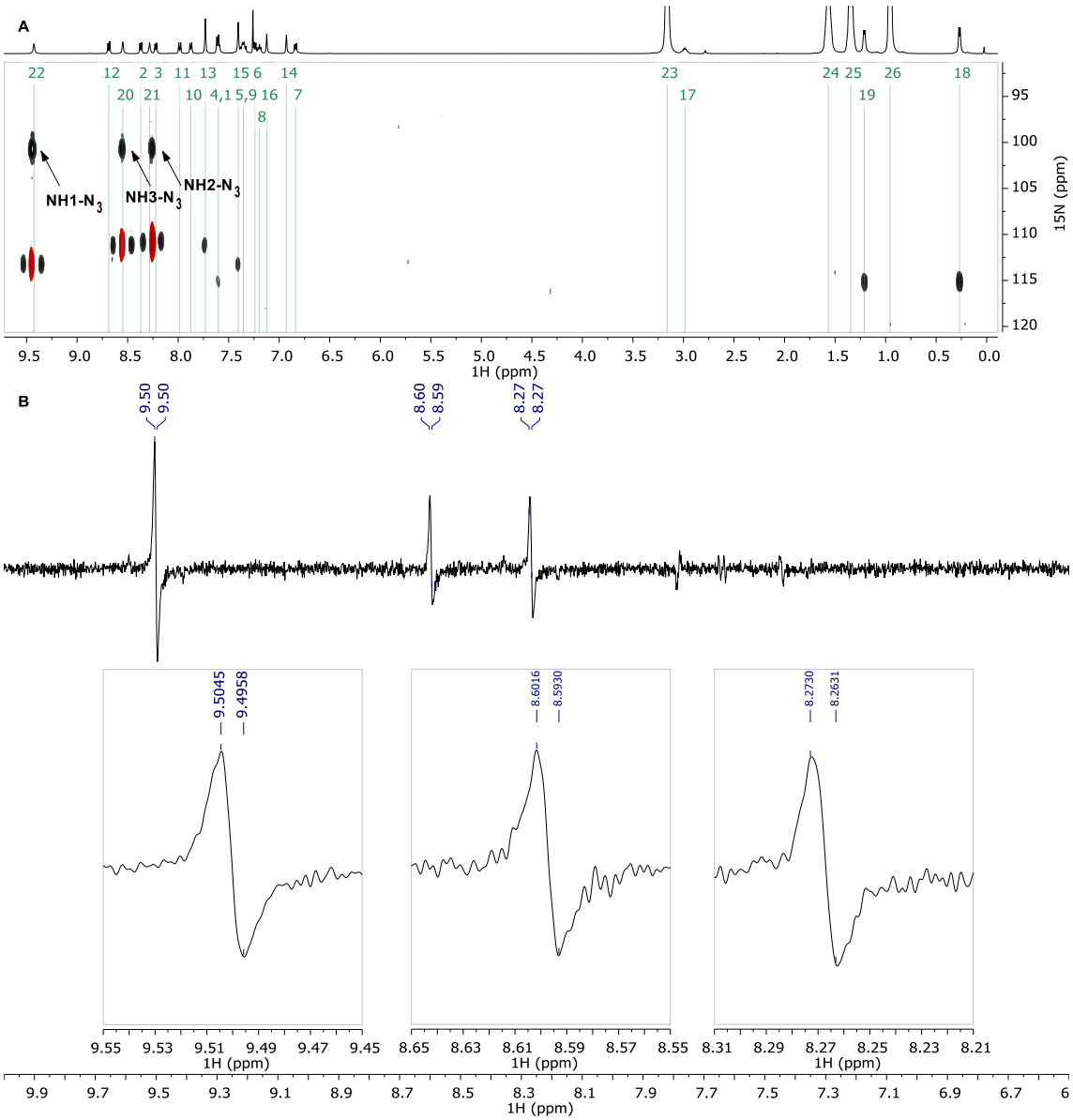


**Figure 2.28** (A) Full view of $^{1}H$-$^{15}N$ HMBC NMR spectra of (*S*)-**2.43b**·$N_3^-$ from (*S*)-**2.43b** and tetrabutylammonium [1-$^{15}N$]azide (2 equiv) (25 mM (*S*)-**2.43b**, $CDCl_3$, 500 MHz, 213 K). (B) 1D $^{1}H$-$^{15}N$ HMBC NMR spectra with inset expansions of antiphase doublets of (*S*)-**2.43b**·$N_3^-$ from (*S*)-**2.43b** and tetrabutylammonium [1-$^{15}N$]azide (2 equiv) (25 mM (*S*)-**2.43b**, $CDCl_3$, 500 MHz, 213 K). Data collected with Prof. T. D. W. Claridge.

These detailed studies in solution by NMR revealed a defined secondary structure of the 1:1 complex of (*S*)-**2.43b** and azide. The data obtained by $^{1}H$-$^{15}N$ NOE and HMBC experiments indicate azide coordination with all three urea NH hydrogen bond donors.

### 2.3.3 Solid state studies

Solid state studies of **2.43b** utilised the racemate owing to its more favourable crystallisation properties, compared to the single enantiomer. Single crystals grown from an amorphous solid of (±)-**2.43b** complexed to tetrabutylammonium azide were analysed by X-ray diffraction

and provided unique insights into the binding of azide with a chiral tridentate hydrogen bond donor.

An amorphous solid of (±)-**2.43b** complexed to tetrabutylammonium azide was prepared by stirring (±)-**2.43b** and tetrabutylammonium azide in MeCN, followed by evaporation of the mixture to dryness (**Scheme 2.12**). The amorphous solid obtained was characterised by NMR and IR. IR spectroscopy of the neat amorphous solid revealed a $\nu_{max}$ characteristic of an azide asymmetric stretch at 2034 $cm^{-1}$ at a noticeable shift from the corresponding signals in tetrabutylammonium azide (1992 $cm^{-1}$) and hydrazoic acid gas (2140 $cm^{-1}$),[55] consistent with a hydrogen bonded azide anion.

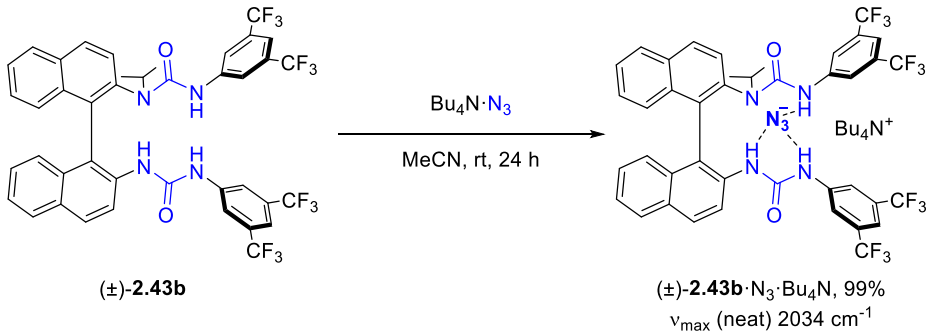


(±)-**2.43b**

(±)-**2.43b**·$N_3$·$Bu_4N$, 99%
$\nu_{max}$ (neat) 2034 $cm^{-1}$

**Scheme 2.12** Preparation of (±)-**2.43b** complexed to tetrabutylammonium azide.

Single crystals of (±)-**2.43b** complexed to tetrabutylammonium azide suitable for X-ray diffraction analysis were successfully grown by slow evaporation of a saturated solution of the amorphous solid in hot hexane and EtOAc. A structure containing both (*R*)-**2.43b** and (*S*)-**2.43b** complexed to individual molecules of azide in the asymmetric unit (Z' = 2) was obtained (**Figure 2.29A**). The azide anions are coordinated at one terminus by three hydrogen bond donors of **2.43b**, with the other terminus in close contact with the tetrabutylammonium cation.

Overlaying a unit of (*S*)-**2.43b** complexed to azide with the previously reported structure of (*S*)-**2.43b** complexed to fluoride[53] revealed exceptionally similar spatial alignments of the (*S*)-BINAM scaffold and 3,5-(bistrifluoromethy)phenyl aromatic rings (**Figure 2.29C**). However, the structure of (*S*)-**2.43b** complexed to azide exhibits an increased hydrogen bonding length

compared to the structure of (*S*)-**2.43b** complexed to fluoride, changing from 2.662(2) Å, 2.667 Å, and 2.690 Å to 2.98(2) Å, 2.81(2) Å, and 2.94(2) Å respectively, consistent with weaker hydrogen bonding interactions.

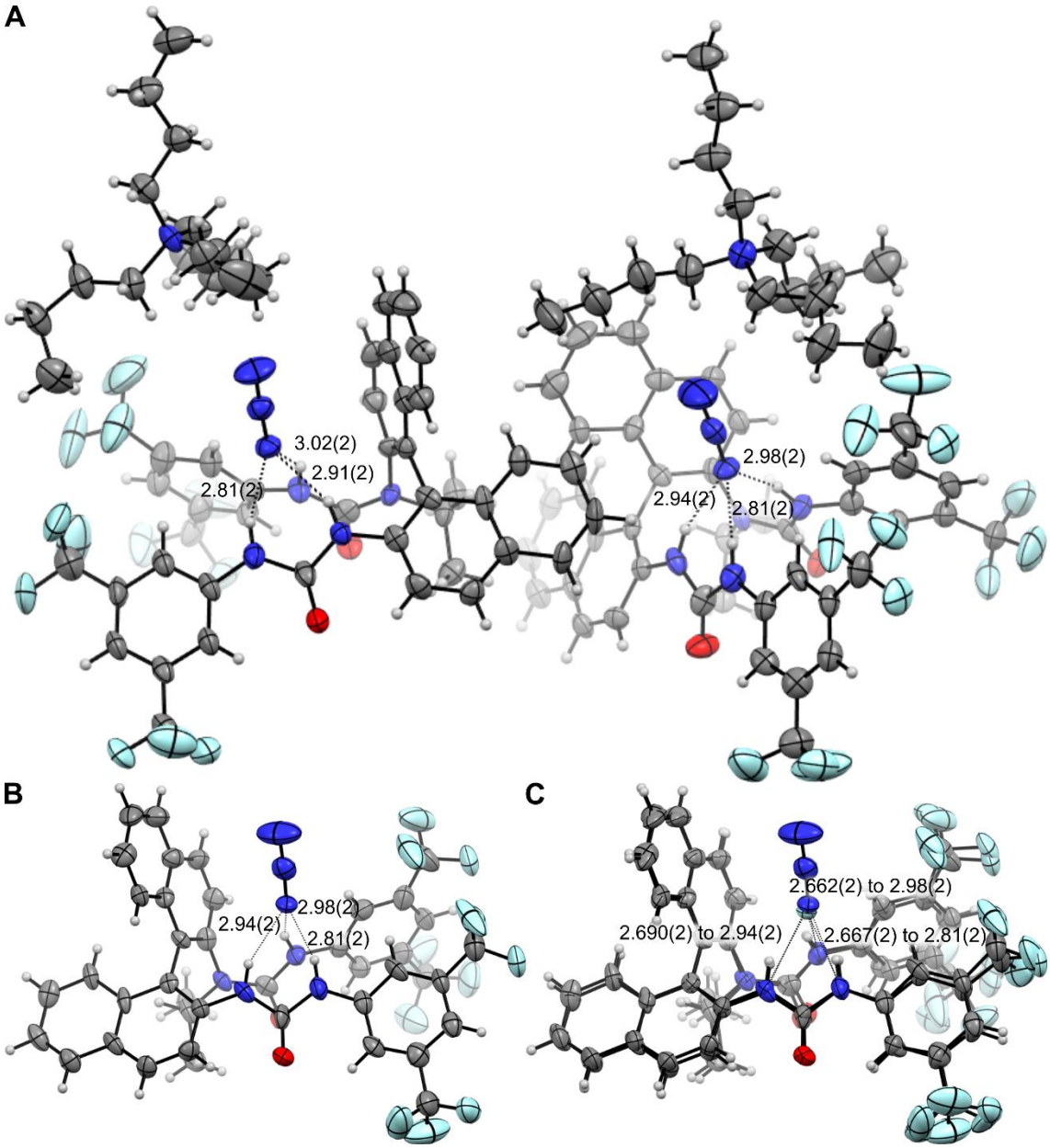


**Figure 2.29** (A) Asymmetric unit of a Z' = 2 crystal structure consisting of both (*R*)-**2.43b** and (*S*)-**2.43b** complexed to tetrabutylammonium azide. (B) View of (*S*)-**2.43b** from the asymmetric unit complexed to azide. (C) (*S*)-**2.43b** complexed to azide overlayed with the reported fluoride structure[53] and the increase in bond lengths. Distances provided in Ångstroms, displacement ellipsoids drawn at 50% probability level. Data collection and analysis by Dr. G. Pupo and Dr. K. E. Christensen.

## 2.4 Reaction development and scope

### 2.4.1 Synthesis of β-thioazides

Although a great effort into optimising the enantioselective synthesis of β-thioazides under HB-PTC with sodium azide was conducted in the Gouverneur group,[52] a brief attempt into further optimising this transformation was undertaken (**Table 2.8**). Minor improvements were observed when changing the solvent to 1,2-difluorobenzene (1,2-DFB) and use of an (*S*)-BINAM derived *N*-alkyl bis-urea, with enantiomeric ratios up to 69:31 and 69.5:30.5 measured. Unfortunately, due to the challenges in improving the enantiomeric ratio of this reaction and the limited applications of β-thioazides, further developments were not pursued.

**Table 2.8** Further optimisation of β-thioazides under HB-PTC.

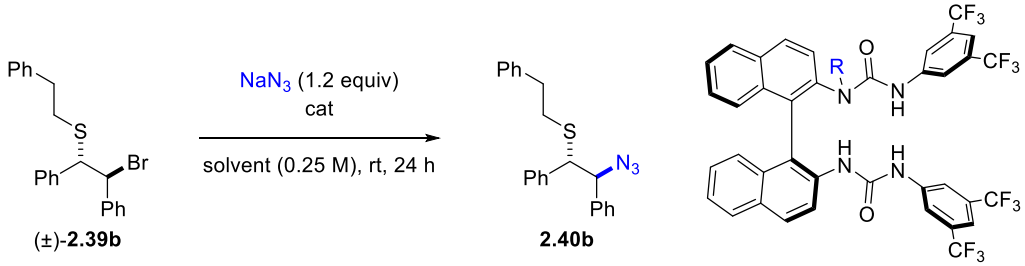


(*S*)-**2.43a** R = H
(*S*)-**2.43b** R = $^{i}$Pr
(*S*)-**2.43c** R = Me

| entry | cat | solvent | NMRy | e.r. |
|---|---|---|---|---|
| 1 | (*S*)-**2.43a** (0.1 equiv) | $CH_2Cl_2$ | 26% | 66:34 |
| 2 | (*S*)-**2.43a** (0.05 equiv) | 1,2-DFB | 21% | 66.5:33.5 |
| 3 | (*S*)-**2.43b** (0.05 equiv) | 1,2-DFB | 76% | 69:31 |
| 4 | (*S*)-**2.43c** (0.05 equiv) | 1,2-DFB | 56% | 69.5:30.5 |

NMRy determined with internal standard. Absolute configuration of **2.40b** not determined. 1,2-DFB = 1,2-difluorobenzene.

### 2.4.2 Racemic synthesis of β-aminoazides

To achieve the synthesis of desirable β-aminoazides from sodium azide under HB-PTC, a suitable *meso*-aziridinium precursor was required. The synthesis of stilbene derived β-aminochloride (±)-**2.46a** was previously reported up to the multi-decagram scale[54] and its preparation was found to be both efficient and robust. (±)-**2.46a** is an easily handled solid powder and stable under ambient conditions for multiple days, although a freezer was used for long term storage. In addition, structural derivatives of the resultant β-aminoazide

products (±)-**2.47a** are frequently found in bioactive compounds such as NMDA receptor antagonists and Kv1.5 blockers,[71–74] hence their enantioenriched counterparts and derivatives may find further utility.

Proof-of-principle was successfully established with (±)-**2.46a**, sodium azide, and Schreiner's urea **2.41a** using conditions adapted from previous studies (**Table 2.9**).[52,53] Stirring (±)-**2.46a** and sodium azide in 1,2-difluorobenzene at 1200 rpm produced only a 2% NMRy of β-aminoazide (±)-**2.47a**, however addition of **2.41a** as catalyst resulted in a 90% NMRy of the desired product. This difference in yield was hypothesised to be linked with the poor organosolubility of sodium azide and are consistent with previous reactions conducted under HB-PTC.[52–54]

**Table 2.9** Initial evaluation for the synthesis of β- aminoazides using sodium azide

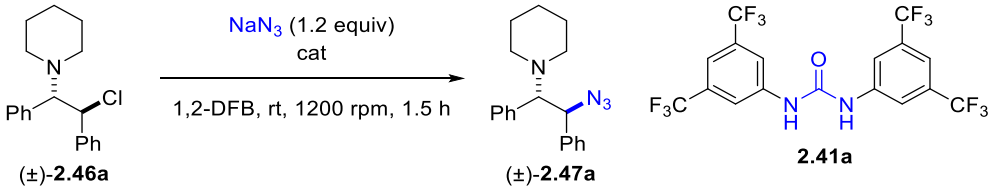


| entry | cat | NMRy |
|---|---|---|
| 1 | **2.41a** (0.1 equiv) | 90% |
| 2 | none | 2% |

1,2-DFB = 1,2-difluorobenzene.

Analysis of the crude NMR spectra showed exclusive formation of a single product, with the predominant remaining mass balance being starting material. Attempts to separate product from the residual starting material by chromatography were unsuccessful due to co-elution, however leaving the reaction for 24 h allowed for full conversion and isolation of the desired (±)-**2.46a** product after chromatography, enabling full characterisation.

The reaction with (±)-**2.46a** was conducted with a diverse selection of achiral dual hydrogen bond donors as catalysts (**Table 2.10**). The relationship of these hydrogen bond donors with azide were previously studied in both solid state and solution, hence their catalytic performance may provide valuable insights into the relationship between azide coordination and reactivity. A range of NMRy from 90% NMRy with **2.41a** down to 2% with **2.41g** were

obtained, suggesting a strong impact of the urea hydrogen bond donor on the reactivity of azide. The highest NMRy were measured with **2.41a**, **2.41c**, and **2.41d** at 90%, 64%, and 40% respectively, and these catalysts represented the most electron deficient 1,3-diarylureas examined. The lowest NMRy were measured with **2.41f** and **2.41g** at 3% and 2% respectively, effectively unchanged from the uncatalysed NMRy of 2%.

**Table 2.10** Study of different hydrogen bond donor catalysts for the synthesis of β-aminoazides.

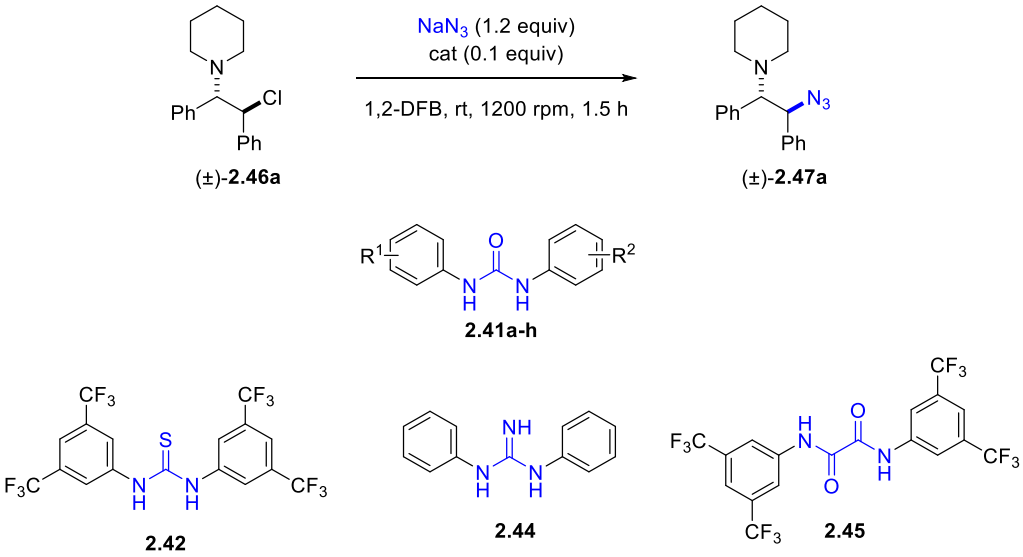


| entry | cat | NMRy |
|---|---|---|
| 1 | **2.41a**, $R^1 = R^2 = 3,5\text{-}CF_3$ | 90% |
| 2 | **2.41b**, $R^1 = R^2 = 3\text{-}Cl$ | 12% |
| 3 | **2.41c**, $R^1 = 3,5\text{-}CF_3$; $R^2 = H$ | 64% |
| 4 | **2.41d**, $R^1 = R^2 = 4\text{-}CF_3$ | 40% |
| 5 | **2.41e**, $R^1 = R^2 = H$ | 11% |
| 6 | **2.41f**, $R^1 = R^2 = 4\text{-}Br$ | 3% |
| 7 | **2.41g**, $R^1 = R^2 = 4\text{-}F$ | 2% |
| 8 | **2.41h**, $R^1 = R^2 = 4\text{-}CN$ | 16% |
| 9 | **2.42** | 18% |
| 10 | **2.44** | 37% |
| 11 | **2.45** | 10% |

NMRy determined with $Ph_3CH$ internal standard. 1,2-DFB = 1,2-difluorobenzene.

These variations were hypothesised to stem from either catalyst structure, electronics, or solubility. Comparing selected results to their association constants with azide suggested potential links between the association constant of the urea catalyst with azide and yield of product produced (**Table 2.11**). From the set of catalysts compared, Schreiner's urea **2.41a** provided product with the highest NMRy at 90% and also possessed the highest $K_{a(1:1)}$ with

azide at 1.57 ± 0.06 × $10^3$ $M^{-1}$, whilst catalysts **2.41e** and **2.41g** with lower association constants with azide at 3.14 ± 0.03 × $10^2$ $M^{-1}$ and 4.82 ± 0.05 × $10^2$ $M^{-1}$ gave the lowest NMRy at 11% and 2% respectively. In general, catalysts forming stronger hydrogen bonds with azide also exhibited superior catalytic performance, consistent with previous reported observations of hydrogen bond donor electronics on HB-PTC with fluoride.[53]

**Table 2.11** Comparison NMRy provided by selected urea catalysts against their $K_{a(1:1)}$ constants with azide.

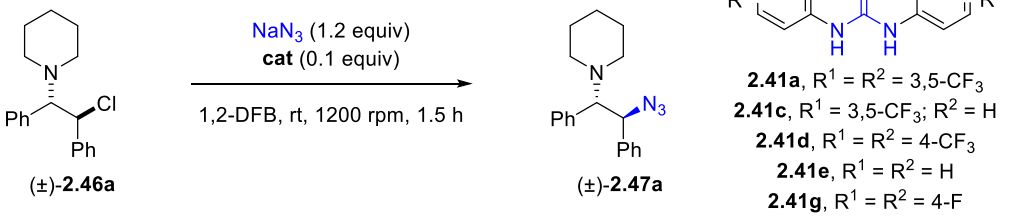


| entry | cat | $K_{a(1:1)}$ ($M^{-1}$) | NMRy |
|---|---|---|---|
| 1 | **2.41a**, $R^1 = R^2$ = 3,5-$CF_3$ | 1.57 ± 0.06 × $10^3$ | 90% |
| 2 | **2.41c**, $R^1$ = 3,5-$CF_3$; $R^2$ = H | 9.4 ± 1.7 × $10^2$ | 64% |
| 3 | **2.41d**, $R^1 = R^2$ = 4-$CF_3$ | 1.25 ± 0.12 × $10^3$ | 40% |
| 4 | **2.41e**, $R^1 = R^2$ = H | 3.14 ± 0.03 × $10^2$ | 11% |
| 5 | **2.41g**, $R^1 = R^2$ = 4-F | 4.82 ± 0.05 × $10^2$ | 2% |

NMRy determined with $Ph_3CH$ internal standard. 1,2-DFB = 1,2-difluorobenzene.

These studies with achiral hydrogen bond donors and *meso*-aziridinium precursors provide a strong foundation for the synthesis of valuable enantioenriched β-aminoazides directly from sodium azide under HB-PTC. With the established knowledge of azide association with these achiral hydrogen bond donors in both solid state and solution, as well as the poor reactivity of the uncatalysed reaction, it appears plausible for these reactions to involve a hydrogen bond mediated phase-transfer.

### 2.4.3 Enantioselective synthesis of β-aminoazides

An enantioselective synthesis of β-aminoazides from sodium azide under HB-PTC was achieved upon stirring (±)-**2.46a** with sodium azide and (*S*)-**2.43b** at 1200 rpm in a range of solvents (**Table 2.12**). Use of 1,2-DFB solvent provided β-aminoazide (*S*,*S*)-**2.47a** in 80% yield and 85:15 e.r. (**Table 2.12**, entry 3). This represented a significant improvement from the

synthesis of β-thioazides from meso-episulfonium precursors, and further optimisation was pursued.

**Table 2.12** Screening of reaction solvent.

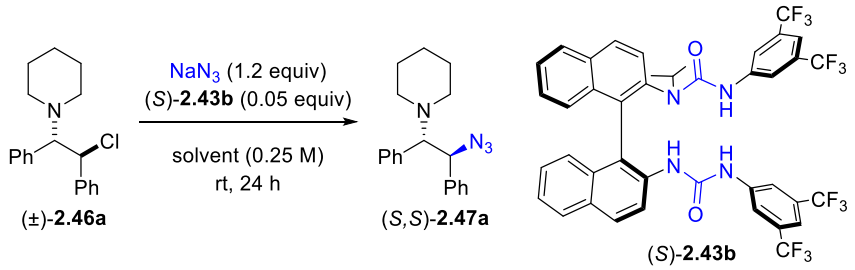


| entry | solvent | yield | e.r. |
|---|---|---|---|
| 1 | $CHCl_3$ | 86% | 77:23 |
| 2 | $CH_2Cl_2$ | 91% | 81:19 |
| **3** | **1,2-DFB** | **80%** | **85:15** |
| 4 | PhMe | 83% | 81:19 |
| 5 | MeCN | 83% | 52:48 |

1,2-DFB = 1,2-difluorobenzene.

Alternative (*S*)-BINAM derived bis-urea catalysts were subsequently examined. (*S*)-BINAM derived tetradentate bis-urea (*S*)-**2.43a** resulted in a 74% yield of (*S*,*S*)-**2.47a**, but with significantly decreased enantioselectivity at only 58:42 e.r. (**Table 2.13**, entry 2), highlighting the crucial effects of *N*-alkylation. A smaller *N*-alkyl group with catalyst (*S*)-**2.43c** maintained a good 80% yield but resulted in a decreased 83:17 e.r. (**Table 2.13**, entry 3).

**Table 2.13** Catalyst optimisation.

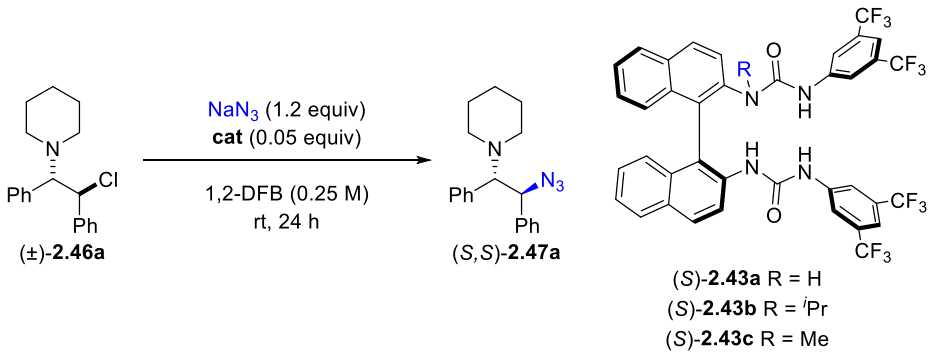


| entry | cat | yield | e.r. |
|---|---|---|---|
| 1 | (*S*)-**2.43a** | 74% | 58:42 |
| **2** | **(*S*)-2.43b** | **80%** | **85:15** |
| 3 | (*S*)-**2.43c** | 80% | 83:17 |

1,2-DFB = 1,2-difluorobenzene.

Enantioselectivity could be increased by reducing the temperature, although this required a higher catalyst loading, azide loading, and a longer reaction time to achieve full conversion for analysis. Use of (*S*)-**2.43b** with $NaN_3$ (2.4 equiv) at -20 °C for 72 h yielded the desired (*S,S*)-**2.47a** product in 74% yield and 93.5:6.5 e.r. (**Table 2.14**, entry 2). A control experiment utilising tetrabutylammonium azide as a soluble azide source resulted in racemic product (**Table 2.14**, entry 3), highlighting the need for an insoluble nucleophile source for enantioselective HB-PTC.

**Table 2.14** Additional reaction optimisation.

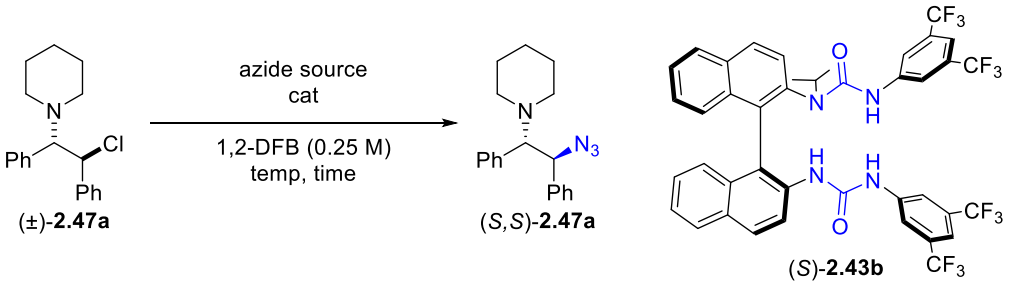


| entry | cat | azide source | temp | time (h) | yield | e.r. |
|---|---|---|---|---|---|---|
| 1 | (*S*)-**2.43b** (0.05 equiv) | $NaN_3$ (1.2 equiv) | rt | 24 | 80% | 85:15 |
| **2** | **(*S*)-2.43b (0.1 equiv)** | **$NaN_3$ (2.4 equiv)** | **-20 °C** | **72** | **74%** | **93.5:6.5** |
| 3[a] | (*S*)-**2.43b** (0.05 equiv) | $Bu_4N{\cdot}N_3$ (1.2 equiv) | rt | 24 | 90% | 50:50 |

[a]Yield determined by NMR with $Ph_3CH$ (0.5 equiv) internal standard, e.r. determined after prep TLC. 1,2-DFB = 1,2-difluorobenzene.

The optimised conditions were successfully applied to a range of *meso*-aziridinium precursors possessing a variety of unprotected nitrogen heterocycles (**Scheme 2.13**). No measures to avoid moisture or oxygen were found necessary to ensure reproducibility. Products containing important saturated heterocycles commonly found in pharmaceuticals[75] including substituted piperidines (*S,S*)-**2.47a-c**, pyrrolidine (*S,S*)-**2.47d**, morpholine (*S,S*)-**2.47e**, piperazine (*S,S*)-**2.47f-g**, and tetrahydroisoquinoline (*S,S*)-**2.47h** motifs were synthesised in good yields and enantioselectivities. Unsymmetrically substituted amine derivatives (*S,S*)-**2.47h-i** were also successfully produced in this reaction, despite the possibility for formation of two diastereomeric *meso*-aziridinium intermediates. The synthesis of azidated analogues of

bioactive *N*-methyl-D-aspartate receptor antagonists diphenidine[73] (*S*,*S*)-**2.47a**, MT-45[74] (*S*,*S*)-**2.47f**, and lefetamine[73] (*S*,*S*)-**2.47j** were achieved in good yields and enantioselectivities.

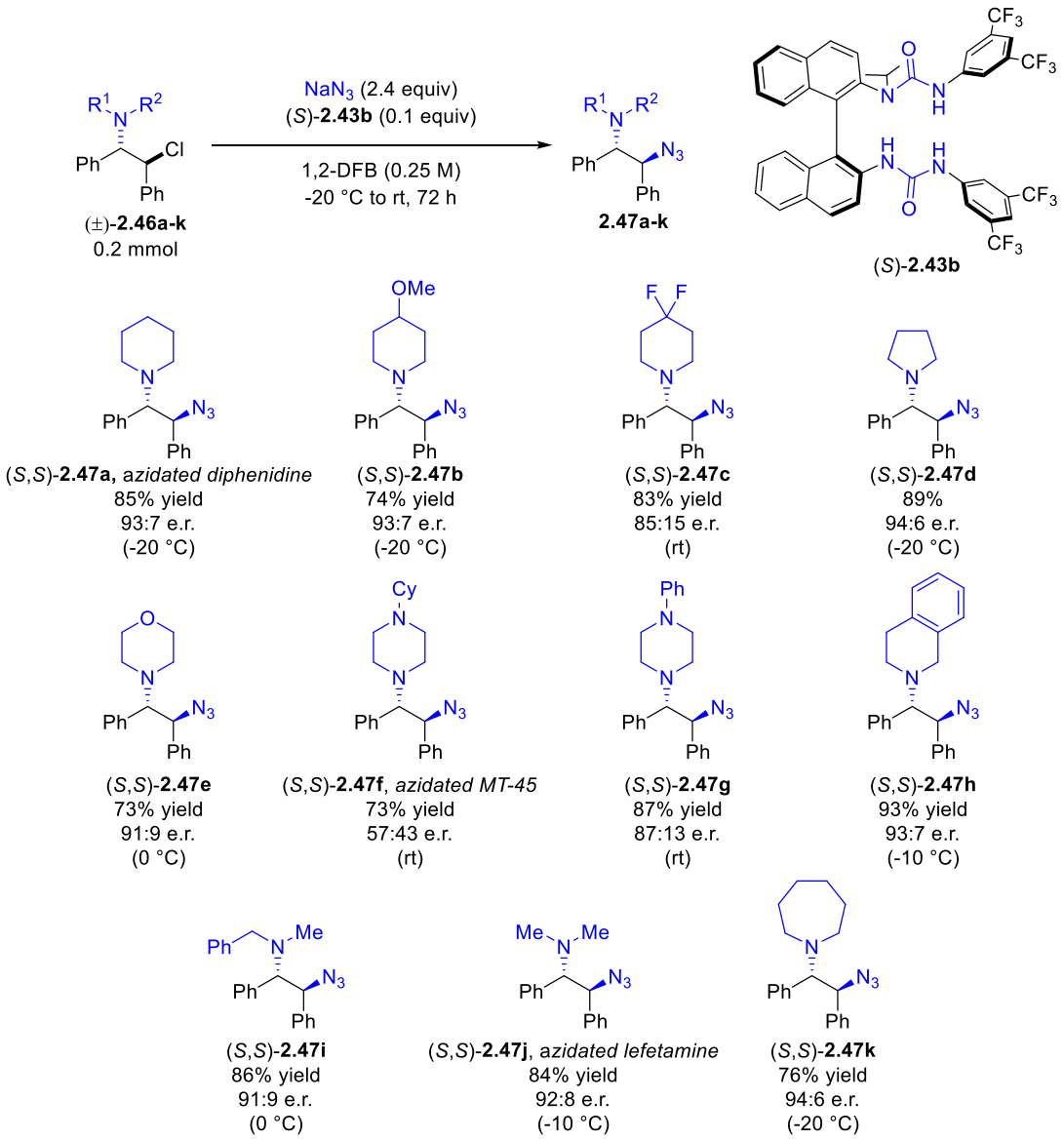


**Scheme 2.13** Substrate scope of amines. Yields are mean of two individual runs. [a]Absolute configuration of major enantiomer not determined. Synthesis of (*S*,*S*)-**3.16h** and (*S*,*S*)-**3.16j** conducted with Dr. M. A. Horwitz.

Additional substrates with variations of the stilbene scaffold were subsequently examined (**Scheme 2.14**). The reaction was found to be tolerant of *meta*- and *para*-halogen substituents ((*S*,*S*)-**2.47l**,**m**,**o**), trifluoromethyl groups ((*S*,*S*)-**2.47n**,**q**), and larger alkyl groups ((*S*,*S*)-**2.47p**). Moving beyond the stilbene scaffold, the bis-pyridyl azide (*S*,*S*)-**2.47r** could be obtained in good yield and enantioselectivity. Although the challenging cycloalkyl amino-chloride

successfully furnished product (*S*,*S*)-**2.47s** in high yield, the enantiomeric ratio remained low, highlighting an area for further improvement.

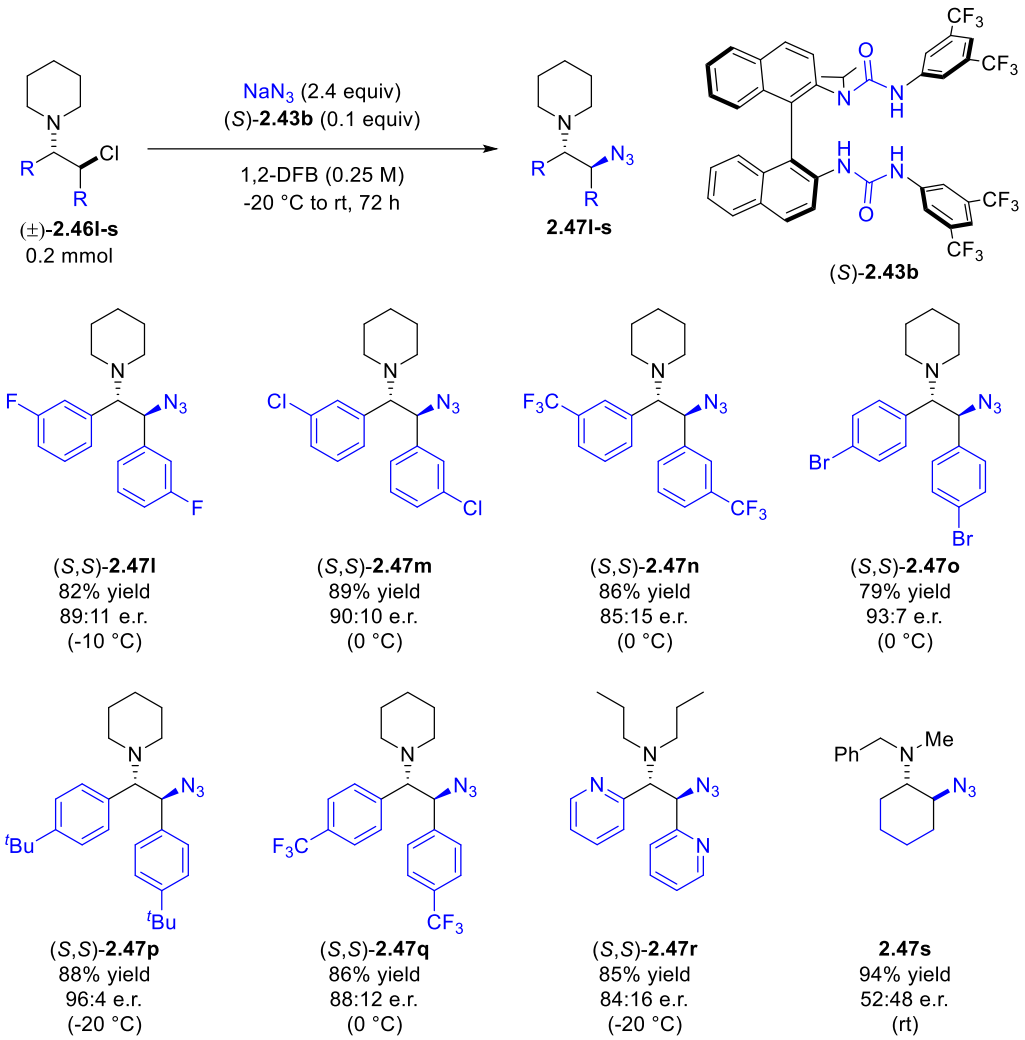


**Scheme 2.14** Substrate scope of backbone. Yields are mean of two individual runs. Absolute configuration of (*S*,*S*)-**2.47s** not determined.

To demonstrate the scalability of this methodology, selected substrates repeated on a larger scale. Conducting a reaction with 0.5 g of substate (±)-**2.46o** containing two aryl bromides afforded product in 69% yield and 98.5:1.5 e.r. after a single recrystallisation (**Scheme 2.15A**). The absolute configuration of (*S*,*S*)-**2.47o** was determined by X-ray crystallography and was used to assign the absolute configuration of (*S*,*S*)-**2.47a-n** and (*S*,*S*)-**2.47p-r** by analogy. Conducting a reaction with 1.5 g (±)-**2.46a** produced 1.23 g of (*S*,*S*)-**2.47a** in 80% yield and 93.5:6.5 e.r. (**Scheme 2.15B**). No measures to avoid moisture or oxygen were found necessary at these larger scales, emphasizing the operationally simple nature of reactions performed

under HB-PTC. Reduction of azide (*S*,*S*)-**2.47a** to the corresponding amine by hydrogenation and subsequent bis-alkylation with 1,5-dibromopentane allowed for the synthesis of enantioenriched Kv1.5 blocker (*S*,*S*)-**2.48**[71,72] from (±)-**2.46a** in 93.5:6.5 e.r.

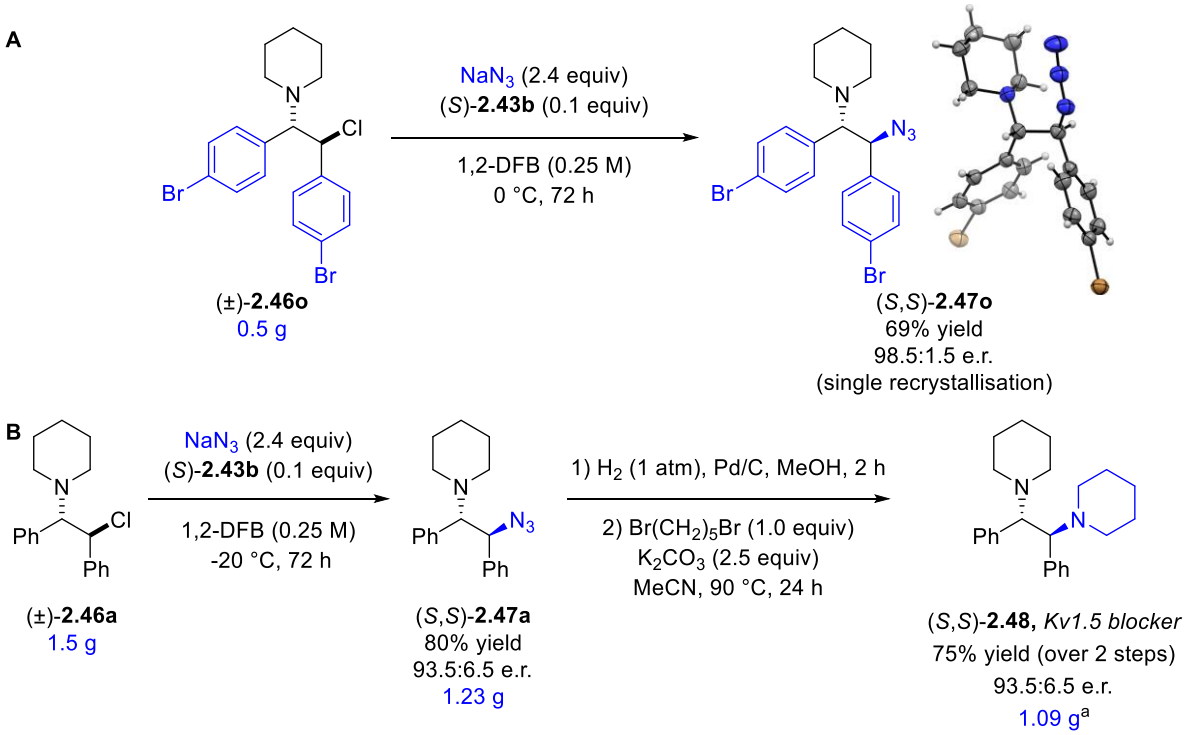


**Scheme 2.15** (A) Scale-up and determination of absolute configuration. 93:7 e.r. prior to recrystallisation. (B) Scale-up and derivatization to Kv1.5 blocker (*S*,*S*)-**2.48**. [a]From 1.29 g (*S*,*S*)-**2.47a**. Displacement ellipsoid plots drawn at 50% probability level. X-ray crystallography data collection and analysis by Dr. K. E. Christensen. 1,2-DFB = 1,2-difluorobenzene.

This development of this reaction represents the first application of HB-PTC to a non-fluoride nucleophile to produce products in high yields and enantiomeric ratios up to the gram scale. Although more investigations are necessary to further understand the reaction mechanism, it is likely a key step involves the solubilisation of sodium azide mediated by the urea catalyst.

## 2.5 Mechanistic studies

### 2.5.1 Achiral HB-PTC with Schreiner's urea

Initial mechanistic studies into the synthesis of β-aminoazides with sodium azide under HB-PTC focused on the achiral transformation with model substrate (±)-**2.46a** and Schreiner's urea **2.41a** as catalyst. Minor modifications to the optimised conditions including performing

the reaction at room temperature and addition of triphenylmethane as internal standard enabled practical study of this reaction (**Scheme 2.16**).

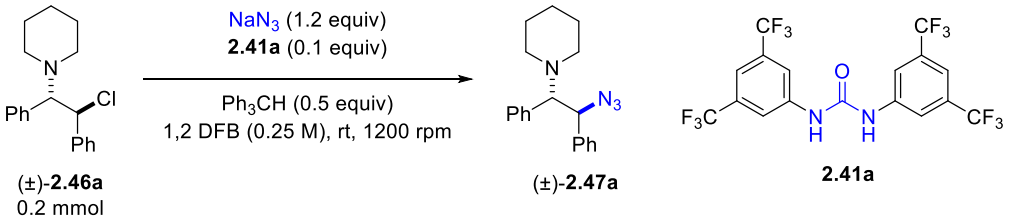


**Scheme 2.16** Standard conditions of the achiral reaction studied. 1,2-DFB = 1,2-difluorobenzene.

Monitoring the rate of reaction of heterogenous systems presents practical challenges due to the strong influence of mass transfer processes on reaction rate, such as stirring speed or removal of aliquots for sampling.[76] *In situ* IR was utilised to enable consistent data collection whilst maintaining a consistent stirring and minimising errors introduced from physical disturbances of the reaction mixture. Reference spectra of (±)-**2.46a** and (±)-**2.47a** revealed an easily discernible absorbance at 2100 $cm^{-1}$ corresponding to product (±)-**2.47a**, but no distinguishing signals for substrate (±)-**2.46a** (**Figure 2.30**). As a result, only data related to formation of product could be directly obtained. Although it was not possible to monitor the change in substrate concentration during the reaction, analysis of incomplete reaction mixtures and crude material at the end of the reaction by quantitative $^{1}H$ NMR typically indicated a mass balance of >99% consisting of only (±)-**2.46** and (±)-**2.47**. Hence side reactions of substrate were considered negligible, and the concentration of substrate was calculated by the difference from the product concentration.

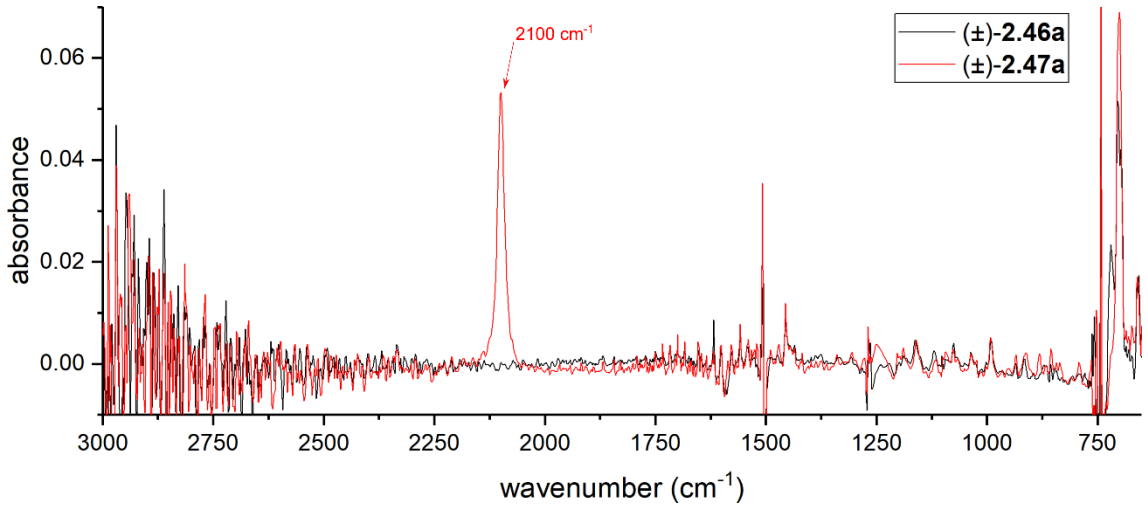


**Figure 2.30** Overlay of the IR spectrum of (±)-**2.46a** and (±)-**2.47a** in 1,2-difluorobenzene taken with a silicon tipped probe.

*In situ* IR spectroscopy utilised a Mettler Toledo ReactIR 15 instrument, equipped with a silicon composite sensor. Extremely careful setup was required to maintain consistency and mitigate the disturbance caused by introducing the probe (**Figure 2.31**). The dimensions and shape of the reaction vessel was consistent with the vessels used during the scope, albeit with modifications to remove the side-arm and reduce the head height. The procedure to monitor this reaction commenced by pre-stirring a suspension of sodium azide and catalyst in half the required solvent with the IR probe for 15 min. At this point, the reaction was initiated by injection of a stock solution containing substrate and internal standard. The IR probe was then carefully raised as high as possible whilst ensuring its position remained as central as possible to minimise both its impact on stirring and any trapping of solution along the walls of the reaction vessel during the reaction. This protocol was complex and more practically demanding than procedure for the reaction scope but was necessary to achieve reproducible results and full conversion. The suspension appeared consistent and was considered a homogenous mixture of both sodium azide and sodium chloride with proportions that vary over time.

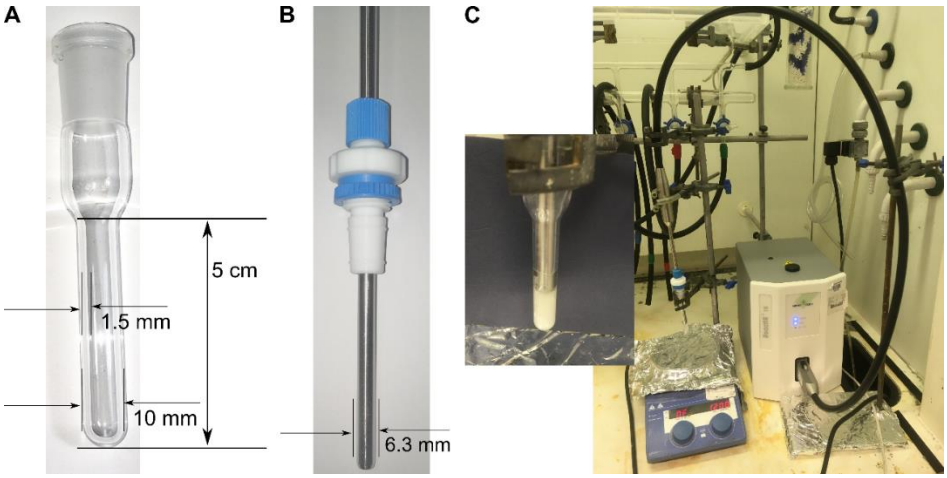


**Figure 2.31** (A) Dimensions of reaction vessel used. (B) Dimension of silicon composite probe used. (C) Reaction setup and inset with stirred reaction mixture at 1200 rpm under standard conditions.

This setup was initially utilised to monitor the model reaction with catalyst **2.41a**, as well as the background reaction of sodium azide and (±)-**2.46a** in the absence of catalyst (**Figure 2.32**). The model reaction with (±)-**2.46a** achieved full conversion after 2 h and produced consistent data with minor variations across three independent trials. In contrast, the background reaction formed (±)-**2.47a** at a much slower rate and exhibited large variations when repeated. Although **2.41a** was not fully soluble in 1,2-difluorobenzene under these conditions, an analysis comparing the initial rate of these two transformations was undertaken to gain a preliminary understanding of this system. A 9$^{th}$ grade polynomial was fit to the mean of each data set, then differentiated to obtain the rate. Comparing the rate of the reaction 20% conversion suggested the catalysed reaction with **2.41a** was approximately 70-times faster than the uncatalysed reaction. This stark difference could be accounted for by the poor solubility of sodium azide in the 1,2-difluorobenzene solvent and these results are consistent with this transformation occurring under HB-PTC.

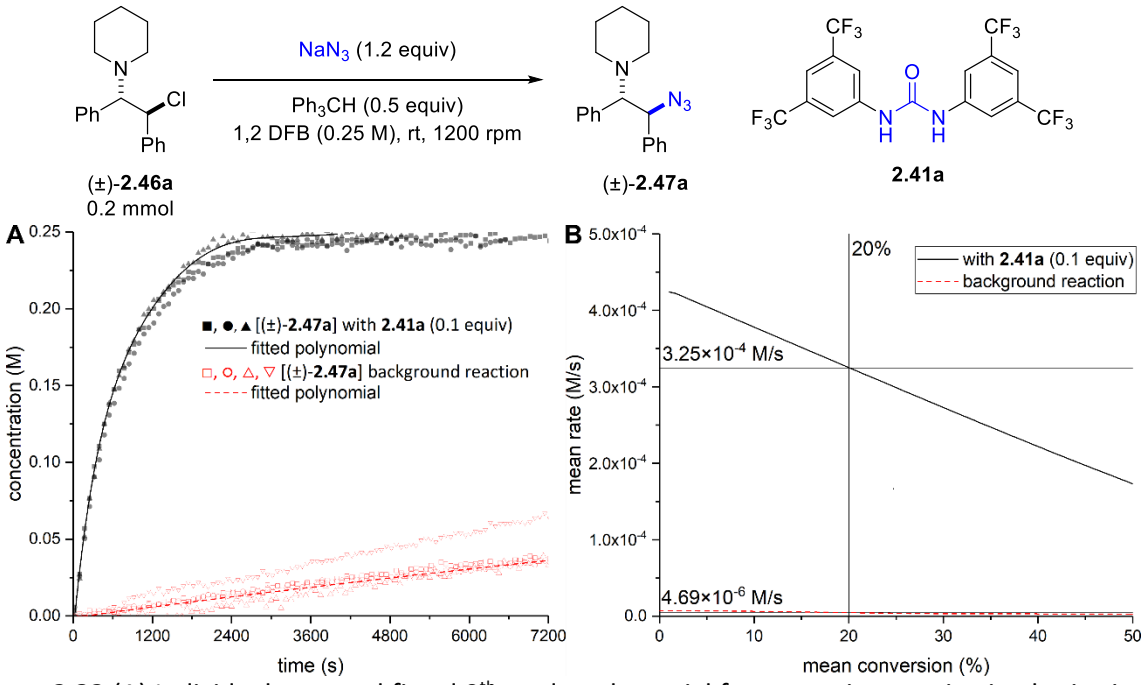


**Figure 2.32** (A) Individual runs and fitted 9th grade polynomial from reaction monitoring by *in situ* IR. (B) Change in reaction rate plot against conversion, and the relative reaction rates at 20% conversion. 1,2-DFB = 1,2-difluorobenzene. Analysis of reaction rates conducted with Dr. F. Ibba.

These reactions involve a chloride leaving group and it is reasonable to propose the presence of Schreiner's urea **2.41a** coordinated to chloride in these systems. Titration of **2.41a** with chloride revealed an association in solution following a 2:1 model with higher association constants than the corresponding values for azide (**Table 2.15**). These values suggest the complex of **2.41a** and chloride is likely to be relevant when developing a catalytic cycle, either as an intermediate or inhibitor.

**Table 2.15** Comparison of the association constants of azide and chloride with Schreiner's urea **2.41a**.

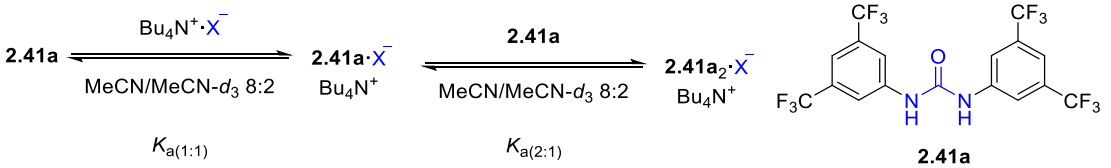


| entry | $X^-$ | $K_{a(1:1)}$ ($M^{-1}$) | $K_{a(2:1)}$ ($M^{-1}$) |
|---|---|---|---|
| 1 | $N_3^-$ | $1.57 \pm 0.06 \times 10^3$ | $7 \pm 3 \times 10^1$ |
| 2 | $Cl^-$ | $4.7 \pm 1.6 \times 10^4$ | $1.7 \pm 0.9 \times 10^2$ |

Titrations conducted at 2 mM, $CH_3CN/CD_3CN$ 8:2, 500 MHz, 298 K. Values are the mean of 3 independent replicas calculated with BindFit v0.5,[64] error is the standard deviation.

The studies with Schreiner's urea **2.41a** established a practical and reproducible setup for data collection of HB-PTC reactions. The data collected is consistent with **2.41a** acting to improve a reaction apparently limited by insolubility of sodium azide. Due to the limitations

predominantly involving catalyst solubility, further studies with **2.41a** was not pursued. In combination with the solid state and solution studies, it is plausible these achiral reactions are under HB-PTC and involve a hydrogen bond mediated phase-transfer process.

### 2.5.2 Uncatalysed azidation with sodium azide

The background reaction exhibited large inconsistencies across multiple trials compared to the catalysed reaction and additional investigations to rationalise these differences were undertaken (**Figure 2.33A**). An apparent slight increase in the initial reaction rate was observed upon close examination of the concentration profiles and suggested the background reaction was not a simple first order transformation. In addition, deviations in concentration profiles between individual trials may reflect a high sensitivity towards initial conditions.

Consideration of a dissolution process could explain the wide variations between trials and the apparent increased initial reaction rate (**Figure 2.33B**). The pre-stirring may result in an initial increased quantity of azide in solution and an increased initial reaction rate. As the reaction continues, if the reaction of azide in solution is faster than its dissolution, the reaction rate would decrease until reaching a dynamic equilibrium. The dissolution process can be highly dependent on small variations to moisture, temperature, or azide granularity, leading to the wide variety of concentration profiles observed.

This hypothesis was probed by conducting the background reaction with 1,2-difluorobenzene (1,2-DFB) pre-saturated with water. Karl Fischer calorimetry (KFC) determined typical batches of ambient 1,2-DFB contained *ca*. 100 ppm of water, rising to *ca*. 1000 ppm when saturated with water. Conducting the background reaction with 1,2-DFB saturated with water resulted in consistently slower concentration profiles. These reactions were also visibly different, with the azide suspension appearing much less fine and coming together in small clumps on the sides of the reaction vessel. The increased cohesion between azide particulates may result in a reduced availability in solution and the reduced reaction rate observed (**Figure 2.33C-D**).

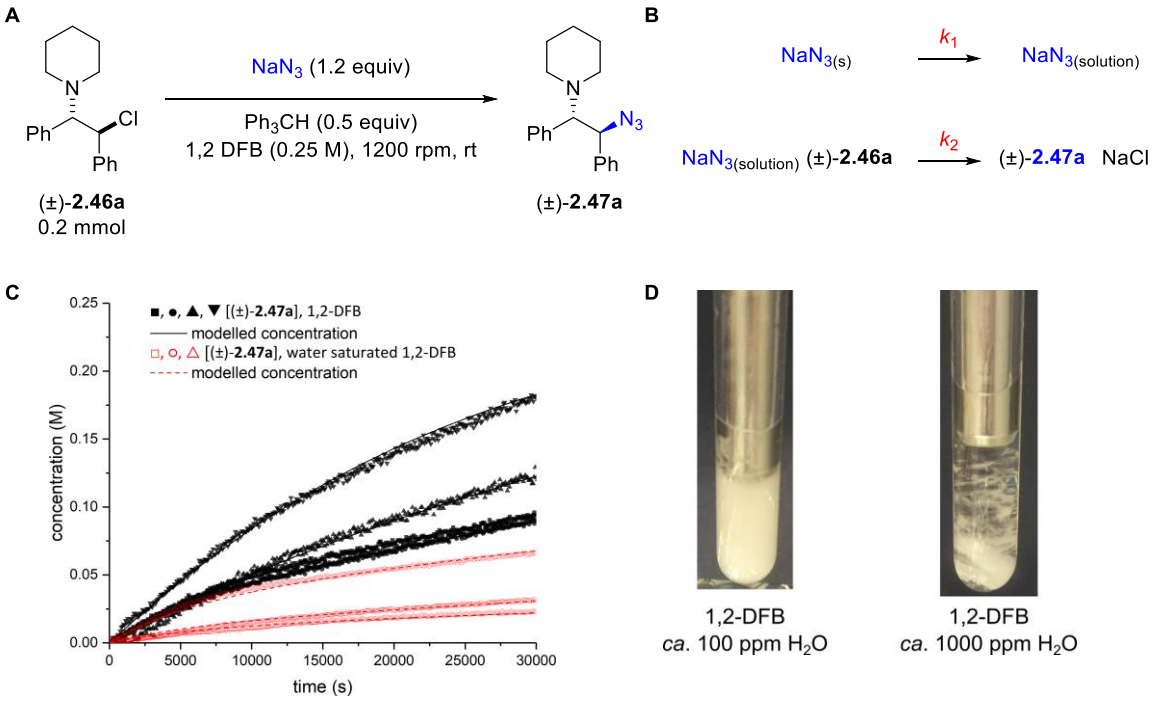


**Figure 2.33** (A) Uncatalysed background reaction studied. (B) Proposed kinetic model. (C) Concentration profiles of the background reaction with different quantities of water in the 1,2-DFB used and the modelled rate based on the kinetic model. (D) Differences in the appearance of the transformation when conducted with 1,2-DFB saturated with water. 1,2-DFB = 1,2-difluorobenzene. Analysis and modelling of kinetic data were performed by Y. Gao and Prof. G. C. Lloyd-Jones.

The proposed kinetic model led to a good fit to each run by adjusting the rate of dissolution and the initial soluble azide quantities whilst keeping the rate of reaction of sodium azide and (±)-**2.46a** ($k_2$) constant at 6.45 × $10^{-4}$ $M^{-1}$ $s^{-1}$ (**Table 2.16**, entry 1-7). Since the experiments conducted with 1,2-DFB saturated with water were likely to cause reduced availability of sodium azide, a model that kept $k_1$ and $k_2$ constant at 8.03 × $10^{-6}$ $s^{-1}$ and 6.45 × $10^{-4}$ $M^{-1}$ $s^{-1}$ respectively whilst adjusting the initial concentration of sodium azide was explored, and produced good fits between experimental and calculated data (**Table 2.16**, entry 8-10). The necessity of these adjustments is consistent with the variations experienced during the practical setup for conducting the background reaction and suggest this model for the background reaction is applicable and valid.

**Table 2.16** Rate constants and initial azide quantities in solution used to fit the model to experimental data.

| entry | $H_2O$ content (ppm) | $k_1$ ($s^{-1}$) | $k_2$ ($M^{-1}$ $s^{-1}$) | initial $[NaN_{3(solution)}]$ (M) | $[NaN_{3(s)}]$ (M) |
|---|---|---|---|---|---|
| 1 | *ca*. 100 | $8.03 \times 10^{-6}$ | $6.45 \times 10^{-4}$ | 0.0488 | 0.3 |
| 2 | | $8.03 \times 10^{-6}$ | | 0.0429 | |
| 3 | | $17.32 \times 10^{-6}$ | | 0.0368 | |
| 4 | | $35.97 \times 10^{-6}$ | | 0.0593 | |
| 5 | *ca*. 1000 | $2.11 \times 10^{-6}$ | $6.45 \times 10^{-4}$ | 0.0167 | 0.3 |
| 6 | | $4.45 \times 10^{-6}$ | | 0.0406 | |
| 7 | | $1.30 \times 10^{-6}$ | | 0.0133 | |
| 8 | *ca*. 1000 | $8.03 \times 10^{-6}$ | $6.45 \times 10^{-4}$ | 0.0154 | 0.0945 |
| 9 | | | | 0.0384 | 0.1893 |
| 10 | | | | 0.0125 | 0.0591 |

Analysis and modelling of kinetic data were performed by Y. Gao and Prof. G. C. Lloyd-Jones.

### 2.5.3 Understanding enantioselective HB-PTC with sodium azide

Further mechanistic studies into the synthesis of β-aminoazides with sodium azide under HB-PTC focused on the enantioselective transformation with model substrate (±)-**2.46a** and chiral catalyst (*S*)-**2.43b**. The improved solubility of (*S*)-**2.43b** and the generation of enantioselectivity enabled collection of data for both the reaction rate and enantioselectivity under multiple conditions to provide insights into this enantioselective transformation.

A titration of (*S*)-**2.43b** with chloride suggested coordination with the same 2:1 model as azide and higher association constants was likely, similar to observations with **2.41a** (**Scheme 2.17A**). The crystal structure used to confirm absolute configuration also established relative configuration and provided additional evidence for this transformation to proceed by a *meso*-aziridinium intermediate (**Scheme 2.17B**). A non-linear effects study found a linear relationship between the enantiomeric excess of the catalyst and the enantiomeric excess of the product (**Scheme 2.17C**). This suggests that one molecule of catalyst (*S*)-**2.43b** is involved with one molecule of substrate (±)-**2.46a** in the enantiodetermining step, which is consistent with existing HB-PTC transformations.[53,54]

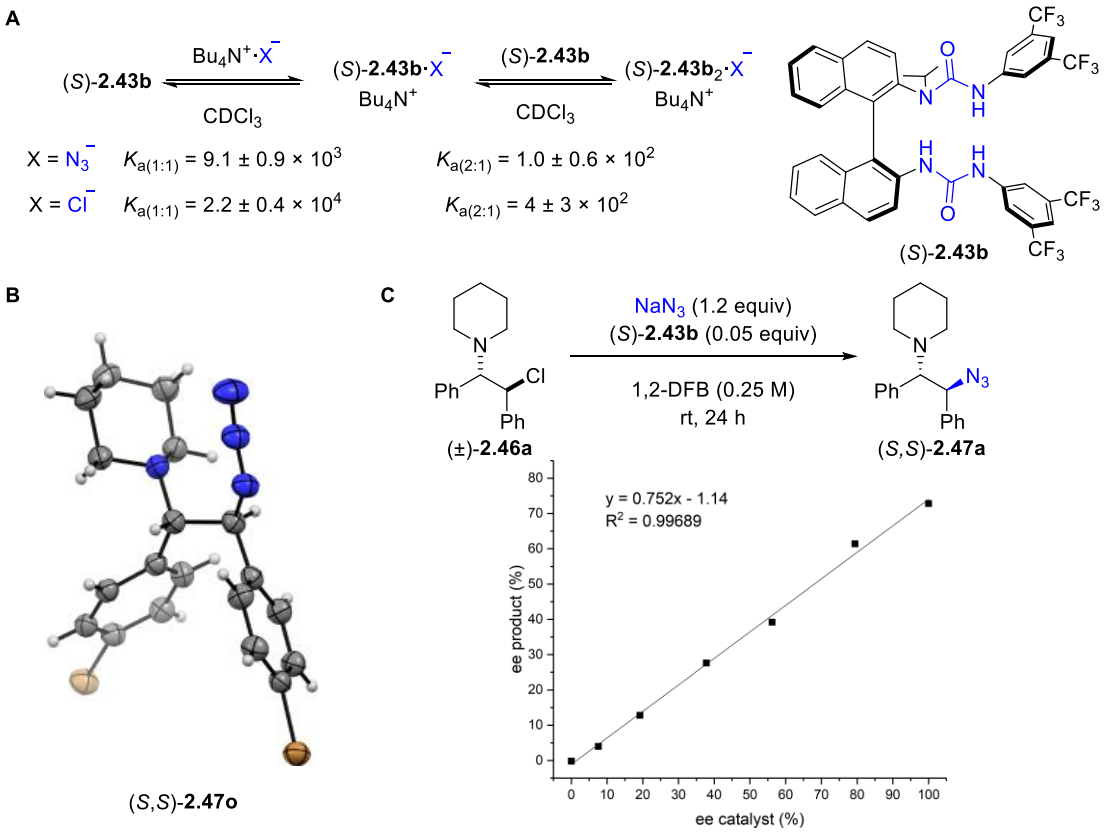


**Scheme 2.17** (A) Chloride titration with (*S*)-**2.43b**. Titrations conducted at 2 mM, $CDCl_3$, 500 MHz, 298 K. Values are the mean of 3 independent replicas calculated with BindFit v0.5,[64] error is the standard deviation. (B) Crystal of (*S*,*S*)-**2.47o** used to determine absolute configuration. Displacement ellipsoid plots drawn at 50% probability level. X-ray crystallography data collection and analysis was performed by Dr. K. E. Christensen. (C) Non-linear effect Average of two runs, major enantiomer of **2.43b** in scalemic mixtures is (*S*). Non-linear effect investigation was conducted with Dr. M. A. Horwitz. 1,2-DFB = 1,2-difluorobenzene.

Further insights into this mechanism were provided by monitoring the model transformation with (*S*)-**2.43b** by *in situ* IR. The setup from the achiral ReactIR experiments were utilised for these studies. However, additional investigations into the physical set up including stirring speed reaction vessel shape, and influence of water were undertaken to understand the influence of the mass transfer process on reaction rate and enantioselectivity, and to ensure the measured reaction rates were predominantly due to the intrinsic rate of the reaction.

A systematic study of stirring speeds provided further confidence in the set up used for data collection but highlighted the low tolerances and high sensitivity to small changes of this system. Conducting the model reaction with 0.1 equiv catalyst and stirring speeds from 1200 down to 400 rpm revealed an improved consistency and higher reaction rate at higher stirring speeds (**Figure 2.34A**). Similar line shapes and only a small reduction in rate was observed

between 1200 and 1000 rpm with 0.1 equiv catalyst (**Figure 2.34A**) or 0.0125 equiv catalyst (**Figure 2.34B**). Since all experiments with identical quantities of catalyst produced product in consistent enantiomeric ratios independent of stirring, 1200 rpm was considered sufficient for ensuring the data collected was predominantly due to the intrinsic rate of the reaction.

Examination of the reaction vessel highlighted the need for a consistent setup (**Figure 2.34C**). A set of custom reaction vessels fabricated with thinner walled glass resulted a small deviation in the stir bar angle in the vessel. When the reaction was monitored with this setup, the rate was consistently slower and less reproducible. This is suspected to deviate from the change in stir bar angle affecting the mass transfer process and rate of reaction.

Finally, a reaction conducted with water saturated 1,2-DFB with *ca*. 1000 ppm $H_2O$ displayed negligible differences in rate and enantiomeric excess compared to the reactions conducted with the standard batch of 1,2-DFB with *ca*. 100 ppm $H_2O$ (**Figure 2.34D**).

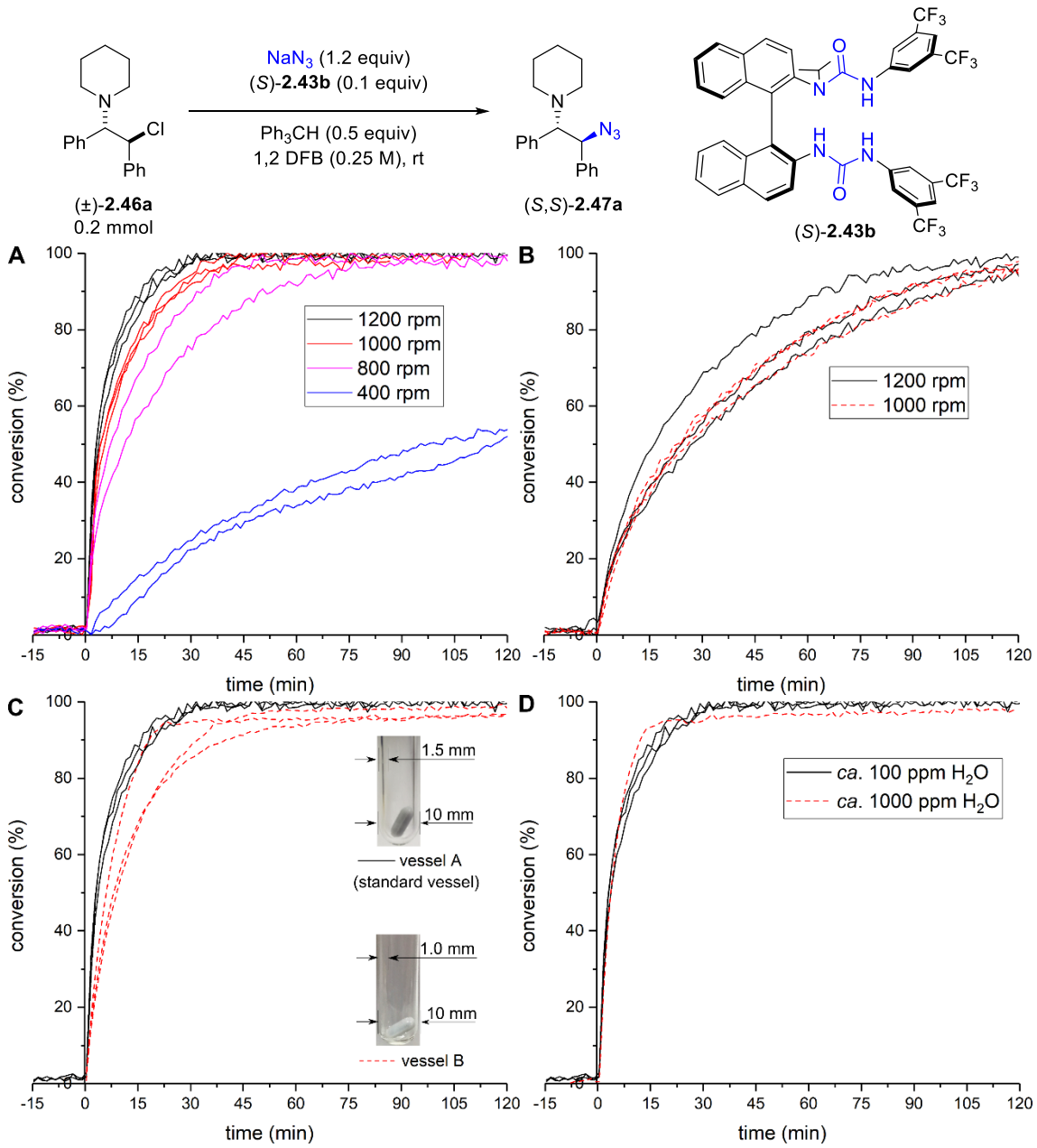


**Figure 2.34** (A) Conversion at 1200, 1000, 800, and 400 rpm with 0.1 equiv (*S*)-**2.43b**. (B) Conversion at 1200 and 1000 rpm with 0.0125 equiv (*S*)-**2.43b**. (C) Conversion with alternate reaction vessel and 0.1 equiv (*S*)-**2.43b** and inset demonstrating the reaction vessels and angle of the 8×3 mm stir bar used. (D) Conversion at 1200 rpm with 1,2-DFB saturated with different quantities of water. 1,2-DFB = 1,2-difluorobenzene.

With full confidence in a robust and reproducible setup, the rate of formation of product (*S*,*S*)-**2.7a** was analysed as a function of the initial concentration of starting material (±)-**2.46a**, catalyst (*S*)-**2.3b**, and the quasi-homogenous mixture of sodium azide and sodium chloride. Eight different initial starting conditions were run in triplicate and the enantiomeric ratio of product was measured for each set of conditions. These experiments, along with the previous investigations into the background reaction, the titration data of (*S*)-**2.43b** with chloride, the

knowledge gained from the X-ray structure of (*S*,*S*)-**2.47o**, and the lack of any non-linear effect, enabled the development and rationalisation of an empirical model for the reaction kinetics. Key assumptions for the proposed mechanism included that only a small proportion of substrate is ionised, the catalyst-anion intermediates are at very low concentration, and the mixture of sodium azide sodium chloride is evenly distributed. Two kinetically indistinguishable models were found to give good fits with the experimental data.

In both models, the formation of product was proposed to involve initial substrate autoionization ($K_i$) and dissociation into separated *meso*-aziridinium and chloride anions by intra-particle diffusion ($K_{IPD}$) (**Scheme 2.18**).

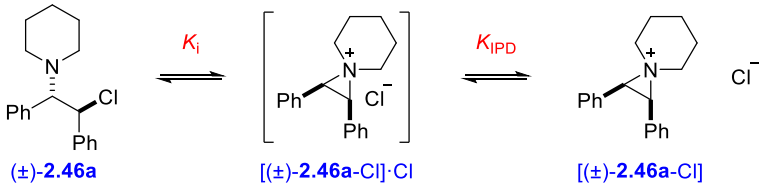


$$K_1 = K_{IPD}K_i \quad (2.1)$$

$$K_{IPD}\,[[(\pm)\text{-}\mathbf{2.46a}\text{-Cl}]\cdot Cl] = [[(\pm)\text{-}\mathbf{2.46a}\text{-Cl}]][Cl^-] \quad (2.2)$$

$$[[(\pm)\text{-}\mathbf{2.46a}\text{-Cl}]] = [Cl^-] = \frac{\sqrt{K_1^2 + 4K_1[(\pm)\text{-}\mathbf{2.46a}]_0} - K_1}{2} \quad (2.3)$$

**Scheme 2.18** Ionisation and separation of substrate (±)-**2.46a** to form meso-aziridinium [(±)-**2.46a**-Cl]. IPD = intraparticle diffusion. Kinetic data analysis and modelling was performed by Y. Gao and Prof. G. C. Lloyd-Jones.

In addition, both proposed mechanisms involved generation of the catalyst (*S*)-**2.43b** coordinating to either azide or chloride anion at, near, or in the phase boundary (**Scheme 2.19**). The solid was considered a mixture of sodium azide and sodium chloride, with proportions that vary systematically as the reactions evolve. The azide bound mole fraction is defined by $\chi_{N3}$.

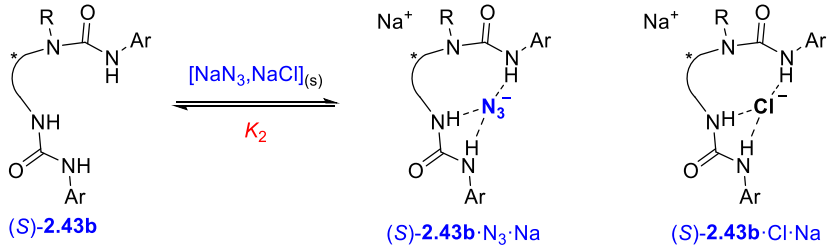


$$K_2[(S)\text{-}\mathbf{2.43b}][[NaN_3,NaCl]] = [[(S)\text{-}\mathbf{2.43b}\cdot N_3\cdot Na,(S)\text{-}\mathbf{2.43b}\cdot Cl\cdot Na]] \quad (2.4)$$

$$\chi_{N3} = \frac{1}{1 + \frac{[NaCl]}{K_2[NaN_3]}} \quad (2.5)$$

**Scheme 2.19** Generation of (*S*)-**2.43b**·$N_3$·Na from (*S*)-**2.43b** and the solid sodium azide and sodium chloride mixture. Kinetic data analysis and modelling was performed by Y. Gao and Prof. G. C. Lloyd-Jones.

The (*S*)-**2.43b**·$N_3$·Na complex forms an ion pair with the *meso*-aziridinium either by direct exchange with the sodium (**Scheme 2.20A**), or by extrusion of sodium chloride and recombination with the *meso*-aziridinium intermediate (**Scheme 2.20B**). These two pathways are kinetically equivalent with identical rate equations, and both result in formation of the (*S*)-**2.43b**·$N_3$·[(±)-**2.46a**-Cl] catalyst-azide-aziridinium ion pair. The (*S*)-**2.43b**·$N_3$ and *meso*-aziridinium ion pair finally react to form enantioenriched (*S*,*S*)-**2.47a** and regenerate (*S*)-**2.43b**.

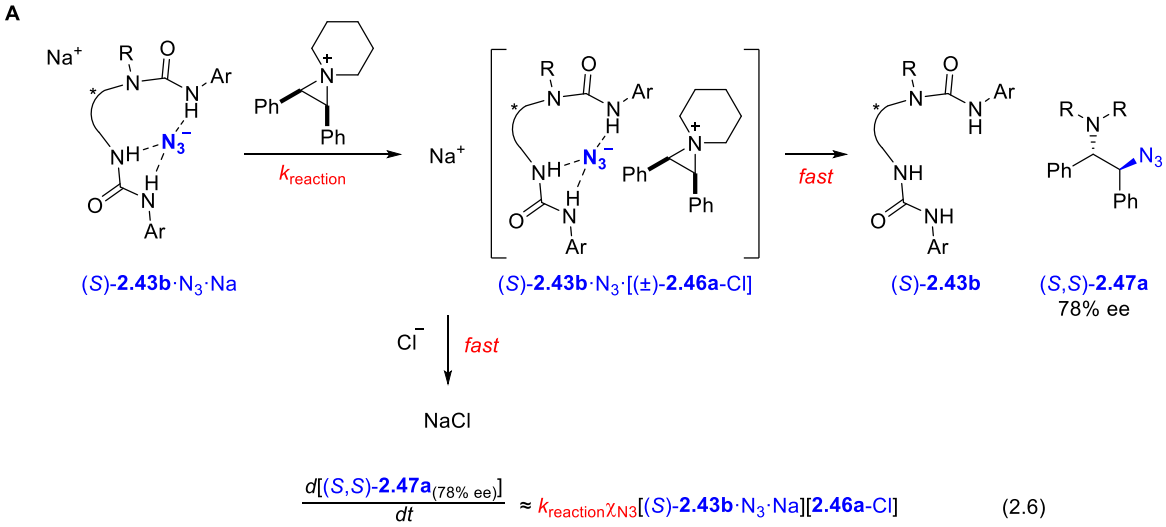


$$\frac{d[(S,S)\text{-}\mathbf{2.47a}_{(78\%\ ee)}]}{dt} \approx k_{reaction}\chi_{N3}[(S)\text{-}\mathbf{2.43b}\cdot N_3\cdot Na][\mathbf{2.46a}\text{-}Cl] \qquad (2.6)$$

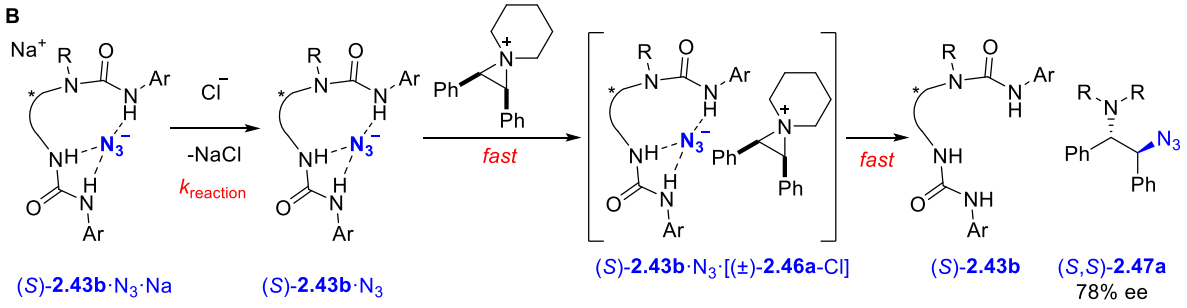


$$\frac{d[(S,S)\text{-}\mathbf{2.47a}_{(78\%\ ee)}]}{dt} \approx k_{reaction}\chi_{N3}[(S)\text{-}\mathbf{2.43b}\cdot N_3\cdot Na][Cl^-] \qquad (2.7)$$

**Scheme 2.20** (A) Formation of the (*S*)-**2.43b**·$N_3$·[(±)-**2.46a**-Cl] ion pair by initial cation exchange. (E) Formation of the (*S*)-**2.43b**·$N_3$·[(±)-**2.46a**-Cl] ion pair by initial formation of (*S*)-**2.43b**·$N_3$ then recombination. Kinetic data analysis and modelling was performed by Y. Gao and Prof. G. C. Lloyd-Jones.

The rate law associated with these models have kinetic orders of 0.5 in substrate (±)-**2.46a** and 1 in catalyst (*S*)-**2.43b**. As the reaction develops, the increasing presence of chloride results in increased catalyst inhibition. The correct enantioselectivity can be calculated when the racemic background racemic reaction (eqn 2.8) is incorporated (**Table 2.17**). However, the background reaction appeared to behave differently to the background reaction in absence of catalyst; this change may be due to a reduction of soluble azide concentration by (*S*)-**2.43b**.

**Table 2.17** Equations for rate of the background reaction with catalyst, rate of formation of (*S*,*S*)-**2.47a**, rate of formation of (*R*,*R*)-**2.47a**, overall rate, and comparison of calculated and experimentally determined ee.

$$rate_{background\ with\ catalyst} \approx c[(\pm)\text{-}\mathbf{2.46a}]^{0.5} \quad (2.8)$$

$$\frac{d[(S,S)\text{-}\mathbf{2.47a}]}{dt} = [(\pm)\text{-}\mathbf{2.46a}]^{0.5}\left[\frac{0.8882a[(S)\text{-}\mathbf{2.43b}]^1}{1 + \frac{b\{\mathrm{NaCl}\}}{\{\mathrm{NaN_3}\}}} + 0.5c\right] \quad (2.9)$$

$$\frac{d[(R,R)\text{-}\mathbf{2.47a}]}{dt} = [(\pm)\text{-}\mathbf{2.46a}]^{0.5}\left[\frac{0.1118a[(S)\text{-}\mathbf{2.43b}]^1}{1 + \frac{b\{\mathrm{NaCl}\}}{\{\mathrm{NaN_3}\}}} + 0.5c\right] \quad (2.10)$$

$$rate_{overall} = [(\pm)\text{-}\mathbf{2.46a}]^{0.5}\left[\frac{\mathrm{a}[(S)\text{-}\mathbf{2.43b}]_0^1}{1 + \frac{\mathrm{b}([(\pm)\text{-}\mathbf{2.46a}]_0 - [(\pm)\text{-}\mathbf{2.46a}]_\mathrm{t})}{\mathrm{ex}[(\pm)\text{-}\mathbf{2.46a}]_0 + [(\pm)\text{-}\mathbf{2.46a}]_\mathrm{t}}} + \mathrm{c}\right] \quad (2.11)$$

$a = 0.081 \pm 0.018$
$\mathrm{b} = 2.1 \pm 0.9$ mean parameter values
$\mathrm{c} = 1.8 \pm 0.5$

| entry | *a* | *b* | *c* ×10$^5$ | ex | ee (calculated) | ee (measured) |
|---|---|---|---|---|---|---|
| 1 | 0.068 | 2.1 | 1.5 | 0.2 | 76.5 | 78 |
| 2 | 0.081 | 2.3 | 1.3 | 0.2 | 75.9 | 76 |
| 3 | 0.063 | 1.7 | 2.1 | 0.22 | 74.0 | 75 |
| 4 | 0.093 | 2.5 | 1.6 | 0.22 | 70.8 | 72 |
| 5 | 0.075 | 1.2 | 1.5 | 0.22 | 68.2 | 69.5 |
| 6 | 0.077 | 1.4 | 1.6 | 0.2 | 59.1 | 60 |
| 7 | 0.083 | 2.9 | 2.3 | 1.48 | 76.1 | 76 |
| 8 | 0.098 | 2.8 | 2.1 | 0.66 | 76.1 | 76 |

Kinetic data analysis and modelling was performed by Y. Gao and Prof. G. C. Lloyd-Jones.

## 2.6 Conclusions and outlook

The study of achiral hydrogen bonded azide complexes supported the formation of dual hydrogen bonded azide in both solution and solid state. The more acidic urea hydrogen bond donors provided evidence of stronger binding to azide. These studies established the ability for azide to be coordinated by a range of the same hydrogen bond donors in solution and in the solid state, and provided insight into the diverse coordination modes of azide.

Investigations into chiral *N*-alkyl (*S*)-BINAM derived urea (*S*)-**2.43b** bound to azide revealed the formation of 1:1 and 2:1 complexes. A combination of $^1$H-$^1$H NOE interactions, $^1$H-$^{15}$N NOE interactions, $^1$H-$^{15}$N HMBC correlations, and X-ray crystallography was used to elucidate the

structure of the 1:1 complex in both solid state and solution and supported the use of *N*-alkyl (*S*)-BINAM derived catalysts for enantioselective azidation.

An enantioselective azidation reaction under HB-PTC using sodium azide for the synthesis of enantioenriched β-aminoazides was developed and explored. A substrate scope demonstrated nineteen examples up to 94% yield and up to 96:4 e.r. Mechanistic insights notably from kinetic studies provided a catalytic cycle highlighting the ability of the chloride leaving group to also act as an inhibitor. This reaction successfully demonstrated a novel nucleophile was capable of enantioselective synthesis under HB-PTC to produce valuable β-aminoazides and indicate this platform may provide a general method for the synthesis of novel enantioenriched organic products from other alkali metal salts consisting of a nucleophilic anion, such as potassium cyanide.

## 2.7 References


1 P. Griess, *Proc. R. Soc. London*, 1864, **13**, 375–384.

2 T. Curtius, *Berichte der Dtsch. Chem. Gesellschaft*, 1890, **23**, 3023–3033.

3 E. F. V. Scriven and K. Turnbull, *Chem. Rev.*, 1988, **88**, 297–368.

4 S. Bräse and K. Banert, *Organic Azides: Syntheses and Applications*, John Wiley & Sons, Ltd, Chichester, UK, 2009.

5 P.-G. Ding, X.-S. Hu, F. Zhou and J. Zhou, *Org. Chem. Front.*, 2018, **5**, 1542–1559.

6 P. Sivaguru, Y. Ning and X. Bi, *Chem. Rev.*, 2021, **121**, 4253–4307.

7 H. Mitsuya, K. J. Weinhold, P. A. Furman, M. H. St Clair, S. N. Lehrman, R. C. Gallo, D. Bolognesi, D. W. Barry and S. Broder, *Proc. Natl. Acad. Sci.*, 1985, **82**, 7096–7100.

8 E. Bengtsson, E. Börje Holmgren and G. Tunevall, *Scand. J. Infect. Dis.*, 1969, **1**, 71–75.

9 P. P. Geurink, W. A. van der Linden, A. C. Mirabella, N. Gallastegui, G. de Bruin, A. E. M. Blom, M. J. Voges, E. D. Mock, B. I. Florea, G. A. van der Marel, C. Driessen, M. van der Stelt, M. Groll, H. S. Overkleeft and A. F. Kisselev, *J. Med. Chem.*, 2013, **56**, 1262–1275.

10 C. U. Kim, W. Lew, M. A. Williams, H. Liu, L. Zhang, S. Swaminathan, N. Bischofberger, M. S. Chen, D. B. Mendel, C. Y. Tai, W. G. Laver and R. C. Stevens, *J. Am. Chem. Soc.*, 1997, **119**, 681–690.

11 Z. P. Demko and K. B. Sharpless, *Org. Lett.*, 2001, **3**, 4091–4094.

12 M. J. Pearson, *J. Chem. Soc., Perkin Trans. 1*, 1981, 2544–2551.

13 M. G. Núñez, A. J. M. Farley and D. J. Dixon, *J. Am. Chem. Soc.*, 2013, **135**, 16348–16351.

14 E. Saxon and C. R. Bertozzi, *Science*, 2000, **287**, 2007–2010.

15 N. J. Agard, J. A. Prescher and C. R. Bertozzi, *J. Am. Chem. Soc.*, 2004, **126**, 15046–15047.

16 F. Kotzyba-Hibert, I. Kapfer and M. Goeldner, *Angew. Chem. Int. Ed.*, 1995, **34**, 1296–1312.

17 H. H. Jobelius and H.-D. Scharff, in *Ullmann's Encyclopedia of Industrial Chemistry*, Wiley-VCH Verlag GmbH & Co. KGaA, Weinheim, Germany, 2000.

18 US Pat., US5176895 A, 1993.

19 S. Alazet, J. Preindl, R. Simonet-Davin, S. Nicolai, A. Nanchen, T. Meyer and J. Waser, *J. Org. Chem.*, 2018, **83**, 12334–12356.

20 J. Kemsley, Explosion injures University of Minnesota graduate student, http://cenblog.org/the-safety-zone/2014/06/explosion-injures-university-of-minnesota-graduate-student, (accessed 8 August 2018).

21 C. M. Hansen, *Hansen Solubility Parameters*, CRC Press, 2007, vol. 118.

22 S. Yoshikawa, K. Shinzawa-Itoh, R. Nakashima, R. Yaono, E. Yamashita, N. Inoue, M. Yao, M. J. Fei, C. P. Libeu, T. Mizushima, H. Yamaguchi, T. Tomizaki and T. Tsukihara, *Science*, 1998, **280**, 1723–1729.

23 M. J. Fei, E. Yamashita, N. Inoue, M. Yao, H. Yamaguchi, T. Tsukihara, K. Shinzawa-Itoh, R. Nakashima and S. Yoshikawa, *Acta Crystallogr. Sect. D Biol. Crystallogr.*, 2000, **56**, 529–535.

24 S. Iwata, C. Ostermeier, B. Ludwig and H. Michel, *Nature*, 1995, **376**, 660–669.

25 J. N. Bandaria, S. Dutta, S. E. Hill, A. Kohen and C. M. Cheatum, *J. Am. Chem. Soc.*, 2008, **130**, 22–23.

26 Q. Guo, L. Gakhar, K. Wickersham, K. Francis, A. Vardi-Kilshtain, D. T. Major, C. M. Cheatum and A. Kohen, *Biochemistry*, 2016, **55**, 2760–2771.

27 G. Hasnaoui-Dijoux, M. Majerić Elenkov, J. H. Lutje Spelberg, B. Hauer and D. B. Janssen, *ChemBioChem*, 2008, **9**, 1048–1051.

28 M. Majerić Elenkov, I. Primožič, T. Hrenar, A. Smolko, I. Dokli, B. Salopek-Sondi and L. Tang, *Org. Biomol. Chem.*, 2012, **10**, 5063.

29 J. H. Lutje Spelberg, J. E. T. van Hylckama Vlieg, L. Tang, D. B. Janssen and R. M. Kellogg, *Org. Lett.*, 2001, **3**, 41–43.

30 S. H. Kim, J. Lee, G. I. Vargas-Zúñiga, V. M. Lynch, B. P. Hay, J. L. Sessler and S. K. Kim, *J. Org. Chem.*, 2018, **83**, 2686–2693.

31 N.-K. Kim, K.-J. Chang, D. Moon, M. S. Lah and K.-S. Jeong, *Chem. Commun.*, 2007, 3401.

32 I. S. Bushmarinov, O. G. Nabiev, R. G. Kostyanovsky, M. Y. Antipin and K. A. Lyssenko, *CrystEngComm*, 2011, **13**, 2930.

33 B. Dietrich, J. Guilhem, J.-M. Lehn, C. Pascard and E. Sonveaux, *Helv. Chim. Acta*, 1984, **67**, 91–104.

34 E. Kimura, H. Anan, T. Koike and M. Shiro, *J. Org. Chem.*, 1989, **54**, 3998–4000.

35 S. O. Kang, V. W. Day and K. Bowman-James, *Inorg. Chem.*, 2010, **49**, 8629–8636.

36 X. Wang, C. Jia, X. Huang and B. Wu, *Inorg. Chem. Commun.*, 2011, **14**, 1508–1510.

37 J. Esteban, M. Font-Bardia and A. Escuer, *Inorg. Chem.*, 2014, **53**, 1113–1121.

38 A. Escuer, J. Esteban and M. Font-Bardia, *Chem. Commun.*, 2012, **48**, 9777.

39 P. G. Urben, Ed., *Bretherick's Handbook of Reactive Chemical Hazards*, Butterworth-Heinemann Ltd, Oxford, 6th edn., 1999.

40 C. Schneider, *Angew. Chem. Int. Ed.*, 2009, **48**, 2082–2084.

41 Z. Li, M. Fernández and E. N. Jacobsen, *Org. Lett.*, 1999, **1**, 1611–1613.

42 Y. Fukuta, T. Mita, N. Fukuda, M. Kanai and M. Shibasaki, *J. Am. Chem. Soc.*, 2006, **128**, 6312–6313.

43 B. Wu, J. C. Gallucci, J. R. Parquette and T. V. RajanBabu, *Chem. Sci.*, 2014, **5**, 1102–1117.

44 S. Nakamura, M. Hayashi, Y. Kamada, R. Sasaki, Y. Hiramatsu, N. Shibata and T. Toru, *Tetrahedron Lett.*, 2010, **51**, 3820–3823.

45 E. B. Rowland, G. B. Rowland, E. Rivera-Otero and J. C. Antilla, *J. Am. Chem. Soc.*, 2007, **129**, 12084–12085.

46 T. Bellavista, S. Meninno, A. Lattanzi and G. Della Sala, *Adv. Synth. Catal.*, 2015, **357**, 3365–3373.

47 M. Nielsen, W. Zhuang and K. A. Jørgensen, *Tetrahedron*, 2007, **63**, 5849–5854.

48 X. Zhang, J. Ren, S. M. Tan, D. Tan, R. Lee and C. Tan, *Science*, 2019, **363**, 400–404.

49 R. da Silva Gomes and E. J. Corey, *J. Am. Chem. Soc.*, 2019, **141**, 20058–20061.

50 J. Humbrías-Martín, M. C. Pérez-Aguilar, R. Mas-Ballesté, A. Dentoni Litta, A. Lattanzi, G. Della Sala, J. A. Fernández-Salas and J. Alemán, *Adv. Synth. Catal.*, 2019, **361**, 4790–4796.

51 M. Tiffner, L. Stockhammer, J. Schörgenhumer, K. Röser and M. Waser, *Molecules*, 2018, **23**, 1142.

52 S. Jing, MChem thesis, University of Oxford, 2017.

53 G. Pupo, F. Ibba, D. M. H. Ascough, A. C. Vicini, P. Ricci, K. E. Christensen, L. Pfeifer, J. R. Morphy, J. M. Brown, R. S. Paton and V. Gouverneur, *Science*, 2018, **360**, 638–642.

54 G. Pupo, A. C. Vicini, D. M. H. Ascough, F. Ibba, K. E. Christensen, A. L. Thompson, J. M. Brown, R. S. Paton and V. Gouverneur, *J. Am. Chem. Soc.*, 2019, **141**, 2878–2883.

55 D. A. Dows and G. C. Pimentel, *J. Chem. Phys.*, 1955, **23**, 1258–1263.

56 L. Pfeifer, K. M. Engle, G. W. Pidgeon, H. A. Sparkes, A. L. Thompson, J. M. Brown and V. Gouverneur, *J. Am. Chem. Soc.*, 2016, **138**, 13314–13325.

57 A. L. Spek, *J. Appl. Crystallogr.*, 2003, **36**, 7–13.

58 J. Y. C. Lim and P. D. Beer, *Eur. J. Inorg. Chem.*, 2017, **2017**, 220–224.

59 S. V. Rosokha, C. L. Stern, A. Swartz and R. Stewart, *Phys. Chem. Chem. Phys.*, 2014, **16**, 12968–12979.

60 G. Jakab, C. Tancon, Z. Zhang, K. M. Lippert and P. R. Schreiner, *Org. Lett.*, 2012, **14**, 1724–1727.

61 P. M. E. Mancini, A. Terenzani, C. Adam and L. R. Vottero, *J. Phys. Org. Chem.*, 1997, **10**, 849–860.

62 S. J. Pike, E. Lavagnini, L. M. Varley, J. L. Cook and C. A. Hunter, *Chem. Sci.*, 2019, **10**, 5943–5951.

63 E. N. W. Howe, M. Bhadbhade and P. Thordarson, *J. Am. Chem. Soc.*, 2014, **136**, 7505–7516.

64 supramolecular.org, http://supramolecular.org, (accessed 18 September 2019).

65 P. Thordarson, *Chem. Soc. Rev.*, 2011, **40**, 1305–1323.

66 F. Ibba, G. Pupo, A. L. Thompson, J. M. Brown, T. D. W. Claridge and V. Gouverneur, *J. Am. Chem. Soc.*, 2020, **142**, 19731–19744.

67 S. H. Hansen and L. Nordholm, *J. Chromatogr. A*, 1981, **204**, 97–101.

68 R. E. Conrow and W. D. Dean, *Org. Process Res. Dev.*, 2008, **12**, 1285–1286.

69 G. Roagna, D. M. H. Ascough, F. Ibba, A. C. Vicini, A. Fontana, K. E. Christensen, A. Peschiulli, D. Oehlrich, A. Misale, A. A. Trabanco, R. S. Paton, G. Pupo and V. Gouverneur, *J. Am. Chem. Soc.*, 2020, **142**, 14045–14051.

70 J. Mason, in *Multinuclear NMR*, ed. J. Mason, Springer US, Boston, MA, 1987, pp. 335–

367.

71 J. Kajanus, T. Antonsson, L. Carlsson, U. Jurva, A. Pettersen, J. Sundell and T. Inghardt, *Bioorg. Med. Chem. Lett.*, 2019, **29**, 1241–1245.

72 J. Boström, *ACS Med. Chem. Lett.*, 2012, **3**, 769–773.

73 H. Morris and J. Wallach, *Drug Test. Anal.*, 2014, **6**, 614–632.

74 A. Helander, M. Bäckberg and O. Beck, *Clin. Toxicol.*, 2014, **52**, 901–904.

75 E. Vitaku, D. T. Smith and J. T. Njardarson, *J. Med. Chem.*, 2014, **57**, 10257–10274.

76 R. Klaewkla, M. Arend and W. F., in *Mass Transfer - Advanced Aspects*, InTech, 2011.

# 3 Hydrogen Bonding Phase-Transfer Catalysis with Potassium Cyanide

## 3.1 Introduction

### 3.1.1 Organonitriles

The nitrile group is a valuable motif in drug discovery, with numerous medicinally active compounds containing an α-chiral (saxagliptin **3.1**, remdesivir **3.2**) or β-chiral nitrile group (ruxolitinib **3.3**, dienogeset **3.4**) (**Figure 3.1**). Nitriles can act as weak hydrogen bond acceptors or as hydroxyl or carboxyl bioisosteres. In addition, the short geometry and polarisation of the nitrile group allows them to make polar interactions and protrude into small pockets in the binding sites of proteins.[1]

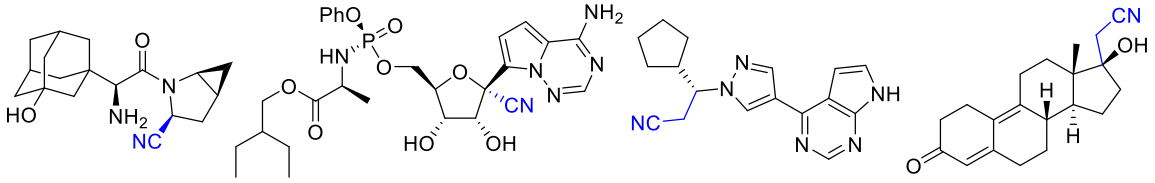


**3.1**, saxagliptin *hypoglycemic* | **3.2**, remdesivir *antiviral* | **3.3**, ruxolitinib *JAK inhibitor* | **3.4**, dienogest *progesetin*

**Figure 3.1** Selected bioactive molecules containing an α-chiral or β-chiral nitrile motif.

Nitriles can serve as a versatile intermediate for the synthesis of a wide variety of functional groups. Many examples of these transformations are used in the preparation of intermediates of medicinally relevant compounds and feature a β-chiral nitrile (**Scheme 3.1**). Nitrile reduction can afford amines in high yields, exemplified by the synthesis of atorvastatin intermediate (*R*,*R*)-**3.6**, a statin generating sales of over $100 billion during its lifetime.[2–4] The reduction of nitriles with DIBAL-H affords aldehydes, a transformation applied in the preparation for intermediate (*S*)-**3.8** in the synthesis of eribulin, a treatment for breast cancer produced with one of the most synthetically complex drugs marketed.[5–7] The nitrile group is also readily transformed into carboxylic acids, a step demonstrated in a synthesis of intermediate (*S*)-**3.10**, used in a preparation of sitagliptin.[8,9] The cycloaddition of a nitrile group with azide to form tetrazoles is also widely used to produced carboxylic acid bioisosteres

and was demonstrated on a β-chiral nitrile substrate (*R*)-**3.11** to produce tetrazole (*R*)-**3.12** in the preparation of a HCV NS5B inhibitor.[10]

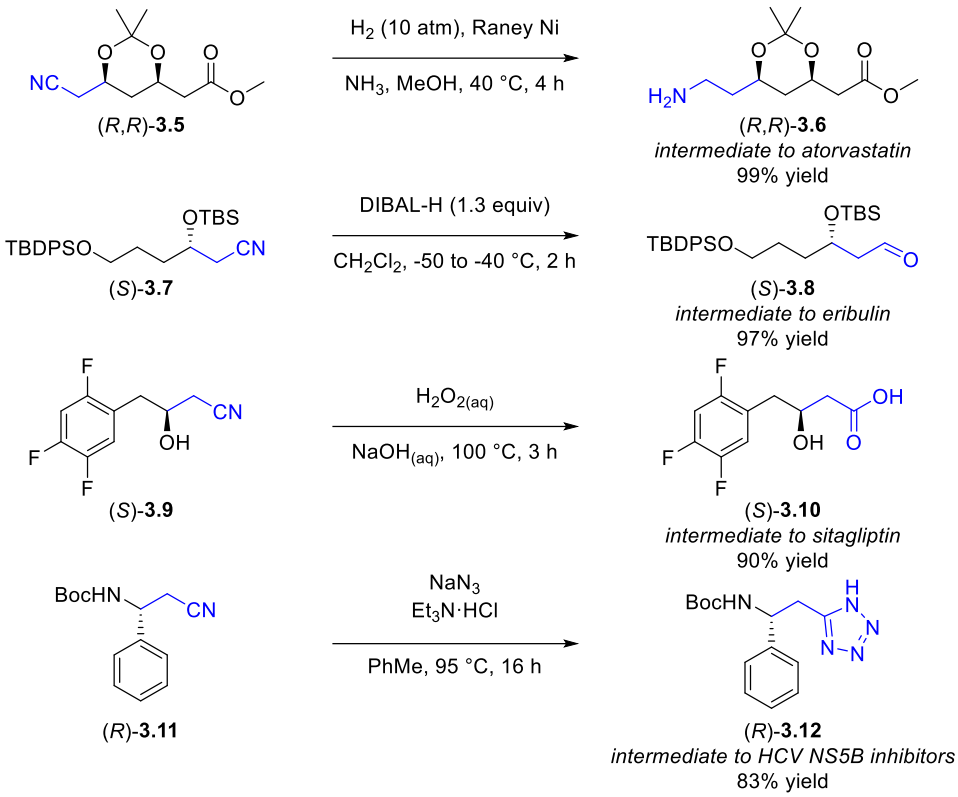


**Scheme 3.1** Selected transformations of β-chiral nitriles to intermediates in the synthesis of medicinally relevant molecules.

A range of reagents capable of introducing a nitrile group are available, with the sodium and potassium cyanide salts of particular interest as they are stable and economical solids available on scale (**Figure 3.2**). Alternatives such as trimethylsilylcyanide, hydrogen cyanide, and acetone cyanohydrin are unfavoured in comparison since they are less economical volatile liquids. Potassium cyanide is often preferred over sodium cyanide due to its improved stability and its easily handled granular supplied form. Potassium cyanide also provides ready access to combinations of its carbon-13 and nitrogen-15 isotopologues for applications in stable isotope labelling. In addition, potassium [$^{14}$C]cyanide is a preferred reagent for carbon-14 radiolabelling and readily available for this purpose, whereas trimethylsilyl[$^{14}$C]cyanide requires an additional synthetic step.[11,12]

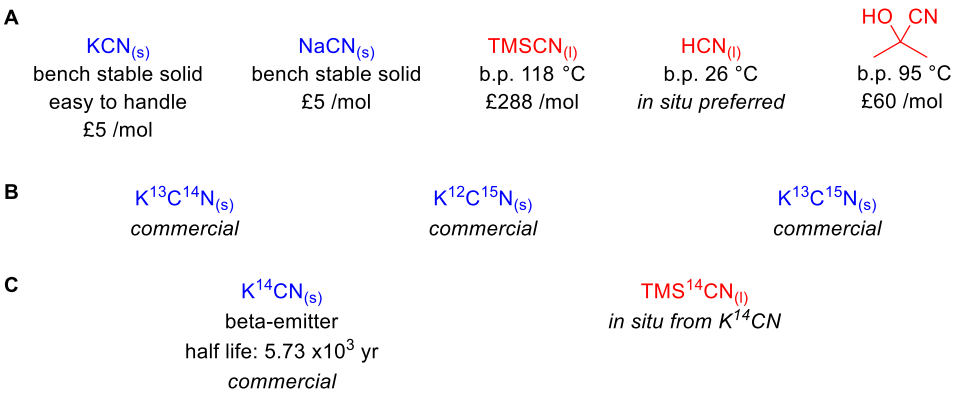


**Figure 3.2** (A) Selected sources of cyanide used in synthesis. (B) Selected sources of stable cyanide isotopologues. (C) Selected sources of [$^{14}$C]cyanide.

### 3.1.2 Enzyme-cyanide structure and reactivity

Cyanide can interact with enzymes and act as an inhibitor through direct coordination with metal cofactors in the active site. Cytochrome c oxidase (CcO) catalyses the oxidation of an iron(II) bound cytochrome c to an iron(III) bound cytochrome c (**Scheme 3.2A**). A crystal structure of cyanide-bound to fully reduced cytochrome c oxidase at 2.05 Å resolution was obtained. The cyanide anion forms a bridge between the iron and copper within the active site and sits nearly equidistant between the two metals (**Scheme 3.2B**).[13]

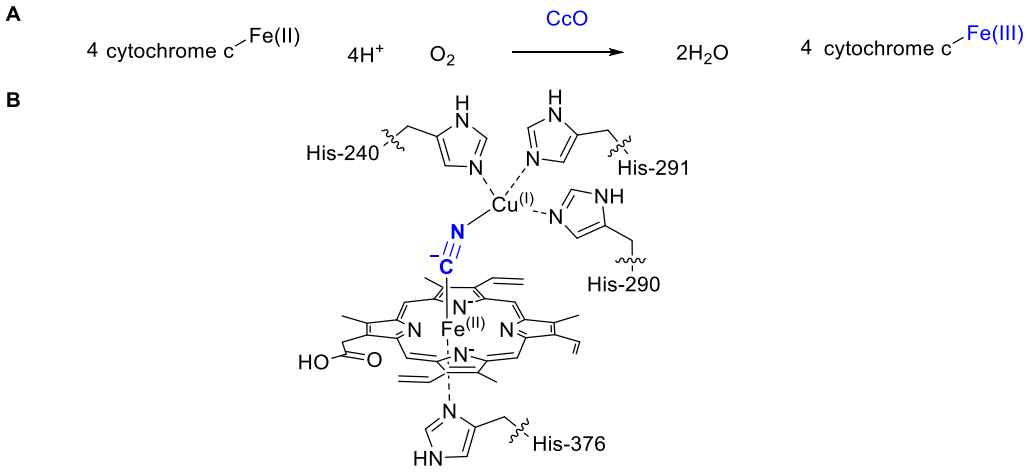


**Scheme 3.2** (A) Oxidation of cytochrome c catalysed by CcO. (B) Cyanide coordination to iron and copper in the CcO active site (PDB 3AG4).[13] CcO = cytochrome c oxidase.

Cyanide can also act as an inhibitor by forming hydrogen bonding interactions with residues in the active site of enzymes. Urate oxidase (UO) catalyses the oxidation of uric acid to 5-hydroxyisourate and is inhibited by cyanide with a loss of activity of 90% (**Scheme 3.3A**).[14] The

cyanide anion forms hydrogen bonds with Asn-254 and Thr-57' and competes reversibly for the place of a water molecule (**Scheme 3.3B**).[15]

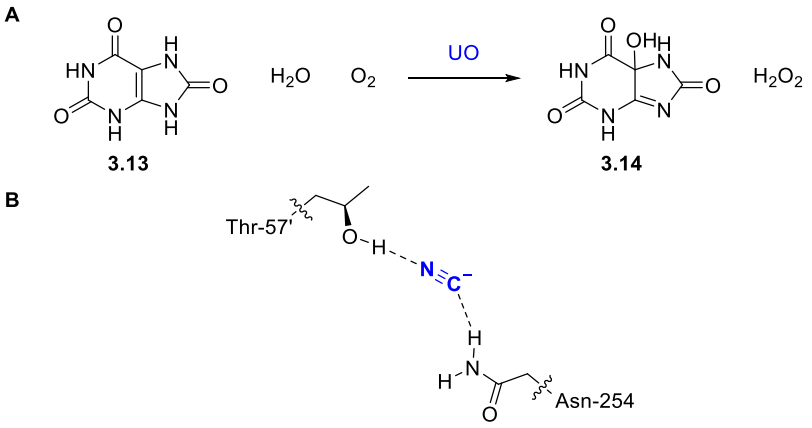


**Scheme 3.3** (A) Oxidation of uric acid **3.13** by UO. (B) Cyanide hydrogen bonded to key residues in the active site of UO (PDB 3BJP).[15] UO = urate oxidase.

In addition, enzymes can control the reactivity of cyanide and a range of enantioenriched nitriles can be prepared with enzyme catalysis (**Scheme 3.4**). The synthesis of enantioenriched cyanohydrins from cyanide with a hydroxynitrile lyase (HNL) was first reported in 1908 using almond emulsin, although this platform gained more attention in the 1960s with the isolation and characterisation of a HNL from bitter almonds.[16,17] A broad scope of enantioenriched cyanohydrins synthesised by a HNL was demonstrated by Becker *et al*. and has since developed into a reliable tool for organic synthesis.[17–19] Halohydrin dehalogenases are also able to utilise the cyanide anion in synthetic transformations, catalysing the kinetic resolution of (±)-**3.15** and producing (*S*)-**3.16** in a 40% yield and 95.5:0.5 e.r.[20–22]

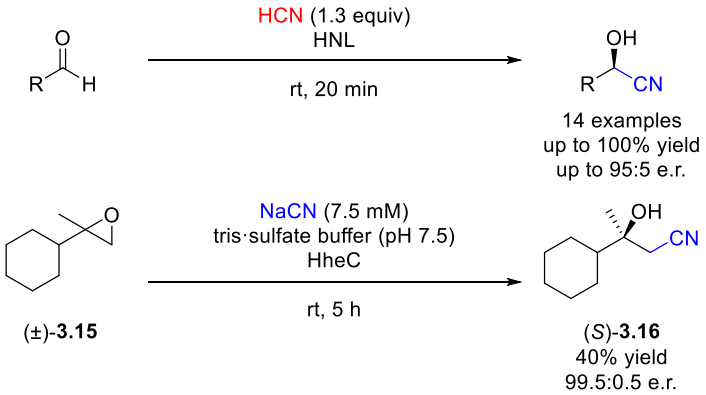


**Scheme 3.4** Selected examples of enantioselective enzyme catalysed cyanation reactions.

### 3.1.3 Structure of hydrogen bonded cyanide complexes

Despite examples of several anion receptors suitable for cyanide coordination, few publications have investigated the structure of hydrogen bonded cyanide complexes, speculated to be due to its basicity (**Figure 3.3**).[23,24] Computational investigations concluded either the carbon or the nitrogen atom in the cyanide anion can function as a hydrogen bond acceptor, although the nitrogen terminus is the stronger acceptor.[23]

Both crystal structures with a hydrogen bond donor coordinating to the nitrogen atom and the carbon atom of cyanide are available. Crystal structures of beryllium-ammonia cluster **3.17** coordinated to cyanide and imidazolium **3.18** coordinated to cyanide display exclusive hydrogen bonding with the nitrogen atom of the cyanide.[25,26] In contrast, the structure of a ternary urea-water-cyanide inclusion complex consists of a disordered cyanide that appears to hydrogen bond exclusively with water in the ternary lattice *via* its carbon atom.[27] Imidazolium salt **3.20** is structurally similar to **3.18**, albeit less hindered around the hydrogen bond donors. The crystal structure of **3.20** coordinated to cyanide appears possess interactions between both the carbon and nitrogen of the cyanide.

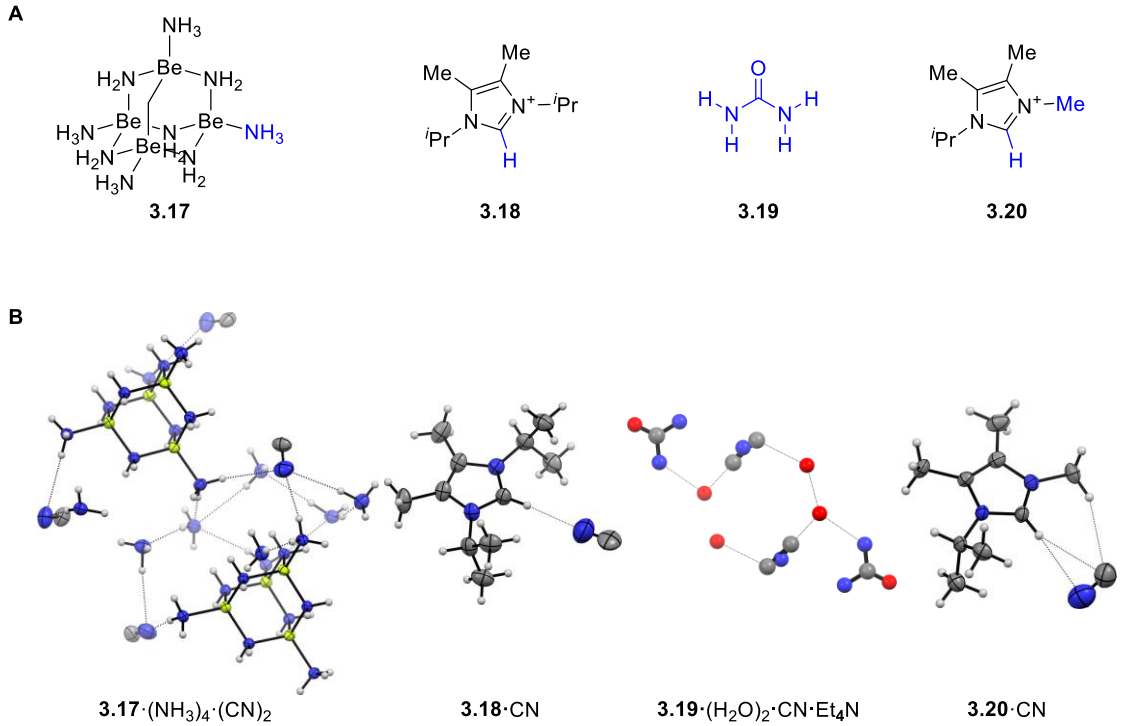


**Figure 3.3** (A) Structure of selected hydrogen bond donors able to coordinate cyanide. (B) Selected crystal structures of hydrogen bonded cyanide complexes. Tetraethylammonium cation omitted for clarity, displacement ellipsoids (if available) drawn at 50% probability level (CCDC 1982302, 615264, 1168018, 615265). Cyanide anion in **3.19**·$(H_2O)_2$·CN·$Et_4N$ is disordered.

### 3.1.4 Enantioselective cyanation

Although metal catalysed processes for enantioselective cyanations are well known,[28,29] organocatalytic platforms often come with environmental and economic advantages.[30] Organocatalytic methods to generate chiral nitriles utilising potassium cyanide are available and typically generate α-chiral nitriles through a 1,2- or 1,4-addition of cyanide to a suitable prochiral electrophile.

The Strecker reaction enables facile access to α-aminonitriles, with a subsequent hydrolysis generating α-amino acids. Enantioselective variants are attractive since they provide rapid access to a broad range of enantioenriched α-amino acids (**Scheme 3.5**).[31] The Jacobsen group published a scalable enantioselective organocatalytic hydrocyanation using potassium cyanide to generate hydrogen cyanide *in situ*.[32] Advances in phase-transfer catalysis have since allowed the same reaction to proceed without generating hydrogen cyanide. Ammonium salt (*R*)-**3.22** can mediate the phase transfer of potassium cyanide from the

aqueous phase to the organic phase, with the chiral cation directing the enantioselectivity of the 1,2-addition, generating enantioenriched α-aminonitriles in good yield and enantiomeric ratios.[33] A chiral neutral crown ether (*R,R*)-**3.23** can also mediate the phase-transfer of potassium cyanide to the organic phase by chelating the potassium cation and direct an enantioselective addition of cyanide onto an *in situ* generated imine.[34]

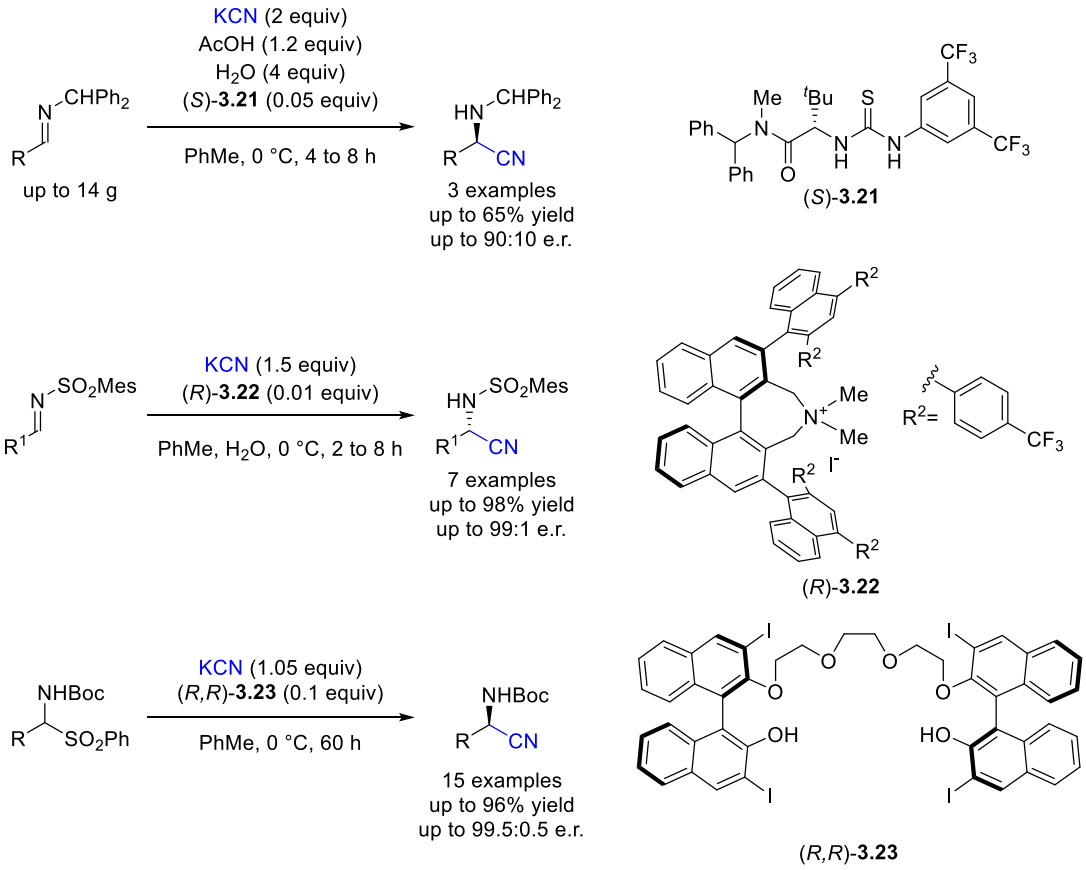


**Scheme 3.5** Selected organocatalytic Strecker reactions using potassium cyanide.

A related transformation involves the desymmetrisation of alkylideneindolenines generated *in situ* from sulfonylalkylindoles to form 2-aryl-3-alkylindole products (**Scheme 3.6**).[35] A triazolium catalyst (*S*)-**3.26** was proposed to act as a phase transfer catalyst and enable the reaction to be conducted under neutral conditions. Initial optimisation revealed potassium cyanide could be applied and synthesise (*R*)-**3.25** in a 53% yield and 90.5:9.5 e.r.

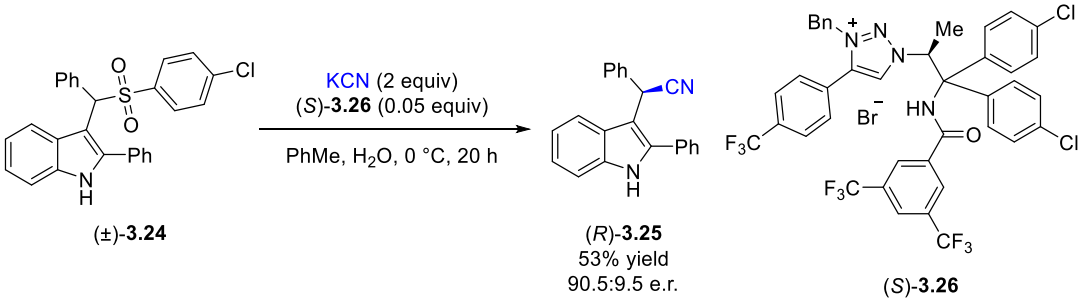


**Scheme 3.6** Synthesis of enantioenriched 2-aryl-3-alkylindole products from potassium cyanide.

Enantioselective conjugate addition of potassium cyanide enables the synthesis of valuable enantioenriched γ-ketonitriles (**Scheme 3.7**). The Maruoka group reported the enantioselective organocatalytic conjugate addition of potassium cyanide with alkylidenemalonate substrates.[36] These reactions utilised a chiral ammonium phase-transfer catalyst (*R*)-**3.27** and although an additional Brønsted acid was required, it was proposed to protonate the substrate instead of generating hydrogen cyanide. A similar reaction disclosed in a patent from Syngenta LTD demonstrated the conjugate addition of potassium cyanide to an enone in a low 28% yield but high 98:2 e.r.[37] Recently, the Ooi group reported a sequential enantioselective conjugate addition of potassium cyanide to an electron deficient alkene and subsequent diastereoselective alkylation to generate enantioenriched nitriles with contiguous α-chiral and β-chiral centres.[38] This reaction utilised chiral triazolium salt (*S*)-**3.31** or (*S*)-**3.32** depending on the reagents and substrates involved.

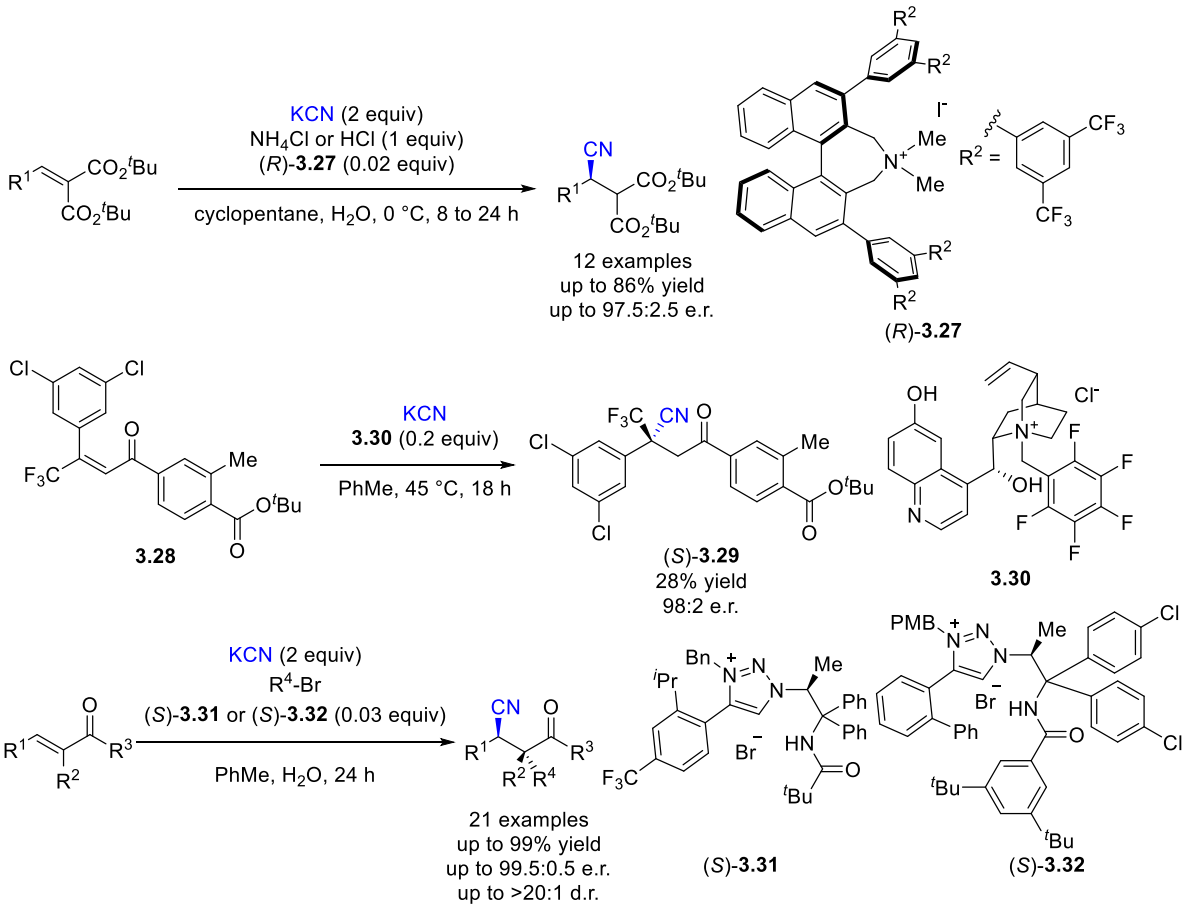


**Scheme 3.7** Enantioselective organocatalytic conjugate addition with potassium cyanide.

Urea-based catalysts are known to facilitate enantioselective cyanation reactions, however mechanistic studies focused on their thiourea counterparts due to their improved catalytic performance.[32,39,40] Organocatalyst (*S*,*S*,*R*)-**3.33** was identified as an effective catalyst for enantioselective Strecker reactions with yields up to 99% and enantiomeric ratios up to 98.5:1.5 using hydrogen cyanide.[41,42] A similar transformation was achieved with urea catalyst (*S*)-**3.34** generating hydrogen cyanide *in situ*, although only 3 examples were presented (**Scheme 3.8**).[39]

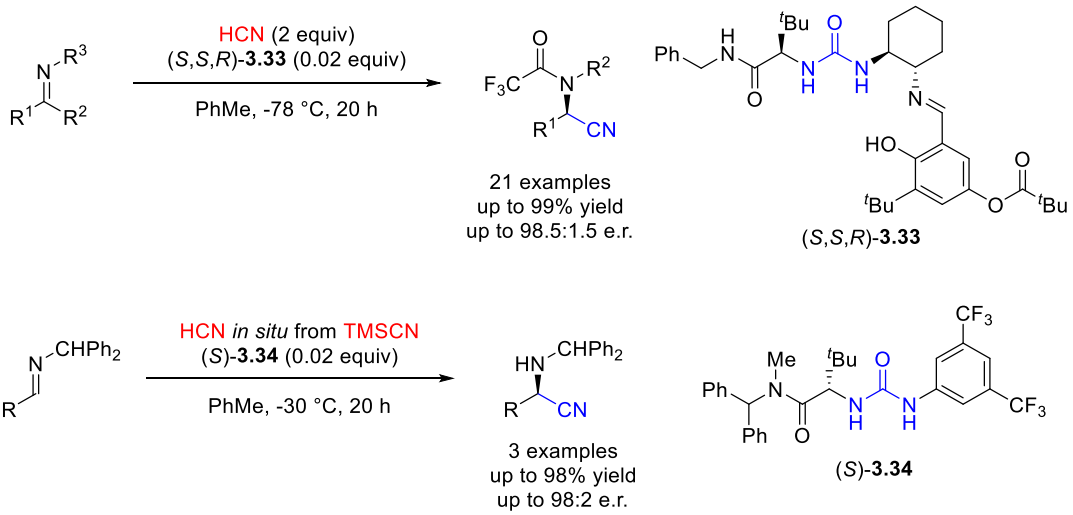


**Scheme 3.8** Selected examples of urea catalysed cyanation reactions.

### 3.1.5 Aims

Initial studies focused on understanding the structure and association of urea-cyanide complexes by crystallography and NMR, providing new insights into their stoichiometry, association strength, and connectivity (**Scheme 3.9A**). Subsequent studies investigated the application of potassium cyanide to HB-PTC for the synthesis of novel enantioenriched β-chiral γ-aminonitriles from preformed azetidinium salts (**Scheme 3.9B**). Together, these studies provided new insights into the reactivity of the hydrogen bonded cyanide anion and established the applicability of HB-PTC to potassium cyanide for enantioselective synthesis.

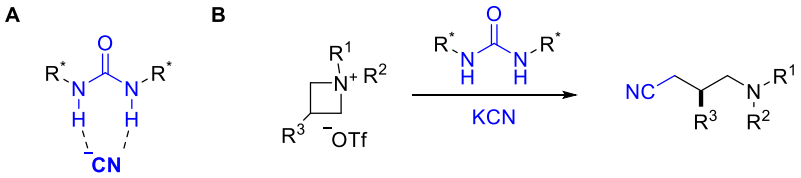


**Scheme 3.9** (A) Proposed urea-cyanide interaction for study. (B) Proposed urea catalysed synthesis of β-chiral γ-aminonitriles from potassium cyanide under HB-PTC.

## 3.2 Structure and coordination in urea-cyanide complexes

### 3.2.1 Solid state studies

Structural insights into the urea-cyanide interaction began with the synthesis and crystallographic study of a urea-cyanide complex. The only previous report of a urea-cyanide complex included a co-crystallised molecule of water disrupting the urea-cyanide interaction, and a disordered cyanide anion.[27] The preparation of a urea-cyanide complex whilst reducing

the potential for co-crystallised water was achieved by adapting a literature procedure from the preparation of urea-fluoride complexes with azeotropic water removal.[43] Schreiner's urea **3.35** was selected for study since it displayed excellent catalytic activity for fluorination[44,45] and azidation under HB-PTC. A complex of **3.35** and cyanide was prepared by heating a suspension of equimolar **3.35** and tetrabutylammonium cyanide in hexanes at reflux for 30 min, followed by collection of the solids by filtration (**Scheme 3.10A**). Visual analysis of the physical product suggested the formation of a single amorphous solid, and its melting point range (101-102 °C) was 140 °C lower than the reported melting point of **3.35** (240-242 °C).

A single crystal suitable for X-ray crystallography was successfully obtained by layering cyclohexane onto a saturated solution of **3.35**·CN·$Bu_4N$ in $Et_2O$ (**Scheme 3.10B**). The crystal structure contained cyanide coordinated to **3.35** in a 1:1 stoichiometry, with both urea hydrogen bond donors coordinating exclusively with the single nitrogen terminus of the cyanide anion. The urea-cyanide hydrogen bond donor lengths were 2.993 Å and 2.964 Å when measured from the urea nitrogen to the cyanide nitrogen, close to the analogous bond lengths observed in the two crystallographically distinct motifs in the complex of **3.35** and tetrabutylammonium azide which ranged from 2.962(4) Å to 3.069(4) Å. These lengths are longer than those observed in the published urea-fluoride complexes,[43] which ranged from 2.648(4) Å to 2.807(8) Å when measured by neutron diffraction.

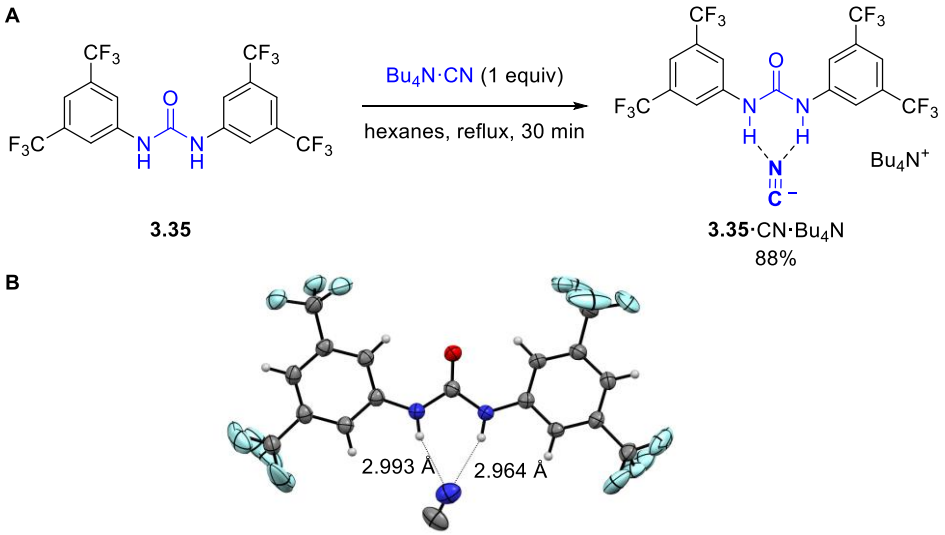


**Scheme 3.10** (A) Synthesis of an amorphous solid of **3.35** complexed to cyanide. (B) Crystal structure of **3.35** complexed to cyanide. Bond distances measured from the urea nitrogen to the cyanide nitrogen Tetrabutylammonium cation omitted for clarity, displacement ellipsoid plots drawn at 50% probability level. X-ray crystallography data collection and analysis by Dr. K. E. Christensen.

The data obtained from the preparation and crystallisation of **3.35**·CN·$Bu_4N$ provided the first evidence for direct urea-cyanide coordination in the solid state by hydrogen bonding. X-ray crystallography established connectivity and identified the nitrogen atom of the cyanide anion to be the exclusive hydrogen bond acceptor.

### 3.2.2 Solution studies

$^1$H NMR titrations were conducted to probe the association and stoichiometry of **3.35** with cyanide in solution, with both 1:1 and full 2:1 equilibrium models considered (**Scheme 3.11**).[46,47] As with the studies of fluoride and azide with achiral 1,3-diarylureas, acetonitrile was selected for solvent as it readily solubilised **3.35**, is itself a poor hydrogen bond acceptor and donor,[48] and is widely available as its deuterated isotopologue. Cyanide was added as its tetrabutylammonium salt due to the cation's non-coordinating nature and desirable solubility profile.[49]

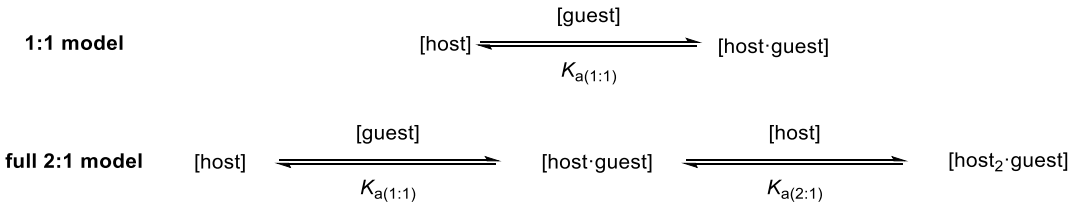


**Scheme 3.11** Equilibria for 1:1 and full 2:1 binding models.

Study of the association of **3.35** and cyanide in solution by $^1$H NMR titration in acetonitrile provided valuable insights (**Figure 3.4**). Upon addition of cyanide, the NH protons of **3.35** no longer remained visible on the $^1$H NMR spectra, a phenomenon indicative of an exchange process. These observations are consistent with the association of cyanide and **3.35** involving the urea NH protons.

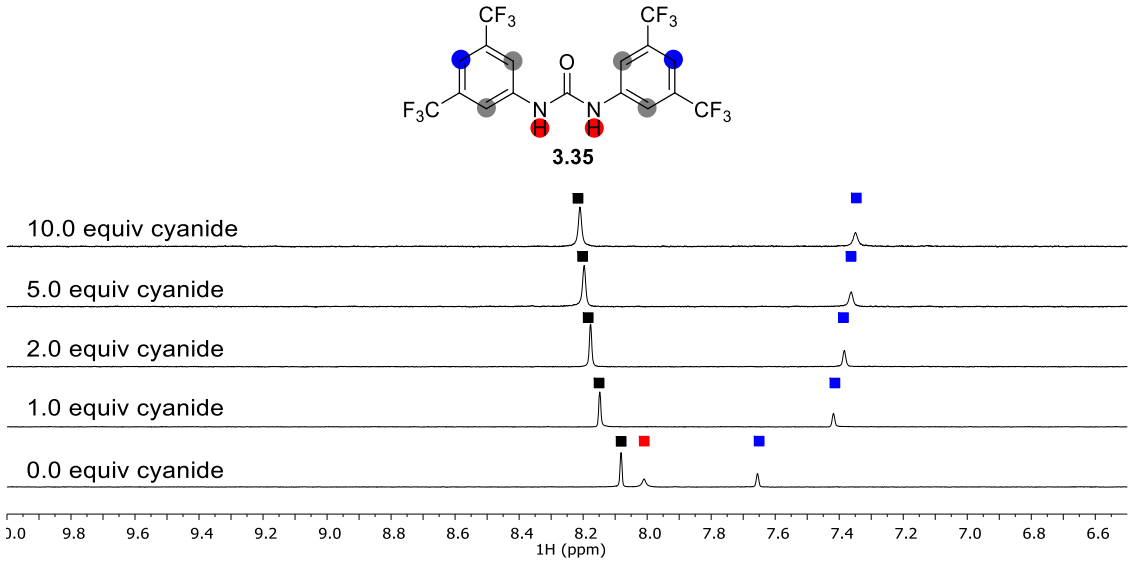


**Figure 3.4** Representative $^1$H NMR spectra from the titration of **3.35** with tetrabutylammonium cyanide with aromatic proton shifts monitored highlighted in black and blue (2 mM **3.35**, $CH_3CN/CD_3CN$ 8:2, 500 MHz, 298 K).

The aromatic proton shifts were tracked across multiple additions, enabling determination of an appropriate binding model. The mean covariance of fit when fitting the data to a 1:1 model was $7.24 \times 10^{-3}$ whereas the mean covariance of fit when fitting the data to a full 2:1 model was $0.2 \times 10^{-3}$, representing an improvement of 36.2-fold (**Table 3.1**). This large difference indicates the full 2:1 model is more likely to be representative of the association of **3.35** and tetrabutylammonium cyanide solution (**Table 3.1**). The $K_{a(1:1)}$ was $2.1 \pm 0.3 \times 10^3$ M$^{-1}$, with a similar $K_{a(2:1)}$ of $1.4 \pm 0.9 \times 10^3$ M$^{-1}$. As with fluoride[43,44,50] and azide the $K_{a(2:1)}$ was smaller than

the $K_{a(1:1)}$, albeit within the same order of magnitude. These results show that solutions of excess cyanide are likely to favour formation of the 1:1 complex, whereas solutions with excess urea would favour formation of the 2:1 complex. The second association of a urea with the 1:1 urea-cyanide complex is likely to involve the additional urea coordinating to the cyanide anion (based on the 2:1 urea-fluoride[43] and 2:1 urea-azide structures), however the precise nature of association cannot be deduced from the available data.

**Table 3.1** Titration modelling and association constants of **3.35** and cyanide.

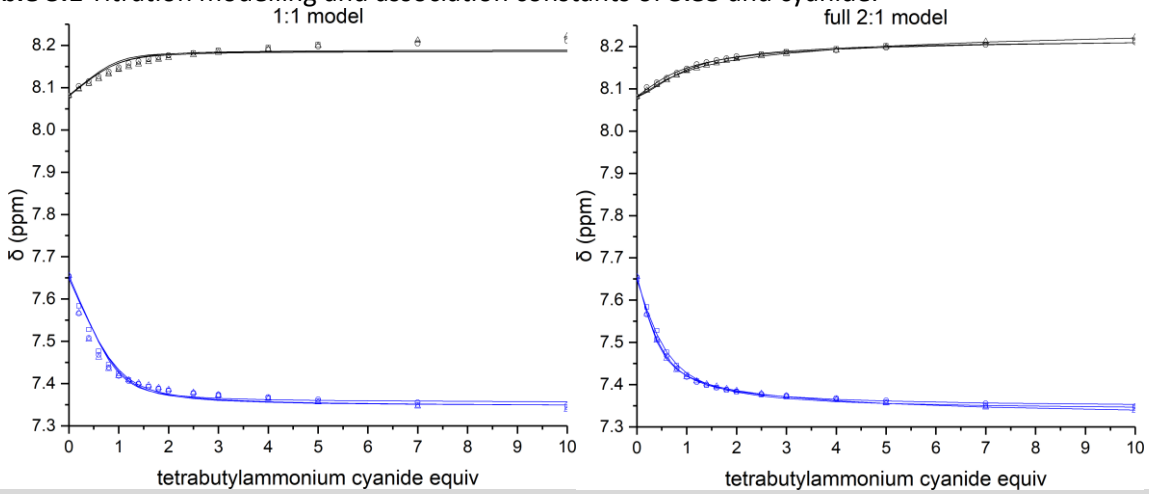


| entry | model | $cov_{fit}$ ($10^{-3}$) | $cov_{fit}$ factor | $K_{a(1:1)}$ ($M^{-1}$) | $K_{a(2:1)}$ ($M^{-1}$) |
|---|---|---|---|---|---|
| 1 | 1:1 | 7.24 | 1 | $5.5 \pm 1.2 \times 10^3$ | - |
| **2** | **full 2:1** | **0.20** | **36.2** | $\mathbf{2.1 \pm 0.3 \times 10^3}$ | $\mathbf{1.4 \pm 0.9 \times 10^3}$ |

One set of symbols (□, ○, △) refers to experimental data from one set of measurements (2 mM, $CH_3CN/CD_3CN$ 8:2, 500 MHz, 298 K). Lines are the calculated isotherms of the described model. $cov_{fit}$ factor is $cov_{fit}$ for the 1:1 model divided by the $cov_{fit}$ for the binding model under study.[47] Values are the mean of 3 independent replicas calculated with BindFit v0.5,[51] error is the standard deviation.

Subsequent studies of the urea-cyanide interaction in solution were undertaken with the prototypical chiral *N*-alkyl (*S*)-BINAM derived bis-urea containing three hydrogen bond donors (*S*)-**3.36a**. Acetonitrile was retained as the solvent for $^1$H NMR titrations since solutions of tetrabutylammonium cyanide in $CD_2Cl_2$ or $CDCl_3$ were insufficiently stable for titrations and changed from colourless to brown within 24 h.

The $^1$H NMR spectra of (*S*)-**3.36a** in $CD_3CN$ were not available and were assigned with additional $^1$H-$^1$H COSY, $^1$H-$^1$H TOCSY, $^1$H-$^1$H NOESY, $^1$H-$^{15}$N HSQC, and $^1$H-$^{15}$N HMBC. Due to the broad and overlapping signals of two NH signals, it was not possible to differentiate between NH1 and NH2 (**Figure 3.5**) from these spectra.

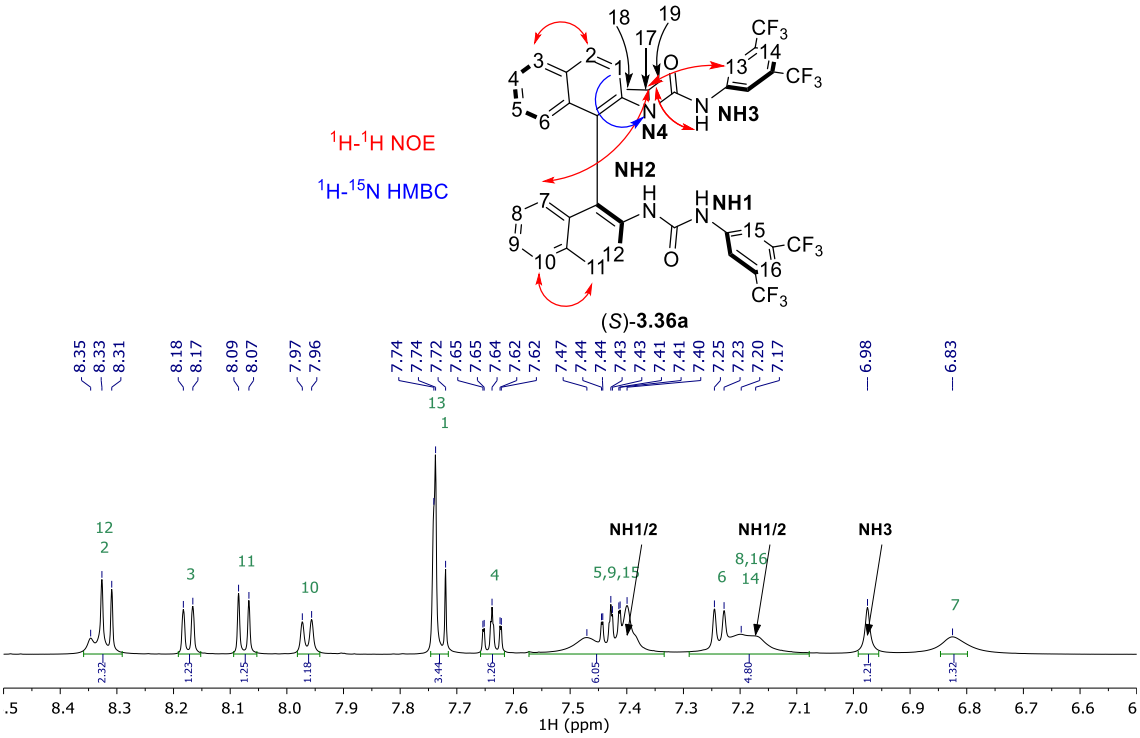


**Figure 3.5** Structure and $^1$H NMR assignment of (*S*)-**3.36a** in $CD_3CN$ (25 mM (*S*)-**3.36a**, $CD_3CN$, 500 MHz, 298 K).

An overlay of the $^1$H-$^{15}$N HSQC and $^1$H-$^{15}$N HMBC NMR spectra displayed the three urea NH $^{15}$N signals at 107.3 ppm, 109.2 ppm, and 109.8 ppm and the tertiary nitrogen of (*S*)-**3.36a** at 113.0 ppm with a correlation with the doublet at 7.73 ppm (**Figure 3.6**). This correlation was used to differentiate the two ring systems of the (*S*)-BINAM backbone, allowing the doublet at 7.73 ppm to be assigned to H1. Two NH signals are present within the multiplets from 7.47 – 7.40 ppm and 7.25 – 7.17 ppm, whilst the third at 6.98 ppm possesses a correlation with the *ortho* protons of a fluorinated aromatic ring at 7.74 ppm and therefore corresponds to NH1 or NH3.

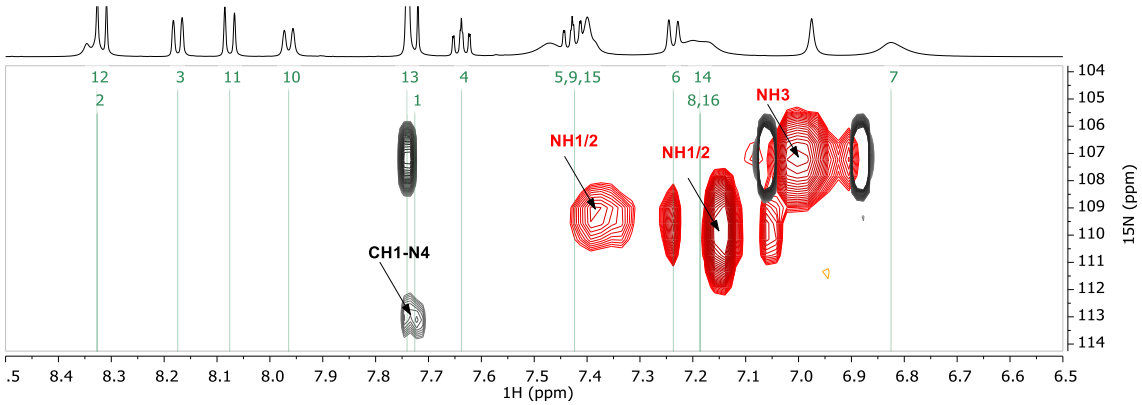


**Figure 3.6** Superimposed $^{1}$H-$^{15}$N HSQC (red) and $^{1}$H-$^{15}$N HMBC (black) NMR spectra of (*S*)-**3.36a** in $CD_3CN$ (25 mM (*S*)-**3.36a**, $CD_3CN$, 500 MHz, 298 K).

Examination of the $^{1}$H-$^{1}$H NOESY NMR spectra revealed NOE interactions between the isopropyl H17 and the *ortho* protons of a fluorinated aromatic ring at 7.74 ppm, the signal corresponding to an NH at 6.98 ppm, and a CH from the (*S*)-BINAM backbone at 6.83 ppm (**Figure 3.7**). Hence the signal at 7.74 ppm was assigned to H13, the NH signal at 6.98 ppm to NH3, and the signal at 6.83 ppm to H7. The interaction between the isopropyl H17 with H7 can be attributed the twist of the (*S*)-BINAM scaffold and was observed in both $CD_2Cl_2$[50] and $CDCl_3$.

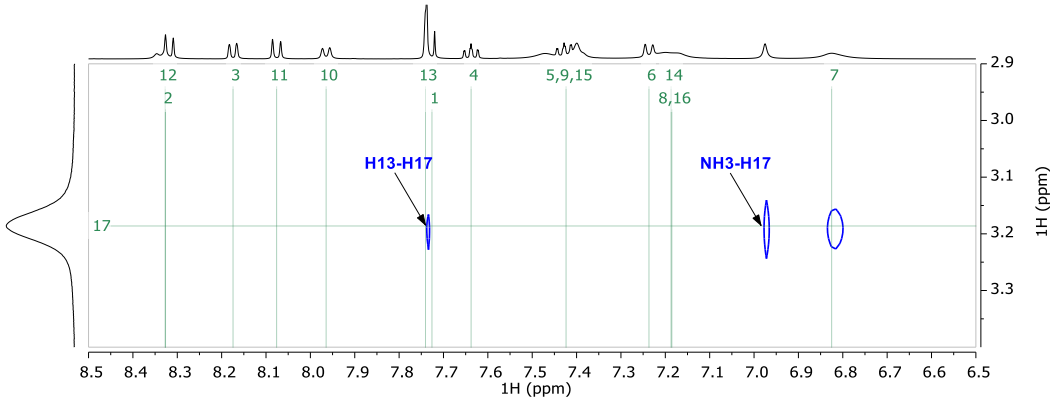


**Figure 3.7** Expansion of the $^{1}$H-$^{1}$H NOESY NMR of (*S*)-**3.36a** in $CD_3CN$ (25 mM (*S*)-**3.36a**, $CD_3CN$, 500 MHz, 298 K).

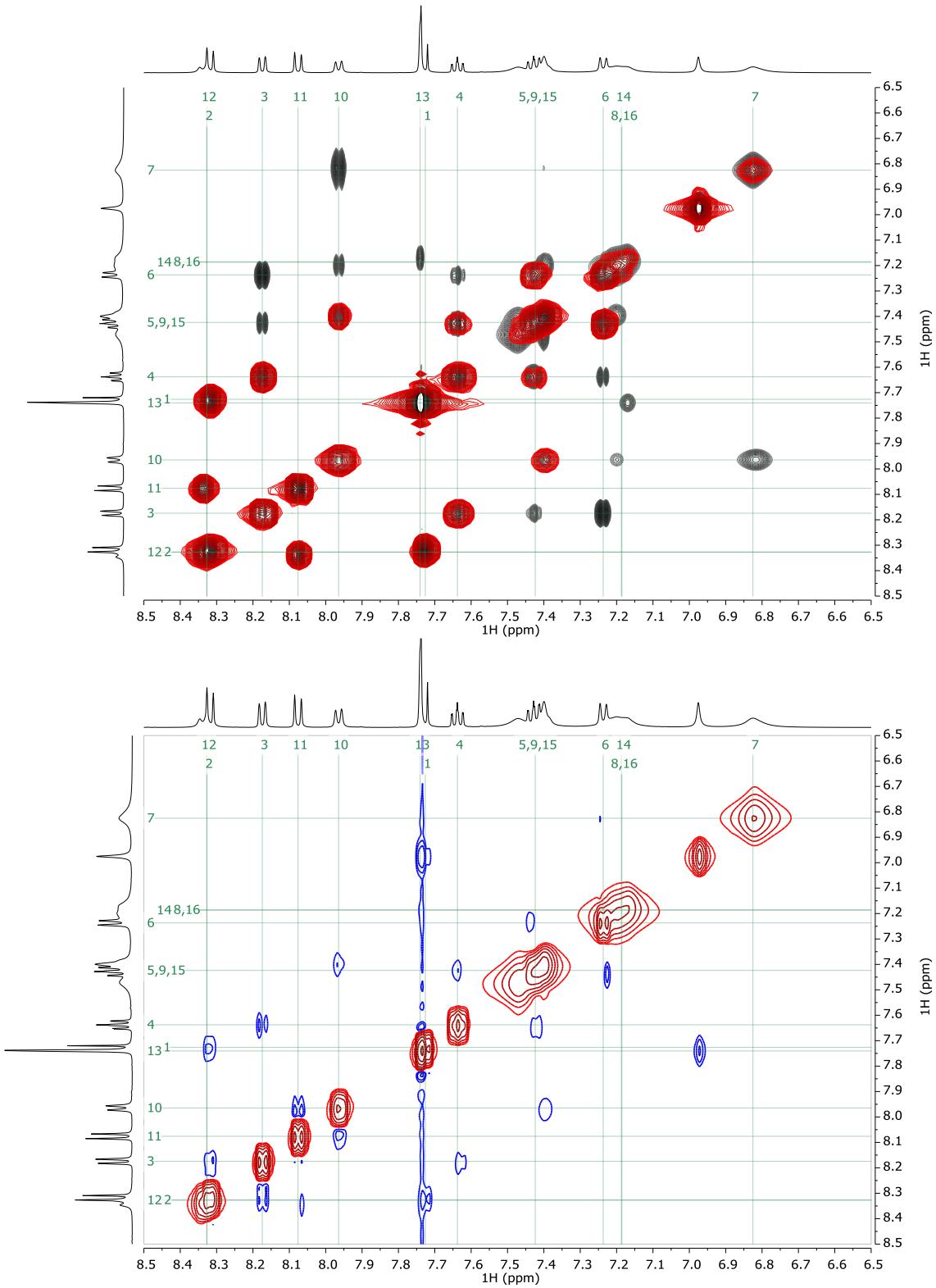


**Figure 3.8** Overlay of $^{1}$H-$^{1}$H COSY (red) and $^{1}$H-$^{1}$H TOCSY (black) NMR spectra, and $^{1}$H-$^{1}$H NOESY (blue and red) NMR spectra of (*S*)-**3.36a** in $CD_3CN$ (25 mM (*S*)-**3.36a**, $CD_3CN$, 500 MHz, 298 K).

With the assignment of H1, H6, and H13 in hand, the remainder of the CH signals in (*S*)-**3.36a** could be assigned with $^{1}$H-$^{1}$H COSY, $^{1}$H-$^{1}$H TOCSY, and $^{1}$H-$^{1}$H NOESY NMR spectra (**Figure 3.9**). The $^{1}$H-$^{1}$H NOESY experiment was necessary to confirm the proximity between the signals

corresponding to H2 and H3, as well as H10 and H11. NH1 could not be differentiated from NH2 with the available spectra due to their broad and overlapped signals.

Despite this ambiguity, all other $^{1}$H NMR shifts were accounted for, and it was possible to obtain association constants by tracking the shifts of selected proton signals (highlighted in black and blue, **Figure 3.9**). The spectra collected from $^{1}$H NMR titrations of tetrabutylammonium cyanide with (*S*)-**3.36a** reflected the observations noted with the titrations of **3.35** and cyanide, with a disappearance of the urea NH proton signals upon addition of titrant.

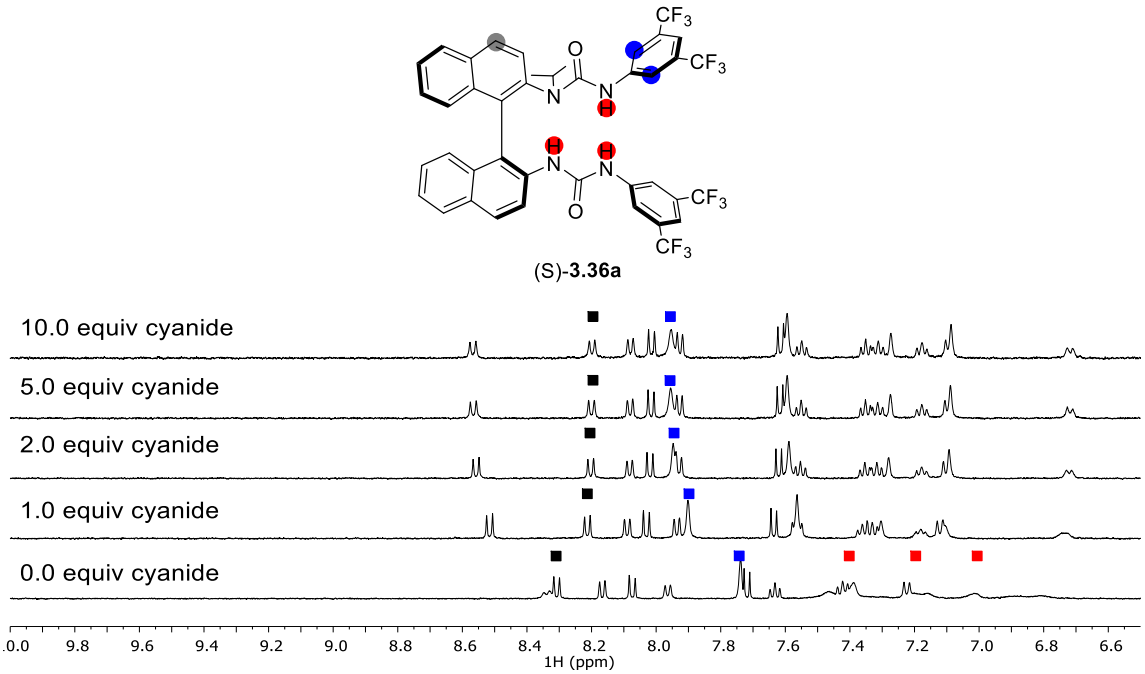


**Figure 3.9** Representative $^{1}$H NMR spectra from the titration of (*S*)-**3.36a** with tetrabutylammonium cyanide. Aromatic proton shifts monitored to determine association constants are highlighted in black and blue, urea NH signals highlighted in red (2 mM (*S*)-**3.36a**, $CH_3CN/CD_3CN$ 8:2, 500 MHz, 298 K).

Tracking selected aromatic proton shifts across (**Figure 3.9**) multiple additions enabled determination of association constants and an appropriate binding model (**Table 3.2**). Application of a full 2:1 model to this data resulted in a 14.2-fold improvement to the mean covariance of fit compared to the 1:1 association model. However, since the $K_{a(1:1)}$ was almost unchanged from the 1:1 model and the $K_{a(2:1)}$ was consistently negative, the association between (*S*)-**3.36a** and tetrabutylammonium cyanide is likely best represented by a 1:1 model

since association constants must be positive and the improvement in $cov_{fit}$ appears more likely due to overfitting. The resulting $K_{a(1:1)}$ was determined to be $1.0 \pm 0.3 \times 10^4$ $M^{-1}$, an order of magnitude higher than the $K_{a(1:1)}$ of tetrabutylammonium cyanide with **3.35**. This also contrasts against the association of (*S*)-**3.36a** with fluoride and azide in $CD_2Cl_2$ and $CHCl_3$ respectively, where a full 2:1 model was applicable. Further investigation into the differences in behaviour of (*S*)-**3.36a** with fluoride, azide, and cyanide with a unified solvent may enable improved understanding into the comparison of these anions.

**Table 3.2** Titration modelling, and association constants of (*S*)-**3.36a** and cyanide.

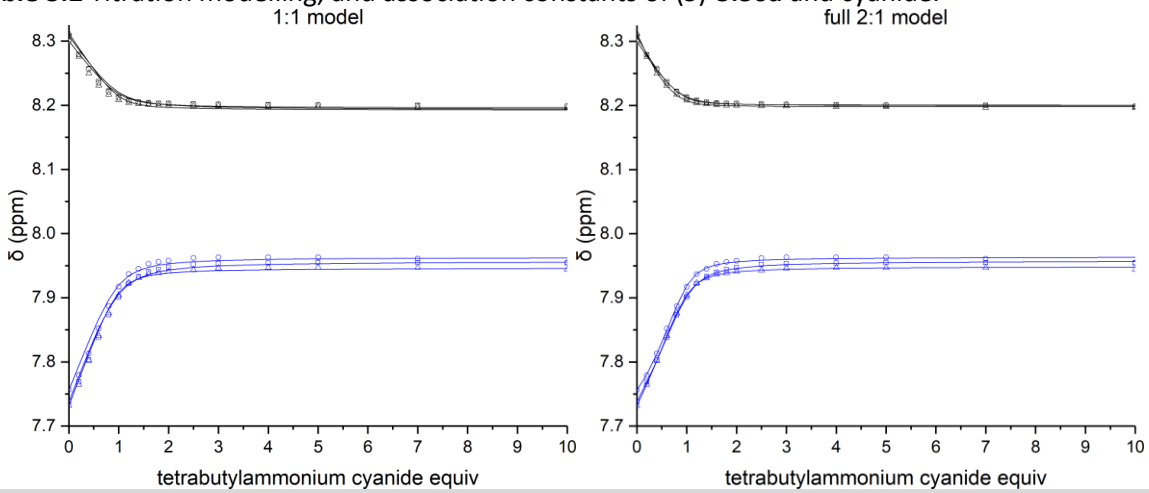


| entry | model | $cov_{fit}$ ($10^{-3}$) | $cov_{fit}$ factor | $K_{a(1:1)}$ ($M^{-1}$) | $K_{a(2:1)}$ ($M^{-1}$) |
|---|---|---|---|---|---|
| **1** | **1:1** | **2.08** | **1** | **$1.0 \pm 0.3 \times 10^4$** | **-** |
| 2 | full 2:1 | 0.24 | 14.2 | $1.1 \pm 0.3 \times 10^4$ | $-1.3 \pm 0.5 \times 10^2$ |

One set of symbols (□, ○, △) refers to experimental data from one set of measurements (2 mM, $CH_3CN/CD_3CN$ 8:2, 500 MHz, 298 K). Lines are the calculated isotherms of the described model. $cov_{fit}$ factor is $cov_{fit}$ for the 1:1 model divided by the $cov_{fit}$ for the binding model under study.[47] Values are the mean of 3 independent replicas calculated with BindFit v0.5,[51] error is the standard deviation.

Studies with (*S*)-**3.36a** at cryogenic temperatures were performed to reduce the rate of exchange and gain further insights into the structure and of (*S*)-**3.36a**·CN·$Bu_4N$ in solution. A change in solvent to $CD_2Cl_2$ enabled access to temperatures down to 193 K. The previously described instability of tetrabutylammonium cyanide in $CD_2Cl_2$ was mitigated by rapid dissolution of the sample in $CD_2Cl_2$ and using it immediately for analysis. A sample consisting of equimolar (*S*)-**3.36a** and tetrabutylammonium cyanide in $CD_2Cl_2$ at 25 mM was prepared by dissolving pre-weighed solid tetrabutylammonium cyanide in an NMR tube with a 25 mM stock solution of (*S*)-**3.36a** in $CD_2Cl_2$.

A $^{1}$H NMR spectra of (*S*)-**3.36a**·CN·$Bu_4N$ in $CD_2Cl_2$ was acquired at 298 K, 273 K, and at 20 °C decrements until 193 K. Signals corresponding to the NH protons of (*S*)-**3.36a** were observed below 253 K, increasing in sharpness and intensity as the temperature was lowered down to 193 K, reducing the exchange processes (**Figure 3.10**). At 193 K, no signals corresponding to a 2:1 urea-cyanide complex were observed, consistent with the titration experiments.

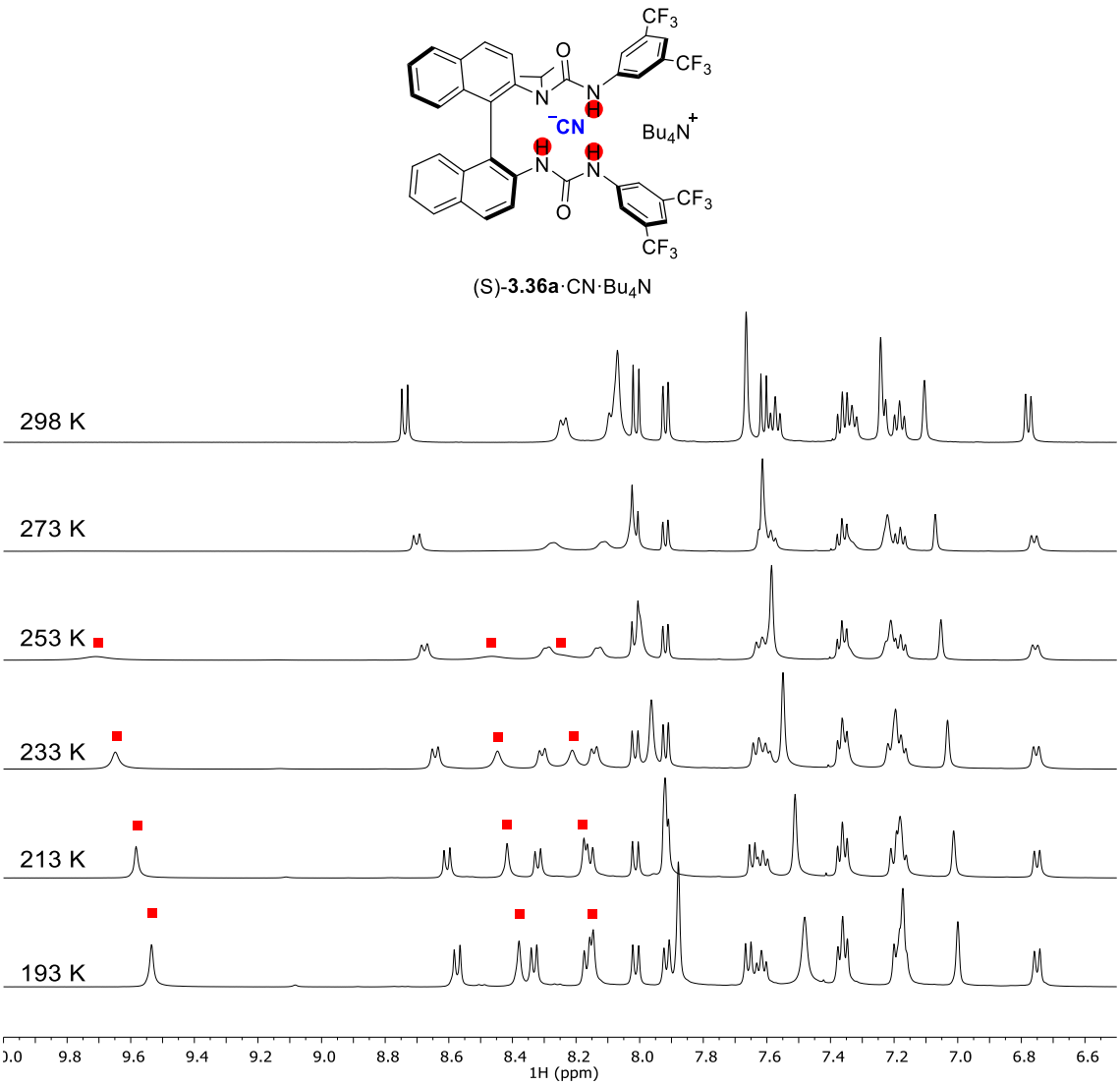


**Figure 3.10** $^{1}$H NMR spectra of (*S*)-**3.36a**·CN·$Bu_4N$ in $CD_2Cl_2$ from 298 K to 193 K. Urea NH signals highlighted in red (25 mM (*S*)-**3.36a**·CN·$Bu_4N$, $CD_2Cl_2$, 500 MHz).

At 193 K, the $^{1}$H NMR spectrum of (*S*)-**3.36a**·CN·$Bu_4N$ was assigned using additional 2D NMR spectra including $^{1}$H-$^{1}$H COSY, $^{1}$H-$^{1}$H NOESY, $^{1}$H-$^{15}$N HSQC, and $^{1}$H-$^{15}$N HMBC (**Figure 3.11**).

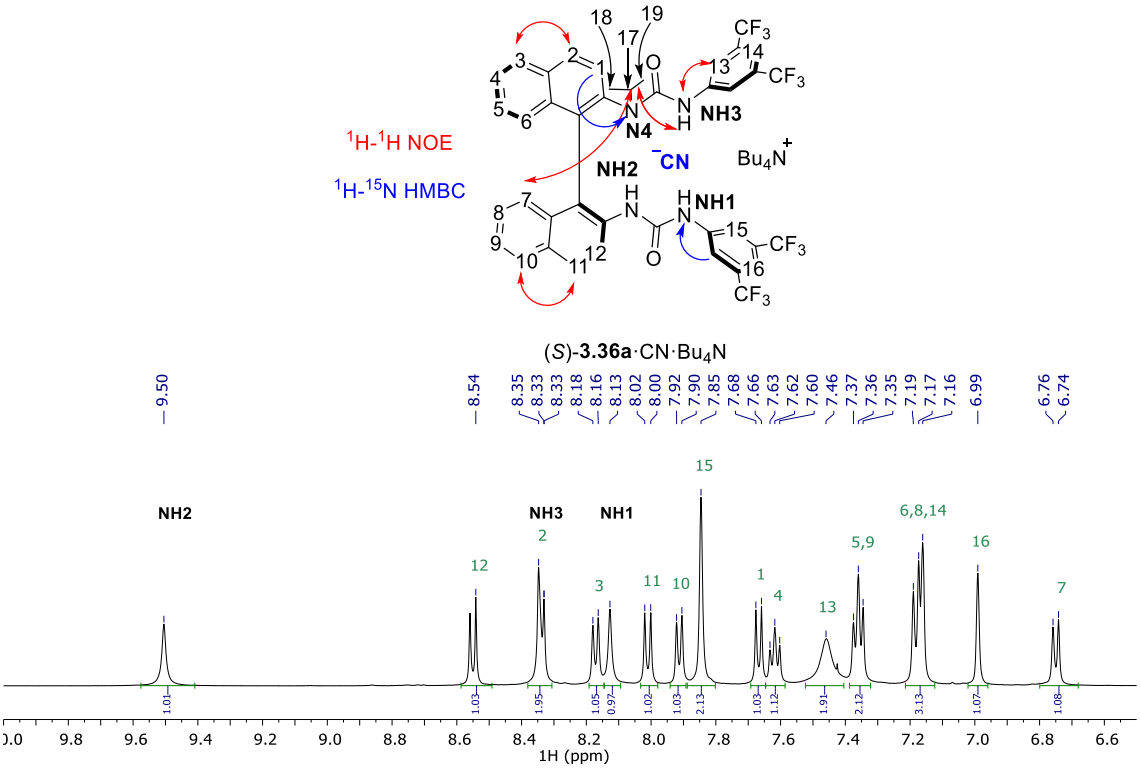


**Figure 3.11** Key interactions, assignment, and $^1$H NMR spectrum of (*S*)-**3.36a**·CN·$Bu_4N$ (25 mM (*S*)-**3.36a**·CN·$Bu_4N$, $CD_2Cl_2$, 500 MHz, 193 K).

An overlay of the $^1$H-$^{15}$N HSQC and $^1$H-$^{15}$N HMBC NMR spectra revealed a $^1$H-$^{15}$N correlation between the tertiary nitrogen and an aromatic proton assigned to H1, which provided a starting point for assignment of the (*S*)-BINAM backbone (**Figure 3.12**).

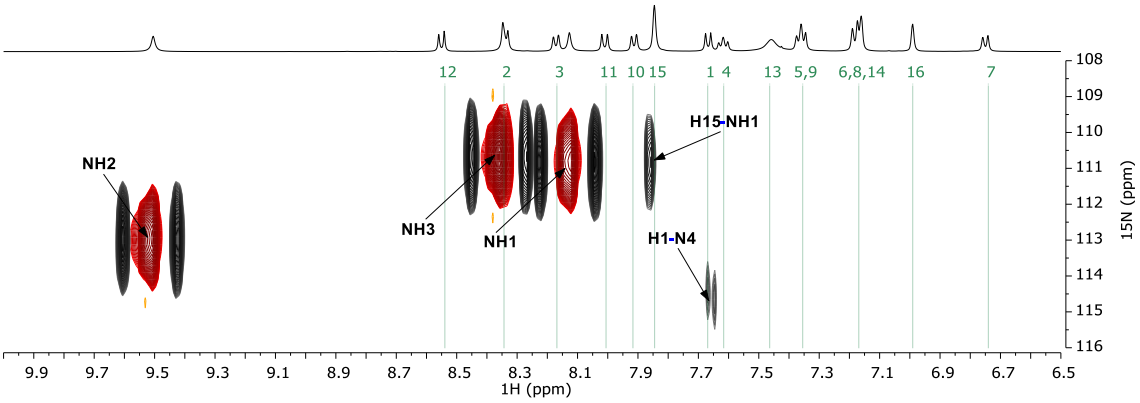


**Figure 3.12** Overlay of $^1$H-$^{15}$N HSQC (red) and $^1$H-$^{15}$N HMBC (black) NMR spectra of (*S*)-**3.36a**·CN·$Bu_4N$ (25 mM (*S*)-**3.36a**·CN·$Bu_4N$, $CD_2Cl_2$, 500 MHz, 193 K).

The remainder of the (*S*)-BINAM backbone was assigned from correlations observed on the $^1$H-$^1$H COSY and $^1$H-$^1$H NOESY NMR spectra (**Figure 3.13**). As before, a $^1$H-$^1$H NOESY experiment was used to confirm the proximity between the signals corresponding to H2 and H3, as well as H10 and H11.

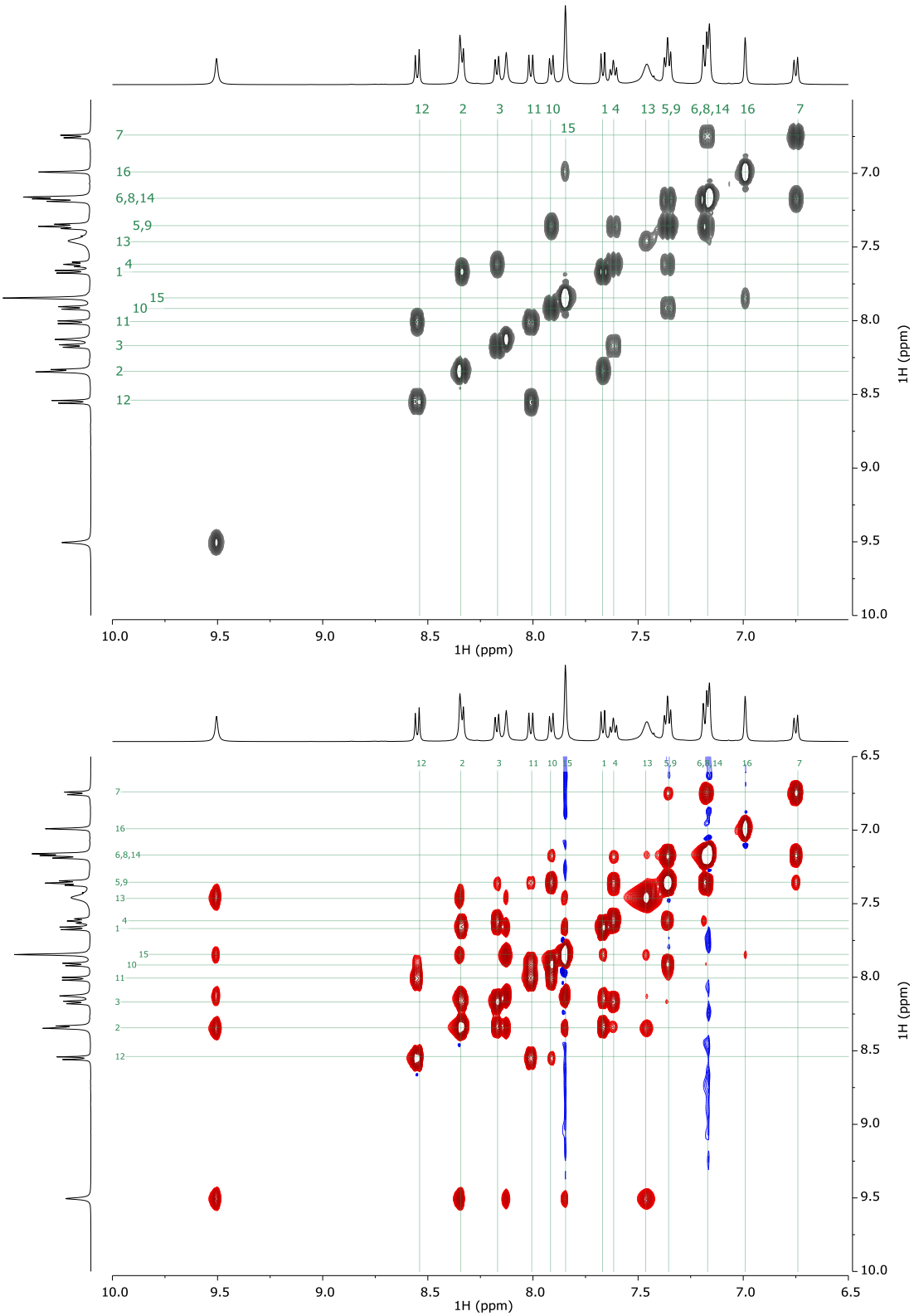


**Figure 3.13** $^{1}$H-$^{1}$H COSY (black) and $^{1}$H-$^{1}$H NOESY (blue and red) NMR spectra of (*S*)-**3.36a**·CN·Bu$_4$N (25 mM (*S*)-**3.36a**·CN·Bu$_4$N, $CD_2Cl_2$, 500 MHz, 193 K).

The individual urea NH proton signals were differentiated by close examination of the $^{1}$H-$^{1}$H NOESY and $^{1}$H-$^{15}$N HMBC NMR spectra. The *ortho* protons of a fluorinated aromatic ring at 7.85 ppm displayed a correlation to an NH signal at 8.13 ppm, which may be assigned to NH1 or NH3 (**Figure 3.14**).

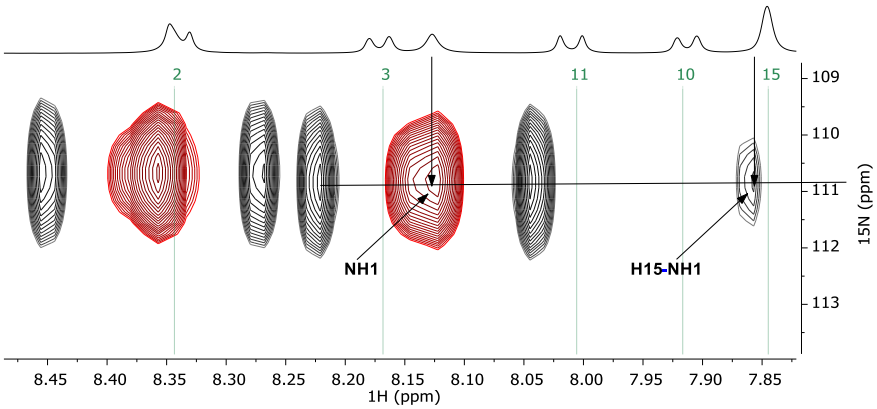


**Figure 3.14** Expansion of the overlay of $^{1}$H-$^{15}$N HSQC (red) and $^{1}$H-$^{15}$N HMBC (black) NMR spectra of (*S*)-**3.36a**·CN·Bu$_4$N (25 mM (*S*)-**3.36a**·CN·Bu$_4$N, $CD_2Cl_2$, 500 MHz, 193 K).

The isopropyl H17 displayed an NOE interaction with the NH at 8.35 ppm, hence the NH signal at 8.13 ppm was assigned to NH1, the NH signal at 8.35 ppm was assigned to NH3, and the most deshielded NH signal at 9.50 ppm was designated as NH2 (**Figure 3.15**).

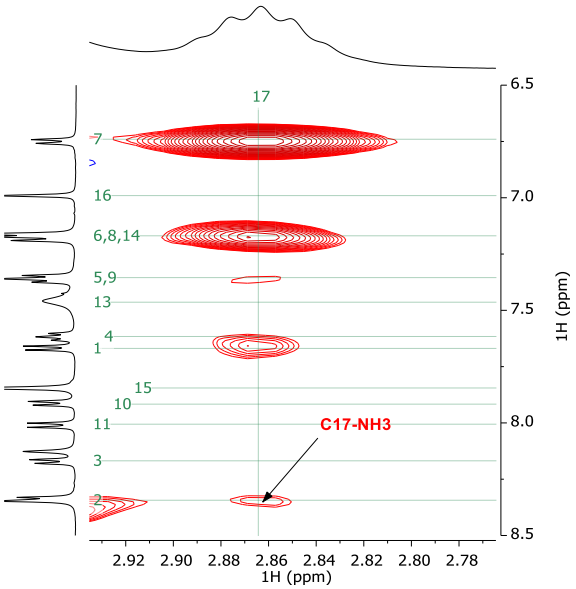


**Figure 3.15** Expansion of the $^{1}$H-$^{1}$H NOESY NMR spectra of (*S*)-**3.36a**·CN·Bu$_4$N (25 mM (*S*)-**3.36a**·CN·Bu$_4$N, $CD_2Cl_2$, 500 MHz, 193 K).

In this system, the most deshielded NH signal corresponded to NH2, followed by NH3 and NH1. This contrasts against the fluoride[50] and azide complexes, where the most deshielded NH signal corresponded to NH1, followed by NH3, and NH2. These were also different from the NH shifts in pure (*S*)-**3.36a** in $CD_2Cl_2$,[50] where NH2 was the most deshielded, followed by NH1, and NH3. These observations are consistent with the hypothesis that cyanide coordinates to (*S*)-**3.36a** in solution and interacts with the three NH protons but may imply a different position of the cyanide anion between the hydrogen bond donors of (*S*)-**3.36a**.

The combined results from these solution studies are consistent with the association of cyanide with urea NH protons of both an achiral mono-urea and chiral tri-coordinate *N*-alkyl bis-urea system. Further investigations with $^{13}C$ or $^{15}N$ labelled cyanide may provide further structural insights into the urea-cyanide relationship by establishing NOE relationships or scalar couplings.[52]

## 3.3 Enantioenriched γ-aminonitriles under HB-PTC

### 3.3.1 Reaction discovery and optimisation

The enantioselective ring opening of 3-substituted azetidinium salts with caesium fluoride was achieved under HB-PTC and produced valuable γ-aminofluorides.[53] These substrates were favoured above other substrates studied under HB-PTC since a similar enantioselective ring opening of 3-substituted azetidinium salts with cyanide would provide access to valuable enantioenriched γ-aminonitriles. It was hypothesised this reaction could be achieved with potassium cyanide under HB-PTC, given this platforms successful application to enantioselective catalysis with caesium fluoride, potassium fluoride,[44,45,50,53] and sodium azide.

Preformed azetidinium salts are prepared by direct alkylation of a corresponding azetidine or through a ring-opening alkylation and subsequent ring-closure (**Scheme 3.12A**).[53,54] A benzhydryl protecting group was required to improve reactivity towards fluoride under HB-

PTC.[53] Two alternative azetidinium salts were considered suitable model substrates; a 3-phenyl derived substrate and 3-hydroxy azetidine derived substrate. The ring opening of these substrates with cyanide may result in either nitriles **3.42a-b** or isonitriles **3.43a-b** as products (**Scheme 3.12B**).

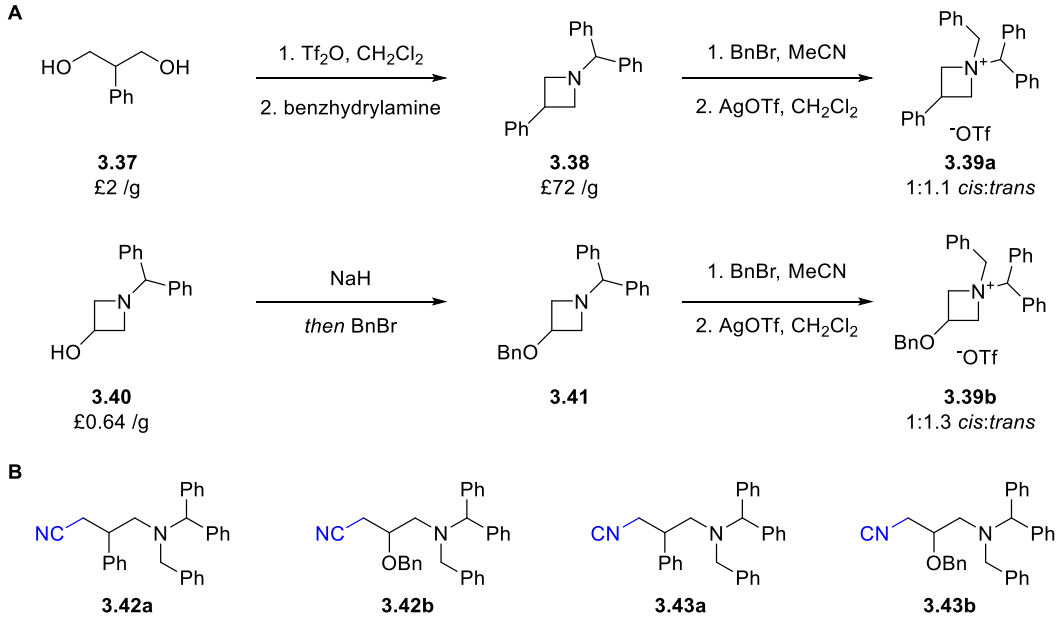


**Scheme 3.12** (A) Preparation of model azetidinium substrates. (B) Potential products from ring opening with cyanide.

Initial investigations to establish proof-of principle utilised substrate **3.39a** and **3.35** as catalyst (**Table 3.3**). Stirring potassium cyanide with azetidinium salt **3.39a** in $CH_2Cl_2$ resulted in a 60% NMRy of racemic nitrile product (±)-**3.42a**, and inclusion of **3.35** (0.1 equiv) provided an improved 70% NMRy of (±)-**3.42a**. The improvement from **3.35** was stronger in $PhCF_3$ solvent, with an uncatalysed NMRy of 5% and a catalysed NMRy of 45%. Exclusive formation of the nitrile product was detected in these experiments, indicating cyanide was exclusively reacting from its carbon atom. These encouraging results demonstrated the strong potential for this system to synthesise enantioenriched γ-aminonitriles, although also highlighted challenges such as a high background reaction that would need to be overcome to produce highly enantioenriched products.

**Table 3.3** Initial results with potassium cyanide and azetidinium **3.39a** in $CH_2Cl_2$.

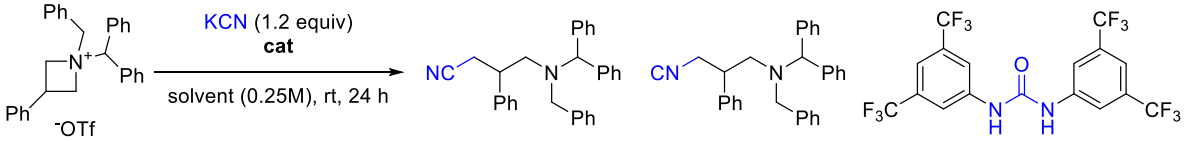


**3.39a**
1:1.1 *cis*:*trans*

(±)-**3.42a**

(±)-**3.43a**

**3.35**

| entry | solvent | cat | (±)-**3.42a** NMRy | (±)-**3.43a** NMRy |
|---|---|---|---|---|
| 1 | $CH_2Cl_2$ | none | 60% | 0 |
| 2 | | **3.35** (0.1 equiv) | 70% | 0 |
| 3 | $PhCF_3$ | none | 5% | 0 |
| 4 | | **3.35** (0.1 equiv) | 45% | 0 |

NMRy determined with $Ph_3CH$ (1 equiv) internal standard.

Investigations into an enantioselective transformation of azetidinium **3.39a** into enantioenriched γ-aminonitrile **3.42a** began with chiral urea catalyst (*S*)-**3.36a**. Stirring **3.39a** with potassium cyanide and (*S*)-**3.36a** in a selection of predominantly aromatic and halogenated solvents successfully produced enantioenriched **3.42a**, with the best results of 74% NMRy and 65:35 e.r. in trifluorotoluene (**Table 3.4**). Additional efforts to preclude moisture resulted in negligible differences to the NMRy or enantiomeric excess of **3.42a**.

**Table 3.4** Initial investigations into the enantioselective synthesis of **3.42a**.

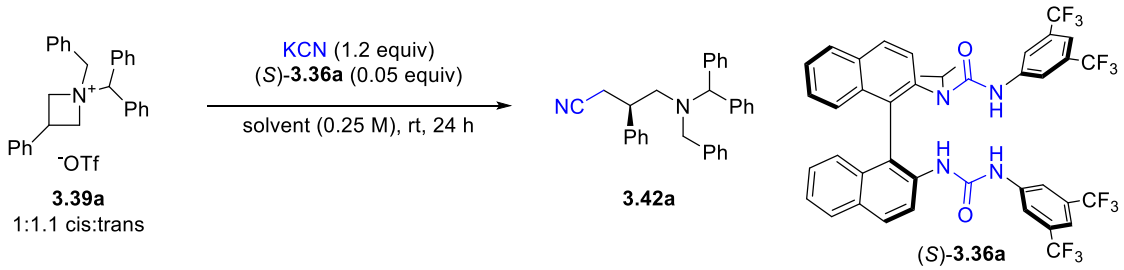


| entry | solvent | NMRy | e.r. |
|---|---|---|---|
| 1 | $CH_2Cl_2$ | 65% | 60:40 |
| **2**[a] | **$PhCF_3$** | **74%** | **65:35** |
| 3 | 1,2-difluorobenzene | 72% | 62:38 |
| 4 | $CHCl_3$ | 62% | 58:42 |
| 5 | 1,2-dichloroethane | 54% | 60:40 |
| 6 | PhF | 56% | 59:41 |
| 7 | PhMe | 61% | 62:38 |
| 8[a] | PhCl | 71% | 64:36 |
| 9[a] | trichloroethylene | 79% | 62:38 |
| 10 | MeCN | 77% | 53:47 |
| 11 | PhH | 71% | 62:38 |
| 12[a] | 1,2-dichlorobenzene | 75% | 64:36 |
| 13 | 1,2,3-trifluorobenzene | 63% | 63:37 |
| 14 | MTBE | 33% | 63:37 |
| 15 | 1,3-bis(trifluoromethyl)benzene | 60% | 64.5:35.5 |
| 16 | 1,2-bis(trifluoromethyl)benzene | 63% | 64.5:35.5 |

[a]NMRy and e.r. are mean of two individual runs. Absolute configuration of **3.42a** not determined. Reaction development was conducted in collaboration with G. Roagna.

With confidence in the reaction setup and procedure, both substrate **3.39a** and **3.39b** were evaluated against a series of catalysts. With (*S*)-**3.36a**, **3.42a** was produced in 74% NMRy and 65:35 e.r, whereas **3.42b** was produced in 76% NMRy and 71:29 e.r. (**Table 3.5**, entries 1 and 7). Tetradentate (*S*)-BINAM derived bis-urea catalyst (*S*)-**3.36b** produced **3.42a** and **3.42b** in similar NMRy at 46% and 76%, although consistently lower enantiomeric ratios at 55:45 and 58:42 respectively (**Table 3.5**, entries 2 and 8). Severely depleted NMRy and enantiomeric ratios were detected with bidentate catalysts (*S*)-**3.36c** and (*S*)-**3.36d**, producing **3.42a** and **3.42b** in up to 27% NMRy or 47:53 e.r. (**Table 3.5**, entries 3, 4, 9, and 10). (*S*)-**3.36e** with a smaller *N*-alkyl group produced **3.42a** and **3.42b** in slightly lower NMRy and e.r. at 68% NMRy and 61:39 and 67% NMRy and 68:32 e.r. respectively (**Table 3.5**, entries 5 and 11). These

studies upheld the advantageous single $^{i}$Pr group of (*S*)-**3.36** and revealed improved enantioselectivity with substrate **3.39b** over **3.39a**.

**Table 3.5** Investigations into the structural features of catalyst (*S*)-**3.36a** in the enantioselective synthesis of **3.42a** and **3.42b**.

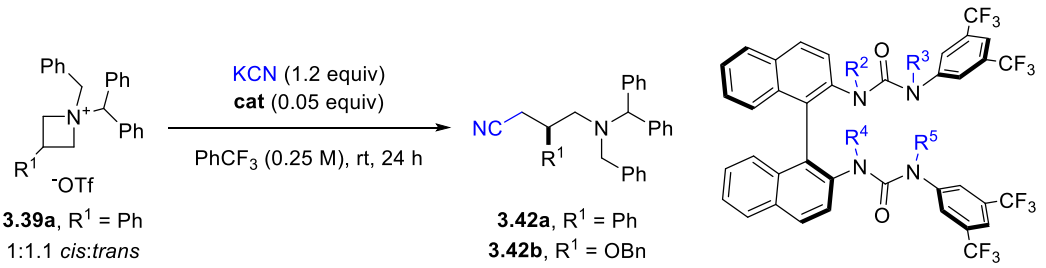


| entry | $R^1$ | cat | $R^2$ | $R^3$ | $R^4$ | $R^5$ | NMRy | e.r. |
|---|---|---|---|---|---|---|---|---|
| **1** | Ph | **(*S*)-3.36a** | **$^{i}$Pr** | **H** | **H** | **H** | **74%** | **65:35** |
| 2 | | (*S*)-**3.36b** | H | H | H | H | 46% | 55:45 |
| 3 | | (*S*)-**3.36c** | Me | H | Me | H | 8% | 44:56 |
| 4 | | (*S*)-**3.36d** | H | Me | H | Me | 3% | 47:53 |
| 5 | | (*S*)-**3.36e** | Me | H | H | H | 68% | 61:39 |
| 6 | | | none | | | | 5% | nd |
| **7** | OBn | **(*S*)-3.36a** | **$^{i}$Pr** | **H** | **H** | **H** | **76%** | **71:29** |
| 8 | | (*S*)-**3.36b** | H | H | H | H | 76% | 58:42 |
| 9 | | (*S*)-**3.36c** | Me | H | Me | H | 15% | 51:49 |
| 10 | | (*S*)-**3.36d** | H | Me | H | Me | 27% | 51:49 |
| 11 | | (*S*)-**3.36e** | Me | H | H | H | 67% | 68:32 |
| 12 | | | none | | | | 18% | nd |

NMRy determined with $Ph_3CH$ (1 equiv) internal standard. Absolute configuration of **3.42a-b** not determined. Reaction development was conducted in collaboration with G. Roagna.

Further catalyst optimisation focused on substrate **3.39b**, and several alternative catalyst classes were investigated (**Table 3.6**). These included commercial chiral thioureas (*S*,*R*,*R*)-**3.44**[55] and (*R*,*R*)-**3.45**,[56] a novel 1,2-diphenylethylenediamine based bis-urea (*R*,*R*)-**3.46**, a cinchona alkaloid derived urea **3.47**,[57] (*S*)-BINAM derived bis-amide (*S*)-**3.48**,[58] and tridentate *N*-alkyl (*S*)-BINAM derived bis-urea with two terphenyl groups (*S*)-**3.49a**.[45] Only (*S*)-**3.49a** produced **3.42b** in a higher enantiomeric ratio than (*S*)-**3.36a**, increasing from 71:29 to 73:27. However this was accompanied by a decrease in NMRy from 76% to 55%.

**Table 3.6** Evaluation of selected alternative catalyst classes.

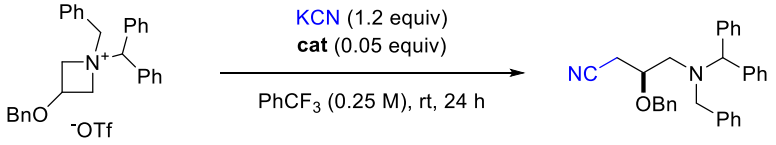


**3.39b**
1:1.3 *cis*:*trans*

**3.42b**

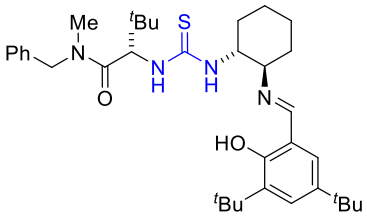

(*S*,*R*,*R*)-**3.44**

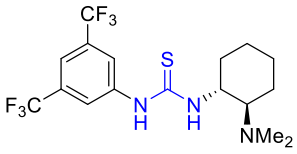

(*R*,*R*)-**3.45**

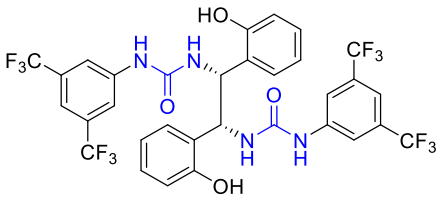

(*R*,*R*)-**3.46**

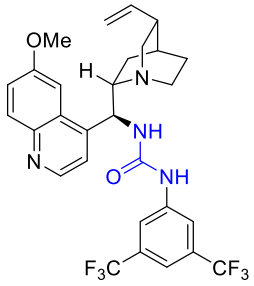

**3.47**

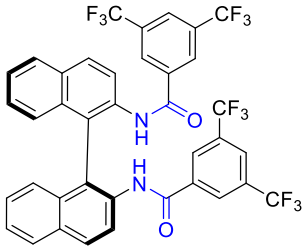

(*S*)-**3.48**

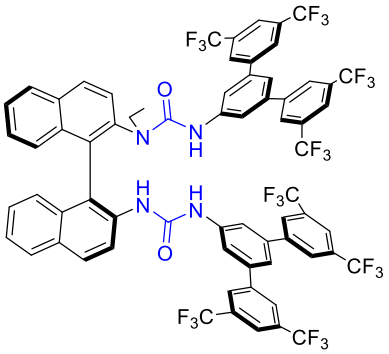

(*S*)-**3.49a**

| entry | cat | NMRy | e.r. |
|---|---|---|---|
| 1 | (*S*,*S*,*R*)-**3.44** | 50% | 51:49 |
| 2 | (*R*,*R*)-**3.45** | 21% | 50:50 |
| 3 | (*R*,*R*)-**3.46** | 32% | 52:48 |
| 4 | **3.47** | 27% | 52:48 |
| 5 | (*S*)-**3.48** | 43% | 54:46 |
| **6** | **(*S*)-3.49a** | **55%** | **73:27** |

NMRy determined with $Ph_3CH$ (1 equiv) internal standard. Absolute configuration of **3.42b** not determined. Reaction development was conducted in collaboration with G. Roagna.

Additional optimisation of reaction conditions with (*S*)-**3.49a** aimed to improve the conversion of starting material **3.39b** to product **3.42b** (**Table 3.7**). Full conversion could be achieved upon increasing the quantity of cyanide to 2.4 equivalents although this also reduced the enantiomeric ratio of the product formed (**Table 3.7**, entry 2). Lowering the reaction temperature to 4 °C improved the enantiomeric ratio to 72.5:27.5 whilst maintaining full conversion (**Table 3.7**, entry 3). Further reduction in temperature to -25 °C improved the enantiomeric ratio to 86:14 but also a significant reduction in NMRy to only 36% (**Table 3.7**,

entry 4). Attempts to achieved full conversion of **3.39b** at -25 °C were unsuccessful and the mass balance was determined by $^{1}$H NMR to be predominantly the *cis* starting material.

These results demonstrated lower enantiomeric ratios at higher conversions, which suggest the individual *cis*:*trans* isomers in the starting material possess different reactivities and lead to product with different levels of enantioselectivity. The comparably small reduction in enantiomeric ratio from 55% NMRy to 92% NMRy (**Table 3.7**, entries 1 and 2) suggest the major enantiomer produced from both starting materials isomers are of the same absolute configuration.

Reaction conditions enabling full conversion were desired for catalyst optimisation to ensure improvements in enantiomeric ratio were representative of an effect of improving the catalyst, and not an effect of unreacted *cis* starting material. Conducting the reaction at 4 °C with 2.4 equivalents of potassium cyanide in trifluorotoluene provided product with full conversion and a good enantiomeric ratio, and these conditions were utilised for further evaluation of catalysts derived from the (*S*)-**3.49a** structure.

**Table 3.7** Optimisation of reagent equivalents and reaction temperature.

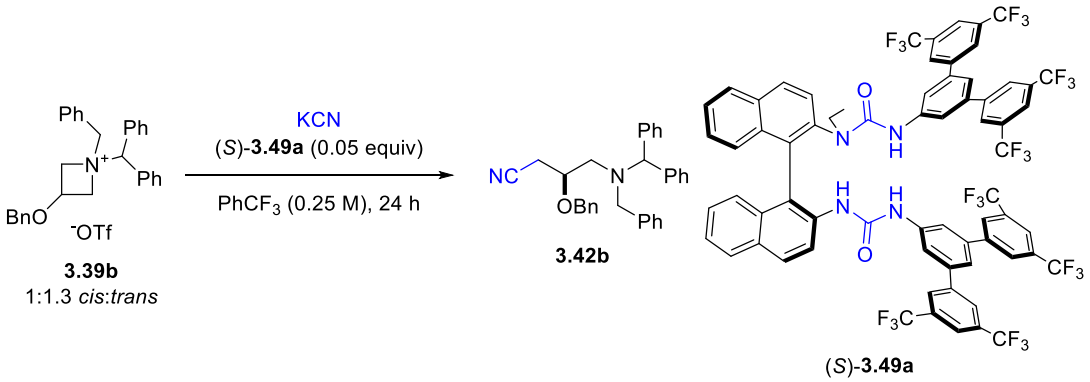


| entry | KCN equiv | temp | NMRy | e.r. |
|---|---|---|---|---|
| 1 | 1.2 | rt | 55% | 73.5:26.5 |
| 2 | 2.4 | rt | 92% | 69:31 |
| **3** | **2.4** | **4 °C** | **94%** | **72.5:27.5** |
| 4 | 2.4 | -25 °C | 36% | 86:14 |

NMRy determined with $Ph_3CH$ (1 equiv) internal standard. Absolute configuration of **3.42b** not determined. Reaction development was conducted in collaboration with G. Roagna.

With these improved conditions in hand, further catalyst synthesis and optimisation was undertaken (**Table 3.8**). A substantial improvement in enantioselectivity was observed by tuning the electronics of the aromatic rings of the catalyst. Whilst bromination of the (*S*)-BINAM backbone resulted in minor differences in the enantiomeric ratio of **3.42b**, addition of electron withdrawing groups *para* to the urea NH on the terphenyl ring resulted in significant improvements to enantioselectivity without compromising the yield. Conducting the reaction with catalyst (*S*)-**3.49h** containing an $OCF_2H$ group produced **3.42b** with full conversion and a high enantiomeric ratio.

**Table 3.8** Optimisation of catalyst electronics.

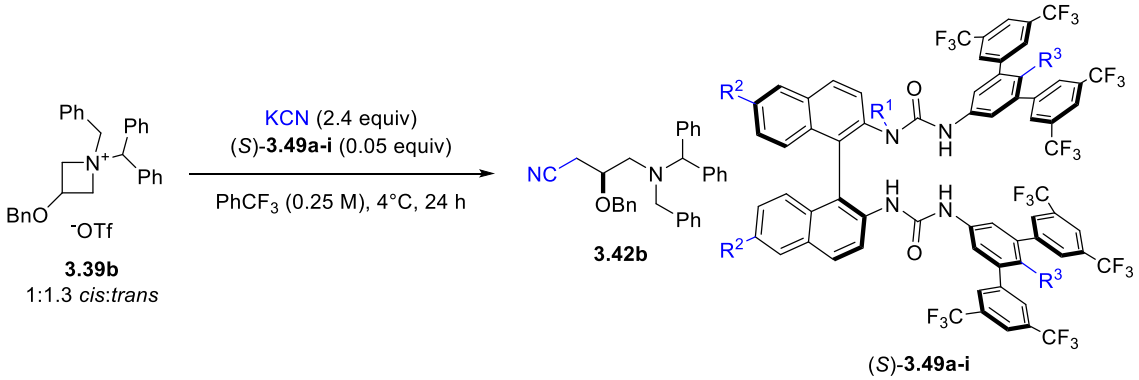


| entry | cat | $R^1$ | $R^2$ | $R^3$ | NMRy | e.r. |
|---|---|---|---|---|---|---|
| 1 | (*S*)-**3.49a** | Et | H | H | 94% | 72.5:27.5 |
| 2 | (*S*)-**3.49b** | $^i$Pr | H | H | 94% | 74:26 |
| 3 | (*S*)-**3.49c** | $^i$Pr | Br | H | 96% | 70:30 |
| 4 | (*S*)-**3.49d** | $^i$Pr | H | F | *quant* | 74:26 |
| 5 | (*S*)-**3.49e** | $^i$Pr | Br | F | 80% | 74.5:25.5 |
| 6 | (*S*)-**3.49f** | $^i$Pr | H | $OCH_2CF_3$ | 87% | 77:23 |
| 7 | (*S*)-**3.49g** | $^i$Pr | Br | $OCH_2CF_3$ | 93% | 77:23 |
| **8** | **(*S*)-3.49h** | **$^i$Pr** | **H** | **$OCF_2H$** | **95%** | **79:21** |
| 9 | (*S*)-**3.49i** | $^i$Pr | Br | $OCF_2H$ | 99% | 78:22 |

NMRy determined with $Ph_3CH$ (1 equiv) internal standard. Absolute configuration of **3.42b** not determined. Reaction development was conducted in collaboration with G. Roagna.

### 3.3.2 Reaction scope

At this stage, preliminary scope to understand the potential of this reaction was undertaken with the current optimal conditions and catalyst structure (**Scheme 3.13**). These included use of 2.4 equivalents of potassium cyanide, catalyst (*S*)-**3.49h**, trifluorotoluene solvent, and a temperature of 4 °C. Whilst these conditions appeared to have reduce effectiveness for the

3-phenylazetidine derived substrate **3.39a**, 3-hydroxyazetidine derived substrates differing in steric and electronic properties provided products **3.42b-d** in high NMR yields and good enantiomeric ratios.

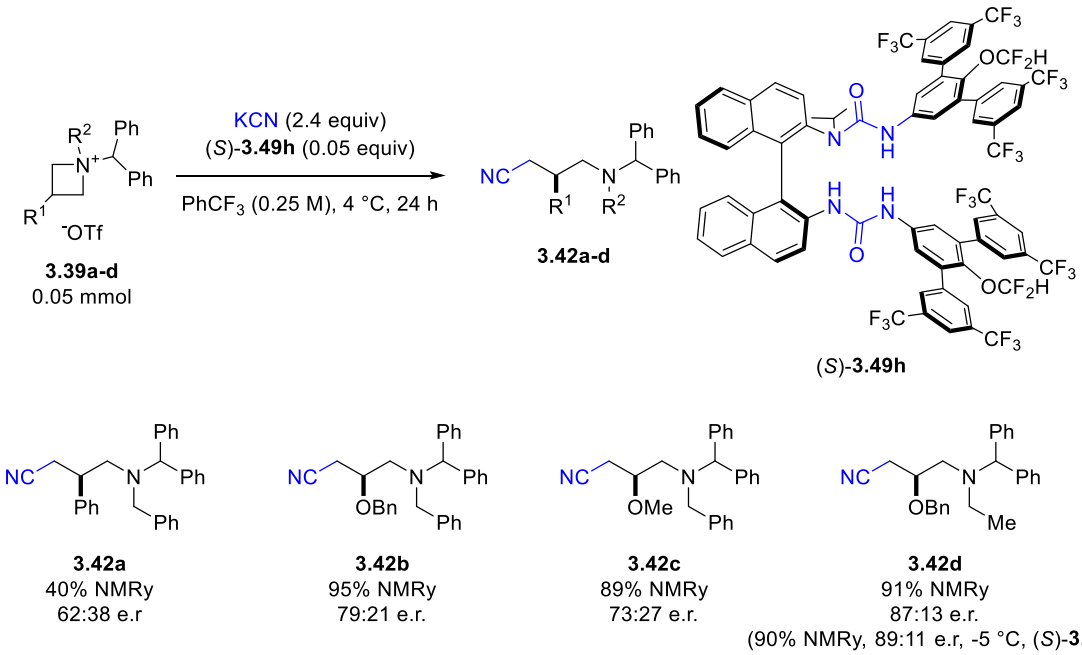


**Scheme 3.13** Preliminary substrate scope. NMRy determined with $Ph_3CH$ (1 equiv) internal standard. Absolute configuration of **3.42a-d** not determined. Reaction development was conducted in collaboration with G. Roagna.

These studies successfully demonstrate an enantioselective cyanation with potassium cyanide under HB-PTC conditions. The protocol developed was both practical and robust, achieving the synthesis of β-chiral nitrile products in high NMRy and good enantiomeric ratios with a suitable hydrogen bond donor catalyst.

## 3.4 Conclusions and outlook

The data obtained from the preparation and crystallisation of **3.35**·CN·$Bu_4N$ provided the first evidence for direct urea-cyanide coordination in the solid state by hydrogen bonding. These studies were reflected in the NMR investigations, reaffirming the ability for both **3.35** and (*S*)-**3.36a** to coordinate cyanide in solution. Further studies in solid state and solution with a broader range of urea hydrogen bond donors may inform the generality of the urea-cyanide relationship observed with **3.35** or (*S*)-**3.36a**, and whether stoichiometry or connectivity remain consistent upon variation of the urea or counter cation. NMR studies with $^{13}C$ or $^{15}N$

enriched cyanide may provide additional structural insights into the urea-cyanide interaction in solution by establishing NOE relationships or scalar couplings.[52]

A practical transformation of azetidinium salts into β-chiral γ-aminonitriles with potassium cyanide under HB-PTC conditions was also successfully developed. The protocol was both practical and robust, achieving the synthesis of β-chiral nitriles in high conversion and good enantiomeric ratios with a suitable hydrogen bond donor catalyst. Further catalyst optimisation may provide continued improvement to the enantioselectivity and scope of this transformation. This transformation also establishes a platform for potentially utilising potassium [$^{14}$C]cyanide for the synthesis of enantioenriched radiolabelled medicinally relevant molecules.[1]

## 3.5 References


1 F. F. Fleming, L. Yao, P. C. Ravikumar, L. Funk and B. C. Shook, *J. Med. Chem.*, 2010, **53**, 7902–7917.

2 P. L. Brower, D. E. Butler, C. F. Deering, T. V. Le, A. Millar, T. N. Nanninga and B. D. Roth, *Tetrahedron Lett.*, 1992, **33**, 2279–2282.

3 X. Chen, F. Xiong, W. Chen, Q. He and F. Chen, *J. Org. Chem.*, 2014, **79**, 2723–2728.

4 H. Ledford, *Nature*, 2011, **480**, 16–17.

5 CN. Pat., CN110922423 A, 2019.

6 T. K. Huyck, W. Gradishar, F. Manuguid and P. Kirkpatrick, *Nat. Rev. Drug Discov.*, 2011, **10**, 173–174.

7 Halaven: Holder of the Record, https://blogs.sciencemag.org/pipeline/archives/2010/11/18/halaven_holder_of_the_record, (accessed 25 August 2021).

8 K. B. Hansen, Y. Hsiao, F. Xu, N. Rivera, A. Clausen, M. Kubryk, S. Krska, T. Rosner, B. Simmons, J. Balsells, N. Ikemoto, Y. Sun, F. Spindler, C. Malan, E. J. J. Grabowski and J.

D. Armstrong, *J. Am. Chem. Soc.*, 2009, **131**, 8798–8804.

9 M. Fistikci, O. Gundogdu, D. Aktas, H. Secen, M. F. Sahin, R. Altundas and Y. Kara, *Tetrahedron*, 2012, **68**, 2607–2610.

10 S. Yan, G. Larson, J. Z. Wu, T. Appleby, Y. Ding, R. Hamatake, Z. Hong and N. Yao, *Bioorg. Med. Chem. Lett.*, 2007, **17**, 63–67.

11 V. Derdau, *J. Label. Compd. Radiopharm.*, 2018, **61**, 1012–1023.

12 R. Voges, J. R. Heys and T. Moenius, *Preparation of Compounds Labeled with Tritium and Carbon-14*, 2009.

13 K. Muramoto, K. Ohta, K. Shinzawa-Itoh, K. Kanda, M. Taniguchi, H. Nabekura, E. Yamashita, T. Tsukihara and S. Yoshikawa, *Proc. Natl. Acad. Sci.*, 2010, **107**, 7740–7745.

14 T. G. Conley and D. G. Priest, *Biochem. J.*, 1980, **187**, 733–738.

15 L. Gabison, T. Prangé, N. Colloc'h, M. El Hajji, B. Castro and M. Chiadmi, *BMC Struct. Biol.*, 2008, **8**, 32.

16 L. Rosenthaler, *Biochem. Z.*, 1908, **14**, 238–253.

17 H. Griengl, H. Schwab and M. Fechter, *Trends Biotechnol.*, 2000, **18**, 252–256.

18 W. Becker, H. Freund and E. Pfeil, *Angew. Chem. Int. Ed.*, 1965, **4**, 1079–1079.

19 P. Bracco, H. Busch, J. von Langermann and U. Hanefeld, *Org. Biomol. Chem.*, 2016, **14**, 6375–6389.

20 M. M. Elenkov, H. W. Hoeffken, L. Tang, B. Hauer and D. B. Janssen, *Adv. Synth. Catal.*, 2007, **349**, 2279–2285.

21 M. M. Elenkov, B. Hauer and D. B. Janssen, *Adv. Synth. Catal.*, 2006, **348**, 579–585.

22 G. Hasnaoui-Dijoux, M. Majerić Elenkov, J. H. Lutje Spelberg, B. Hauer and D. B. Janssen, *ChemBioChem*, 2008, **9**, 1048–1051.

23 R. O. Ramabhadran, Y. Hua, A. H. Flood and K. Raghavachari, *J. Phys. Chem. A*, 2014, **118**, 7418–7423.

24 T. W. Hudnall, C. W. Chiu and F. P. Gabbat, *Acc. Chem. Res.*, 2009, **42**, 388–397.

25 M. Müller, A. J. Karttunen and M. R. Buchner, *Chem. Sci.*, 2020, **11**, 5415–5422.

26 N. Kuhn, K. Eichele, M. Steimann, A. Al-Sheikh, B. Doser and C. Ochsenfeld, *Zeitschrift für Anorg. und Allg. Chemie*, 2006, **632**, 2268–2275.

27 T. C. W. Mak and R. K. McMullan, *J. Incl. Phenom.*, 1988, **6**, 473–481.

28 W. B. Wu, J. S. Yu and J. Zhou, *ACS Catal.*, 2020, **10**, 7668–7690.

29 N. ul H. Khan, R. I. Kureshy, S. H. R. Abdi, S. Agrawal and R. V. Jasra, *Coord. Chem. Rev.*, 2008, **252**, 593–623.

30 P. I. Dalko and L. Moisan, *Angew. Chem. Int. Ed.*, 2001, **40**, 3726–3748.

31 J. Wang, X. Liu and X. Feng, *Chem. Rev.*, 2011, **111**, 6947–6983.

32 S. J. Zuend, M. P. Coughlin, M. P. Lalonde and E. N. Jacobsen, *Nature*, 2009, **461**, 968–970.

33 T. Ooi, Y. Uematsu and K. Maruoka, *J. Am. Chem. Soc.*, 2006, **128**, 2548–2549.

34 H. Yan, J. Suk Oh, J.-W. Lee and C. Eui Song, *Nat. Commun.*, 2012, **3**, 1212.

35 K. Ohmatsu, Y. Furukawa, D. Nakaguro and T. Ooi, *Chem. Lett.*, 2015, **44**, 1350–1352.

36 Y. Liu, S. Shirakawa and K. Maruoka, *Org. Lett.*, 2013, **15**, 1230–1233.

37 US Pat., US9233920 (B2), 2016.

38 K. Ohmatsu, Y. Morita, M. Kiyokawa and T. Ooi, *J. Am. Chem. Soc.*, 2021, **143**, 11218–11224.

39 S. J. Zuend and E. N. Jacobsen, *J. Am. Chem. Soc.*, 2009, **131**, 15358–15374.

40 S. J. Zuend and E. N. Jacobsen, *J. Am. Chem. Soc.*, 2007, **129**, 15872–15883.

41 M. S. Sigman and E. N. Jacobsen, *J. Am. Chem. Soc.*, 1998, **120**, 4901–4902.

42 M. S. Sigman, P. Vachal and E. N. Jacobsen, *Angew. Chem. Int. Ed.*, 2000, **39**, 1279–1281.

43 L. Pfeifer, K. M. Engle, G. W. Pidgeon, H. A. Sparkes, A. L. Thompson, J. M. Brown and V. Gouverneur, *J. Am. Chem. Soc.*, 2016, **138**, 13314–13325.

44 G. Pupo, F. Ibba, D. M. H. Ascough, A. C. Vicini, P. Ricci, K. E. Christensen, L. Pfeifer, J. R. Morphy, J. M. Brown, R. S. Paton and V. Gouverneur, *Science*, 2018, **360**, 638–642.

45 G. Pupo, A. C. Vicini, D. M. H. Ascough, F. Ibba, K. E. Christensen, A. L. Thompson, J. M. Brown, R. S. Paton and V. Gouverneur, *J. Am. Chem. Soc.*, 2019, **141**, 2878–2883.

46 P. Thordarson, *Chem. Soc. Rev.*, 2011, **40**, 1305–1323.

47 E. N. W. Howe, M. Bhadbhade and P. Thordarson, *J. Am. Chem. Soc.*, 2014, **136**, 7505–7516.

48 P. M. E. Mancini, A. Terenzani, C. Adam and L. R. Vottero, *J. Phys. Org. Chem.*, 1997, **10**, 849–860.

49 S. J. Pike, E. Lavagnini, L. M. Varley, J. L. Cook and C. A. Hunter, *Chem. Sci.*, 2019, **10**, 5943–5951.

50 F. Ibba, G. Pupo, A. L. Thompson, J. M. Brown, T. D. W. Claridge and V. Gouverneur, *J. Am. Chem. Soc.*, 2020, **142**, 19731–19744.

51 supramolecular.org, http://supramolecular.org, (accessed 18 September 2019).

52 H.-J. Mo, Y. Shen and B.-H. Ye, *Inorg. Chem.*, 2012, **51**, 7174–7184.

53 G. Roagna, D. M. H. Ascough, F. Ibba, A. C. Vicini, A. Fontana, K. E. Christensen, A. Peschiulli, D. Oehlrich, A. Misale, A. A. Trabanco, R. S. Paton, G. Pupo and V. Gouverneur, *J. Am. Chem. Soc.*, 2020, **142**, 14045–14051.

54 D. Qian, M. Chen, A. C. Bissember and J. Sun, *Angew. Chem. Int. Ed.*, 2018, **57**, 3763–3766.

55 A. G. Wenzel and E. N. Jacobsen, *J. Am. Chem. Soc.*, 2002, **124**, 12964–12965.

56 T. Okino, Y. Hoashi and Y. Takemoto, *J. Am. Chem. Soc.*, 2003, **125**, 12672–12673.

57 W. Wu, L. Min, L. Zhu and C.-S. Lee, *Adv. Synth. Catal.*, 2011, **353**, 1135–1145.

58 Y. Sudo, D. Shirasaki, S. Harada and A. Nishida, *J. Am. Chem. Soc.*, 2008, **130**, 12588–12589.

1 F. F. Fleming, L. Yao, P. C. Ravikumar, L. Funk and B. C. Shook, *J. Med. Chem.*, 2010, **53**, 7902–7917.

2 P. L. Brower, D. E. Butler, C. F. Deering, T. V. Le, A. Millar, T. N. Nanninga and B. D. Roth, *Tetrahedron Lett.*, 1992, **33**, 2279–2282.

3 X. Chen, F. Xiong, W. Chen, Q. He and F. Chen, *J. Org. Chem.*, 2014, **79**, 2723–2728.

4 H. Ledford, *Nature*, 2011, **480**, 16–17.

5 CN. Pat., CN110922423 A, 2019.

6 T. K. Huyck, W. Gradishar, F. Manuguid and P. Kirkpatrick, *Nat. Rev. Drug Discov.*, 2011, **10**, 173–174.

7 Halaven: Holder of the Record, https://blogs.sciencemag.org/pipeline/archives/2010/11/18/halaven_holder_of_the_record, (accessed 25 August 2021).

8 K. B. Hansen, Y. Hsiao, F. Xu, N. Rivera, A. Clausen, M. Kubryk, S. Krska, T. Rosner, B. Simmons, J. Balsells, N. Ikemoto, Y. Sun, F. Spindler, C. Malan, E. J. J. Grabowski and J. D. Armstrong, *J. Am. Chem. Soc.*, 2009, **131**, 8798–8804.

9 M. Fistikci, O. Gundogdu, D. Aktas, H. Secen, M. F. Sahin, R. Altundas and Y. Kara, *Tetrahedron*, 2012, **68**, 2607–2610.

10 S. Yan, G. Larson, J. Z. Wu, T. Appleby, Y. Ding, R. Hamatake, Z. Hong and N. Yao, *Bioorg. Med. Chem. Lett.*, 2007, **17**, 63–67.

11 V. Derdau, *J. Label. Compd. Radiopharm.*, 2018, **61**, 1012–1023.

12 R. Voges, J. R. Heys and T. Moenius, *Preparation of Compounds Labeled with Tritium and Carbon-14*, 2009.

13 K. Muramoto, K. Ohta, K. Shinzawa-Itoh, K. Kanda, M. Taniguchi, H. Nabekura, E. Yamashita, T. Tsukihara and S. Yoshikawa, *Proc. Natl. Acad. Sci.*, 2010, **107**, 7740–7745.

14 T. G. Conley and D. G. Priest, *Biochem. J.*, 1980, **187**, 733–738.

15 L. Gabison, T. Prangé, N. Colloc'h, M. El Hajji, B. Castro and M. Chiadmi, *BMC Struct. Biol.*, 2008, **8**, 32.

16 L. Rosenthaler, *Biochem. Z.*, 1908, **14**, 238–253.

17 H. Griengl, H. Schwab and M. Fechter, *Trends Biotechnol.*, 2000, **18**, 252–256.

18 W. Becker, H. Freund and E. Pfeil, *Angew. Chemie Int. Ed.*, 1965, **4**, 1079–1079.

19 P. Bracco, H. Busch, J. von Langermann and U. Hanefeld, *Org. Biomol. Chem.*, 2016, **14**, 6375–6389.

20 M. M. Elenkov, H. W. Hoeffken, L. Tang, B. Hauer and D. B. Janssen, *Adv. Synth. Catal.*, 2007, **349**, 2279–2285.

21 M. M. Elenkov, B. Hauer and D. B. Janssen, *Adv. Synth. Catal.*, 2006, **348**, 579–585.

22 G. Hasnaoui-Dijoux, M. Majerić Elenkov, J. H. Lutje Spelberg, B. Hauer and D. B. Janssen, *ChemBioChem*, 2008, **9**, 1048–1051.

23 R. O. Ramabhadran, Y. Hua, A. H. Flood and K. Raghavachari, *J. Phys. Chem. A*, 2014, **118**, 7418–7423.

24 T. W. Hudnall, C. W. Chiu and F. P. Gabbat, *Acc. Chem. Res.*, 2009, **42**, 388–397.

25 M. Müller, A. J. Karttunen and M. R. Buchner, *Chem. Sci.*, 2020, **11**, 5415–5422.

26 N. Kuhn, K. Eichele, M. Steimann, A. Al-Sheikh, B. Doser and C. Ochsenfeld, *Zeitschrift für Anorg. und Allg. Chemie*, 2006, **632**, 2268–2275.

27 T. C. W. Mak and R. K. McMullan, *J. Incl. Phenom.*, 1988, **6**, 473–481.

28 W. B. Wu, J. S. Yu and J. Zhou, *ACS Catal.*, 2020, **10**, 7668–7690.

29 N. ul H. Khan, R. I. Kureshy, S. H. R. Abdi, S. Agrawal and R. V. Jasra, *Coord. Chem. Rev.*, 2008, **252**, 593–623.

30 P. I. Dalko and L. Moisan, *Angew. Chemie Int. Ed.*, 2001, **40**, 3726–3748.

31 J. Wang, X. Liu and X. Feng, *Chem. Rev.*, 2011, **111**, 6947–6983.

32 S. J. Zuend, M. P. Coughlin, M. P. Lalonde and E. N. Jacobsen, *Nature*, 2009, **461**, 968–970.

33 T. Ooi, Y. Uematsu and K. Maruoka, *J. Am. Chem. Soc.*, 2006, **128**, 2548–2549.

34 H. Yan, J. Suk Oh, J.-W. Lee and C. Eui Song, *Nat. Commun.*, 2012, **3**, 1212.

35 K. Ohmatsu, Y. Furukawa, D. Nakaguro and T. Ooi, *Chem. Lett.*, 2015, **44**, 1350–1352.

36 Y. Liu, S. Shirakawa and K. Maruoka, *Org. Lett.*, 2013, **15**, 1230–1233.

37 US Pat., US9233920 (B2), 2016.

38 K. Ohmatsu, Y. Morita, M. Kiyokawa and T. Ooi, *J. Am. Chem. Soc.*, 2021, **143**, 11218–11224.

39 S. J. Zuend and E. N. Jacobsen, *J. Am. Chem. Soc.*, 2009, **131**, 15358–15374.

40 S. J. Zuend and E. N. Jacobsen, *J. Am. Chem. Soc.*, 2007, **129**, 15872–15883.

41 M. S. Sigman and E. N. Jacobsen, *J. Am. Chem. Soc.*, 1998, **120**, 4901–4902.

42 M. S. Sigman, P. Vachal and E. N. Jacobsen, *Angew. Chemie Int. Ed.*, 2000, **39**, 1279–1281.

43 L. Pfeifer, K. M. Engle, G. W. Pidgeon, H. A. Sparkes, A. L. Thompson, J. M. Brown and V. Gouverneur, *J. Am. Chem. Soc.*, 2016, **138**, 13314–13325.

44 G. Pupo, F. Ibba, D. M. H. Ascough, A. C. Vicini, P. Ricci, K. E. Christensen, L. Pfeifer, J. R. Morphy, J. M. Brown, R. S. Paton and V. Gouverneur, *Science*, 2018, **360**, 638–642.

45 G. Pupo, A. C. Vicini, D. M. H. Ascough, F. Ibba, K. E. Christensen, A. L. Thompson, J. M. Brown, R. S. Paton and V. Gouverneur, *J. Am. Chem. Soc.*, 2019, **141**, 2878–2883.

46 P. Thordarson, *Chem. Soc. Rev.*, 2011, **40**, 1305–1323.

47 E. N. W. Howe, M. Bhadbhade and P. Thordarson, *J. Am. Chem. Soc.*, 2014, **136**, 7505–7516.

48 P. M. E. Mancini, A. Terenzani, C. Adam and L. R. Vottero, *J. Phys. Org. Chem.*, 1997, **10**, 849–860.

49 S. J. Pike, E. Lavagnini, L. M. Varley, J. L. Cook and C. A. Hunter, *Chem. Sci.*, 2019, **10**, 5943–5951.

50 F. Ibba, G. Pupo, A. L. Thompson, J. M. Brown, T. D. W. Claridge and V. Gouverneur, *J. Am. Chem. Soc.*, 2020, **142**, 19731–19744.

51 supramolecular.org, http://supramolecular.org, (accessed 18 September 2019).

52 H.-J. Mo, Y. Shen and B.-H. Ye, *Inorg. Chem.*, 2012, **51**, 7174–7184.

53 G. Roagna, D. M. H. Ascough, F. Ibba, A. C. Vicini, A. Fontana, K. E. Christensen, A. Peschiulli, D. Oehlrich, A. Misale, A. A. Trabanco, R. S. Paton, G. Pupo and V. Gouverneur, *J. Am. Chem. Soc.*, 2020, **142**, 14045–14051.

54 D. Qian, M. Chen, A. C. Bissember and J. Sun, *Angew. Chemie Int. Ed.*, 2018, **57**, 3763–3766.

55 A. G. Wenzel and E. N. Jacobsen, *J. Am. Chem. Soc.*, 2002, **124**, 12964–12965.

56 T. Okino, Y. Hoashi and Y. Takemoto, *J. Am. Chem. Soc.*, 2003, **125**, 12672–12673.

57 W. Wu, L. Min, L. Zhu and C.-S. Lee, *Adv. Synth. Catal.*, 2011, **353**, 1135–1145.

58 Y. Sudo, D. Shirasaki, S. Harada and A. Nishida, *J. Am. Chem. Soc.*, 2008, **130**, 12588–12589.

# 4 Supporting Information

## 4.1 General Considerations

### 4.1.1 Reagents and solvents

All reagents and solvents were purchased from commercial suppliers and used without further purification unless stated otherwise. Sodium cyanide was ground before use. Tetrabutylammonium azide and cyanide were purchased from Sigma-Aldrich, dried over $P_2O_5$ and stored under nitrogen. Dry THF, $CH_2Cl_2$ and MeCN were obtained from a MBRAUN SPS-5 bench-top unit. $CDCl_3$ was purchased from Sigma-Aldrich and stored over $K_2CO_3$.

### 4.1.2 Equipment and analysis

Reactions at 4 °C were conducted in a cold room. Other reactions requiring prolonged refrigeration were kept cold with an ethanol or isopropyl alcohol bath cooled using a Thermo Scientific HAAKE EK immersion cooler.

Melting points were measured with a Gallenkamp melting point apparatus equipped with a mercury 76 mm partial immersion thermometer.

Infrared spectra were recorded on a Bruker Tensor 27 FT-IR spectrometer equipped with a diamond ATR module.

NMR spectra for characterisation were obtained on Bruker AVANCE III HD 400 and 500 MHz spectrometers. Chemical shifts are reported in ppm and coupling constants are reported in Hz and rounded to the nearest 0.5 Hz. $^{1}H$ and $^{13}C$ chemical shifts are referenced to the appropriate residual solvent signal.[1] $^{19}F$ chemical shifts were observed directly and referenced to external $CFCl_3$. $^{15}N$ chemical shifts were observed directly and referenced to external $NH_{3(l)}$.

High resolution mass spectra were recorded by the University of Oxford, Department of Chemistry High Resolution Sample Submission Service. High resolution values are calculated to four decimal places from the molecular formula, and all values are within a tolerance of 5 ppm.

Specific rotations were recorded on a UniPol L2000 Polarimeter with a path length of 10 cm using the sodium D-line (589 nm). Specific rotations are reported in units of ° $dm^2$ $g^{-1}$. Concentration (c) is given in g/100 mL.

Single crystal X-ray diffraction data were obtained by the University of Oxford, Department of Chemistry X-Ray Service.

Analytical chiral HPLC was performed on a SHIMADZU Prominence-*i* LC2030-LT instrument.

**4.1.3 Azide quench**

Glassware and equipment contaminated with azide (from $NaN_3$, $Bu_4N{\cdot}N_3$ etc.) were washed with water into a glass beaker/conical flask and quenched according to a modified literature procedure.[2]

The collected washings were diluted such that the azide concentration was <5% (w/w). A >40% excess (with respect to azide) of $NaNO_2$ (20% in $H_2O$) was added, followed by careful addition of $H_2SO_4$ (20% in $H_2O$) with gentle stirring. This generates nitrous acid in situ, which reacts fast with sodium azide to form $N_2O$ and $N_2$ gas.[3] The order of addition is important to avoid releasing hydrazoic acid. After gas evolution ceased, the solution was checked with litmus and starch-iodide paper to ensure it was acidic and contained excess nitrite. The mixture was then disposed of as standard aqueous waste.

**4.1.4 Cyanide quench**

Glassware and equipment contaminated with cyanide was washed with water and collected. The solution was basified to above pH 8.5 with 1 M NaOH. Excess bleach was added carefully to beaker/conical flask, and the mixture was left standing overnight. This results in oxidation of the cyanide.[4] The mixture was then disposed of as standard aqueous waste.

## 4.2 General procedure for $^1$H NMR titrations

### 4.2.1 Titration procedure

$^1$H NMR spectra were recorded on Bruker AVANCE III HD 500 MHz spectrometers at 298 K. A solution of host (0.5 mL, 2 mM) was placed in an NMR tube. A $^1$H NMR spectrum was recorded followed by stepwise addition (0.0 equiv, 0.2 equiv, 0.4 equiv, 0.6 equiv, 0.8 equiv, 1.0 equiv, 1.2 equiv, 1.4 equiv, 1.6 equiv, 1.8 equiv, 2.0 equiv, 2.5 equiv, 3.0 equiv, 4.0 equiv, 5.0 equiv, 7.0 equiv, 10.0 equiv) of a solution of the selected salt (100 mM) using a 25 or 50 µL Hamilton Microlitre syringe. After each addition, the sample was shaken thoroughly.

### 4.2.2 Data analysis & model fitting

Data was analysed with BindFit v0.5,[5] enabling a 'global analysis' approach, improving the quality of the resultant fits.[5,6] Errors in association constants provided are the standard deviation from three independent repetitions.

Details of BindFit v0.5,[5] derivation of equations,[6] and descriptions of models implemented and respective equations have been previously published and are briefly summarized below.[7,8]

**1:1 Binding model**

$$\underset{\mathbf{H}}{\text{urea}} \quad \underset{\mathbf{G}}{\text{anion}} \quad \overset{K_{a,1:1}}{\rightleftharpoons} \quad \underset{\mathbf{HG}}{\text{urea-anion}}$$

$$K_{a,1:1} = \frac{[\mathbf{HG}]}{[\mathbf{H}][\mathbf{G}]} \tag{4.1}$$

$$[\mathbf{G}]_0 = [\mathbf{G}] + [\mathbf{HG}] \tag{4.2}$$

$$[\mathbf{H}]_0 = [\mathbf{H}] + [\mathbf{HG}] \tag{4.3}$$

$$\Delta\delta_{obs} = \delta_{\Delta HG}\left(\frac{[\mathbf{HG}]}{[\mathbf{H}]_0}\right) \tag{4.4}$$

The concentration of urea **H**, anion **G**, and the urea-anion complex **HG** during the titration is unknown but can be related to their initial concentrations $[\mathbf{H}]_0$ and $[\mathbf{G}]_0$ through eqn (2) and (3).

Assuming unbound **G** has negligible impact on the chemical shift of **H**, the change in the observed chemical shift $\Delta\delta_{obs}$ can be described as a function of the chemical shift change of pure **HG** $\delta_{\Delta HG}$, weighted by its mole fraction (eqn (4.4)).[6]

Rearrangement of eqn (4.1), (4.2), (4.3), and (4.4) provides eqn (4.5), which relates $\Delta\delta_{obs}$ to $K_{a(1:1)}$ with known constants.

$$\Delta\delta_{obs} = \frac{\delta_{\Delta HG}}{[\mathbf{H}]_0} \cdot \frac{1}{2}\left(\left([\mathbf{G}]_0 + [\mathbf{H}]_0 + \frac{1}{K_{a,1:1}}\right) - \sqrt{\left([\mathbf{G}]_0 + [\mathbf{H}]_0 + \frac{1}{K_{a,1:1}}\right)^2 - 4[\mathbf{H}]_0[\mathbf{G}]_\mathbf{0}}\right) \quad (4.5)$$

**2:1 Binding model**


$$K_{a,1:1} = \frac{[\mathbf{HG}]}{[\mathbf{H}][\mathbf{G}]} \quad (4.1)$$

$$K_{a,2:1} = \frac{[\mathbf{H_2G}]}{[\mathbf{H}][\mathbf{HG}]} \quad (4.6)$$

$$[\mathbf{H}]_0 = [\mathbf{H}] + [\mathbf{HG}] + 2[\mathbf{H_2G}] \quad (4.7)$$

$$[\mathbf{G}]_0 = [\mathbf{G}] + [\mathbf{HG}] + [\mathbf{H_2G}] \quad (4.8)$$

$$\Delta\delta_{obs} = \delta_{\Delta HG}\left(\frac{[\mathbf{HG}]}{[\mathbf{H}]_0}\right) + 2\delta_{\Delta H_2G}\left(\frac{[\mathbf{H_2G}]}{[\mathbf{H}]_0}\right) \quad (4.9)$$

The concentration of urea **H**, anion **G**, the urea-anion complex **HG** and the bis-urea-anion complex **H₂G** during the titration is unknown but can be related to their initial concentrations $[\mathbf{H}]_0$ and $[\mathbf{G}]_0$ through eqn (4.7) and (4.8).

Assuming unbound **G** has negligible impact on the chemical shift of **H**, the change in the observed chemical shift $\Delta\delta_{obs}$ can be described as the sum of the chemical shift changes of pure **HG** $\delta_{\Delta HG}$ and pure **H₂G** $\delta_{\Delta H_2G}$ weighted by their respective mole fractions (eqn (4.9)).[6]

Rearrangement of eqn (4.1), (4.6), (4.7), (4.8), and (4.9) provides eqn (4.10), which relates $\Delta\delta_{obs}$ to $K_{a(1:1)}$, $K_{a(2:1)}$, $\delta_{\Delta HG}$, and $\delta_{\Delta H_2G}$ in terms of **H**. The cubic equation for **H** in terms of known constants is given by eqn (4.11) and can be derived from eqn (4.1), (4.6), (4.7), and (4.8).

$$\Delta\delta_{obs} = \frac{\delta_{\Delta HG}K_{a,1:1}[\mathbf{H}][\mathbf{G}]_0 + 2\delta_{\Delta H_2G}K_{a,1:1}K_{a,2:1}[\mathbf{G}]_0[\mathbf{H}]^2}{[\mathbf{H}]_0\left(1 + K_{a,1:1}[\mathbf{H}] + K_{a,1:1}K_{a,2:1}[\mathbf{H}]^2\right)} \quad (4.10)$$

$$\begin{gathered} A[\mathbf{H}]^3 + B[\mathbf{H}]^2 + C[\mathbf{H}] - [\mathbf{H}]_0 = 0 \\ A = K_{a,1:1}K_{a,2:1} \\ B = K_{a,1:1}\left(2K_{a,2:1}[\mathbf{G}]_0 - K_{a,2:1}[\mathbf{H}]_0 + 1\right) \\ C = K_{a,1:1}([\mathbf{G}]_0 - [\mathbf{H}]_0) + 1 \end{gathered} \quad (4.11)$$

## 4.3 Supporting Information for Chapter 2

### 4.3.1 General procedures

**General procedure 2.1 (GP2.1, synthesis of hydrogen bonded azide complexes)**
Dry MeCN (0.10 M) was added to tetrabutylammonium azide (1.00 equiv) and hydrogen bond donor **2.41-2.45** (1.00 equiv). The reaction mixture stirred at rt for 24 h. The reaction mixture was evaporated to dryness to afford an amorphous solid. The solids obtained were used without further purification.

**General procedure 2.2 (GP2.2, synthesis of racemic reference samples)**
1,2-difluorobenzene (0.40 mL, 0.25 M) was added to a 1.75 mL vial charged sequentially with substrate (0.10 mmol, 1.00 equiv), **2.41a** (4.8 mg, 0.01 mmol, 0.10 equiv), and sodium azide (7.8 mg, 1.20 mmol, 1.20 equiv). The reaction mixture was stirred at rt and 1200 rpm for 24 h. The reaction mixture was purified by flash silica chromatography.

**NB**: Reference for **2.47s** required 50 °C.

**General procedure 2.3 (GP2.3, optimisation for the enantioselective synthesis of β-thioazides)**
Solvent was added to a 1.75 mL vial charged sequentially (±)-**2.39b** (19.9 mg, 0.05 mmol, 1.00 equiv), catalyst, and sodium azide (3.9 mg, 1.20 mmol, 1.20 equiv). The reaction mixture was stirred at rt and 1200 rpm for 24 h. The reaction mixture filtered through a silica plug, eluted with $Et_2O$, and concentrated to afford crude product. The NMRy was determined by $^1H$ NMR with $CH_2Br_2$ internal standard. The enantiomeric ratio was determined with HPLC on a sample purified by pTLC.

**General procedure 2.4 (GP2.4, achiral reaction screening)**
1,2-difluorobenzene (0.20 mL, 0.25 M) was added to a 1.75 mL vial charged sequentially with (±)-**2.46a** (15 mg, 0.05 mmol, 1.00 equiv), catalyst (0.10 equiv), and sodium azide (3.9 mg, 0.06 mmol, 1.20 equiv), and in a 1.75 mL vial. The reaction mixture was stirred at rt and 1200 rpm for 90 min. The reaction mixture was filtered through silica, eluted with $Et_2O$, and

concentrated. Yield was determined by quantitative $^1$H NMR with $Ph_3CH$ (6.1 mg, 0.025 mmol, 0.50 equiv) as internal standard.

**General procedure 2.5 (GP2.5, optimisation for the enantioselective synthesis of β-aminoazides)**
1,2-difluorobenzene (0.40 mL, 0.25 M) was added to a 1.75 mL vial charged sequentially with (±)-**2.46a** (30 mg, 0.10 mmol, 1.00 equiv), catalyst, and azide source. The suspension was stirred at the indicated temperature at 1200 rpm for the indicated time. The reaction mixture was applied directly to a silica column and purified by flash silica chromatography (elution gradient 0 to 10% $Et_2O$ in pentane) to afford **2.47**. **HPLC** DAICEL CHIRALPAK® IB-3, 0.1% $BuNH_2$ and 0.9% IPA in heptane, 1 mL min$^{-1}$, $t_1$ = 3.23, $t_2$ = 3.73.

**General procedure 2.6 (GP2.6, synthesis of β-amino alcohols)**
The amine and epoxide (1.00 equiv) were stirred in a pressure tube at 100 °C for the indicated time. The reaction mixture was concentrated to afford crude product. The crude product was purified as indicated.

**General procedure 2.7 (GP2.7, synthesis of β-amino chlorides)**
Methanesulfonyl chloride (1.50 equiv) was added dropwise to a solution of the β-amino alcohol (1.00 equiv) and triethylamine (1.50 equiv) in $CH_2Cl_2$ (0.2 M) at 0 °C under $N_2$. The reaction mixture was stirred at rt for 2 h. The reaction mixture was washed with sat. $NaHCO_3$ and sat. brine, dried with $MgSO_4$, filtered, and concentrated to afford crude product. The crude product was purified as indicated. All β-amino chlorides were stored in the freezer.

**NB**: Degradation of β-amino chlorides was observed upon prolonged exposure to silica.

**General procedure 2.8 (GP2.8, synthesis of enantioenriched β-amino azides)**
**Standard scale**: A 2 mL Schlenk tube (7 mm internal diameter) was charged sequentially with substrate (0.20 mmol, 1.00 equiv), (*S*)-**2.43b** (16.7 mg, 0.02 mmol, 0.10 equiv), and sodium azide (31.2 mg, 0.48 mmol, 2.40 equiv) under air. 1,2-difluorobenzene (0.8 mL, 0.25 M) was added to the Schlenk tube. The suspension was stirred at the indicated temperature at 1200 rpm for 72 h. The reaction mixture was diluted with $Et_2O$ (2 mL) and washed with $H_2O$ (2

mL). **Aqueous washings containing the excess azide were quenched according to the method described *vida supra*.** The organic layer was dried with $MgSO_4$, filtered, and concentrated to afford crude product. The crude product was purified as indicated.

Reported yields are the mean of two independent reactions.

**4.3.2 Synthesis of hydrogen bond donors**

**2.41a**,[9] **2.41b**,[10] **2.41c**,[11] **2.41d**,[12] **2.41e**,[12] **2.41g**,[12] **2.41h**,[13] **2.42**,[11] and (*S*)-**2.43a-c**,[14] were prepared according to the reported literature procedures.

***N*$^1$,*N*$^2$-bis(3,5-bis(trifluoromethyl)phenyl)oxalamide (2.45)**

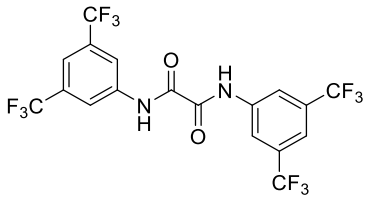

Oxalyl chloride (0.43 mL, 5.1 mmol, 0.51 equiv) was added to a solution of 3,5-bis(trifluoromethyl)aniline (1.56 mL, 10 mmol, 1.00 equiv) in dry THF (20 mL) under $N_2$. The reaction mixture was heated to reflux for 18 h. The reaction mixture was concentrated to dryness to afford crude product. The crude solid was washed with pentane, then dried to afford the title compound (2.04 g, 3.98 mmol, 80%) as a white solid.

**mp** 263-265 °C; **$\nu_{max}$** (neat) /cm$^{-1}$ 2161, 2033, 1676, 1543, 1375, 1274, 1129, 891, 681; **$^1$H NMR** (400 MHz, Acetone-$d_6$) δ 10.73 (s, 2H), 8.61 (s, 4H), 7.84 (s, 2H); **$^{19}$F NMR** (377 MHz, Acetone-$d_6$) δ -63.72; **$^{13}$C NMR** (101 MHz, Acetone-$d_6$) δ 159.2, 140.3, 132.7 (q, *J* = 33.5 Hz), 124.3 (q, *J* = 272.0 Hz), 121.2 (q, *J* = 4.0 Hz), 118.8 (p, *J* = 4.0 Hz); **HRMS** (ESI$^+$) calc. for $C_{18}H_7O_2N_2F_{12}^+$ ([M-H]$^-$): 511.0321; found: 511.0317.

**(±)-*N*$^2$-isopropyl-[1,1'-binaphthalene]-2,2'-diamine**

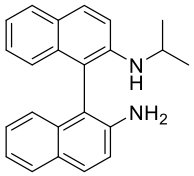

Prepared according to the literature procedure for (*S*)-*N*$^2$-isopropyl-[1,1'-binaphthalene]-2,2'-diamine using (±)-1,1'-bi(2-naphthylamine) instead of (*S*)-1,1'-bi(2-naphthylamine).[14]

**NB**: All spectra identical to (*S*)-*N*$^2$-isopropyl-[1,1'-binaphthalene]-2,2'-diamine.[14]

**(±)-3-(3,5-bis(trifluoromethyl)phenyl)-1-(2'-(3-(3,5-bis(trifluoromethyl)phenyl)ureido)-[1,1'-binaphthalen]-2-yl)-1-isopropylurea ((±)-2.43b)**

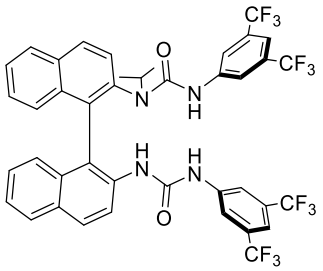

Prepared according to the literature procedure for (*S*)-**2.43b** with (±)-*N*$^2$-isopropyl-[1,1'-binaphthalene]-2,2'-diamine instead of (*S*)-*N*$^2$-isopropyl-[1,1'-binaphthalene]-2,2'-diamine.[14]

**NB**: All spectra identical to (*S*)-**2.43b**.[14]

### 4.3.3 Synthesis and crystallisation of hydrogen bonded azide complexes

**1,3-bis(3,5-bis(trifluoromethyl)phenyl)urea·tetrabutylammonium azide (2.41a·$N_3$·$Bu_4N$)**

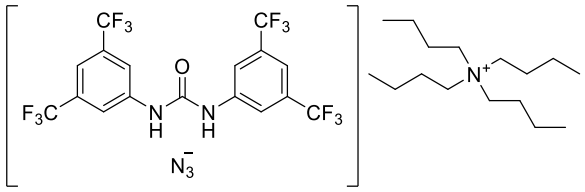

Prepared according to GP2.1 with 1,3-bis(3,5-bis(trifluoromethyl)phenyl)urea (484 mg, 1.00 mmol, 1.00 equiv) to afford the title compound as a yellow solid (732 mg, 0.95 mmol, 95%). Single crystals suitable for X-ray crystallography were grown by vapour diffusion of cyclohexane into a saturated solution of the title compound in EtOAc.

**mp** 100-102 °C; **$\nu_{max}$** (neat) /cm$^{-1}$ 2961, 2004, 1706, 1574, 1471, 1376, 1273, 1229, 1170, 1124, 927, 880, 682; **$^1$H NMR** (400 MHz, Acetone-*d*$_6$) δ 10.62 (s, 2H), 8.23 (s, 4H), 7.57 (s, 2H), 3.51 – 3.35 (m, 8H), 1.81 (p, *J* = 8.0 Hz, 8H), 1.40 (h, *J* = 7.5 Hz, 8H), 0.95 (td, *J* = 7.5, 1.2 Hz, 12H); **$^{19}$F NMR** (377 MHz, Acetone-*d*$_6$) δ -63.55; **$^{13}$C NMR** (101 MHz, Acetone-*d*$_6$) δ 153.9, 143.0, 132.6

(q, *J* = 33.0 Hz), 124.6 (q, *J* = 272.0 Hz), 118.8 (d, *J* = 4.0 Hz), 115.5 (p, *J* = 4.0 Hz), 59.4 (t, *J* = 3.0 Hz), 24.4, 20.4, 13.9.

**1,3-bis(3,5-bis(trifluoromethyl)phenyl)urea·azide sodium·15-crown-5 (2.41a·$N_3$·Na·15-crown-5)**

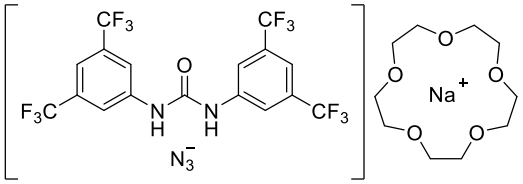

15-crown-5 (0.099 mL, 0.50 mmol, 1.00 equiv) was added to sodium azide (32.5 mg, 0.50 mmol, 1.00 equiv) and 1,3-bis(3,5-bis(trifluoromethyl)phenyl)urea (1.00 mmol, 2.00 equiv) in dry MeCN (5 mL). The reaction mixture was stirred at rt for 24 h. The reaction mixture was evaporated to dryness to afford the title compound (385 mg, 0.50 mmol, *quant*) as a white solid. Single crystals of **2.41a**·$N_3$·Na·15-crown-5 suitable for X-ray crystallography were grown by layering cyclohexane onto a saturated solution of the title compound in THF. Single crystals of **2.41a**$_2$·$N_3$·Na·15-crown-5 suitable for X-ray crystallography were grown by layering PhMe onto a saturated solution of the title compound in MeCN.

**mp** 126-128 °C; **$\nu_{max}$** (neat) /cm$^{-1}$ 2921, 2068, 1706, 1471, 1280, 1113, 927, 682; **$^1$H NMR** (500 MHz, Acetone-$d_6$) δ 10.40 (br s, 2H), 8.23 (s, 4H), 7.58 (s, 2H), 3.70 (s, 20H); **$^{19}$F NMR** (470 MHz, Acetone-$d_6$) δ -63.56; **$^{13}$C NMR** (126 MHz, Acetone-$d_6$) δ 158.0, 147.1, 136.8 (q, *J* = 33.0 Hz), 128.8 (q, *J* = 272.0 Hz), 123.9 – 122.5 (m), 120.2 – 119.4 (m), 74.1.

**1,3-bis(3-chlorophenyl)urea·tetrabutylammonium azide (2.41b·$N_3$·$Bu_4N$)**

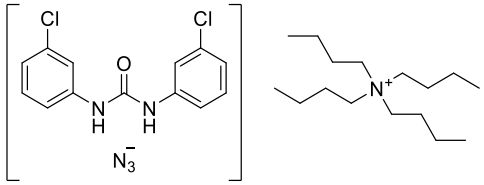

Prepared according to GP2.1 with 1,3-bis(3-chlorophenyl)urea (140 mg, 0.50 mmol, 1.00 equiv) to afford the title compound as a yellow solid (281 mg, 0.50 mmol, *quant*.). Single crystals suitable for X-ray crystallography were grown by layering cyclohexane onto a saturated solution of the title compound in EtOAc.

**mp** 67-69 °C; **$\nu_{max}$** (neat) /cm$^{-1}$ 2961, 2015, 1709, 1587, 1537, 1195, 879, 783, 713; **$^{1}$H NMR** (400 MHz, $CD_3CN$) δ 9.33 (s, 2H), 7.72 (t, *J* = 2.0 Hz, 2H), 7.31 (ddd, *J* = 8.5, 2.0, 1.0 Hz, 2H), 7.24 (t, *J* = 8.0 Hz, 2H), 6.97 (ddd, *J* = 8.0, 2.0, 1.0 Hz, 2H), 3.11 – 3.01 (m, 8H), 1.67 – 1.49 (m, 8H), 1.33 (h, *J* = 7.5 Hz, 8H), 0.95 (t, *J* = 7.5 Hz, 12H); **$^{13}$C NMR** (101 MHz, $CD_3CN$) δ 154.0, 142.5, 134.8, 131.2, 122.5, 118.8, 117.6, 59.3 (t, *J* = 3.0 Hz), 24.3, 20.3 (t, *J* = 1.5 Hz), 13.8.

**1-(3,5-bis(trifluoromethyl)phenyl)-3-phenylurea·tetrabutylammonium azide (2.41c·$N_3$·$Bu_4N$)**

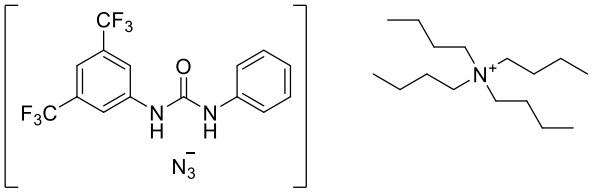


Prepared according to GP2.1 with 1-(3,5-bis(trifluoromethyl)phenyl)-3-phenylurea (174 mg, 0.50 mmol, to afford the title compound as a white solid (316 mg, 0.50 mmol, *quant*.). Single crystals suitable for X-ray crystallography were grown by layering cyclohexane onto a saturated solution of the title compound in THF.

**mp** 86-88 °C; **$\nu_{max}$** (neat) /cm$^{-1}$ 2963, 2023, 1708, 1582, 1551, 1473, 1447, 1392, 1307, 1276, 1232, 1204, 1186, 1168, 1152, 1123, 1084, 1024, 877, 755, 681; **$^{1}$H NMR** (400 MHz, $CD_3CN$) δ 9.82 (s, 1H), 9.04 (s, 1H), 8.15 – 8.05 (m, 2H), 7.55 – 7.48 (m, 3H), 7.36 – 7.23 (m, 2H), 7.08 – 6.95 (m, 1H), 3.12 – 3.01 (m, 8H), 1.66 – 1.52 (m, 8H), 1.33 (h, *J* = 7.5 Hz, 8H), 0.95 (t, *J* = 7.5 Hz, 12H); **$^{19}$F NMR** (377 MHz, $CD_3CN$) -63.58; **$^{13}$C NMR** (151 MHz, $CD_3CN$) δ 154.1, 143.3, 140.5, 132.4 (q, *J* = 33.0 Hz), 129.9, 124.7 (q, *J* = 272.0 Hz), 123.5, 119.7, 118.9 (q, *J* = 3.5 Hz), 115.4 (p, *J* = 4.0 Hz), 59.4 (t, *J* = 3.0 Hz), 24.3, 20.3, 13.8.

**1,3-bis(4-trifluoromethylphenyl)urea·tetrabutylammonium azide (2.41d·$N_3$·$Bu_4N$)**

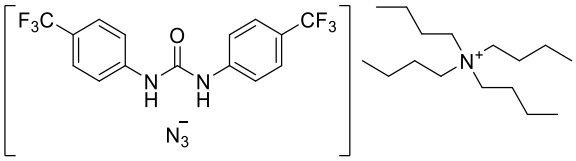

Prepared according to GP2.1 with 1,3-bis(4-trifluoromethyl)urea (174 mg, 0.50 mmol, 1.00 equiv) to afford the title compound as an off-white solid (321 mg, 0.49 mmol, 99%). Single crystals suitable for X-ray crystallography were grown by slow diffusion of PhMe into a saturated solution of the title compound in MeCN.

**mp** 99-101 °C; **$\nu_{max}$** (neat) /$cm^{-1}$ 2963, 2006, 1711, 1603, 858; **$^1$H NMR** (400 MHz, Acetone-$d_6$) δ 10.11 (s, 2H), 7.78 (d, *J* = 8.5 Hz, 4H), 7.60 (d, *J* = 8.5 Hz, 4H), 3.53 – 3.31 (m, 8H), 1.86 – 1.75 (m, 8H), 1.41 (h, *J* = 7.5 Hz, 8H), 0.96 (t, *J* = 7.5 Hz, 12H); **$^{19}$F NMR** (376 MHz, Acetone-$d_6$) δ -62.06; **$^{13}$C NMR** (101 MHz, Acetone-$d_6$) δ 153.8, 144.9, 126.8 (q, *J* = 4.0 Hz), 125.7 (q, *J* = 270.0 Hz), 123.5 (q, *J* = 32.0 Hz), 118.7, 59.4 (t, *J* = 3.0 Hz), 24.5, 20.4 (t, *J* = 1.5 Hz), 13.8.

**1,3-diphenylurea·tetrabutylammonium azide (2.41e·$N_3$·$Bu_4N$)**

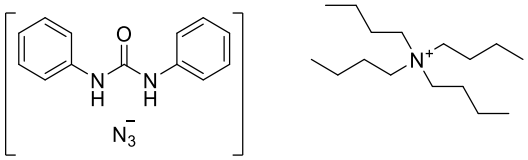

Prepared according to GP2.1 with 1,3-diphenylurea (106 mg, 0.50 mmol, 1 equiv) to afford the title compound as a white solid (248 mg, 0.50 mmol, *quant*.). Single crystals suitable for X-ray crystallography were grown by layering cyclohexane onto a saturated solution of the title compound in EtOAc.

**mp** 69-71 °C; **$\nu_{max}$** (neat) /$cm^{-1}$ 3279, 2962, 2022 ,1706, 1594, 1545, 1488, 1445, 1384, 1297, 1201, 1173, 892, 754, 696; **$^1$H NMR** (400 MHz, Acetone-$d_6$) δ 9.41 (s, 2H), 7.67 – 7.53 (m, 4H), 7.31 – 7.15 (m, 4H), 6.90 (tt, *J* = 7.5, 1.0 Hz, 2H), 3.49 – 3.35 (m, 8H), 1.80 (p, *J* = 8.0 Hz, 8H), 1.41 (h, *J* = 7.5 Hz, 8H), 0.96 (t, *J* = 7.5 Hz, 12H); **$^{13}$C NMR** (101 MHz, Acetone-$d_6$) δ 141.8, 129.4, 122.0, 118.9, 118.8, 59.3, 30.4, 24.4, 20.4, 13.9.

**1,3-bis(4-bromophenyl)urea·tetrabutylammonium azide (2.41f·$N_3$·$Bu_4N$)**

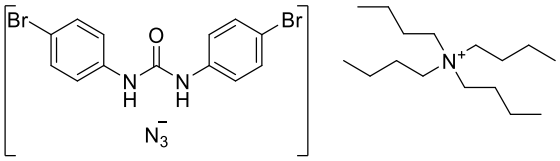

Prepared according to GP2.1 with 1,3-bis(4-bromophenyl)urea (185 mg, 0.50 mmol, 1.00 equiv) to afford the title compound as an off-white solid (326 mg, 0.50 mmol, *quant*.). Single crystals suitable for X-ray crystallography were grown by layering cyclohexane onto a saturated solution of the title compound in THF.

**mp** 118-120 °C; **$\nu_{max}$** (neat) /$cm^{-1}$ 2961, 2020, 1704, 1485, 1174, 817; **$^1$H NMR** (400 MHz, DMSO-$d_6$) δ 8.95 (s, 2H), 7.64 – 7.29 (m, 8H), 3.21 – 3.00 (m, 8H), 1.56 (td, *J* = 11.5, 10.0, 6.0 Hz, 8H), 1.30 (h, *J* = 7.5 Hz, 8H), 0.93 (t, *J* = 7.5 Hz, 12H); **$^{13}$C NMR** (101 MHz, DMSO-$d_6$) δ 152.3, 139.0, 131.5, 120.2, 113.3, 57.5 (t, *J* = 3.0 Hz), 23.1, 19.2 (t, *J* = 3.0 Hz), 13.5.

**1,3-bis(4-fluorophenyl)urea·tetrabutylammonium azide (2.41g·$N_3$·$Bu_4N$)**

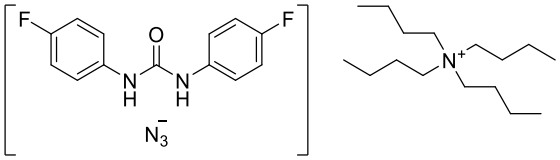

Prepared according to GP2.1 with 1,3-bis(4-fluorophenyl)urea (248 mg, 1.00 mmol, 1.00 equiv) to afford the title compound as an off-white solid (504 mg, 0.95 mmol, 95%). Single crystals suitable for X-ray crystallography were grown by layering cyclohexane onto a saturated solution of the title compound in EtOAc.

**mp** 88-90 °C; **$\nu_{max}$** (neat) /$cm^{-1}$ 2961, 2021, 1705, 1613, 1561, 1503, 1305, 1200, 737; **$^1$H NMR** (400 MHz, $CD_3CN$) δ 8.68 (s, 2H), 7.51 – 7.42 (m, 4H), 7.08 – 6.97 (m, 4H), 3.12 – 3.02 (m, 8H), 1.59 (ddd, *J* = 12.0, 10.0, 6.5 Hz, 8H), 1.34 (h, *J* = 7.5 Hz, 8H), 0.96 (t, *J* = 7.5 Hz, 12H); **$^{19}$F NMR** (376 MHz, $CD_3CN$) δ -123.40; **$^{13}$C NMR** (101 MHz, $CD_3CN$) δ 159.0 (d, *J* = 238.0 Hz), 154.4, 137.4 (d, *J* = 2.0 Hz), 121.2 (d, *J* = 7.5 Hz), 116.1 (d, *J* = 22.5 Hz), 59.3 (t, *J* = 3.0 Hz), 24.3, 20.3 (t, *J* = 1.5 Hz), 13.8.

**1,3-bis(4-cyanophenyl)urea·tetrabutylammonium azide (2.41h·$N_3$·$Bu_4N$)**

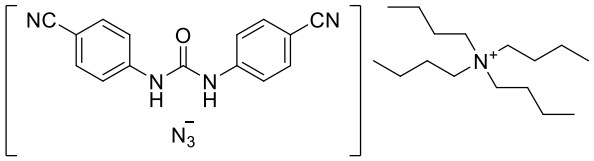

Prepared according to GP21 with 1,3-bis(4-cyanophenyl)urea (131 mg, 0.50 mmol, 1.00 equiv) to afford the title compound as an off-white solid (272 mg, 0.50 mmol, *quant*.). Single crystals of **2.41h**$_2$·$Bu_4N$·$N_3$·$(H_2O)_2$ suitable for X-ray crystallography were grown by layering cyclohexane onto a saturated solution of the title compound in THF.

**mp** 96-98 °C; **$\nu_{max}$** (neat) /$cm^{-1}$ 2962, 2222, 2014, 1719, 1590, 1170; **$^1$H NMR** (400 MHz, Acetone-$d_6$) δ 10.33 (s, 2H), 7.78 – 7.71 (m, 4H), 7.71 – 7.62 (m, 4H), 3.50 – 3.32 (m, 8H), 1.99 – 1.70 (m, 8H), 1.42 (h, *J* = 7.5 Hz, 8H), 0.96 (t, *J* = 7.5 Hz, 8H); **$^{13}$C NMR** (101 MHz, Acetone-$d_6$) δ 152.6, 144.5, 133.0, 119.0, 118.2, 104.2, 58.5 (t, *J* = 3.0 Hz), 23.5, 19.5 (t, *J* = 1.5 Hz), 13.0.

**1,3-bis(3,5-bis(trifluoromethyl)phenyl)thiourea·tetrabutylammonium azide (2.42·$N_3$·$Bu_4N$)**

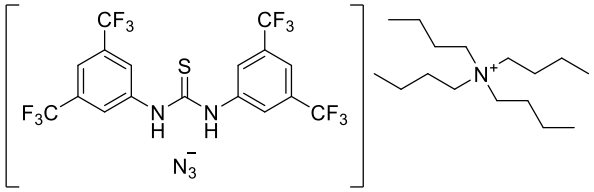

Prepared according to GP2.1 with 1,3-bis(3,5-bis(trifluoromethyl)phenyl)thiourea (250 mg, 0.50 mmol, 1.00 equiv) to afford the title compound as a pale yellow solid (386 mg, 98%). Single crystals of [**2.42**-H]·$Bu_4N$ suitable for X-ray crystallography were grown by vapour diffusion of cyclohexane into a saturated solution of the title compound in $CH_2Cl_2$.

**mp** 70-72 °C; **$\nu_{max}$** (neat) /$cm^{-1}$ 2966, 2058, 2027, 1572, 1470, 1418, 1371, 1328, 1273, 1169, 1122, 1000, 885, 678; **$^1$H NMR** (500 MHz, $CDCl_3$) δ 10.77 (br s, 2 H), 8.27 (s, 4H), 7.56 (s, 2H), 3.41 – 2.75 (m, 8H), 1.58 (dq, *J* = 12.0, 8.0 Hz, 8H), 1.36 (h, *J* = 7.5 Hz, 8H), 0.95 (t, *J* = 7.5 Hz, 12H); **$^{19}$F NMR** (470 MHz, $CDCl_3$) δ -62.84; **$^{13}$C NMR** (126 MHz, $CDCl_3$) δ 180.0, 141.3, 131.5 (q, *J* = 33.5 Hz), 123.4 (q, *J* = 272.5 Hz), 123.3, 117.6 (p, *J* = 4.0 Hz), 59.0 (t, *J* = 2.5 Hz), 23.9, 19.7, 13.5.

**diphenylguanidine·tetrabutylammonium azide (2.44·$N_3$·$Bu_4N$)**

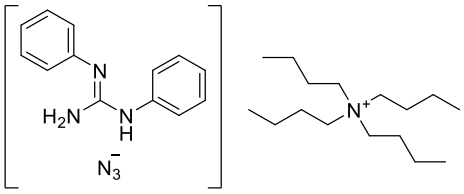

Prepared according to GP2.1 with diphenylguanidine (106 mg, 0.50 mmol, 1.00 equiv) to afford the title compound as a white solid (248 mg, 0.50 mmol, *quant*.). Single crystals of suitable for X-ray crystallography were grown by layering cyclohexane onto a saturated solution of the title compound in acetone.

**mp** 93-95 °C; **$\nu_{max}$** (neat) /$cm^{-1}$ 2960, 2011, 1665, 1554, 700; **$^1$H NMR** (400 MHz, $CDCl_3$) δ 7.26 – 7.20 (m, 8H), 6.98 – 6.90 (m, 2H), 3.30 – 3.14 (m, 8H), 1.58 (dq, *J* = 12.0, 8.0 Hz, 8H), 1.40 (h, *J* = 7.5 Hz, 8H), 0.98 (t, *J* = 7.5 Hz, 12H); **$^{13}$C NMR** (101 MHz, $CDCl_3$) δ 149.1, 145.3, 129.2, 122.0, 121.8, 58.6, 23.9, 19.8, 13.8.

***N*$^1$,*N*$^2$-bis(3,5-bis(trifluoromethyl)phenyl)oxalamide·tetrabutylammonium azide (2.45·$N_3$·$Bu_4N$)**

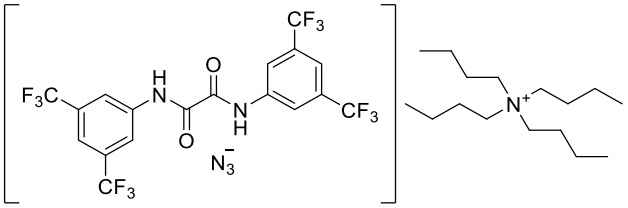

Prepared according to GP2.1 with *N*$^1$,*N*$^2$-bis(3,5-bis(trifluoromethyl)phenyl)oxalamide (256 mg, 0.50 mmol, 1.00 equiv) to afford the title compound as an off-white solid (398 mg, 0.50 mmol, *quant*.). Single crystals suitable for X-ray crystallography were grown by layering cyclohexane onto a saturated solution of the title compound in THF.

**mp** 140-142 °C; **$\nu_{max}$** (neat) /$cm^{-1}$ 2964, 2033, 1683, 1537, 1373, 1129, 890; **$^1$H NMR** (500 MHz, Acetone-$d_6$) δ 8.66 (s, 4H), 7.81 (s, 2H), 4.20 – 2.96 (m, 8H), 1.82 (dq, *J* = 12.0, 7.5 Hz, 8H), 1.43 (h, *J* = 7.5 Hz, 8H), 0.97 (t, *J* = 7.5 Hz, 12H); **$^{19}$F NMR** (470 MHz, Acetone-$d_6$) δ -63.58; **$^{13}$C NMR** (126 MHz, Acetone-$d_6$) δ 159.6, 141.0, 132.6 (q, *J* = 33.0 Hz), 124.4 (q, *J* = 272.0 Hz), 121.8 – 121.1 (m), 119.0 – 117.8 (m), 59.3 (t, *J* = 3.0 Hz), 24.4, 20.4 (t, *J* = 1.5 Hz), 13.9.

### 4.3.4 Evaluation of achiral hydrogen bond donor solubility

Hydrogen bond donor (0.005 mmol, 1.00 equiv) was added to 1.75 mL vial. The selected solvent (3.125 mM, 1.6 mL) was added, and the vial was shaken vigorously for 10 s. The compound was deemed suitably soluble for the $^1$H NMR titrations if no visible solid persisted.

**Table 4.1** Evaluation of hydrogen bond donor solubility.

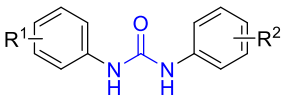

**2.41a-h**

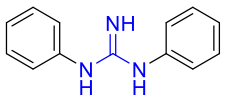

**2.44**

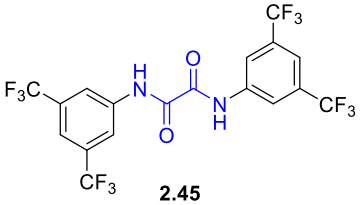

**2.45**

| entry | hydrogen bond donor | visually soluble | | |
|---|---|---|---|---|
| | | 1,2-DFB | $CHCl_3$ | MeCN |
| 1 | **2.41a**, $R^1 = R^2 = 3,5\text{-}CF_3$ | ✓ | ✓ | ✓ |
| 2 | **2.41b**, $R^1 = R^2 = 3\text{-}Cl$ | | | |
| 3 | **2.41c**, $R^1 = 3,5\text{-}CF_3$; $R^2 = H$ | | ✓ | ✓ |
| 4 | **2.41d**, $R^1 = R^2 = 4\text{-}CF_3$ | | | ✓ |
| 5 | **2.41e**, $R^1 = R^2 = H$ | | | ✓ |
| 6 | **2.41f**, $R^1 = R^2 = 4\text{-}Br$ | | | |
| 7 | **2.41g**, $R^1 = R^2 = 4\text{-}F$ | | | ✓ |
| 8 | **2.41h**, $R^1 = R^2 = 4\text{-}CN$ | | | |
| 9 | **2.44** | ✓ | ✓ | ✓ |
| 10 | **2.45** | ✓ | | |

1,2-DFB = 1,2-difluorobenzene.

### 4.3.5 $^{1}$H NMR titrations of achiral HBDs and tetrabutylammonium azide

### 2.41a and tetrabutylammonium azide

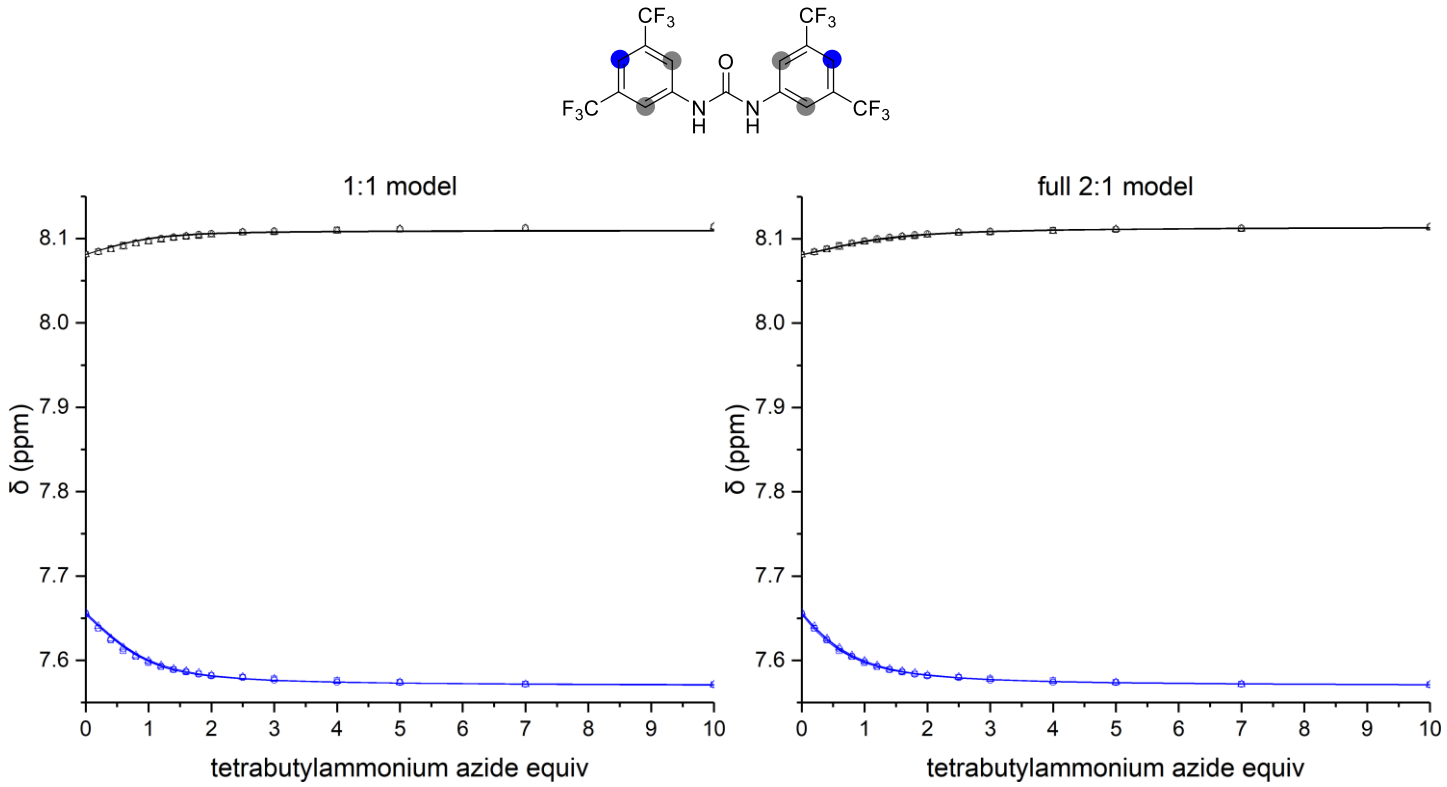


**Figure 4.1** $^{1}$H NMR titration data of **2.41a** with tetrabutylammonium azide. One set of symbols (□, ○, △) refers to experimental data from one set of measurements. Lines are the calculated isotherms of the described model. (2 mM **2.41a**, $CH_3CN/CD_3CN$ 8:2, 500 MHz, 298 K).

**Table 4.2** Comparison of binding models.

| model | entry | $cov_{fit}$ ($10^{-3}$) | $cov_{fit}$ factor | $K_{a(1:1)}$ ($M^{-1}$) | $K_{a(2:1)}$ ($M^{-1}$) | $\Delta G_{(1:1)}$ (kJ $mol^{-1}$) | $\Delta G_{(2:1)}$ (kJ $mol^{-1}$) |
|---|---|---|---|---|---|---|---|
| 1:1 | 1 | 2.26 | 1 | $2.86 \times 10^3$ | - | | |
| | 2 | 1.81 | 1 | $2.68 \times 10^3$ | - | | |
| | 3 | 2.04 | 1 | $2.45 \times 10^3$ | - | | |
| | **mean** | **2.04** | **1** | **$2.66 \pm 0.18 \times 10^3$** | **-** | **-19.54 ± 0.17** | **-** |
| **full 2:1** | 1 | 0.14 | 16.1 | $1.55 \times 10^3$ | $1.06 \times 10^2$ | | |
| | 2 | 0.062 | 29.2 | $1.65 \times 10^3$ | $6.62 \times 10^1$ | | |
| | 3 | 0.083 | 24.6 | $1.50 \times 10^3$ | $3.23 \times 10^1$ | | |
| | **mean** | **0.095** | **23.3** | **$1.57 \pm 0.06 \times 10^3$** | **$7 \pm 3 \times 10^1$** | **-18.23 ± 0.09** | **-10.4 ± 1.1** |

$cov_{fit}$ factor is $cov_{fit}$ for the 1:1 model divided by the $cov_{fit}$ for the binding model under study.[7] Values calculated with BindFit v0.5,[5] error is the standard deviation from 3 independent replicas.

The mean $cov_{fit}$ for the full 2:1 model is significantly higher than the mean $cov_{fit}$ for the 1:1 model, suggesting this system is best described by the full 2:1 model.

**2.41c and tetrabutylammonium azide**

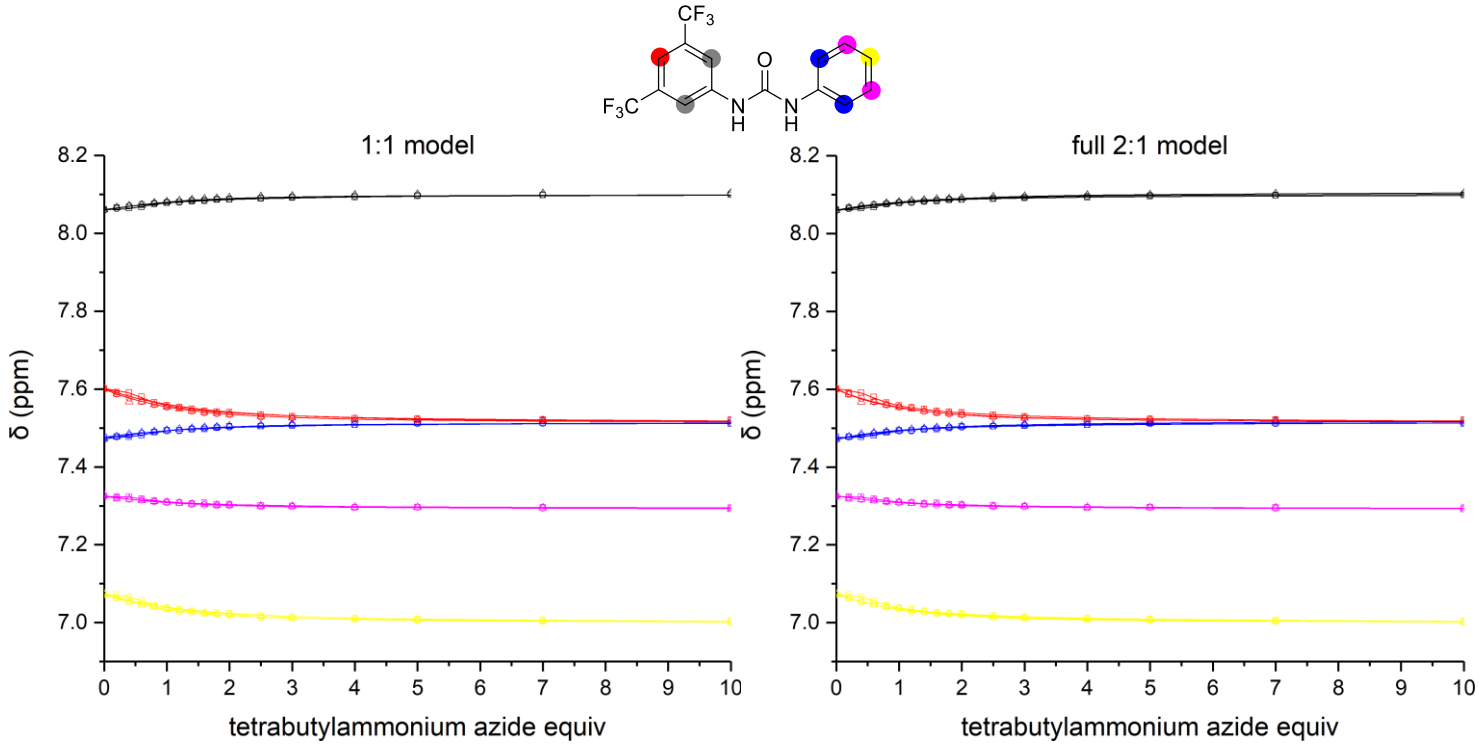


**Figure 4.2** $^{1}$H NMR titration data of **2.41c** with tetrabutylammonium azide. One set of symbols (□, ○, △) refers to experimental data from one set of measurements. Lines are the calculated isotherms of the described model. (2 mM **2.41c**, $CH_3CN/CD_3CN$ 8:2, 500 MHz, 298 K).

**Table 4.3** Comparison of binding models.

| model | entry | $cov_{fit}$ ($10^{-3}$) | $cov_{fit}$ factor | $K_{a(1:1)}$ ($M^{-1}$) | $K_{a(2:1)}$ ($M^{-1}$) | $\Delta G_{(1:1)}$ (kJ $mol^{-1}$) | $\Delta G_{(2:1)}$ (kJ $mol^{-1}$) |
|---|---|---|---|---|---|---|---|
| **1:1** | 1 | 6.43 | 1 | $6.93 \times 10^2$ | - | | |
| | 2 | 1.11 | 1 | $1.06 \times 10^3$ | - | | |
| | 3 | 1.62 | 1 | $1.06 \times 10^3$ | - | | |
| | **mean** | **3.05** | **1** | **$9.4 \pm 1.7 \times 10^2$** | **-** | **-17.0 ± 0.4** | **-** |
| full 2:1 | 1 | 1.54 | 4.2 | $4.57 \times 10^5$ | $2.37 \times 10^5$ | | |
| | 2 | 0.74 | 1.5 | $2.77 \times 10^2$ | $-5.95 \times 10^1$ | | |
| | 3 | 0.84 | 1.9 | $4.75 \times 10^2$ | $6.84 \times 10^1$ | | |
| | **mean** | **1.04** | **2.5** | **$2 \pm 2 \times 10^4$** | **$8 \pm 11 \times 10^3$** | **-24.5 ± 24.5** | **-16.6 ± 3.4** |

$cov_{fit}$ factor is $cov_{fit}$ for the 1:1 model divided by the $cov_{fit}$ for the binding model under study.[7] Values calculated with BindFit v0.5,[5] error is the standard deviation from 3 independent replicas.

The mean $cov_{fit}$ for the full 2:1 model is not significantly higher than the mean $cov_{fit}$ for the 1:1 model, suggesting this system is best described by the 1:1 model. In addition the $K_{a(2:1)}$ cannot be negative, hence it is likely the fits from the full 2:1 models do not need to be considered.

**2.41d and tetrabutylammonium azide**

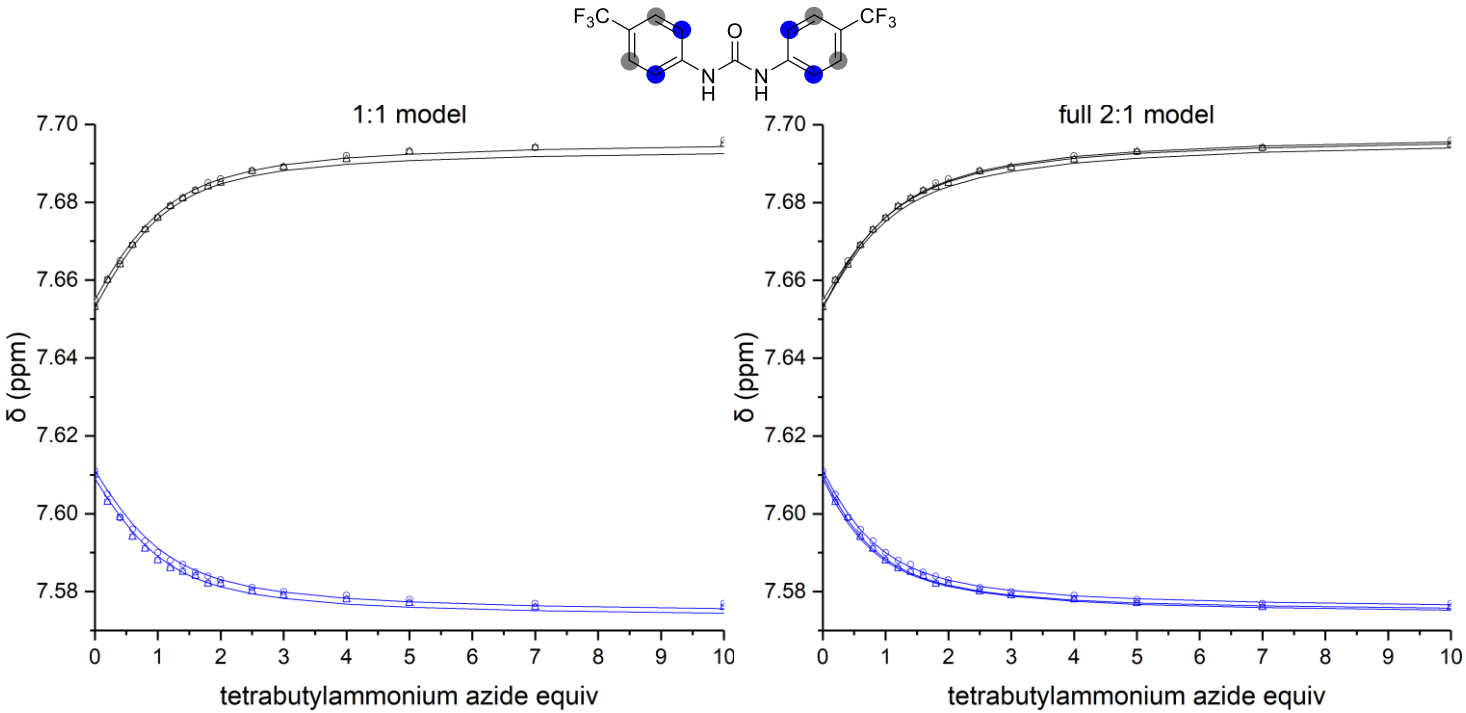


**Figure 4.3** $^{1}$H NMR titration data of **2.41d** with tetrabutylammonium azide. One set of symbols (□, ○, △) refers to experimental data from one set of measurements. Lines are the calculated isotherms of the described model. (2 mM **2.41d**, $CH_3CN/CD_3CN$ 8:2, 500 MHz, 298 K)..

**Table 4.4** Comparison of binding models.

| model | entry | $cov_{fit}$ ($10^{-3}$) | $cov_{fit}$ factor | $K_{a(1:1)}$ ($M^{-1}$) | $K_{a(2:1)}$ ($M^{-1}$) | $\Delta G_{(1:1)}$ (kJ $mol^{-1}$) | $\Delta G_{(2:1)}$ (kJ $mol^{-1}$) |
|---|---|---|---|---|---|---|---|
| 1:1 | 1 | 1.08 | 1 | $1.39 \times 10^3$ | - | | |
| | 2 | 0.94 | 1 | $1.24 \times 10^3$ | - | | |
| | 3 | 0.94 | 1 | $1.48 \times 10^3$ | - | | |
| | **mean** | **0.99** | **1** | **$1.4 \pm 0.1 \times 10^3$** | **-** | **-17.95 ± 0.18** | **-** |
| **full 2:1** | 1 | 0.16 | 6.8 | $1.31 \times 10^3$ | $1.99 \times 10^2$ | | |
| | 2 | 0.16 | 5.9 | $1.37 \times 10^3$ | $1.20 \times 10^2$ | | |
| | 3 | 0.15 | 6.3 | $1.08 \times 10^3$ | $7.47 \times 10^1$ | | |
| | **mean** | **0.16** | **6.3** | **$1.25 \pm 0.12 \times 10^3$** | **$1.3 \pm 0.5 \times 10^2$** | **-17.7 ± 0.2** | **-12 ± 1** |

$cov_{fit}$ factor is $cov_{fit}$ for the 1:1 model divided by the $cov_{fit}$ for the binding model under study.[7] Values calculated with BindFit v0.5,[5] error is the standard deviation from 3 independent replicas.

The mean $cov_{fit}$ for the full 2:1 model is significantly higher than the mean $cov_{fit}$ for the 1:1 model, suggesting this system is best described by the full 2:1 model.

**2.41e and tetrabutylammonium azide**

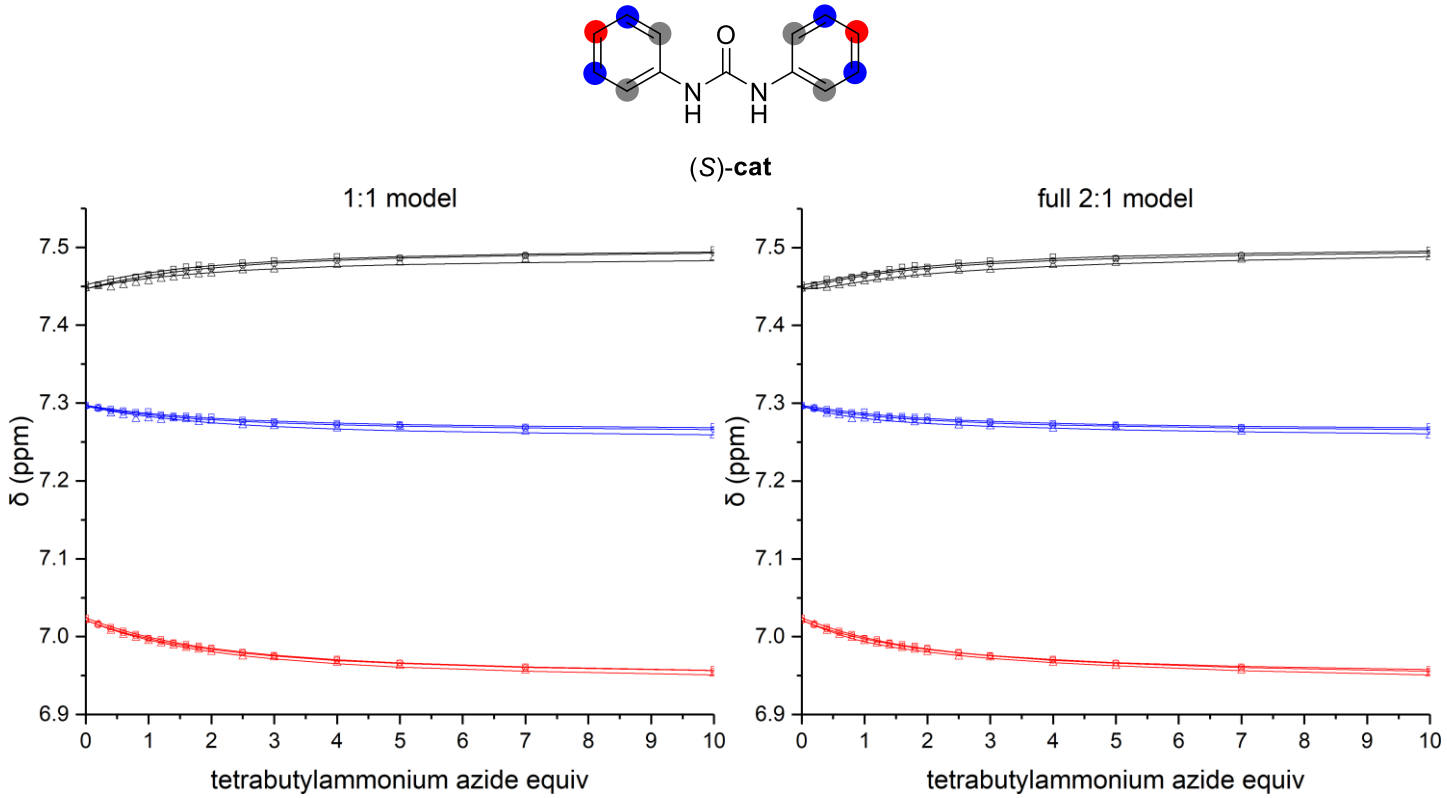


**Figure 4.4** $^{1}$H NMR titration data of **2.41e** with tetrabutylammonium azide. One set of symbols (□, ○, △) refers to experimental data from one set of measurements. Lines are the calculated isotherms of the described model. (2 mM **2.41e**, $CH_3CN/CD_3CN$ 8:2, 500 MHz, 298 K).

**Table 4.5** Comparison of binding models.

| model | entry | $cov_{fit}$ ($10^{-3}$) | $cov_{fit}$ factor | $K_{a(1:1)}$ ($M^{-1}$) | $K_{a(2:1)}$ ($M^{-1}$) | $\Delta G_{(1:1)}$ (kJ $mol^{-1}$) | $\Delta G_{(2:1)}$ (kJ $mol^{-1}$) |
|---|---|---|---|---|---|---|---|
| **1:1** | 1 | 2.95 | 1 | $3.14 \times 10^2$ | - | | |
| | 2 | 0.18 | 1 | $3.17 \times 10^2$ | - | | |
| | 3 | 7.09 | 1 | $3.10 \times 10^2$ | - | | |
| | **mean** | **3.41** | **1** | **$3.14 \pm 0.03 \times 10^2$** | **-** | **-14.3 ± 0.2** | **-** |
| full 2:1 | 1 | 2.45 | 1.2 | $6.67 \times 10^2$ | $2.88 \times 10^2$ | | |
| | 2 | 0.093 | 1.9 | $3.64 \times 10^2$ | $1.51 \times 10^2$ | | |
| | 3 | 2.51 | 2.8 | $8.38 \times 10^2$ | $1.65 \times 10^3$ | | |
| | **mean** | **1.68** | **2.0** | **$6 \pm 2 \times 10^2$** | **$7 \pm 7 \times 10^2$** | **-15.8 ± 0.8** | **-11 ± 2** |

$cov_{fit}$ factor is $cov_{fit}$ for the 1:1 model divided by the $cov_{fit}$ for the binding model under study.[7] Values calculated with BindFit v0.5,[5] error is the standard deviation from 3 independent replicas.

The mean $cov_{fit}$ for the full 2:1 model is not significantly higher than the mean $cov_{fit}$ for the 1:1 model, suggesting this system is best described by the 1:1 model.

**2.41g and tetrabutylammonium azide**

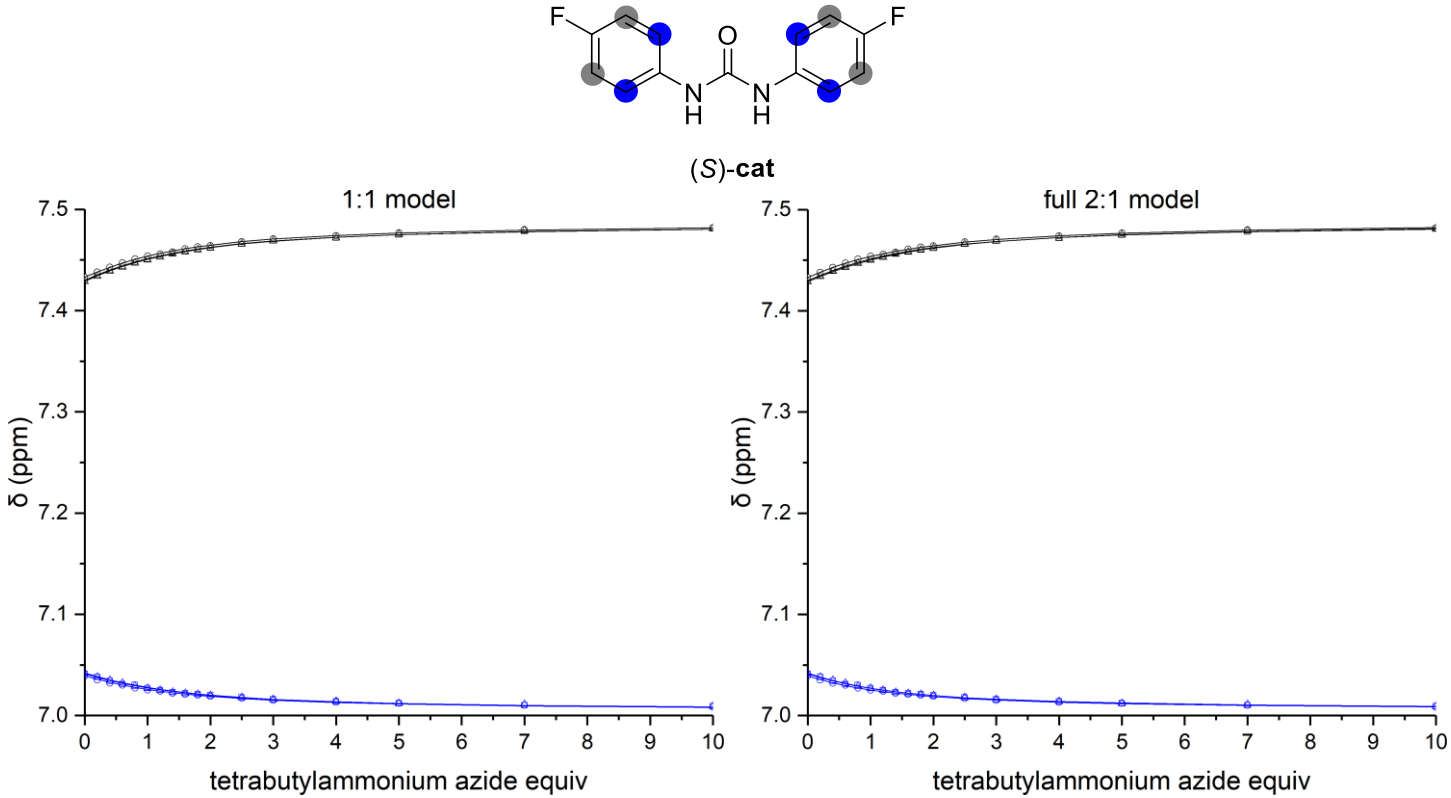


**Figure 4.5** $^{1}$H NMR titration data of **2.41g** with tetrabutylammonium azide. One set of symbols (□, ○, △) refers to experimental data from one set of measurements. Lines are the calculated isotherms of the described model. (2 mM **2.41g**, $CH_3CN/CD_3CN$ 8:2, 500 MHz, 298 K).

**Table 4.6** Comparison of binding models.

| model | entry | $cov_{fit}$ ($10^{-3}$) | $cov_{fit}$ factor | $K_{a(1:1)}$ ($M^{-1}$) | $K_{a(2:1)}$ ($M^{-1}$) | $\Delta G_{(1:1)}$ (kJ $mol^{-1}$) | $\Delta G_{(2:1)}$ (kJ $mol^{-1}$) |
|---|---|---|---|---|---|---|---|
| **1:1** | 1 | 0.19 | 1 | $4.81 \times 10^2$ | - | | |
| | 2 | 0.29 | 1 | $4.88 \times 10^2$ | - | | |
| | 3 | 0.40 | 1 | $4.77 \times 10^2$ | - | | |
| | **mean** | **0.29** | **1** | **$4.82 \pm 0.05 \times 10^2$** | **-** | **-15.31 ± 0.03** | **-** |
| full 2:1 | 1 | 0.14 | 1.4 | $7.85 \times 10^2$ | $2.72 \times 10^2$ | | |
| | 2 | 0.16 | 1.8 | $4.56 \times 10^2$ | $6.5 \times 10^1$ | | |
| | 3 | 0.091 | 4.4 | $6.11 \times 10^2$ | $8.9 \times 10^1$ | | |
| | **mean** | **0.13** | **2.5** | **$6.17 \pm 0.13 \times 10^2$** | **$1.4 \pm 0.9 \times 10^2$** | **-15.92 ± 0.05** | **-12.2 ± 1.6** |

$cov_{fit}$ factor is $cov_{fit}$ for the 1:1 model divided by the $cov_{fit}$ for the binding model under study.[7] Values calculated with BindFit v0.5,[5] error is the standard deviation from 3 independent replicas.

The mean $cov_{fit}$ for the full 2:1 model is not significantly higher than the mean $cov_{fit}$ for the 1:1 model, suggesting this system is best described by the 1:1 model.

**2.44 and tetrabutylammonium azide**

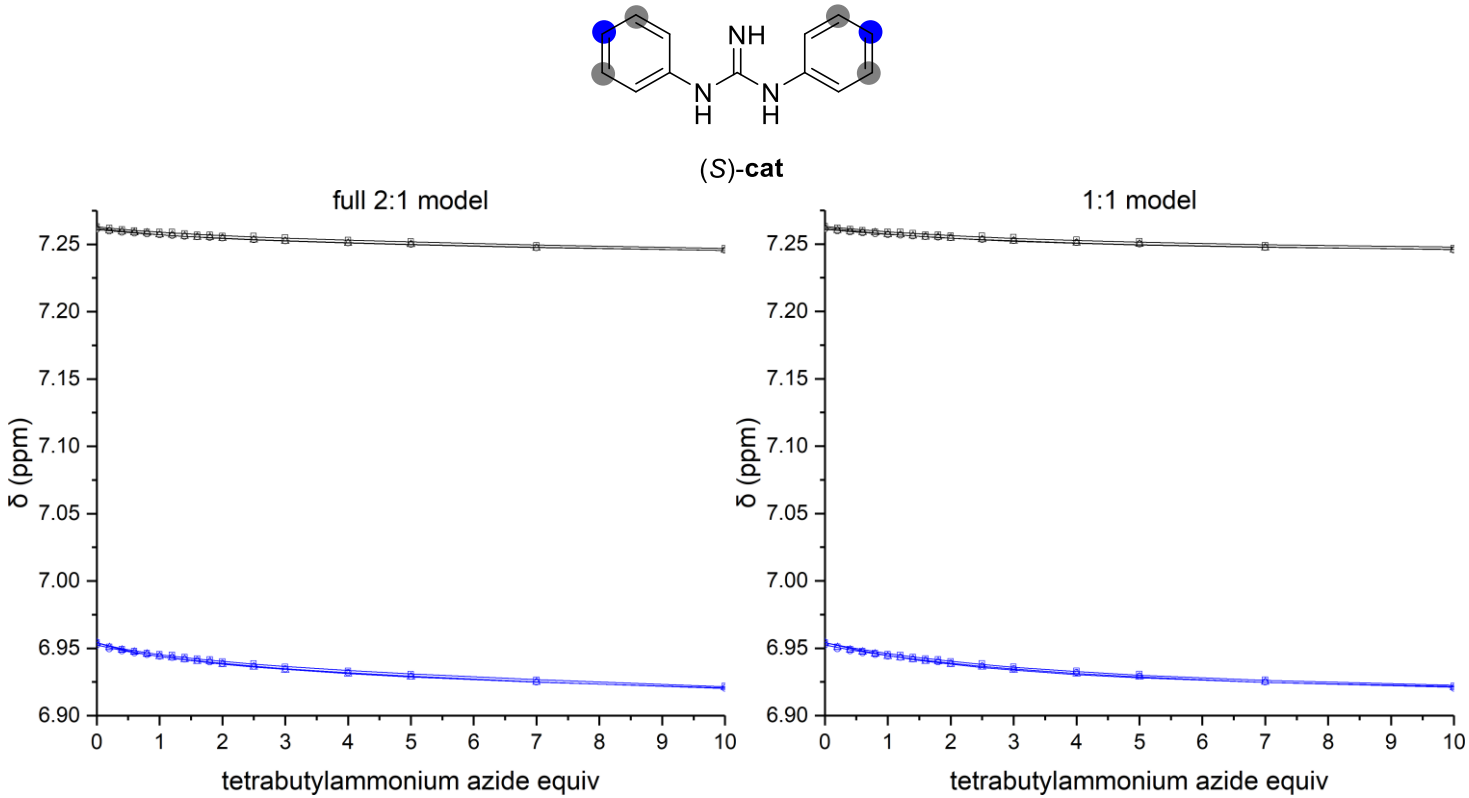


**Figure 4.6** $^{1}$H NMR titration data of **2.44** with tetrabutylammonium azide. One set of symbols (□, ○, △) refers to experimental data from one set of measurements. Lines are the calculated isotherms of the described model. (2 mM **2.44**, $CH_3CN/CD_3CN$ 8:2, 500 MHz, 298 K).

**Table 4.7** Comparison of binding models.

| model | entry | $cov_{fit}$ ($10^{-3}$) | $cov_{fit}$ factor | $K_{a(1:1)}$ ($M^{-1}$) | $K_{a(2:1)}$ ($M^{-1}$) | $\Delta G_{(1:1)}$ (kJ $mol^{-1}$) | $\Delta G_{(2:1)}$ (kJ $mol^{-1}$) |
|---|---|---|---|---|---|---|---|
| **1:1** | 1 | 6.70 | 1 | $1.23 \times 10^2$ | - | | |
| | 2 | 2.29 | 1 | $1.17 \times 10^2$ | - | | |
| | 3 | 4.48 | 1 | $1.79 \times 10^2$ | - | | |
| | **mean** | **4.49** | **1** | **$1.4 \pm 0.3 \times 10^2$** | **-** | **-12.2 ± 0.5** | **-** |
| full 2:1 | 1 | 2.59 | 2.6 | $1.73 \times 10^1$ | $7.40 \times 10^3$ | | |
| | 2 | 0.55 | 4.2 | $6.34 \times 10^1$ | $1.04 \times 10^3$ | | |
| | 3 | 1.86 | 2.4 | $9.24 \times 10^1$ | $9.53 \times 10^2$ | | |
| | **mean** | **1.67** | **3.1** | **$6 \pm 3 \times 10^1$** | **$3 \pm 3 \times 10^3$** | **-10.1 ± 1.2** | **-20 ± 2** |

$cov_{fit}$ factor is $cov_{fit}$ for the 1:1 model divided by the $cov_{fit}$ for the binding model under study.[7] Values calculated with BindFit v0.5,[5] error is the standard deviation from 3 independent replicas.

The mean $cov_{fit}$ for the full 2:1 model is not significantly higher than the mean $cov_{fit}$ for the 1:1 model, suggesting this system is best described by the 1:1 model.

### 4.3.6 Chiral urea bound azide - solution studies – establishing association

**(*S*)-2.43b $^{1}$H assignment ($CDCl_3$)**

Full characterisation of (*S*)-**2.43b** with $^{1}$H, $^{19}$F, and $^{13}$C spectra in $CDCl_3$ has been reported.[14] Full assignment of (*S*)-**2.43b** in $CD_2Cl_2$ has been reported.[15] The $^{1}$H assignment of (*S*)-**2.43b** in $CDCl_3$ was assisted with 2D $^{1}$H-$^{1}$H COSY, $^{1}$H-$^{1}$H NOESY, $^{1}$H-$^{15}$N HSQC, and $^{1}$H-$^{15}$N HMBC spectra, and is in good agreement with the $^{1}$H assignment of (*S*)-**2.43b** in $CD_2Cl_2$.

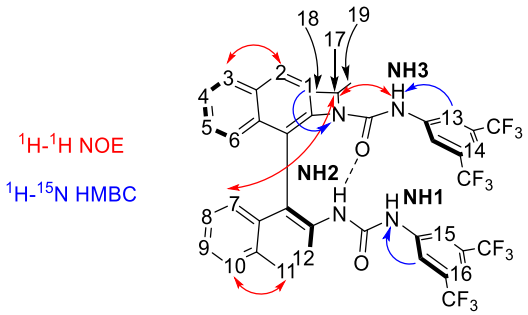


(*S*)-**2.1**

**$^{1}$H NMR** (500 MHz, $CDCl_3$) δ 8.54 (d, *J* = 9.0 Hz, 1H, **H12**), 8.14 (d, *J* = 9.0 Hz, 1H, **H2**), 8.02 (d, *J* = 9.0 Hz, 1H, **H11**), 7.99 (d, *J* = 8.0 Hz, 1H, **H3**), 7.92 (d, *J* = 8.0 Hz, 1H, **H10**), 7.82 (s, 2H, **H13**), 7.61 (s, 2H, **H15**), 7.56-7.51 (m, 4 H, **H4, H1, H14, NH2**), 7.43 – 7.38 (m, 2H, **H9, H16**), 7.30 (ddd, *J* = 8.0, 6.5, 1.0 Hz, 1H, **H5**), 7.26 – 7.22 (m, 1H, **H8**), 7.17 (d, *J* = 8.5 Hz, 1H, **H6**), 7.06 (s, 1H, **NH1**), 6.90 (d, *J* = 8.5 Hz, 1H, **H7**), 6.80 (s, 1H, **NH3**), 3.66 (sept, *J* = 7.0 Hz, 1H, **H17**), 1.06 (d, *J* = 7.0 Hz, 3H, **H19**), 0.67 (d, *J* = 7.0 Hz, 3H, **H18**).

**$^1$H NMR titration of (*S*)-2.43b and tetrabutylammonium azide**

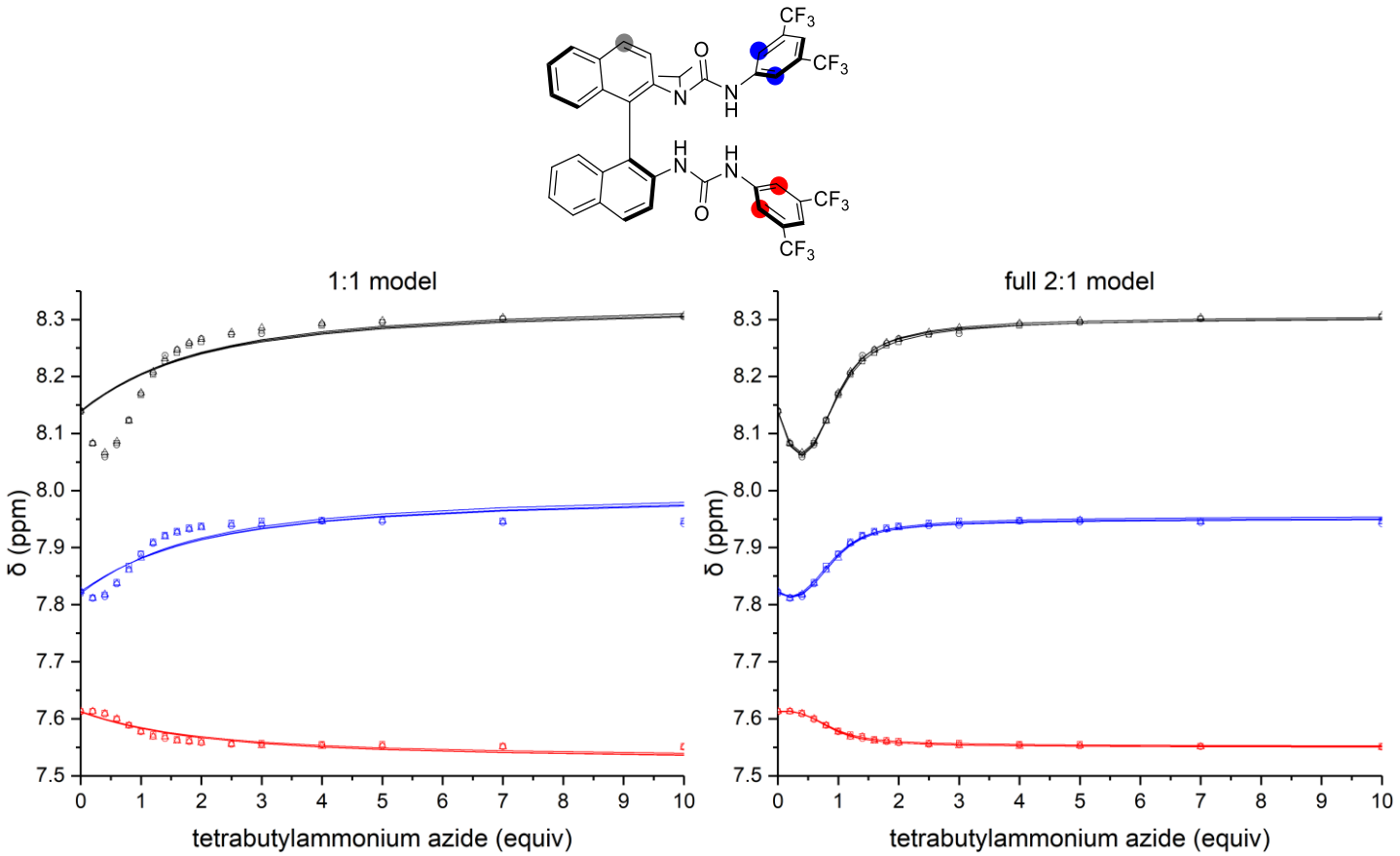


**Figure 4.7** $^1$H NMR titration data of (*S*)-**2.43b** with tetrabutylammonium azide. One set of symbols (□, ○, △) refers to experimental data from one set of measurements. Lines are the calculated isotherms of the described model. (2 mM (*S*)-**2.43b**, $CDCl_3$ 8:2, 500 MHz, 298 K).

**Table 4.8** Comparison of binding models.

| model | entry | $cov_{fit}$ ($10^{-3}$) | $cov_{fit}$ factor | $K_{a(1:1)}$ ($M^{-1}$) | $K_{a(2:1)}$ ($M^{-1}$) | $\Delta G_{(1:1)}$ (kJ $mol^{-1}$) | $\Delta G_{(2:1)}$ (kJ $mol^{-1}$) |
|---|---|---|---|---|---|---|---|
| 1:1 | 1 | 126.72 | 1 | $3.77 \times 10^2$ | - | | |
| | 2 | 137.94 | 1 | $3.68 \times 10^2$ | - | | |
| | 3 | 127.35 | 1 | $3.58 \times 10^2$ | - | | |
| | **mean** | **130.67** | **1** | **$3.68 \pm 0.08 \times 10^2$** | **-** | **-14.64 ± 0.05** | **-** |
| **full 2:1** | 1 | 0.67 | 189.1 | $9.17 \times 10^3$ | $1.67 \times 10^2$ | | |
| | 2 | 0.96 | 143.7 | $1.03 \times 10^4$ | $1.16 \times 10^2$ | | |
| | 3 | 0.53 | 240.3 | $7.95 \times 10^3$ | $1.69 \times 10^1$ | | |
| | **mean** | **0.72** | **191.0** | **$9.1 \pm 0.9 \times 10^3$** | **$1.0 \pm 0.6 \times 10^2$** | **-22.7 ± 0.2** | **-11.4 ± 1.5** |

$cov_{fit}$ factor is $cov_{fit}$ for the 1:1 model divided by the $cov_{fit}$ for the binding model under study.[7] Values calculated with BindFit v0.5,[5] error is the standard deviation from 3 independent replicas.

The mean $cov_{fit}$ for the full 2:1 model is significantly higher than the mean $cov_{fit}$ for the 1:1 model, suggesting this system is best described by the full 2:1 model.

**$^{14}$N studies**

$^{14}$N NMR spectra were obtained on a Bruker AVANCE III 500 MHz spectrometer equipped with a 5 mm z-gradient broadband X-$^{19}$F/$^{1}$H BBFO SMART probe. An anti-ringing proton decoupled pulse sequence 'aringdec' was used. Chemical shifts referenced to external $NH_{3(l)}$.

25 mM solutions of tetrabutylammonium azide, (*S*)-**2.43b,** and (*S*)-**2.43b**·$N_3$·$Bu_4N$·were measured. The (*S*)-**2.43b**·$N_3$·$Bu_4N$ sample was prepared by dissolving tetrabutylammonium azide (5 mg) with a solution of (*S*)-**2.43b** in $CDCl_3$ (0.7 mL, 25 mM).

**4.3.7 Chiral urea bound azide - solution studies – understanding structure**

**Tetrabutylammonium [1-$^{15}$N]azide**

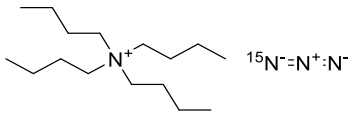


Prepared according to an adapted literature procedure.[16] Tetrabutylammonium hydroxide (40% in $H_2O$, 2.76 mL, 4.24 mmol, 1.1 equiv) was washed with $CH_2Cl_2$ (2 mL). The aqueous layer was added to a solution of sodium [1-$^{15}$N]azide (250 mg, 3.85 mmol, 1 equiv) in $H_2O$ (1 mL) in a separatory funnel. The aqueous layer was extracted with $CHCl_3$ (3×5 mL). The organic layer was dried with $MgSO_4$, filtered, and concentrated to afford crude product. The crude product was concentrated under reduced pressure, then evaporated to dryness under reduced pressure (0.05 mbar) over $P_2O_5$ to afford the title compound as a white solid, used without further purification (1.03 g, 3.61 mmol, 94%). The title compound was stored under nitrogen.

**$\nu_{max}$** (neat) /cm$^{-1}$ 2959, 2873, 1983, 1489, 885, 743; **$^{1}$H NMR** (500 MHz, $CDCl_3$) δ 3.40 – 3.24 (m, 8H), 1.74 – 1.62 (m, 8H), 1.52 – 1.37 (m, 8H), 1.02 (t, *J* = 7.5 Hz, 12H); **$^{13}$C NMR** (126 MHz, $CDCl_3$) δ 58.8, 24.1, 19.9, 13.8; **$^{15}$N NMR** (51 MHz, $CDCl_3$) δ 101.2.

**NB**: Only $^{15}$N label on terminal azide observed on $^{15}$N NMR.

**Concentration dependence of spectra**

A 1:1 mixture of (*S*)-**2.43b**·[1-$^{15}$N]$N_3$·$Bu_4N$ at 100 mM was prepared by dissolving (*S*)-**2.43b** (83.7 mg) and tetrabutylammonium [1-$^{15}$N]azide (28.5 mg) with $CDCl_3$ in a 1 mL volumetric flask.

A 25 mM solution was prepared with 250 µL of (*S*)-**2.43b**·[1-$^{15}$N]$N_3$·$Bu_4N$ (100 mM) and $CDCl_3$ in a 1 mL volumetric flask.

A 2.5 mM solution was prepared with 100 µL of (*S*)-**2.43b**·[1-$^{15}$N]$N_3$·$Bu_4N$ (25 mM) and $CDCl_3$ in a 1 mL volumetric flask.

**(*S*)-2.43b·[1-$^{15}$N]$N_3$·$Bu_4N$ sample preparation**

Subsequent samples for analysis were prepared by weighing tetrabutylammonium [1-$^{15}$N]azide (5.2 mg, 1 equiv) into an NMR tube equipped with a J. Young valve under $N_2$. A solution of (*S*)-**2.43b** in $CDCl_3$ (0.73 mL, 0.25 mM, 1 equiv) was added, and the sample was frozen with liquid $N_2$, evacuated, and flushed with $N_2$ once.

**(*S*)-2.43b·[1-$^{15}$N]$N_3$·$Bu_4N$ ($CDCl_3$, 25 mM) assignment**

The assignment of the $^1$H shifts of (*S*)-**2.43b**·[1-$^{15}$N]$N_3$·$Bu_4N$ in $CDCl_3$ at rt was achieved by tracking $^1$H CH signals along the titration, with additional assistance from 2D $^1$H-$^1$H COSY and $^1$H-$^1$H NOESY spectra. Additional support for NH assignments was provided by the variable temperature NMR studies of both this sample, and variable temperature (VT) NMR studies of a sample containing excess tetrabutylammonium [1-$^{15}$N]azide.

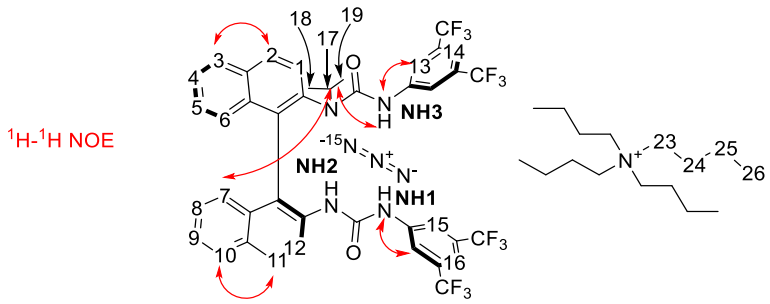


**$^1$H NMR** (600 MHz, $CDCl_3$) δ 9.49 (s, 1H, **H22**), 8.85 (d, *J* = 9.0 Hz, 1H, **H12**), 8.23 (s, 1H, **H20**), 8.10 (br s, 1H, **H2**), 7.98 (d, *J* = 9.0 Hz, 1H, **H11**), 7.94 – 7.80 (m, 4H, **H3**, **H10**, **H20**, **H13**), 7.59 (s, 2H, **H15**), 7.52 (d, *J* = 8.5 Hz, 1H, **H1**), 7.39 (br s, 1H, **H4**), 7.31 (t, *J* = 7.5 Hz, 1H, **H8**), 7.25 (s,

1H, **H16**), 7.21 – 7.10 (m, 3H, **H5**, **H6**, **H9**), 7.06 (s, 1H, **H14**), 6.75 (d, *J* = 8.0 Hz, 1H, **H7**), 3.14 – 2.98 (m, 9H, **H23**, **H17**), 1.62 – 1.41 (m, 8H, **H24**), 1.34 (sept, *J* = 7.5 Hz, 8H, **H25**), 1.18 (d, *J* = 6.5 Hz, 3H, **H19**), 0.95 (t, *J* = 7.5 Hz, 12H, **H26**), 0.37 (d, *J* = 6.5 Hz, 3H, **H18**).

**$^{15}$N [1-$^{15}$N]-Azide $T_1$ Measurement**

The previously prepared 25 mM sample of (*S*)-**2.43b**·[1-$^{15}$N]$N_3$·$Bu_4N$ in $CDCl_3$ was studied. A 25 mM sample of tetrabutylammonium [1-$^{15}$N]azide in $CDCl_3$ was also prepared.

$^{15}$N $T_1$ measurements were conducted on a Bruker AVIII HD 600 MHz spectrometer equipped with a Prodigy $N_2$ broadband cryoprobe. $T_1$ measurements used the inversion-recovery method.

The data were fitted to eqn (4.12) using TopSpin 4.0.2 in order to determine the $^{15}$N [1-$^{15}$N]azide $T_1$ of each sample. $I[0]$ is the relative equilibrium peak intensity (ideal = 1) and $P$ is the inverted peak intensity factor that is variable in the fit to allow for an imperfect initial inversion condition ($P = -2 \cdot I[0]$ for ideal inversion).

$$I[t] = I[0] + Pe^{-\frac{t}{T_1}} \tag{4.12}$$

**Table 4.9** [1-$^{15}$N]-azide $T_1$ acquisition parameters and values.

| entry | initial concentrations (*S*)-**2.43b** (mM) | [1-$^{15}$N]$N_3$ (mM) | F1 (slices/scans) | *t* (s) | $T_1$ (s) |
|---|---|---|---|---|---|
| 1 | 0 | 25 | 8/8 | 0.001, 10, 50, 80, 120, 180, 240, 300 | 39 |
| 2 | 25 | 25 | 10/8 | 0.001, 1, 3, 5, 8, 10, 15, 20, 25, 50 | 3.5 |
| 3 | 25 | 50 | 10/8 | 0.001, 1, 3, 5, 8, 10, 15, 20, 25, 50 | 8 |

**$^{1}$H-$^{15}$N Heteronuclear NOE experiments**

$^{1}$H-$^{15}$N NOE measurements were conducted on a Bruker AVIII HD 600 MHz spectrometer equipped with a Prodigy $N_2$ broadband cryoprobe. $^{1}$H chemical shifts are referenced to residual $CHCl_3$ and $^{15}$N chemical shifts are referenced to external $NH_{3(l)}$.

Steady-state $^{1}$H to $^{15}$N NOEs were generated using selective presaturation of $^{1}$H resonances followed by acquisition of the $^{15}$N 1D spectrum (**Figure 4.8A**). Control experiments were performed by off-resonance irradiation at ±20 ppm for all measurements. Due to crowding of the $^{1}$H resonances, various $B_1$ *rf* field strengths for $^{1}$H presaturation were investigated,

providing a balance of selectivity versus extent of $^1$H saturation, as directly observed in $^1$H NMR spectra following selective presaturation (**Figure 4.8B**). Series of NOE experiments were recorded using $B_1$ *rf* fields of 25 and 5 Hz, the former providing stronger NOEs but with spill over of saturation to neighbouring resonances in the $^1$H spectrum, whereas the latter provided for greater selectivity but weaker NOEs. Total $^1$H irradiation times of up to 40 s (>5×$T_1$) were employed.

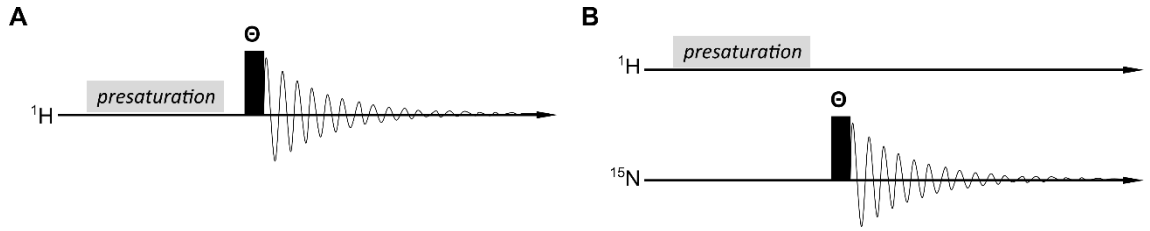


**Figure 4.8** (A) Schematic NMR sequences for $^1$H-$^{15}$N steady state NOE observations. (B) Schematic NMR sequences for optimisation of $^1$H presaturation conditions. Grey box indicates presaturation of a $^1$H resonance during relaxation delay and black rectangle indicates excitation pulse for acquisition (θ = 30° or 90°).

**Variable temperature studies of (*S*)-2.43b·[1-$^{15}$N]$N_3$·$Bu_4N$ ($CDCl_3$, 25 mM)**

Variable temperature studies were conducted on a Bruker AVANCE III 500 MHz spectrometer. The previously prepared 25 mM sample of (*S*)-**2.43b**·[1-$^{15}$N]$N_3$·$Bu_4N$ in $CDCl_3$ was studied. A $^1$H NMR spectra was taken at 298 K, then the temperature was reduced from 283 K to 213 K in 10 K decrements, and a $^1$H NMR spectra was acquired at every decrement.

At 213 K, decoalescence of an additional minor species was observed. The major species was designated the 1:1 (*S*)-**2.43b**·[1-$^{15}$N]$N_3$·$Bu_4N$ complex, and the minor species was tentatively designated as a 2:1 (*S*)-**2.43b**$_2$·[1-$^{15}$N]$N_3$·$Bu_4N$ complex, supported by the titration data. The presence of this species was suppressed in the sample of (*S*)-**2.43b** containing excess azide, further supporting this hypothesis.

**Variable temperature studies of (*S*)-2.43b ($CDCl_3$, 25 mM) and excess [1-$^{15}$N]$N_3$·$Bu_4N$**

$CDCl_3$ was further dried over activated 4 Å molecular sieves. The sample was prepared by weighing tetrabutylammonium [1-$^{15}$N]azide (10.4 mg, 2 equiv) and (*S*)-**2.43b** (15.2 mg, 1 equiv) into a flame dried NMR tube equipped with a J. Young valve under $N_2$. Dry $CDCl_3$ (0.73 mL, 0.25 mM) was added, and the sample was frozen with liquid $N_2$, evacuated, and flushed

with $N_2$ once. Variable temperature studies were conducted on a Bruker AVANCE III 500 MHz spectrometer. A $^1$H NMR spectra was taken at 298 K, then the temperature was reduced from 283 K to 213 K in 10 K decrements, and a $^1$H NMR spectra was acquired at every decrement. A significantly reduced quantity of the previously observed minor species at 213 K was observed, supporting the hypothesis those signals corresponded to a 2:1 (*S*)-**2.43b**$_2$·[1-$^{15}$N]$N_3$·$Bu_4N$ complex.

The assignment of the $^1$H shifts of (*S*)-**2.43b**·[1-$^{15}$N]$N_3$·$Bu_4N$ in $CDCl_3$ at 213 K was achieved by tracking $^1$H signals along the titration and temperature change, with additional assistance from 2D $^1$H-$^1$H COSY and $^1$H-$^1$H NOESY spectra, and supported the assignment at rt.

$^{1h}J_{HN}$ coupling constants was studied by 1D $^1$H-$^{15}$N HMBC.

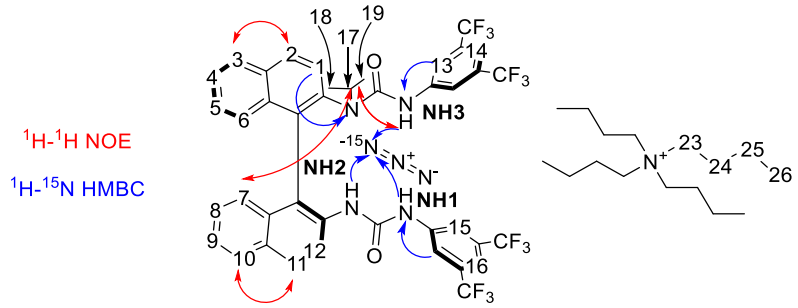


**$^1$H NMR** (500 MHz, $CDCl_3$, 213 K) δ 9.43 (s, 1H, **NH1**), 8.69 (d, *J* = 9.0 Hz, 1H, **H12**), 8.55 (s, 1H, **NH3**), 8.37 (d, *J* = 8.5 Hz, 1H, **H2**), 8.28 (s, 1H, **NH2**), 8.22 (d, *J* = 8.5 Hz, 1H, **H3**), 7.98 (d, *J* = 9.0 Hz, 1H, **H11**), 7.87 (d, *J* = 8.0 Hz, 1H, **H10**), 7.73 (s, 2H, **H13**), 7.64 – 7.55 (m, 2H, **H4, H1**), 7.41 (s, 2H, **H15**), 7.39 – 7.32 (m, 2H, **H5, H9**), 7.26 – 7.22 (m, 1H, **H6**), 7.22 – 7.16 (m, 1H, **H8**), 7.12 (s, 1H, **H16**), 6.93 (s, 1H, **H14**), 6.84 (d, *J* = 8.5 Hz, 1H, **H7**), 3.22 – 3.13 (m, 16H, **H23**), 3.02 – 2.94 (m, 1H, **H17**), 1.57 (s, 16H, **H24**), 1.41 – 1.27 (m, 16H, **H25**), 1.21 (d, *J* = 6.5 Hz, 1H, **H19**), 0.96 (t, *J* = 7.0 Hz, 24H, **H26**), 0.27 (d, *J* = 6.5 Hz, 1H, **H18**).

### 4.3.8 Chiral urea bound azide - solid state studies

**(±)-3-(3,5-bis(trifluoromethyl)phenyl)-1-(2'-(3-(3,5-bis(trifluoromethyl)phenyl)ureido)-[1,1'-binaphthalen]-2-yl)-1-isopropylurea·tetrabutylammonium azide ((±)-2.43b·$N_3$·$Bu_4N$)**

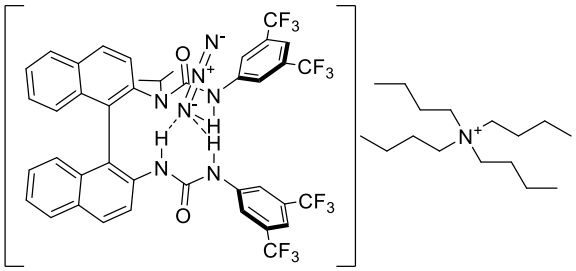

MeCN (2.5 mL) was added to (±)-**2.43b** (209 mg, 0.25 mmol, 1 equiv) and tetrabutylammonium azide (71.2 mg, 0.25 mmol, 1 equiv). The reaction mixture was stirred at rt for 24 h. The reaction mixture was evaporated to dryness to afford the title compound as a white solid (277 mg, 0.25 mmol, 99%).

Single crystals suitable for X-ray crystallography were grown by slow evaporation of a saturated solution of the title compound in hot hexane with a minimal quantity of EtOAc.

**mp** 85-87 °C; **$\nu_{max}$** (neat) /$cm^{-1}$ 2034, 1709, 1666, 1388, 1277, 1175, 1121, 880, 747, 681; **$^1$H NMR** (500 MHz, $CDCl_3$) δ 9.27 (br s, 1H), 8.84 (d, *J* = 8.0 Hz, 1H), 8.28 (br s, 1H), 8.03 – 7.80 (m, 7H), 7.51 – 7.40 (m, 4H), 7.32 (t, *J* = 7.5 Hz, 1H), 7.20 – 7.14 (m, 4H), 7.04 (s, 1H), 6.77 (d, *J* = 8.5 Hz, 1H), 3.12 – 3.02 (m, 9H), 1.57 – 1.51 (m, 8H), 1.38 – 1.30 (m, 8H), 1.20 (d, *J* = 6.5 Hz, 3H), 0.95 (t, *J* = 7.5 Hz, 12H), 0.36 (d, *J* = 6.5 Hz, 3H); **$^{19}$F NMR** (471 MHz, $CDCl_3$) δ -62.82, -63.02; **$^{13}$C NMR** (126 MHz, $CDCl_3$) δ 153.9, 153.0, 141.6, 141.0, 140.6, 136.8, 134.8, 133.4×2, 131.9, 131.6, 131.4 (q, *J* = 33.0 Hz), 131.1 (q, *J* = 33.0 Hz), 130.0, 129.1, 128.7, 128.2, 127.4, 127.1, 126.7, 126.5, 126.4, 125.3, 124.0, 123.4 (q, *J* = 272.5 Hz), 123.4 (q, *J* = 273.0 Hz), 120.8 (q, *J* = 5.0 Hz), 120.3, 119.7, 117.4 (q, *J* = 5.0 Hz), 114.8, 114.5, 58.9, 56.4, 23.9, 20.0, 19.7, 19.1, 13.6.

### 4.4.3 Synthesis of β-thioazides under HB-PTC

Substrate (±)-**2.39b** was prepared according to reported literature procedure.[14]

**(2-azido-1,2-diphenylethyl)(phenethyl)sulfane (2.40b)**

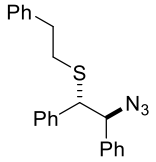

**Racemic product**: Prepared according to GP2.2 from (±)-**2.39b** to afford the title compound as a clear oil.

**Enantioenriched product**: Prepared according to GP2.3 from (±)-**2.39b** to afford the title compound (56% NMRy, 69.5:30.5 e.r.).

**$\nu_{max}$** (thin film) /$cm^{-1}$ 3028, 2917, 2098, 1494, 1453, 1251, 1074, 1030, 697; **$^{1}$H NMR** (400 MHz, $CDCl_3$) δ 7.42 – 6.96 (m, 15H), 4.82 (d, *J* = 9.0 Hz, 1H), 4.13 (d, *J* = 9.0 Hz, 1H), 2.89 – 2.74 (m, 2H), 2.66 – 2.59 (m, 2H); **$^{13}$C NMR** (101 MHz, $CDCl_3$) δ 140.5, 138.6, 137.5, 128.8, 128.6, 128.5, 128.5, 128.5, 128.4, 127.7, 127.6, 126.4, 71.2, 56.3, 36.2, 33.3; **HPLC** DAICEL CHIRALPAK® IA-3, 1% IPA in heptane, 1 mL $min^{-1}$, $t_{major}$ = 3.23, $t_{minor}$ = 3.73.

**NB**: Characterisation of racemic product provided.

**4.4.4 Synthesis of β-aminoazides under HB-PTC**

Substrates (±)-**2.46a,d,e,f,h,j** were prepared according to reported literature procedures.[17]

**(±)-2-(4-methoxypiperidin-1-yl)-1,2-diphenylethan-1-ol**

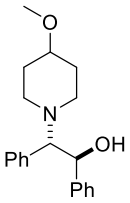

Prepared according to GP2.6 (48 h) with *cis*-stilbene oxide (2.00 g, 10.19 mmol, 1.00 equiv) and 4-methoxy-piperidine (5.87 g, 50.96 mmol, 5.00 equiv). The crude product was purified by flash silica chromatography (elution gradient 0 to 20% $Et_2O$ in pentane) to afford the title compound as a white solid (2.96 g, 9.50 mmol, 93%).

**mp** 115-117 °C; **$\nu_{max}$** (thin film) /$cm^{-1}$ 2926, 2360, 1452, 1084, 701; **$^{1}$H NMR** (400 MHz, $CDCl_3$) δ 7.26 – 7.18 (m, 5H), 7.17 – 7.05 (m, 5H), 5.19 (s, 1H), 5.02 (d, *J* = 10.5 Hz, 1H), 3.58 (d, *J* = 10.5 Hz, 1H), 3.27 (s, 3H), 3.08 (quin, *J* = 4.5 Hz, 1H), 3.03 – 2.91 (m, 1H), 2.76 – 2.62 (m, 1H),

2.41 (t, *J* = 10.5 Hz, 1H), 2.05 – 1.92 (m, 3H), 1.75 – 1.57 (m, 2H); **$^{13}$C NMR** (101 MHz, $CDCl_3$) δ 141.6, 133.3, 130.0, 128.1, 128.0, 127.9, 127.5, 127.4, 76.6, 70.7, 55.7, 45.3, 31.8, 31.5; **HRMS** ($ESI^+$) calc. for $C_{20}H_{26}O_2N$ ($[M+H]^+$): 312.1958; found: 321.1958.

**NB**: Two fewer $^{13}$C resonances observed due to overlapping signals from diastereotopic carbons.

**(±)-1-(2-chloro-1,2-diphenylethyl)-4-methoxypiperidine (2.46b)**

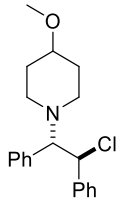


Prepared according to GP2.7 with (±)-2-(4-methoxypiperidin-1-yl)-1,2-diphenylethan-1-ol (2.90 g, 9.31 mmol, 1.00 equiv). The crude product was purified by flash silica chromatography (elution gradient 0 to 20% $Et_2O$ in pentane) to afford the title compound as a white solid (2.15 g, 6.52 mmol, 70%).

**mp** 97-99 °C; **$\nu_{max}$** (thin film) /$cm^{-1}$ 2940, 2819, 2361, 1452, 1139, 1090, 697; **$^1$H NMR** (400 MHz, $CDCl_3$) δ 7.23 – 7.06 (m, 8H), 6.97 – 6.92 (m, 2H), 5.37 (d, *J* = 10.5 Hz, 1H), 4.08 (d, *J* = 10.5 Hz, 1H), 3.28 (s, 3H), 3.07 (tt, *J* = 8.5, 4.5 Hz, 1H), 2.97 – 2.88 (m, 1H), 2.80 – 2.71 (m, 1H), 2.23 (td, *J* = 10.5, 3.0 Hz, 1H), 2.10 (td, *J* = 10.5, 3.0 Hz, 1H), 2.03 – 1.85 (m, 2H), 1.77 – 1.56 (m, 2H); **$^{13}$C NMR** (101 MHz, $CDCl_3$) δ 140.0, 135.0, 129.2, 128.3, 128.2, 128.0, 127.9, 127.4, 76.9, 74.9, 63.1, 55.6, 48.9, 45.4, 31.6, 31.4; **HRMS** ($ESI^+$) calc. for $C_{20}H_{25}ON^{35}Cl$ ($[M+H]^+$): 330.1619; found: 330.1618.

**(±)-2-(4,4-difluoropiperidin-1-yl)-1,2-diphenylethan-1-ol**

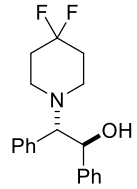


*cis*-Stilbene oxide (1.00 g, 5.10 mmol, 1.00 equiv) was added to a mixture of 4,4-difluoropiperidine hydrochloride (2.41 g, 15.29 mmol, 3.00 equiv) and NaOH (1.22 g, 30.57 mmol, 6.00 equiv) in $^i$PrOH (12.75 mL) and $H_2O$ (12.75 mL). The reaction mixture was stirred

at 90 °C in a sealed tube for 60 h. The reaction mixture was cooled to rt, diluted with EtOAc (50 mL), washed with $H_2O$ (25 mL), sat. brine (25 mL), dried with $MgSO_4$, filtered, and concentrated to afford crude product. The crude product was purified by flash silica chromatography (elution gradient 0 to 20% $Et_2O$ in pentane) to afford the title compound as a white solid (1.26 g, 3.97 mmol, 78%).

**mp** 123-124 °C; **$\nu_{max}$** (thin film) /$cm^{-1}$ 2845, 1366, 1155, 1129, 1072, 1005, 701; **$^1$H NMR** (500 MHz, DMSO-$d_6$) δ 7.29 – 7.24 (m, 2H), 7.24 – 7.11 (m, 7H), 7.11 – 7.05 (m, 1H), 5.14 (d, *J* = 10.0 Hz, 1H), 4.90 (d, *J* = 1.0 Hz, 1H), 3.80 (d, *J* = 10.0 Hz, 1H), 2.66 (br s, 2H), 2.37 (br s, 2H), 2.16 – 1.94 (m, 4H); **$^{19}$F NMR** (471 MHz, DMSO-$d_6$) δ -95.32 (br s); **$^{13}$C NMR** (126 MHz, DMSO-$d_6$) δ 142.3, 133.8, 129.6, 127.8, 127.6×2, 127.2, 127.0, 122.8 (t, *J* = 241.0 Hz), 74.2, 70.3, 45.5, 33.7 (t, *J* = 22.0 Hz); **HRMS** ($ESI^+$) calc. for $C_{19}H_{22}ONF_2$ ($[M+H]^+$): 318.1664; found: 318.1662.

**(±)-1-(2-chloro-1,2-diphenlethyl)-4,4-difluoropiperidine (2.46c)**

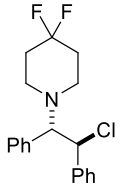


Prepared according to GP2.7 with (±)-2-(4,4-difluoropiperidin-1-yl)-1,2-diphenylethan-1-ol (1.18 g, 3.72 mmol, 1.00 equiv). The crude product was purified by flash silica chromatography (elution gradient 0 to 10% $Et_2O$ in pentane) to afford the title compound as a white solid (1.16 g, 3.45 mmol, 93%).

**mp** 120-121 °C; **$\nu_{max}$** (thin film) /$cm^{-1}$ 2832, 2361, 1453, 1362, 1125, 1081, 946, 697; **$^1$H NMR** (400 MHz, $CDCl_3$) δ 7.25 – 7.08 (m, 8H), 7.03 – 6.89 (m, 2H), 5.36 (d, *J* = 11.0 Hz, 1H), 4.13 (d, *J* = 11.0 Hz, 1H), 2.78 – 2.61 (m, 2H), 2.61 – 2.42 (m, 2H), 2.22 – 1.92 (m, 4H); **$^{19}$F NMR** (377 MHz, $CDCl_3$) δ -97.34 (br s); **$^{13}$C NMR** (101 MHz, $CDCl_3$) δ 139.7, 134.6, 128.9, 128.4, 128.2, 128.2, 128.1, 127.8, 122.3 (t, *J* = 241.5 Hz), 74.5, 63.1, 40.0, 34.6 (t, *J* = 22.5 Hz); **HRMS** ($ESI^+$) calc. for $C_{19}H_{21}N^{35}ClF_2$ ($[M+H]^+$): 336.1325; found: 336.1324.

**(±)-1,2-diphenyl-2-(4-phenylpiperazin-1-yl)ethan-1-ol**

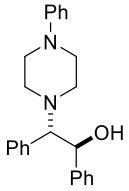


Prepared according to GP2.6 (48 h) with *cis*-stilbene oxide (1.00 g, 5.10 mmol, 1.00 equiv) and 1-phenylpiperazine (3.89 g, 25.50 mmol, 5.00 equiv). The crude product was purified by flash silica chromatography (elution gradient 0 to 30% $Et_2O$ in pentane) to afford the title compound as a white solid (1.46 g, 4.07 mmol, 80%).

**mp** 174-176 °C; **$\nu_{max}$** (thin film) /$cm^{-1}$ 2836, 1599, 1239, 761, 749, 701, 690; **$^1$H NMR** (400 MHz, $CDCl_3$) δ 7.20 – 6.99 (m, 12H), 6.84 – 6.73 (m, 3H), 5.53 – 4.75 (m, 2H), 3.58 (d, *J* = 10.5 Hz, 1H), 3.25 – 3.08 (m, 4H), 2.81 – 2.71 (m, 2H), 2.53 – 2.42 (m, 2H); **$^{13}$C NMR** (101 MHz, $CDCl_3$) δ 151.3, 141.3, 132.8, 130.0, 129.2, 128.1×2, 128.0, 127.6, 127.4, 120.2, 116.4, 76.5, 70.6, 49.9, 49.1; **HRMS** ($ESI^+$) calc. for $C_{24}H_{27}ON_2$ ($[M+H]^+$): 359.2129; found: 359.2120.

**(±)-1-(2-chloro-1,2-diphenylethyl)-4-phenylpiperazine (2.46g)**

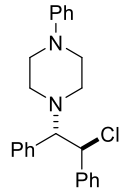


Prepared according to GP2.7 with (±)-1,2-diphenyl-2-(4-phenylpiperazin-1-yl)ethan-1-ol (1.42 g, 3.96 mmol, 1.00 equiv). The crude product was purified by flash silica chromatography (elution gradient 0 to 20% EtOAc in $CH_2Cl_2$) to afford the title compound as white solid (1.10 g, 3.96 mmol, 74%).

**mp** 135-137 °C; **$\nu_{max}$** (thin film) /$cm^{-1}$ 2824, 2361, 1598, 1233, 694; **$^1$H NMR** (400 MHz, $CDCl_3$) δ 7.21 – 7.13 (m, 4H), 7.13 – 6.99 (m, 6H), 6.96 – 6.86 (m, 2H), 6.87 – 6.79 (m, 2H), 6.79 – 6.68 (m, 1H), 5.36 (d, *J* = 10.5 Hz, 1H), 4.07 (d, *J* = 10.5 Hz, 1H), 3.25 – 3.08 (m, 4H), 2.73 – 2.50 (m, 4H); **$^{13}$C NMR** (101 MHz, $CDCl_3$) δ 151.6, 139.7, 134.5, 129.3, 129.2, 128.4, 128.2, 128.1, 128.0, 127.6, 119.9, 116.4, 75.0, 62.7, 49.8, 49.3; **HRMS** ($ESI^+$) calc. for $C_{24}H_{26}N_2{}^{35}Cl$ ($[M+H]^+$): 377.1779; found: 377.1782.

**(±)-2-(benzyl(methyl)amino)-1,2-diphenylethan-1-ol**

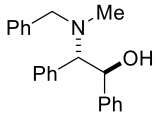

Yttrium(III) trifluoromethanesulfonate (1.09 g, 2.04 mmol, 0.20 equiv) was added to a solution of *N*-benzylmethylamine (1.32 mL, 10.19 mmol, 1.00 equiv) and *cis*-stilbene oxide (2.00 g, 10.19 mmol, 1.00 equiv) in dry THF (20 mL) under $N_2$. The reaction mixture was heated under reflux for 18 h. The reaction mixture was cooled to rt, diluted with $Et_2O$ (50 mL), washed with sat. $NaHCO_3$ (50 mL), sat. brine (50 mL), dried with $MgSO_4$, filtered, and concentrated to afford crude product. The crude product was purified by flash silica chromatography (elution gradient 0 to 50% $Et_2O$ in pentane) to afford the title compound as a white solid (2.17 g, 6.84 mmol, 67%).

**mp** 119-120 °C; **$\nu_{max}$** (thin film) /$cm^{-1}$ 3029, 1494, 1452, 1399, 1079, 1053, 913, 879, 758, 737, 699; **$^1$H NMR** (400 MHz, $CDCl_3$) δ 7.41 – 7.34 (m, 4H), 7.34 – 7.26 (m, 4H), 7.19 – 7.07 (m, 7H), 5.27 (s, 1H), 5.11 (d, *J* = 10.5 Hz, 1H), 3.74 (d, *J* = 10.5 Hz, 1H), 3.65 (d, *J* = 13.0 Hz, 1H), 3.41 (d, *J* = 13.0 Hz, 1H), 2.21 (s, 3H); **$^{13}$C NMR** (101 MHz, $CDCl_3$) δ 141.5, 138.5, 133.0, 130.3, 129.2, 128.7, 128.1, 128.0, 127.9, 127.5×3, 74.3, 71.2, 58.8, 36.9; **HRMS** ($ESI^+$) calc. for $C_{22}H_{24}ON$ ($[M+H]^+$): 318.1852; found 318.1851.

**(±)-*N*-benzyl-2-chloro-*N*-methyl-1,2-diphenylethan-1-amine (2.46i)**

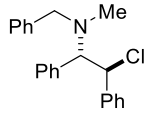

Prepared according to GP2.7 with (±)-2-(benzyl(methyl)amino)-1,2-diphenylethan-1-ol (2.15 g, 6.77 mmol, 1.00 equiv). The crude product was triturated with $CH_2Cl_2$. The solids were collected and dried to afford the title compound as white solid (1.17 g, 3.45 mmol, 51%).

**mp** 156-157 °C; **$\nu_{max}$** (thin film) /$cm^{-1}$ 3028, 2361, 1492, 1452, 761, 703; **$^1$H NMR** (400 MHz, $CDCl_3$) δ 7.52 – 7.45 (m, 2H), 7.39 – 7.33 (m, 2H), 7.31 – 7.26 (m, 1H), 7.24 – 7.06 (m, 8H), 7.01 – 6.95 (m, 2H), 5.49 (d, *J* = 11.0 Hz, 1H), 4.24 (d, *J* = 11.0 Hz, 1H), 3.80 (d, *J* = 13.5 Hz, 1H), 3.33 (d, *J* = 13.5 Hz, 1H), 2.25 (s, 3H); **$^{13}$C NMR** (101 MHz, $CDCl_3$) δ 140.0, 139.5, 134.3, 129.3, 129.0,

128.4×2, 128.2, 128.1, 128.0, 127.5, 127.1, 73.0, 63.4, 58.0, 37.6; **HRMS** ($ESI^+$) calc. for $C_{22}H_{23}N^{35}Cl$ ($[M+H]^+$): 412.1514; found: 412.1512.

**(±)-2-(azepan-1-yl)-1,2-diphenylethan-1-ol**

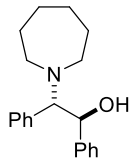


Prepared according to GP2.6 (72 h) with *cis*-stilbene oxide (2.00 g, 10.19 mmol, 1.00 equiv) and azepane (5.74 mL, 50.96 mmol, 5.00 equiv). The crude product was purified by flash silica chromatography (elution gradient 0 to 20% EtOAc in pentane), then triturated with pentane to afford the title compound as a white solid (2.05 g, 6.94 mmol, 68%).

**mp** 81-83 °C; **$\nu_{max}$** (thin film) /$cm^{-1}$ 2923, 2852, 1451, 1047, 759, 699; **$^1$H NMR** (400 MHz, $CDCl_3$) δ 7.25 – 7.18 (m, 5H), 7.17 – 7.08 (m, 5H), 5.34 (s, 1H), 4.98 (d, *J* = 10.5 Hz, 1H), 3.64 (d, *J* = 10.5 Hz, 1H), 2.89 – 2.74 (m, 2H), 2.60 – 2.45 (m, 2H), 1.80 – 1.65 (m, 4H), 1.62 – 1.56 (m, 4H); **$^{13}$C NMR** (101 MHz, $CDCl_3$) δ 141.7, 135.0, 129.8, 128.0×2, 127.7, 127.5, 127.4, 77.6, 71.3, 52.1, 29.4, 26.7; **HRMS** ($ESI^+$) calc. for $C_{20}H_{26}ON$ ($[M+H]^+$): 296.2009; found 296.2007.

**(±)-2-chloro-1,2-diphenylethyl)azepane (2.46k)**

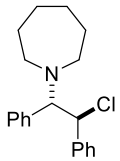


Prepared according to GP2.7 with (±)-2-(azepan-1-yl)-1,2-diphenylethan-1-ol (2.05 g, 6.94 mmol, 1.00 equiv). The crude product was purified by flash silica chromatography (elution gradient 0 to 20% $Et_2O$ in pentane) to afford the title compound as a white solid (1.47 g, 4.68 mmol, 67%).

**mp** 77-78 °C; **$\nu_{max}$** (thin film) /$cm^{-1}$ 2924, 2361, 1494, 1451, 1158, 1076, 695; **$^1$H NMR** (400 MHz, $CDCl_3$) δ 7.24 – 6.84 (m, 10H), 5.29 (d, *J* = 10.5 Hz, 1H), 4.08 (d, *J* = 10.5 Hz, 1H), 2.87 – 2.65 (m, 2H), 2.65 – 2.42 (m, 2H), 1.67 – 1.55 (m, 4H), 1.52 – 1.41 (m, 4H); **$^{13}$C NMR** (101 MHz, $CDCl_3$) δ 140.3, 137.4, 128.7, 128.3, 128.2, 127.9, 127.8, 127.0, 75.5, 64.5, 51.6, 29.7, 27.2; **HRMS** ($ESI^+$) calc. for $C_{20}H_{25}N^{35}Cl$ ($[M+H]^+$): 314.1670; found 314.1668.

**(±)-1,2-bis(3-fluorophenyl)-2-(piperidin-1-yl)ethan-1-ol**

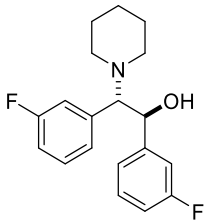


Prepared according to GP2.6 (30 h) with *cis*-2,3-bis(3-fluorophenyl)oxirane[18] (1.30 g, 5.60 mmol, 1.00 equiv) and piperidine (2.76 mL, 28.00 mmol, 5.00 equiv). The crude product was purified by flash silica chromatography (elution gradient 0 to 20% $Et_2O$ in pentane) to afford the title compound as a white solid (1.42 g, 4.48 mmol, 80%).

**mp** 108-110 °C; $\nu_{max}$ (thin film) /$cm^{-1}$ 2936, 1590, 1488, 1445, 1250, 1136, 1157, 780, 732, 706, 695; **$^1$H NMR** (500 MHz, $CDCl_3$) δ 7.23 (td, *J* = 8.0, 6.0 Hz, 1H), 7.09 (td, *J* = 8.0, 6.0 Hz, 1H), 7.00 (dt, *J* = 10.0, 2.0 Hz, 1H), 6.97 – 6.91 (m, 2H), 6.86 (d, *J* = 7.5 Hz, 1H), 6.84 – 6.79 (m, 2H), 5.29 (s, 1H), 4.97 (d, *J* = 10.5 Hz, 1H), 3.47 (d, *J* = 10.5 Hz, 1H), 2.62 (br s, 2H), 2.28 (br s, 2H), 1.70 – 1.59 (m, 4H), 1.37 (br s, 2H); **$^{19}$F NMR** (471 MHz, $CDCl_3$) δ -113.00, -113.44; **$^{13}$C NMR** (126 MHz, $CDCl_3$) δ 162.8 (d, *J* = 245.0 Hz), 162.4 (d, *J* = 246.5 Hz), 144.3 (d, *J* = 7.0 Hz), 135.9 (d, *J* = 6.5 Hz), 129.5 (d, *J* = 8.0 Hz), 129.4 (d, *J* = 8.0 Hz), 125.7 (d, *J* = 3.0 Hz), 123.1 (d, *J* = 3.0 Hz), 116.7 (d, *J* = 21.0 Hz), 114.9 (d, *J* = 21.0 Hz), 114.4 (d, *J* = 21.0 Hz), 114.0 (d, *J* = 22.0 Hz), 76.8 (d, *J* = 1.5 Hz), 70.0 (d, *J* = 2.0 Hz), 50.4, 26.6, 24.3; **HRMS** ($ESI^+$) calc. for $C_{19}H_{22}ONF_2$ ($[M+H]^+$): 318.1664 found: 318.1662.

**(±)-1-(2-chloro-1,2-bis(3-fluorophenyl)ethyl)piperidine (2.46l)**

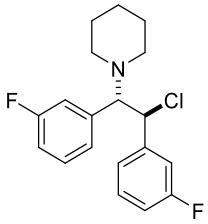


Prepared according to GP2.7 with (±)-1-(2-chloro-1,2-bis(3-fluorophenyl)ethyl)piperidine (1.36 g, 4.29 mmol, 1.00 equiv). The crude product was purified by flash silica chromatography (elution gradient 0 to 20% $Et_2O$ in pentane) to afford the title compound as a white solid (1.10 g, 3.26 mmol, 76%).

**mp** 120-122 °C; **$\nu_{max}$** (thin film) /$cm^{-1}$ 2934, 1590, 1488, 1447, 1245, 878, 773; **$^{1}$H NMR** (500 MHz, $CDCl_3$) δ 7.19 – 7.06 (m, 2H), 7.00 – 6.92 (m, 2H), 6.89 – 6.78 (m, 2H), 6.73 (d, *J* = 7.5 Hz, 1H), 6.67 (d, *J* = 9.5 Hz, 1H), 5.30 (d, *J* = 10.5 Hz, 1H), 3.97 (d, *J* = 10.5 Hz, 1H), 2.56 – 2.43 (m, 2H), 2.42 – 2.27 (m, 2H), 1.74 – 1.63 (m, 2H), 1.63 – 1.52 (m, 2H), 1.41 – 1.31 (m, 2H); **$^{19}$F NMR** (471 MHz, $CDCl_3$) δ -112.67, -113.13; **$^{13}$C NMR** (126 MHz, $CDCl_3$) δ 162.6 (d, *J* = 246.5 Hz), 162.4 (d, *J* = 246.0 Hz), 142.2 (d, *J* = 7.5 Hz), 137.5 (d, *J* = 6.0 Hz), 129.9 (d, *J* = 8.5 Hz), 129.3 (d, *J* = 8.0 Hz), 124.9 (d, *J* = 3.0 Hz), 124.0 (d, *J* = 3.0 Hz), 115.9 (d, *J* = 21.0 Hz), 115.2 (d, *J* = 21.0 Hz), 115.2 (d, *J* = 22.5 Hz), 114.5 (d, *J* = 21.0 Hz), 75.2, 61.6, 50.6, 26.5, 24.7; **HRMS** ($ESI^+$) calc. for $C_{19}H_{21}N^{35}ClF_2$ ($[M+H]^+$): 336.1325 found: 336.1325.

**(±)-1,2-bis(3-chlorophenyl)-2-(piperidin-1-yl)ethan-1-ol**

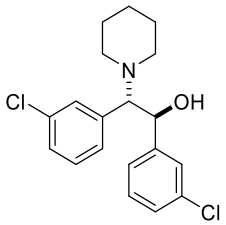


Prepared according to GP2.6 (48 h) with *cis*-2,3-bis(3-chlorophenyl)oxirane[19] (1.48 g, 7.54 mmol, 1.00 equiv) and piperidine (3.72 mL, 50.90 mmol, 6.75 equiv). The crude product was purified by flash silica chromatography (elution gradient 0 to 10% $Et_2O$ in pentane) to afford the title compound as a white solid (1.67 g, 4.77 mmol, 63%).

**mp** 99-101 °C; **$\nu_{max}$** (thin film) /$cm^{-1}$ 2936, 2360, 1596, 1572, 1475, 1429, 1191, 1157, 1055, 883, 733, 695; **$^{1}$H NMR** (400 MHz, $CDCl_3$) δ 7.34 – 7.29 (m, 1H), 7.26 – 7.18 (m, 2H), 7.13 – 7.02 (m, 3H), 7.00 – 6.92 (m, 2H), 5.27 (s, 1H), 4.94 (d, *J* = 10.5 Hz, 1H), 3.44 (d, *J* = 10.5 Hz, 1H), 2.60 (br s, 2H), 2.27 (br s, 2H), 1.76 – 1.59 (m, 4H), 1.37 (br s, 2H); **$^{13}$C NMR** (101 MHz, $CDCl_3$) δ 143.7, 135.3, 134.2, 134.1, 129.9, 129.3×2, 128.2, 128.0, 127.8, 127.3, 125.8, 76.8, 70.0, 50.3, 26.6, 24.3; **HRMS** ($ESI^+$) calc. for $C_{19}H_{22}ON^{35}Cl_2$ ($[M+H]^+$): 350.1073; found: 350.1076.

**(±)-1-(2-chloro-1,2-bis(3-chlorophenyl)ethyl)piperidine (2.46m)**

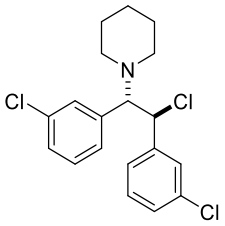


Prepared according to GP2.7 with (±)-1,2-bis(3-chlorophenyl)-2-(piperidin-1-yl)ethan-1-ol (1.65 g, 4.71 mmol, 1.00 equiv). The crude product was purified by flash silica chromatography (elution gradient 0 to 10% $Et_2O$ in pentane) to afford the title compound as a white solid (1.22 g, 3.30 mmol, 70%).

**mp** 140-142 °C; **$\nu_{max}$** (thin film) /$cm^{-1}$ 2933, 2360, 1573, 1429, 1098, 1079, 717, 694; **$^1$H NMR** (400 MHz, $CDCl_3$) δ 7.25 – 7.21 (m, 1H), 7.13 – 7.04 (m, 5H), 6.96 – 6.93 (m, 1H), 6.87 – 6.80 (m, 1H), 5.28 (d, *J* = 10.5 Hz, 1H), 3.94 (d, *J* = 10.5 Hz, 1H), 2.50 (ddd, *J* = 11.0, 7.0, 3.5 Hz, 2H), 2.34 (ddd, *J* = 11.0, 7.0, 3.5 Hz, 2H), 1.72 – 1.56 (m, 4H), 1.42 – 1.32 (m, 2H); **$^{13}$C NMR** (101 MHz, $CDCl_3$) δ 141.7, 136.9, 134.3, 134.0, 129.7, 129.1×2, 128.4×2, 127.8, 127.3, 126.4, 75.2, 61.5, 50.7, 26.4, 24.7; **HRMS** ($ESI^+$) calc. for $C_{19}H_{21}N^{35}Cl_3$ ($[M+H]^+$): 368.0734; found: 368.0735.

**(±)-2-(piperidin-1-yl)-1,2-bis(3-(trifluoromethyl)phenyl)ethan-1-ol**

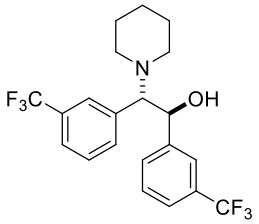


Prepared according to GP2.6 (48 h) with 2,3-bis(3-(trifluoromethyl)phenyl)oxirane[19] (1.00 g, 3.01 mmol, 1.00 equiv) and piperidine (1.44 mL, 15.05 mmol, 5.00 equiv). The crude product was purified by flash silica chromatography (elution gradient 0 to 20% $Et_2O$ in pentane) to afford the title compound as a pale-yellow oil (0.95 g, 2.29 mmol, 76%).

**$\nu_{max}$** (thin film) /$cm^{-1}$ 2939, 1446, 1326, 1160, 1120, 1073, 900, 804, 704, 665; **$^1$H NMR** (400 MHz, $CDCl_3$) δ 7.55 – 7.48 (m, 2H), 7.43 – 7.36 (m, 2H), 7.34 – 7.21 (m, 4H), 5.27 (s, 1H), 5.08 (d, *J* = 10.5 Hz, 1H), 3.53 (d, *J* = 10.5 Hz, 1H), 2.63 (br s, 2H), 2.30 (br s, 2H), 1.76 – 1.54 (m, 4H), 1.38 (s, 2H); **$^{19}$F NMR** (377 MHz, $CDCl_3$) δ -62.72, -62.81; **$^{13}$C NMR** (101 MHz, $CDCl_3$) δ 142.5,

134.3, 133.3, 130.7, 130.6 (q, *J* = 32.5 Hz), 130.6 (q, *J* = 32.5 Hz), 128.6, 128.6, 126.4 (q, *J* = 4.0 Hz), 125.0 (q, *J* = 4.0 Hz), 124.5 (q, *J* = 4.0 Hz), 124.2 (q, *J* = 272.0 Hz), 124.1 (q, *J* = 272.5 Hz), 124.0 (q, *J* = 4.0 Hz), 77.1, 70.2, 50.4, 26.6, 24.3; **HRMS** ($ESI^+$) calc. for $C_{21}H_{22}ONF_6$ ($[M+H]^+$): 418.1600; found: 418.1589.

**(±)-1-(2-chloro-1,2-bis(3-(trifluoromethyl)phenyl)ethyl)piperidine (2.46n)**

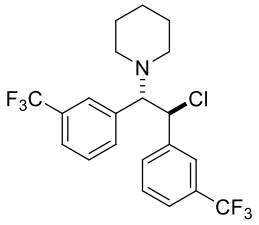


Prepared according to GP2.7 with (±)-2-(piperidin-1-yl)-1,2-bis(3-(trifluoromethyl)phenyl)ethan-1-ol (902 mg, 2.16 mmol, 1.00 equiv). The crude product was purified by flash silica chromatography (elution gradient 0 to 20% $Et_2O$ in pentane) to afford the title compound as a white solid (687 mg, 1.58 mmol, 73%).

**mp** 89-90 °C; **$\nu_{max}$** (thin film) /$cm^{-1}$ 2937, 1446, 1327, 1162, 1120, 1073, 700; **$^1$H NMR** (500 MHz, $CDCl_3$) δ 7.46 – 7.37 (m, 4H), 7.35 – 7.27 (m, 2H), 7.18 (br s, 1H), 7.16 – 7.12 (m, 1H), 5.47 (d, *J* = 9.5 Hz, 1H), 4.06 (d, *J* = 9.5 Hz, 1H), 2.63 – 2.46 (m, 2H), 2.46 – 2.37 (m, 2H), 1.76 – 1.61 (m, 4H), 1.48 – 1.34 (m, 2H); **$^{19}$F NMR** (471 MHz, $CDCl_3$) δ -62.84, -62.96; **$^{13}$C NMR** (126 MHz, $CDCl_3$) δ 140.4, 136.0, 132.6, 131.4, 130.7 (q, *J* = 32.5 Hz), 130.5 (d, *J* = 32.5 Hz), 128.9, 128.4, 125.7 (q, *J* = 4.0 Hz), 125.2 (q, *J* = 4.0 Hz), 125.0 (d, *J* = 4.0 Hz), 124.5 (q, *J* = 4.0 Hz), 124.1 (q, *J* = 272.5 Hz), 123.8 (q, *J* = 272.5 Hz), 75.8, 61.3, 51.0, 26.4, 24.6; **HRMS** ($ESI^+$) calc. for $C_{21}H_{21}N^{35}ClF_6$ ($[M+H]^+$): 436.1261; found: 436.1269.

**(±)-1,2-bis(4-bromophenyl)-2-(piperidin-1-yl)ethan-1-ol**

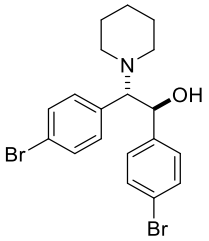


Prepared according to GP2.6 (48 h) with 2,3-bis(4-bromophenyl)oxirane[20] (2.25 g, 6.36 mmol, 1.00 equiv). The crude product was purified by flash silica chromatography (elution gradient

0 to 15% $Et_2O$ in pentane), then triturated with pentane to afford the title compound as a white solid (1.46 g, 3.32 mmol, 52%).

**mp** 130-132 °C; $\nu_{max}$ (thin film) /$cm^{-1}$ 2934, 2361, 1591, 1488, 1395, 1071, 1010, 908, 871, 822, 728; **$^1$H NMR** (400 MHz, $CDCl_3$) δ 7.40 (d, *J* = 8.5 Hz, 2H), 7.28 (d, *J* = 8.5 Hz, 2H), 7.06 (d, *J* = 8.5 Hz, 2H), 6.93 (d, *J* = 8.5 Hz, 2H), 5.26 (s, 1H), 4.92 (d, *J* = 10.5 Hz, 1H), 3.41 (d, *J* = 10.5 Hz, 1H), 2.58 (br s, 2H), 2.25 (br s, 2H), 1.80 – 1.51 (m, 4H), 1.36 (s, 2H); **$^{13}$C NMR** (101 MHz, $CDCl_3$) δ 140.7, 132.2, 131.5, 131.3, 131.2, 129.0, 122.1, 121.4, 76.7, 70.0, 50.5, 26.6, 24.3; **HRMS** ($ESI^+$) calc. for $C_{19}H_{22}ON^{79}Br_2$ ($[M+H]^+$): 438.0063; found: 438.0059.

**(±)-1-(1,2-bis(4-bromophenyl)-2-chloroethyl)piperidine (2.46o)**

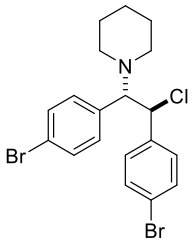


Prepared according to GP2.7 with (±)-1,2-bis(4-bromophenyl)-2-(piperidin-1-yl)ethan-1-ol (1.62 g, 3.69 mmol, 1.00 equiv). The crude product was purified by flash silica chromatography (elution gradient 0 to 10% $Et_2O$ in pentane) to afford the title compound as a white solid (1.05 g, 2.29 mmol, 62%).

**mp** 119-120 °C; $\nu_{max}$ (thin film) /$cm^{-1}$ 2993, 1488, 1103, 1074, 1010, 750; **$^1$H NMR** (400 MHz, $CDCl_3$) δ 7.34 – 7.27 (m, 4H), 7.10 – 6.98 (m, 2H), 6.87 – 6.75 (m, 2H), 5.29 (d, *J* = 10.5 Hz, 1H), 3.93 (d, *J* = 10.5 Hz, 1H), 2.53 – 2.40 (m, 2H), 2.40 – 2.27 (m, 2H), 1.73 – 1.52 (m, 4H), 1.47 – 1.30 (m, 2H); **$^{13}$C NMR** (101 MHz, $CDCl_3$) δ 138.8, 133.8, 131.6, 131.1, 130.7, 129.9, 122.1, 121.5, 75.0, 61.6, 50.6, 26.4, 24.7; **HRMS** ($ESI^+$) calc. for $C_{19}H_{21}N^{79}Br_2{}^{35}Cl$ ($[M+H]^+$): 455.9724; found 455.9722.

**(*Z*)-1,2-bis(4-(*tert*-butyl)phenyl)ethene**

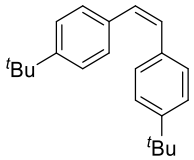


A solution of $^{n}$BuLi in hexane (27.5 mL, 1.6 M, 44.08 mmol, 4.00 equiv) was added dropwise over 5 min to a solution of titanium(IV) isopropoxide (6.53 mL, 22.04 mmol, 2.00 equiv) and 1,2-bis(4-(*tert*-butyl)phenyl)ethyne[21,22] (3.20 g, 11.02 mmol, 1.00 equiv) in dry THF (44 mL, 0.25 M) under $N_2$ at -78 °C. The reaction mixture was stirred at rt for 2 h. The reaction mixture was cooled to 0 °C, then diluted with sat. $NH_4Cl$ (50 mL). The reaction mixture was extracted with $Et_2O$ (50 mL), washed with sat. brine (50 mL), dried with $MgSO_4$, filtered, and concentrated to afford crude product. The crude product was purified by filtration through a silica plug (elution with 100% pentane) to afford the title compound as a pale-yellow oil (2.34 g, 8.00 mmol, 73%).

**$\nu_{max}$** (thin film) /cm$^{-1}$ 2961, 2361, 1511, 1463, 1363, 1269, 1108, 1018, 883, 842, 824; **$^{1}$H NMR** (400 MHz, $CDCl_3$) δ 7.18 – 7.16 (m, 8H), 6.42 (s, 2H), 1.23 (s, 18H); **$^{13}$C NMR** (101 MHz, $CDCl_3$) δ 150.2, 134.7, 129.6, 128.7, 125.2, 34.7, 31.5; **HRMS** (EI) calc. for $C_{22}H_{28}$ ([M]$^{+}$): 292.2186; found 292.2191.

**NB**: Both (*E*)-1,2-bis(4-(tert-butyl)phenyl)ethene and a mixture of (*E*)-1,2-bis(4-(tert-butyl)phenyl)ethene and (*Z*)-1,2-bis(4-(tert-butyl)phenyl)ethene have been previously characterised.[23,24]

**2,3-bis(4-(*tert*-butyl)phenyl)oxirane**

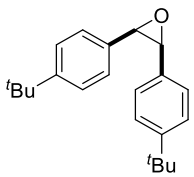


*m*CPBA (2.69 g, 12.00 mmol, 1.50 equiv) was added to (*Z*)-1,2-bis(4-(*tert*-butyl)phenyl)ethene (2.34 g, 8.00 mmol, 1.00 equiv) in $CH_2Cl_2$ (16 mL, 0.5 M) at 0 °C. The reaction mixture was stirred at rt for 24 h. The reaction mixture was filtered through celite. The filtrate was washed with sat. $Na_2SO_3$ (20 mL), sat. brine (20 mL), dried with $MgSO_4$, filtered, and concentrated to

afford crude product. The crude product was purified by flash silica chromatography (elution gradient 0 to 5% $Et_2O$ in pentane) to afford the title compound as a pale-yellow oil (2.30 g, 7.46 mmol, 93%).

**$\nu_{max}$** (thin film) /$cm^{-1}$ 2962, 2361, 1517, 1392, 1268, 805; **$^1$H NMR** (400 MHz, $CDCl_3$) δ 7.24 – 7.19 (m, 4H), 7.15 – 7.08 (m, 4H), 4.31 (s, 2H), 1.25 (s, 18H); **$^{13}$C NMR** (101 MHz, $CDCl_3$) δ 150.5, 131.7, 126.9, 124.8, 60.1, 34.6, 31.4; **HRMS** ($ESI^+$) calc. for $C_{22}H_{29}O$ ($[M+H]^+$): 309.2213; found: 309.2214.

**(±)-1,2-bis(4-(*tert*-butyl)phenyl)-2-(piperidin-1-yl)ethan-1-ol**

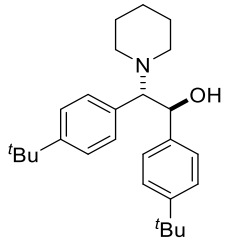


Prepared according to GP2.6 (72 h) with 2,3-bis(4-(*tert*-butyl)phenyl)oxirane (737 mg, 2.39 mmol, 1.00 equiv). The crude product was purified by flash silica chromatography (elution gradient 0 to 20% $Et_2O$ in pentane) to afford the title compound as a white solid (823 mg, 2.09 mmol, 88%).

**mp** 125-127 °C; **$\nu_{max}$** (thin film) /$cm^{-1}$ 2961, 2360, 1364, 1271, 1110, 828; **$^1$H NMR** (400 MHz, $CDCl_3$) δ 7.27 – 7.22 (m, 2H), 7.20 – 7.12 (m, 4H), 7.05 – 7.00 (m, 2H), 5.48 (s, 1H), 5.01 (d, *J* = 10.5 Hz, 1H), 3.54 (d, *J* = 10.5 Hz, 1H), 2.62 (br s, 2H), 2.24 (br s, 2H), 1.80 – 1.49 (m, 4H), 1.40 – 1.31 (m, 2H), 1.28 (s, 9H), 1.22 (s, 9H); **$^{13}$C NMR** (101 MHz, $CDCl_3$) δ 150.3, 149.9, 139.0, 130.7, 129.7, 127.0, 124.9, 124.6, 76.1, 69.9, 50.4, 34.6, 34.5, 31.5, 31.4, 26.7, 24.4; **HRMS** ($ESI^+$) calc. for $C_{27}H_{40}ON$ ($[M+H]^+$): 394.3104; found: 394.3099.

**(±)-1-(1,2-bis(4-(*tert*-butyl)phenyl)-2-chloroethyl)piperidine (2.46p)**

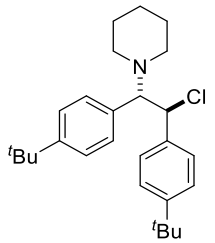

Prepared according to GP2.7 with (±)-1,2-bis(4-(*tert*-butyl)phenyl)-2-(piperidin-1-yl)ethan-1-ol (832 mg, 1.89 mmol, 1.00 equiv). The crude product was purified by flash silica chromatography (elution gradient 0 to 10% $Et_2O$ in pentane) to afford the title compound as a white solid (289 mg, 0.70 mmol, 35%).

**mp** 117-119 °C; **$\nu_{max}$** (thin film) /$cm^{-1}$ 2962, 2360, 908, 731, 697; **$^1$H NMR** (400 MHz, $CDCl_3$) δ 7.17 – 6.95 (m, 6H), 6.85 – 6.71 (m, 2H), 5.29 (d, *J* = 10.5 Hz, 1H), 3.93 (d, *J* = 10.5 Hz, 1H), 2.47 (br s, 2H), 2.30 (br s, 2H), 1.67 – 1.37 (m, 4H), 1.34 – 1.20 (m, 2H), 1.14 (s, 9H), 1.11 (s, 9H); **$^{13}$C NMR** (101 MHz, $CDCl_3$) δ 150.6, 149.8, 137.3, 132.3, 129.0, 127.8, 125.0, 124.4, 75.1, 63.2, 50.6, 34.5, 34.4, 31.4, 31.3, 26.5, 24.8; **HRMS** ($ESI^+$) calc. for $C_{27}H_{39}N^{35}Cl$ ($[M+H]^+$): 412.2766; found: 412.2764.

**(±)-2-(piperidin-1-yl)-1,2-bis(4-(trifluoromethyl)phenyl)ethan-1-ol**

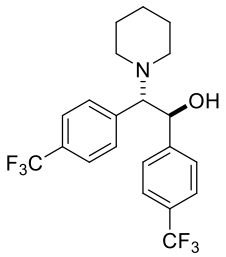

Prepared according to GP2.6 (48 h) with 2,3-bis(3-(trifluoromethyl)phenyl)oxirane[19] (1.00 g, 3.01 mmol, 1.00 equiv) and piperidine (1.44 mL, 15.05 mmol, 5.00 equiv). The crude product was purified by flash silica chromatography (elution gradient 0 to 20% $Et_2O$ in pentane) to afford the title compound as a white solid (0.84 g, 2.02 mmol, 67%).

**mp** 118-119 °C; **$\nu_{max}$** (thin film) /$cm^{-1}$ 2939, 1322, 1161, 1109, 1067, 1018, 873, 836; **$^1$H NMR** (500 MHz, $CDCl_3$) δ 7.55 (d, *J* = 8.0 Hz, 2H), 7.42 (d, *J* = 8.0 Hz, 2H), 7.31 (d, *J* = 8.0 Hz, 2H), 7.21 (d, *J* = 8.0 Hz, 2H), 5.33 (s, 1H), 5.08 (d, *J* = 10.5 Hz, 1H), 3.54 (d, *J* = 10.5 Hz, 1H), 2.62 (br s, 2H), 2.28 (br s, 2H), 1.74 – 1.59 (m, 4H), 1.38 (br s, 2H); **$^{19}$F NMR** (471 MHz, $CDCl_3$) δ -62.56, -62.60;

**$^{13}$C NMR** (126 MHz, $CDCl_3$) δ 145.6, 137.2, 130.3 (q, *J* = 32.5 Hz), 130.2, 129.8 (q, *J* = 32.5 Hz), 127.6, 125.2 (q, *J* = 4.0 Hz), 125.1 (q, *J* = 3.5 Hz), 124.2 (q, *J* = 272.0 Hz), 124.1 (q, *J* = 272.0), 76.9, 70.0, 50.5, 26.6, 24.2; **HRMS** ($ESI^+$) calc. for $C_{21}H_{22}ONF_6$ ($[M+H]^+$): 418.1600; found: 418.1596.

**NB**: In the $^{13}$C spectra, one resonance of the quartet at 124.1 overlaps with the quartet at 125.2.

**(±)-1-(2-chloro-1,2-bis(4-(trifluoromethyl)phenyl)ethyl)piperidine (2.46q)**

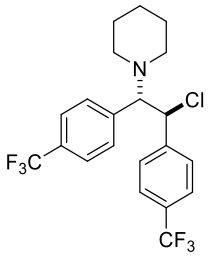


Prepared according to GP2.7 with (±)-2-(piperidin-1-yl)-1,2-bis(4-(trifluoromethyl)phenyl)ethan-1-ol (792 mg, 1.89 mmol, 1.00 equiv). The crude product was purified by flash silica chromatography (elution gradient 0 to 20% $Et_2O$ in pentane) to afford the title compound as a white solid (559 mg, 1.29 mmol, 68%).

**mp** 125-127 °C; **$\nu_{max}$** (thin film) /$cm^{-1}$ 2937, 1323, 1164, 1110, 1068, 1018, 877, 848, 760, 720, 671; **$^1$H NMR** (500 MHz, $CDCl_3$) δ 7.47 – 7.41 (m, 4H), 7.33 (d, *J* = 8.0 Hz, 2H), 7.07 (d, *J* = 8.0 Hz, 2H), 5.43 (d, *J* = 10.0 Hz, 1H), 4.07 (d, *J* = 10.0 Hz, 1H), 2.54 – 2.46 (m, 2H), 2.40 – 2.32 (m, 2H), 1.69 – 1.58 (m, 4H), 1.41 – 1.33 (m, 2H); **$^{19}$F NMR** (471 MHz, $CDCl_3$) δ -62.59, -62.76; **$^{13}$C NMR** (126 MHz, $CDCl_3$) δ 143.4, 138.7, 130.4 (q, *J* = 32.5 Hz), 129.8 (q, *J* = 32.5 Hz), 129.4, 128.6, 125.5 (q, *J* = 4.0 Hz), 124.9 (q, *J* = 3.5 Hz), 124.1 (q, *J* = 272.0 Hz), 123.9 (q, *J* = 272.5 Hz), 75.2, 61.3, 50.1, 26.4, 24.6; **HRMS** ($ESI^+$) calc. for $C_{21}H_{21}N^{35}ClF_6$ ($[M+H]^+$): 436.1261; found: 436.1250.

**NB**: In the $^{13}$C spectra, one resonance of the quartet at 124.1 overlaps with the quartet at 124.9.

**(±)-*N*-(2-chloro-1,2-di(pyridin-2-yl)ethyl)-*N*-propylpropan-1-amine (2.46r)**

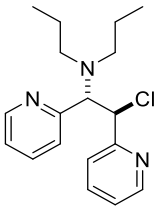


Prepared according to GP2.7 with (±)-2-(dipropylamino)-1,2-di(pyridin-2-yl)ethan-1-ol[25] (550 mg, 1.84 mmol, 1.00 equiv). The crude product was purified by flash silica chromatography (elution gradient 0 to 100% $Et_2O$ in pentane) to afford the title compound as a yellow oil (461 mg, 1.45 mmol, 79%).

**$\nu_{max}$** (thin film) /$cm^{-1}$ 2958, 1589, 1570, 1470, 1434, 746; **$^1$H NMR** (400 MHz, $CDCl_3$) δ 8.49 – 8.23 (m, 2H), 7.49 – 7.37 (m, 2H), 7.23 (dt, *J* = 8.0, 1.0 Hz, 1H), 7.04 – 6.86 (m, 3H), 5.78 (d, *J* = 10.5 Hz, 1H), 4.68 (d, *J* = 10.5 Hz, 1H), 2.85 (ddd, *J* = 13.0, 8.5, 7.0 Hz, 2H), 2.35 (ddd, *J* = 13.0, 8.5, 5.0 Hz, 2H), 1.69 – 1.36 (m, 4H), 0.92 (t, *J* = 7.5 Hz, 6H); **$^{13}$C NMR** (101 MHz, $CDCl_3$) δ 159.1, 158.1, 149.4, 148.4, 136.3, 135.5, 124.6, 123.9, 122.5, 121.7, 69.2, 63.9, 53.0, 22.3, 12.0; **HRMS** ($ESI^+$) calc. for $C_{18}H_{25}N_3{}^{35}Cl$ ($[M+H]^+$): 318.1732; found: 318.1733.

**(±)-*N*-benzyl-2-chloro-*N*-methylcyclohexan-1-amine (2.46s)**

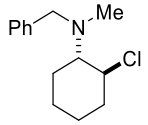


Prepared according to GP2.7 with (±)-2-(benzyl(methyl)amino)cyclohexan-1-ol[26] (500 mg, 2.28 mmol, 1.00 equiv). The crude product was purified by flash silica chromatography (elution gradient 0 to 10% $Et_2O$ in pentane) to afford the title compound as a white solid (273 mg, 1.14 mmol, 50%).

**mp** 37-38 °C; **$\nu_{max}$** (thin film) /$cm^{-1}$ 2936, 1450, 734, 698; **$^1$H NMR** (400 MHz, $CDCl_3$) δ 7.44 – 7.38 (m, 2H), 7.34 – 7.28 (m, 2H), 7.25 – 7.19 (m, 1H), 3.96 (ddd, *J* = 11.0, 10.5, 4.5 Hz, 1H), 3.81 (d, *J* = 13.5 Hz, 1H), 3.59 (d, *J* = 13.5 Hz, 1H), 2.61 (ddd, *J* = 11.5, 10.5, 3.5 Hz, 1H), 2.35 – 2.28 (m, 1H), 2.26 (s, 3H), 2.03 – 1.95 (m, 1H), 1.81 – 1.63 (m, 3H), 1.36 – 1.21 (m, 3H); **$^{13}$C NMR** (101 MHz, $CDCl_3$) δ 140.4, 128.8, 128.3, 126.9, 68.3, 62.3, 58.3, 37.8, 36.8, 26.4×2, 25.2; **HRMS** ($ESI^+$) calc. for $C_{14}H_{21}N^{35}Cl$ ($[M+H]^+$): 238.1357; found: 238.1358.

**1-((1*S*,2*S*)-2-azido-1,2-diphenylethyl)piperidine (2.47a)**

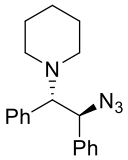


**Standard scale**: Prepared according to GP2.8 from (±)-**2.46a**. The reaction mixture was stirred at -20 °C. The crude product was purified by flash silica chromatography (elution gradient 0 to 10% $Et_2O$ in pentane) to afford the title compound as a white solid (52 mg, 0.17 mmol, 85%, 93:7 e.r.).

**Gram scale**: A 50 mL pear-shaped Schlenk flask was charged sequentially with (±)-**2.46a** (1.50 g, 5.00 mmol, 1.00 equiv), sodium azide (781 mg, 12.00 mmol, 2.40 equiv), and (*S*)-**3.10a** (419 mg, 0.50 mmol, 0.10 equiv) under air. 1,2-difluorobenzene (20 mL, 0.25 M) was added to the Schlenk flask. The suspension was stirred at -20 °C at 900 rpm for 72 h. The reaction mixture was diluted with $Et_2O$ (25 mL) and washed with $H_2O$ (25 mL). **Aqueous washings containing the excess azide were quenched according to the method described *vida supra*.** The organic layer was dried with $MgSO_4$, filtered, and concentrated to afford crude product. The crude product was purified by flash silica chromatography (elution gradient 0 to 10% $Et_2O$ in pentane) to afford the title compound as an off-white solid (1.23 g, 4.01 mmol, 80%, 93.5:6.5 e.r.). Continued elution (20% EtOAc in pentane) enabled recovery of crude catalyst (*S*)-**3.10a**. The crude catalyst was purified by recrystallization, layering pentane over a saturated solution of crude catalyst in $Et_2O$ overnight. The solids were collected and dried to afford recovered (*S*)-**3.10** (304 mg, 0.36 mmol, 73%) as a white solid.

**mp** 44-45 °C; $\boldsymbol{\nu_{max}}$ (thin film) /$cm^{-1}$ 3031, 2933, 2852, 2805, 2094, 698; **$^1$H NMR** (400 MHz, $CDCl_3$) δ 7.21 – 7.06 (m, 8H), 7.00 – 6.93 (m, 2H), 5.01 (d, *J* = 11.0 Hz, 1H), 3.94 (d, *J* = 11.0 Hz, 1H), 2.65 – 2.50 (m, 2H), 2.35 (br s, 2H), 1.72 – 1.60 (m, 4H), 1.34 (quin, *J* = 6.0 Hz, 2H); **$^{13}$C NMR** (101 MHz, $CDCl_3$) δ 138.2, 133.7, 129.5, 128.4, 128.0, 127.9, 127.7, 127.3, 75.1, 65.0, 50.9, 26.2, 24.7; **HRMS** ($ESI^+$) calc. for $C_{19}H_{23}N_4$ ($[M+H]^+$): 307.1917; found: 307.1917; $[\boldsymbol{\alpha}]_{\boldsymbol{D}}^{\mathbf{25}}$ +30.6° (*c* 1.00, $CHCl_3$); **HPLC** DAICEL CHIRALPAK® IB-3, 0.1% $BuNH_2$ and 0.9% IPA in heptane, 1 mL $min^{-1}$, $t_{major}$ = 3.73, $t_{minor}$ = 3.23.

**1-((1*S*,2*S*)-2-azido-1,2-diphenylethyl)-4-methoxypiperidine (3.16b)**

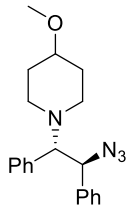

Prepared according to GP2.8 from (±)-**2.46b**. The reaction mixture was stirred at -20 °C. The crude product was purified by flash silica chromatography (elution gradient 0 to 10% $Et_2O$ in pentane) to afford the title compound as a viscous oil (50 mg, 0.15 mmol, 74%, 93:7 e.r.).

**$\nu_{max}$** (thin film) /$cm^{-1}$ 2941, 2821, 2093, 1452, 1087, 946, 751, 698; **$^1$H NMR** (400 MHz, $CDCl_3$) δ 7.21 – 7.05 (m, 8H), 7.01 – 6.92 (m, 2H), 4.98 (d, *J* = 10.5 Hz, 1H), 3.98 (d, *J* = 10.5 Hz, 1H), 3.27 (s, 3H), 3.08 (ddt, *J* = 13.0, 8.5, 4.0 Hz, 1H), 3.02 – 2.91 (m, 1H), 2.77 (dt, *J* = 10.0, 4.5 Hz, 1H), 2.33 (ddd, *J* = 11.5, 10.0, 3.0 Hz, 1H), 2.16 – 2.04 (m, 1H), 2.04 – 1.92 (m, 2H), 1.83 – 1.59 (m, 2H); **$^{13}$C NMR** (101 MHz, $CDCl_3$) δ 138.1, 133.7, 129.4, 128.4, 128.0×2, 127.8, 127.4, 76.7, 74.3, 65.3, 55.5, 49.1, 45.8, 31.4, 30.8; **HRMS** ($ESI^+$) calc. for $C_{20}H_{25}N_4$ ($[M+H]^+$): 337.2023; found: 337.2022; $[\alpha]_D^{25}$ +14.4° (*c* 1.00, $CHCl_3$); **HPLC** DAICEL CHIRALPAK® IB-3, 0.1% $BuNH_2$ and 0.9% IPA in heptane, 1 mL $min^{-1}$, $t_{major}$ = 6.41, $t_{minor}$ = 5.07.

**1-((1*S*,2*S*)-2-azido-1,2-diphenylethyl)-4,4-difluoropiperidine (3.16c)**

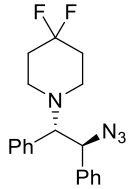

Prepared according to GP2.8 from (±)-**2.46c**. The reaction mixture was stirred at rt. The crude product was purified by flash silica chromatography (elution gradient 0 to 10% $Et_2O$ in pentane) to afford the title compound as a white solid (59 mg, 0.17 mmol, 86%, 84:16 e.r.).

**mp** 82-84 °C; **$\nu_{max}$** (thin film) /$cm^{-1}$ 2093, 1363, 1160, 1082, 938, 699; **$^1$H NMR** (400 MHz, $CDCl_3$) δ 7.24 – 7.09 (m, 8H), 7.03 – 6.95 (m, 2H), 4.98 (d, *J* = 10.5 Hz, 1H), 4.05 (d, *J* = 10.5 Hz, 1H), 2.82 – 2.71 (m, 2H), 2.59 – 2.49 (m, 2H), 2.19 – 2.00 (m, 4H); **$^{19}$F NMR** (377 MHz, $CDCl_3$) δ -97.43 (br s); **$^{13}$C NMR** (101 MHz, $CDCl_3$) δ 137.7, 133.4, 129.1, 128.5, 128.2, 128.1, 127.9, 127.8, 122.0 (t, *J* = 241.5 Hz), 73.9, 65.4, 46.5, 34.3 (t, *J* = 22.5 Hz); **HRMS** ($ESI^+$) calc. for $C_{19}H_{21}N_4F_2$

([M+H]$^+$): 343.1729; found: 343.1730; $[\alpha]_D^{25}$ +10.9° (*c* 1.00, $CHCl_3$); **HPLC** DAICEL CHIRALPAK® IB-3, 1% IPA in heptane, 1 mL min$^{-1}$, $t_{major}$ = 7.13, $t_{minor}$ = 5.34.

**1-((1*S*,2*S*)-2-azido-1,2-diphenylethyl)pyrrolidine (2.47d)**

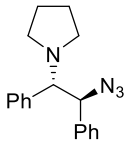


Prepared according to GP2.8 from (±)-**2.46d**. The reaction mixture was stirred at -20 °C. The crude product was purified by flash silica chromatography (elution gradient 0 to 10% $Et_2O$ in pentane) to afford the title compound as a viscous oil (52 mg, 0.18 mmol, 89%, 94:6 e.r.).

**$\nu_{max}$** (thin film) /cm$^{-1}$ 2968, 2803, 2094, 1453, 1252, 757, 698; **$^1$H NMR** (400 MHz, $CDCl_3$) δ 7.21 – 7.11 (m, 6H), 7.11 – 7.07 (m, 2H), 7.02 – 6.97 (m, 2H), 5.03 (d, *J* = 8.5 Hz, 1H), 3.94 (d, *J* = 8.5 Hz, 1H), 2.68 – 2.55 (m, 4H), 1.80 – 1.70 (m, 4H); **$^{13}$C NMR** (101 MHz, $CDCl_3$) δ 137.6, 136.0, 129.6, 128.2, 128.1, 127.9, 127.7, 127.3, 72.0, 67.9, 50.5, 23.1; **HRMS** (ESI$^+$) calc. for $C_{18}H_{21}N_4$ ([M+H]$^+$): 293.1716; found: 293.1757; $[\alpha]_D^{25}$ +73.6° (*c* 1.00, $CHCl_3$); **HPLC** DAICEL CHIRALPAK® IA-3, 0.1% $BuNH_2$ and 0.15% IPA in heptane, 1 mL min$^{-1}$, $t_{major}$ = 4.77, $t_{minor}$ = 6.12.

**4-((1*S*,2*S*)-2-azido-1,2-diphenylethyl)morpholine (2.47e)**

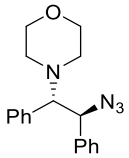


Prepared according to GP2.8 from (±)-**2.46e**. The reaction mixture was stirred at 0 °C. The crude product was purified by flash silica chromatography (elution gradient 0 to 20% $Et_2O$ in pentane) to afford the title compound as a white solid (45 mg, 0.15 mmol, 73%, 91:9 e.r.).

**mp** 96-98 °C; **$\nu_{max}$** (thin film) /cm$^{-1}$ 2861, 2090, 1494, 1452, 1251, 1113, 1002, 881, 759, 699; **$^1$H NMR** (400 MHz, $CDCl_3$) δ 7.22 – 7.10 (m, 8H), 7.01 – 6.97 (m, 2H), 5.01 (d, *J* = 10.5 Hz, 1H), 3.95 (d, *J* = 10.5 Hz, 1H), 3.85 – 3.71 (m, 4H), 2.70 – 2.60 (m, 2H), 2.52 – 2.44 (m, 2H); **$^{13}$C NMR** (101 MHz, $CDCl_3$) δ 137.7, 133.4, 129.4, 128.4, 128.1, 127.9×2, 127.7, 74.6, 67.1, 64.9, 50.1; **HRMS** (ESI$^+$) calc. for $C_{18}H_{21}ON_4$ ([M+H]$^+$): 309.1710; found: 309.1710; $[\alpha]_D^{25}$ +28.9° (*c* 1.00,

$CHCl_3$); **HPLC** DAICEL CHIRALPAK® IB-3, 0.1% $BuNH_2$ and 0.9% IPA in heptane, 1 mL $min^{-1}$, $t_{major}$ = 12.13, $t_{minor}$ = 8.67.

**1-((1*S*,2*S*)-2-azido-1,2-diphenylethyl)-4-cyclohexylpiperazine (2.47f)**

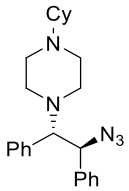


Prepared according to GP2.8 from (±)-**2.46f**. The reaction mixture was stirred at rt. The crude product was purified by flash silica chromatography (elution gradient 0 to 20% EtOAc in $CH_2Cl_2$) to afford the title compound as a white solid (57 mg, 0.15 mmol, 73%, 57:43 e.r.).

**mp** 78-80 °C; **$\nu_{max}$** (thin film) /$cm^{-1}$ 2928, 2094, 1452, 755, 731, 698; **$^1$H NMR** (500 MHz, $CDCl_3$) δ 7.18 – 7.05 (m, 8H), 7.01 – 6.92 (m, 2H), 5.01 (d, *J* = 10.5 Hz, 1H), 3.95 (d, *J* = 10.5 Hz, 1H), 2.68 (s, 6H), 2.48 (s, 2H), 2.26 – 2.07 (m, 1H), 1.90 – 1.80 (m, 2H), 1.80 – 1.70 (m, 2H), 1.66 – 1.53 (m, 1H), 1.29 – 1.01 (m, 5H); **$^{13}$C NMR** (126 MHz, $CDCl_3$) δ 138.0, 133.4, 129.5, 128.4, 128.0, 128.0, 127.9, 127.4, 74.2, 65.0, 63.6, 49.6, 49.2, 29.2, 29.1, 26.4, 26.0×2; **HRMS** ($ESI^+$) calc. for $C_{24}H_{32}N_5$ ($[M+H]^+$): 390.2652; found: 390.2645; $[\alpha]_D^{25}$ +6.1° (*c* 1.00, $CHCl_3$); **HPLC** DAICEL CHIRALPAK® IB-3, 0.1% $BuNH_2$ and 0.9% IPA in heptane, 1 mL $min^{-1}$, $t_{major}$ = 4.58, $t_{minor}$ = 3.89.

**1-((1*S*,2*S*)-2-azido-1,2-diphenylethyl)-4-phenylpiperazine (2.47g)**

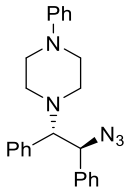


Prepared according to GP2.8 from (±)-**2.46g**. The reaction mixture was stirred at rt. The crude product was purified by flash silica chromatography (elution gradient 0 to 20% $Et_2O$ in pentane) to afford the title compound as a white solid (67 mg, 0.17 mmol, 87%, 87:13 e.r.).

**mp** 103-105 °C; **$\nu_{max}$** (thin film) /$cm^{-1}$ 2827, 2095, 1599, 1234, 755, 695; **$^1$H NMR** (400 MHz, $CDCl_3$) δ 7.18 – 7.11 (m, 2H), 7.11 – 7.00 (m, 8H), 6.94 – 6.89 (m, 2H), 6.83 – 6.78 (m, 2H), 6.78 – 6.72 (m, 1H), 4.95 (d, *J* = 10.5 Hz, 1H), 3.95 (d, *J* = 10.5 Hz, 1H), 3.25 – 3.11 (m, 4H), 2.76 –

2.68 (m, 2H), 2.57 – 2.49 (m, 2H); **$^{13}$C NMR** (101 MHz, $CDCl_3$) δ 151.5, 137.8, 133.4, 129.4, 129.1, 128.5, 128.1, 128.0, 127.9, 127.6, 119.8, 116.3, 74.3, 65.1, 49.6, 49.5; **HRMS** ($ESI^+$) calc. for $C_{26}H_{26}N_5$ ($[M+H]^+$): 384.2194; found: 384.2184; $[\alpha]_D^{25}$ +15.6° (*c* 1.00, $CHCl_3$); **HPLC** DAICEL CHIRALPAK® IB-3, 1% IPA in heptane, 1 mL min$^{-1}$, $t_{major}$ = 11.71, $t_{minor}$ =8.38.

**2-((1*S*,2*S*)-2-azido-1,2-diphenylethyl)-1,2,3,4-tetrahydroisoquinoline (2.47h)**

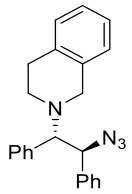


Prepared according to GP2.8 from (±)-**2.46h**. The reaction mixture was stirred at -10 °C. The crude product was purified by flash silica chromatography (elution gradient 0 to 10% $Et_2O$ in pentane) to afford the title compound as a viscous oil (66 mg, 0.19 mmol, 93%, 93:7 e.r.).

**$\nu_{max}$** (thin film) /cm$^{-1}$ 2360, 2095, 1495, 1454, 1251, 1095, 741, 697; **$^1$H NMR** (400 MHz, $CDCl_3$) δ 7.26 – 7.09 (m, 13H), 7.08 – 7.01 (m, *J* = 3.0 Hz, 1H), 5.16 (d, *J* = 10.5 Hz, 1H), 4.19 (d, *J* = 10.5 Hz, 1H), 3.85 – 3.73 (m, 2H), 3.21 – 3.05 (m, 2H), 3.03 – 2.90 (m, 1H), 2.68 – 2.59 (m, 1H); **$^{13}$C NMR** (101 MHz, $CDCl_3$) δ 137.9, 135.1, 134.5, 133.8, 129.5, 128.8, 128.5, 128.1, 128.0, 128.0, 127.6, 126.6×2, 125.6, 73.6, 65.6, 52.8, 46.6, 29.6; **HRMS** ($ESI^+$) calc. for $C_{23}H_{23}N_4$ ($[M+H]^+$): 355.1917; found: 355.1911; $[\alpha]_D^{25}$ +31.3° (*c* 1.00, $CHCl_3$); **HPLC** DAICEL CHIRALPAK® IB-3, 1% IPA in heptane, 1 mL min$^{-1}$, $t_{major}$ = 7.04, $t_{minor}$ = 5.44.

**(1*S*,2*S*)-2-azido-*N*-benzyl-*N*-methyl-1,2-diphenylethan-1-amine (2.47i)**

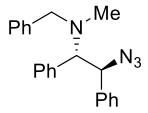


Prepared according to GP2.8 from (±)-**2.46i**. The reaction mixture was stirred at 0 °C. The crude product was purified by flash silica chromatography (elution gradient 0 to 10% $Et_2O$ in pentane) to afford the title compound as a white solid (59 mg, 0.17 mmol, 86%, 91:9 e.r.).

**mp** 131-132 °C; **$\nu_{max}$** (thin film) /cm$^{-1}$ 2962, 2095, 1492, 1451, 1225, 1014, 701; **$^1$H NMR** (500 MHz, $CDCl_3$) δ 7.53 – 7.48 (m, 2H), 7.44 – 7.39 (m, 2H), 7.36 – 7.30 (m, 1H), 7.28 – 7.23 (m, 2H), 7.23 – 7.13 (m, 6H), 7.08 – 7.04 (m, 2H), 5.09 (d, *J* = 11.0 Hz, 1H), 4.17 (d, *J* = 11.0 Hz, 1H),

3.75 (d, *J* = 13.0 Hz, 1H), 3.47 (d, *J* = 13.0 Hz, 1H), 2.30 (s, 3H); **$^{13}$C NMR** (126 MHz, $CDCl_3$) δ 139.2, 137.9, 133.7, 129.5, 129.0, 128.5×2, 128.1, 128.0, 127.9, 127.5, 127.2, 71.4, 65.7, 58.9, 37.4; **HRMS** ($ESI^+$) calc. for $C_{22}H_{23}N_4$ ($[M+H]^+$): 343.1917; found: 343.1914; $[\boldsymbol{\alpha}]_{\boldsymbol{D}}^{\mathbf{25}}$ +43.1° (*c* 1.00, $CHCl_3$); **HPLC** DAICEL CHIRALPAK® IB-3, 1% IPA in heptane, 1 mL $min^{-1}$, $t_{major}$ = 5.06, $t_{minor}$ = 4.23.

**(1*S*,2*S*)-2-azido-*N*,*N*-dimethyl-1,2-diphenylethan-1-amine (2.47j)**

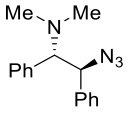


Prepared according to GP2.8 from (±)-**2.46j**. The reaction mixture was stirred at -10 °C. The crude product was purified by flash silica chromatography (elution gradient 0 to 20% EtOAc in $CH_2Cl_2$) to afford the title compound as a viscous oil (45 mg, 0.17 mmol, 84%, 92:8 e.r.).

**$\nu_{max}$** (thin film) /$cm^{-1}$ 2936, 2785, 2096, 1453, 1256, 752, 698; **$^1$H NMR** (500 MHz, $CDCl_3$) δ 7.22 – 7.06 (m, 8H), 7.02 – 6.92 (m, 2H), 4.99 (d, *J* = 11.0 Hz, 1H), 3.90 (d, *J* = 11.0 Hz, 1H), 2.29 (s, 6H); **$^{13}$C NMR** (126 MHz, $CDCl_3$) δ 137.6, 133.1, 129.6, 128.5, 128.2, 128.1, 127.8, 127.5, 73.1, 65.9, 41.2; **HRMS** ($ESI^+$) calc. for $C_{16}H_{19}N_4$ ($[M+H]^+$): 267.1604; found 267.1604; $[\boldsymbol{\alpha}]_{\boldsymbol{D}}^{\mathbf{25}}$ +61.4° (*c* 1.00, $CHCl_3$); **HPLC** DAICEL CHIRALPAK® IB-3, 0.1% $BuNH_2$ and 0.9% IPA in heptane, 1 mL $min^{-1}$, $t_{major}$ = 4.92, $t_{minor}$ = 3.83.

**1-((1*S*,2*S*)-2-azido-1,2-diphenylethyl)azepane (2.47k)**

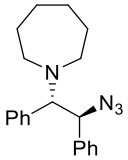


Prepared according to GP2.8 from (±)-**2.46k**. The reaction mixture was stirred at -20 °C. The crude product was purified by flash silica chromatography (elution gradient 0 to 10% $Et_2O$ in pentane) to afford the title compound as a viscous oil (49 mg, 0.15 mmol, 76%, 94:6 e.r.).

**$\nu_{max}$** (thin film) /$cm^{-1}$ 2925, 2361, 2093, 1452, 1249, 758, 696; **$^1$H NMR** (400 MHz, $CDCl_3$) δ 7.19 – 7.09 (m, 8H), 7.06 – 7.01 (m, 2H), 4.87 (d, *J* = 11.0 Hz, 1H), 4.07 (d, *J* = 11.0 Hz, 1H), 2.86 (ddd, *J* = 11.5, 6.0, 4.5 Hz, 2H), 2.64 (ddd, *J* = 12.0, 7.5, 4.0 Hz, 2H), 1.77 – 1.64 (m, 4H), 1.62 – 1.54 (m, 4H); **$^{13}$C NMR** (101 MHz, $CDCl_3$) δ 138.5, 136.2, 129.1, 128.5, 128.0, 127.9, 127.8, 127.1,

74.2, 66.4, 52.2, 29.3, 27.0; **HRMS** (ESI$^+$) calc. for $C_{20}H_{25}N_4$ ([M+H]$^+$): 321.2074; found: 321.2070; $[\alpha]_D^{25}$ -9.1° (*c* 1.00, $CHCl_3$); **HPLC** DAICEL CHIRALPAK® IB-3, 0.1% $BuNH_2$ and 0.9% IPA in heptane, 1 mL min$^{-1}$, $t_{major}$ = 3.46, $t_{minor}$ = 3.03.

**1-((1*S*,2*S*)-2-azido-1,2-bis(3-fluorophenyl)ethyl)piperidine (2.47l)**

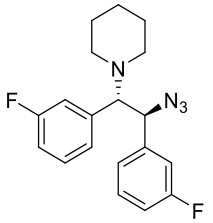


Prepared according to GP2.8 from (±)-**2.46l**. The reaction mixture was stirred at -10 °C. The crude product was purified by flash silica chromatography (elution gradient 0 to 10% $Et_2O$ in pentane) to afford the title compound as a white solid (56 mg, 0.16 mmol, 82%, 89:11 e.r.).

**mp** 67-68 °C; **$\nu_{max}$** (thin film) /cm$^{-1}$ 2936, 2100, 1615, 1591, 1489, 1449, 1249, 1142, 777, 695; **$^1$H NMR** (500 MHz, $CDCl_3$) δ 7.19 – 7.09 (m, 2H), 6.93 – 6.80 (m, 4H), 6.78 – 6.73 (m, 1H), 6.69 (dt, *J* = 10.0, 2.0 Hz, 1H), 4.95 (d, *J* = 10.5 Hz, 1H), 3.88 (d, *J* = 10.5 Hz, 1H), 2.70 – 2.53 (m, 2H), 2.53 – 2.29 (m, 2H), 1.71 – 1.48 (m, 4H), 1.36 (quin, *J* = 6.0 Hz, 2H); **$^{19}$F NMR** (471 MHz, $CDCl_3$) δ -112.46, -112.47; **$^{13}$C NMR** (126 MHz, $CDCl_3$) δ 162.7 (d, *J* = 246.5 Hz), 162.4 (d, *J* = 246.0 Hz), 142.2 (d, *J* = 7.5 Hz), 137.5 (d, *J* = 6.0 Hz)., 130.0 (d, *J* = 8.5 Hz), 129.3 (d, *J* = 8.0 Hz), 125.1 (d, *J* = 3.0 Hz), 123.8 (d, *J* = 3.0 Hz), 116.1 (d, *J* = 21.0 Hz), 115.1 (d, *J* = 21.0 Hz), 114.9 (d, *J* = 22.0 Hz), 114.5 (d, *J* = 21.0 Hz), 74.9 (d, *J* = 1.5 Hz), 64.2 (d, *J* = 2.0 Hz), 51.0, 26.1, 24.6; **HRMS** (ESI$^+$) calc. for $C_{19}H_{21}N_4F_2$ ([M+H]$^+$): 343.1729; found: 343.1729; $[\alpha]_D^{25}$ +12.5° (*c* 1.00, $CHCl_3$, 89:11 e.r.); **HPLC** DAICEL CHIRALPAK® IB-3, 1% IPA in heptane, 1 mL min$^{-1}$, $t_{major}$ = 4.55, $t_{minor}$ = 3.72.

**NB**: Recrystallisation of **3l** (45 mg, 0.13 mmol) from hot hexanes afforded **3l** (14 mg, 0.04 mmol, 30%, 98:2 e.r.).

**1-((1*S*,2*S*)-2-azido-1,2-bis(3-chlorophenyl)ethyl)piperidine (2.47m)**

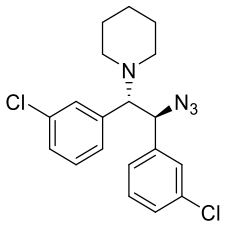


Prepared according to GP2.8 from (±)-**2.46m**. The reaction mixture was stirred at 0 °C. The crude product was purified by flash silica chromatography (elution gradient 0 to 10% $Et_2O$ in pentane) to afford the title compound as a viscous oil (67 mg, 0.18 mmol, 89%, 90:10 e.r.). **$\nu_{max}$** (thin film) /$cm^{-1}$ 2962, 2095, 1270, 785, 714, 693; **$^1$H NMR** (400 MHz, $CDCl_3$) δ 7.18 – 7.06 (m, 5H), 7.02 – 6.95 (m, 2H), 6.88 – 6.83 (m, 1H), 4.93 (d, *J* = 10.5 Hz, 1H), 3.84 (d, *J* = 10.5 Hz, 1H), 2.58 (dt, *J* = 11.0, 5.0 Hz, 2H), 2.33 (dt, *J* = 9.5, 5.0 Hz, 2H), 1.71 – 1.62 (m, 4H), 1.36 (quin, *J* = 6.0 Hz, 2H); **$^{13}$C NMR** (101 MHz, $CDCl_3$) δ 139.9, 135.6, 134.4, 133.9, 129.7, 129.3, 129.1, 128.3, 128.1, 127.7, 127.5, 126.2, 74.9, 64.2, 51.0, 26.0, 24.6; **HRMS** ($ESI^+$) calc. for $C_{19}H_{21}N_4{}^{35}Cl_2$ ($[M+H]^+$): 375.1138; found: 375.1142; $[\boldsymbol{\alpha}]_{\boldsymbol{D}}^{\mathbf{25}}$ -5.3° (*c* 1.00, $CHCl_3$); **HPLC** DAICEL CHIRALPAK® IA-3, 1% IPA in heptane, 1 mL $min^{-1}$, $t_{major}$ = 6.96, $t_{minor}$ = 5.49.

**1-((1*S*,2*S*)-2-azido-1,2-bis(3-(trifluoromethyl)phenyl)ethyl)piperidine (2.47n)**

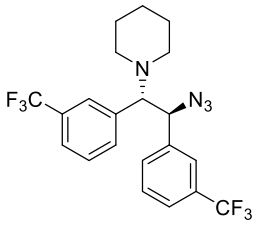

Prepared according to GP2.8 from (±)-**2.46n**. The reaction mixture was stirred at 0 °C. The crude product was purified by flash silica chromatography (elution gradient 0 to 10% $Et_2O$ in pentane) to afford the title compound as a white solid (76 mg, 0.17 mmol, 86%, 85:15 e.r.).

**mp** 43-44 °C; **$\nu_{max}$** (thin film) /$cm^{-1}$ 2938, 2100, 1326, 1162, 1120, 1074, 702; **$^1$H NMR** (400 MHz, $CDCl_3$) δ 7.40 – 7.22 (m, 6H), 7.20 – 7.15 (m, 1H), 7.12 – 7.07 (m, 1H), 5.07 (d, *J* = 10.0 Hz, 1H), 3.90 (d, *J* = 10.0 Hz, 1H), 2.69 – 2.48 (m, 2H), 2.48 – 2.21 (m, 2H), 1.70 – 1.61 (m, 4H), 1.41 – 1.28 (m, 2H); **$^{19}$F NMR** (377 MHz, $CDCl_3$) δ -62.85, -62.99; **$^{13}$C NMR** (101 MHz, $CDCl_3$) δ 138.8, 134.7, 132.8, 131.3, 130.9 (q, *J* = 32.5 Hz), 130.3 (q, *J* = 32.5 Hz), 129.0, 128.5, 125.8 (q, *J* = 4.0 Hz), 125.0 (q, *J* = 4.0 Hz), 124.9 (q, *J* = 4.0 Hz), 124.4 (q, *J* = 3.7 Hz), 124.1 (q, *J* = 272.5 Hz), 123.9 (q, *J* = 272.5 Hz), 75.6, 64.3, 51.2, 26.0, 24.5; **HRMS** ($ESI^+$) calc. for $C_{21}H_{21}N_4F_6$ ($[M+H]^+$): 442.4765; found: 442.4753; $[\alpha]_D^{25}$ +13.9° (*c* 1.00, $CHCl_3$); **HPLC** DAICEL CHIRALPAK® IB-3, 0.5% IPA in heptane, 1 mL $min^{-1}$, $t_{major}$ = 4.95, $t_{minor}$ = 3.79.

**1-((1*S*,2*S*)-2-azido-1,2-bis(4-bromophenyl)ethyl)piperidine (2.47o)**

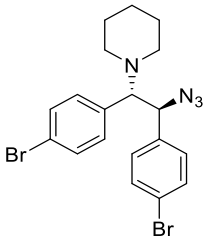

**Standard scale**: Prepared according to GP2.8 from (±)-**2.46o**. The reaction mixture was stirred at 0 °C. The crude product was purified by flash silica chromatography (elution gradient 0 to 10% $Et_2O$ in pentane) to afford the title compound as a white solid (73 mg, 0.16 mmol, 79%, 93:7 e.r.).

**Half-gram scale**: A Schlenk flask was charged sequentially with (±)-**2.46o** (0.50 g, 1.09 mmol, 1.00 equiv), sodium azide (170 mg, 2.62 mmol, 2.40 equiv), and (*S*)-**3.10** (91 mg, 0.11 mmol,

0.10 equiv) under air. 1,2-difluorobenzene (4.36 mL, 0.25 M) was added to the Schlenk flask. The suspension was stirred at 0 °C at 900 rpm for 72 h. The reaction mixture was diluted with $Et_2O$ (10 mL) and washed with $H_2O$ (10 mL). **Aqueous washings containing the excess azide were quenched according to the method described *vida supra*.** The organic layer was dried with $MgSO_4$, filtered, and concentrated to afford crude product. The crude product was purified by flash silica chromatography (elution gradient 0 to 10% $Et_2O$ in pentane) to afford an off-white solid (459 mg, 0.99 mmol, 91%, 93:7 e.r.). A sample of this (144 mg, 0.31 mmol, 1.00 equiv) was recrystallized from hot hexane to afford the title compound as an off-white crystalline solid, suitable for X-ray crystallography (110 mg, 0.24 mmol, 76%, 98.5:1.5 e.r.).

**mp** 120-122 °C; **$\nu_{max}$** (thin film) /$cm^{-1}$ 2934, 2098, 1488, 1097, 1010, 908, 815, 728; **$^1$H NMR** (400 MHz, $CDCl_3$) δ 7.34 – 7.27 (m, 4H), 7.01 – 6.96 (m, 2H), 6.85 – 6.79 (m, 2H), 4.92 (d, *J* = 10.5 Hz, 1H), 3.83 (d, *J* = 10.5 Hz, 1H), 2.59 – 2.42 (m, 2H), 2.42 – 2.13 (m, 2H), 1.71 – 1.57 (m, 4H), 1.49 – 1.24 (m, 2H); **$^{13}$C NMR** (101 MHz, $CDCl_3$) δ 137.0, 132.5, 131.7, 131.1, 130.9, 129.6, 122.1, 121.5, 74.6, 64.1, 50.9, 26.0, 24.6; **HRMS** ($ESI^+$) calc. for $C_{19}H_{21}N_4{}^{79}Br_2$ ($[M+H]^+$): 463.0128; found: 463.0125; $[\alpha]_D^{25}$ -2.6° (*c* 1.00, $CHCl_3$, 95.5:1.5 e.r.); **HPLC** DAICEL CHIRALPAK® OJ-3, 1% EtOH in heptane, 1 mL $min^{-1}$, $t_{major}$ = 14.00, $t_{minor}$ = 9.03.

**1-((1*S*,2*S*)-2-azido-1,2-bis(4-(*tert*-butyl)phenyl)ethyl)piperidine (2.47p)**

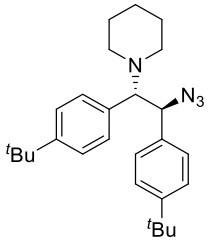


Prepared according to GP2.8 from (±)-**2.46p**. The reaction mixture was stirred at -20 °C. The crude product was purified by flash silica chromatography (elution gradient 0 to 10% $Et_2O$ in pentane) to afford the title compound as a white solid (74 mg, 0.18 mmol, 88%, 96:4 e.r.).

**mp** 62-63 °C; **$\nu_{max}$** (thin film) /$cm^{-1}$ 2935, 2097, 1270, 1110, 909, 823, 733; **$^1$H NMR** (400 MHz, $CDCl_3$) δ 7.20 – 7.10 (m, 4H), 7.09 – 7.03 (m, 2H), 6.95 – 6.87 (m, 2H), 4.96 (d, *J* = 10.5 Hz, 1H),

3.92 (d, *J* = 10.5 Hz, 1H), 2.75 – 2.54 (m, 2H), 2.54 – 2.25 (m, 2H), 1.74 – 1.57 (m, 4H), 1.43 – 1.33 (m, 2H), 1.24 (s, 9H), 1.21 (s, 9H); **$^{13}$C NMR** (101 MHz, $CDCl_3$) δ 150.5, 149.8, 135.3, 131.1, 129.2, 127.6, 125.2, 124.4, 74.4, 65.1, 51.0, 34.5, 34.4, 31.4, 31.3, 26.3, 24.7; **HRMS** ($ESI^+$) calc. for $C_{27}H_{39}N_4$ ($[M+H]^+$): 419.3169; found: 419.3174; $[\alpha]_D^{25}$ +11.2° (*c* 1.00, $CHCl_3$); **HPLC** DAICEL CHIRALPAK® IA-3 0.5% IPA in heptane, 1 mL min$^{-1}$, $t_{major}$ = 6.96, $t_{minor}$ = 5.49.

**1-((1*S*,2*S*)-2-azido-1,2-bis(4-(trifluoromethyl)phenyl)ethyl)piperidine (2.47q)**

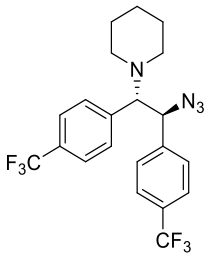


Prepared according to GP2.8 from (±)-**2.46q**. The reaction mixture was stirred at 0 °C. The crude product was purified by flash silica chromatography (elution gradient 0 to 10% $Et_2O$ in pentane) to afford the title compound as a white solid (76 mg, 0.17 mmol, 86%, 88:12 e.r.).

**mp** 60-62 °C; **$\nu_{max}$** (thin film) /cm$^{-1}$ 2938, 2102, 1322, 1163, 1109, 1067, 829; **$^1$H NMR** (400 MHz, $CDCl_3$) δ 7.46 – 7.37 (m, 4H), 7.25 – 7.19 (m, 2H), 7.10 – 7.03 (m, 2H), 5.04 (d, *J* = 10.5 Hz, 1H), 3.94 (d, *J* = 10.5 Hz, 1H), 2.61 – 2.50 (m, 2H), 2.37 – 2.26 (m, 2H), 1.70 – 1.60 (m, 4H), 1.38 – 1.28 (m, 2H); **$^{19}$F NMR** (377 MHz, $CDCl_3$) δ -62.62, -62.78; **$^{13}$C NMR** (101 MHz, $CDCl_3$) δ 141.7, 137.4, 130.4 (q, *J* = 32.5 Hz), 129.8 (q, *J* = 32.5 Hz), 129.5, 128.4, 125.6 (q, *J* = 4.0 Hz), 124.9 (q, *J* = 4.0 Hz), 124.1 (q, *J* = 272.0 Hz), 123.9 (q, *J* = 272.5 Hz), 75.0, 64.2, 51.1, 26.0, 24.5; **HRMS** ($ESI^+$) calc. for $C_{21}H_{21}N_4F_6$ ($[M+H]^+$): 442.4765; found: 442.4750; $[\alpha]_D^{25}$ +11.3° (*c* 1.00, $CHCl_3$); **HPLC** DAICEL CHIRALPAK® OJ-3, 1% EtOH in heptane, 1 mL min$^{-1}$, $t_{major}$ = 16.23, $t_{minor}$ = 6.52.

***N*-((1*R*,2*R*)-2-azido-1,2-di(pyridin-2-yl)ethyl)-*N*-propylpropan-1-amine (2.47r)**

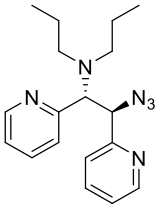

$NaN_3$ (31.2 mg, 0.48 mmol, 2.40 equiv) was added to a solution of (±)-**2.46r** (64 mg, 0.2 mmol, 1.00 equiv) and (*S*)-**3.10** (16.7 mg, 0.02 mmol, 0.1.00 equiv) in 1,2-difluorobenzene (0.8 mL, 0.25 M) in a 2 mL Schlenk tube (5 mm internal diameter) under air. The suspension was stirred at -20 °C at 1200 rpm for 72 h. The reaction mixture was diluted with $Et_2O$ (2 mL) and washed with $H_2O$ (2 mL). **Aqueous washings containing the excess azide were quenched according to the method described *vida supra*.** The organic layer was were dried with $MgSO_4$, filtered, and concentrated to afford crude product. The crude product was purified by flash silica chromatography (elution gradient 0 to 20% EtOAc in $CH_2Cl_2$) to afford the title compound as a clear oil (55 mg, 0.17 mmol, 85%, 84:16 e.r.).

**$\nu_{max}$** (thin film) /$cm^{-1}$ 2959, 2095, 1589, 1570, 1470, 1434, 996, 782, 747; **$^1$H NMR** (400 MHz, $CDCl_3$) δ 8.47 – 8.35 (m, 2H), 7.43 – 7.34 (m, 2H), 7.08 (dt, *J* = 8.0, 1.0 Hz, 1H), 7.00 – 6.90 (m, 3H), 5.21 (d, *J* = 10.5 Hz, 1H), 4.58 (d, *J* = 10.5 Hz, 1H), 2.81 (ddd, *J* = 13.0, 9.5, 6.5 Hz, 2H), 2.36 – 2.25 (m, 2H), 1.64 – 1.42 (m, 4H), 0.89 (t, *J* = 7.5 Hz, 6H); **$^{13}$C NMR** (101 MHz, $CDCl_3$) δ 158.1, 157.0, 149.4, 148.5, 136.1, 135.5, 124.7, 123.9, 122.5, 121.8, 68.1, 65.6, 53.0, 21.9, 11.9; **HRMS** (ESI$^+$) calc. for $C_{18}H_{25}N_6$ ([M+H]$^+$): 325.2135; found: 325.2139; $[\alpha]_D^{25}$ +37.2° (*c* 1.00, $CHCl_3$); **HPLC** DAICEL CHIRALPAK® IC-3, 0.1% $BuNH_2$ and 0.9% IPA in heptane, 1 mL $min^{-1}$, $t_{major}$ = 6.48, $t_{minor}$ = 5.52.

**2-azido-*N*-benzyl-*N*-methylcyclohexan-1-amine (2.47s)**

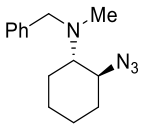

Prepared according to GP2.8 from (±)-**2.46s**. The reaction mixture was stirred at rt. The crude product was purified by flash silica chromatography (elution gradient 0 to 10% $Et_2O$ in pentane) to afford the title compound as a clear oil (46 mg, 0.19 mmol, 94%, 52:48 e.r.).

**$\nu_{max}$** (thin film) /$cm^{-1}$ 2933, 2089, 1451, 1460, 737, 698; **$^{1}$H NMR** (400 MHz, $CDCl_3$) δ 7.40 – 7.35 (m, 2H), 7.32 – 7.26 (m, 2H), 7.24 – 7.18 (m, 1H), 3.71 (d, *J* = 13.5 Hz, 1H), 3.60 (d, *J* = 13.5 Hz, 1H), 3.29 (td, *J* = 10.5, 4.5 Hz, 1H), 2.50 (ddd, *J* = 11.5, 10.5, 3.5 Hz, 1H), 2.20 (s, 3H), 2.08 – 1.98 (m, 1H), 1.96 – 1.86 (m, 1H), 1.79 – 1.65 (m, 2H), 1.33 – 1.11 (m, 4H); **$^{13}$C NMR** (101 MHz, $CDCl_3$) δ 139.9, 128.8, 128.3, 127.0, 66.3, 61.5, 59.0, 36.2, 32.4, 25.1, 25.0, 24.2; **HRMS** ($ESI^+$) calc. for $C_{14}H_{21}N_4$ ($[M+H]^+$): 245.1761; found: 245.1761; **HPLC** DAICEL CHIRALPAK® IF-3 0.1% IPA in heptane, 1 mL $min^{-1}$, $t_{major}$ = 7.57, $t_{minor}$ = 6.51.

**NB**: Absolute configuration of major enantiomer not determined.[17]

**(1*S*,2*S*)-1,2-diphenyl-2-(piperidin-1-yl)ethan-1-amine**

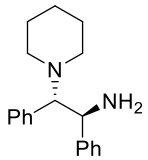


Pd/C (10 wt. %, 224 mg, 0.21 mmol, 0.05 equiv) was added to a suspension of (*S*,*S*)-**2.47a** (1.29 g, 4.21 mmol, 1.00 equiv, 93.5:6.5 e.r.) in MeOH (16.8 mL) at rt under $N_2$. The reaction mixture was purged with $H_2$ (balloon), then stirred at rt for 2 h under $H_2$ (1 atm). The reaction mixture was filtered through celite and concentrated to afford crude product. The crude product was purified by flash silica chromatography (elution gradient 20 to 60% EtOAc in pentane) to afford the title compound as a white solid (0.94 g, 3.35 mmol, 80%, 93.5:6.5 e.r.).

**mp** 76-78 °C; **$\nu_{max}$** (neat) /cm$^{-1}$ 2933, 1490, 1451, 1303, 696; **$^1$H NMR** (400 MHz, $CDCl_3$) δ 7.25 – 7.20 (m, 2H), 7.19 – 7.07 (m, 5H), 7.07 – 6.96 (m, 3H), 4.49 (d, *J* = 10.5 Hz, 1H), 3.62 (d, *J* = 10.5 Hz, 1H), 2.55 (br s, 2H), 2.28 (br s, 2H), 1.95 (br s, 2H), 1.74 – 1.61 (m, 2H), 1.61 – 1.47 (m, 2H), 1.39 – 1.26 (m, 2H); **$^{13}$C NMR** (101 MHz, $CDCl_3$) δ 143.5, 135.0, 129.7, 128.2, 128.1, 127.4, 126.9, 126.8, 76.6, 55.1, 50.6, 26.9, 24.8; **HRMS** (ESI$^+$) calc. for $C_{19}H_{25}N_2$ ([M+H]$^+$): 281.2012; found: 281.2012; $[\alpha]_D^{25}$ -22.0° (*c* 0.5, EtOH); **HPLC** DAICEL CHIRALPAK® IA-3, 0.1% $BuNH_2$ and 4.9% IPA in heptane, 1 mL min$^{-1}$, $t_{major}$ = 6.43, $t_{minor}$ = 5.40.

**NB**: Synthesis of (1*R*,2*R*)-1,2-diphenyl-2-(piperidin-1-yl)ethan-1-amine from commercial (1*R*,2*R*)-(+)-1,2-diphenylethane-1,2-diamine according to the literature procedure[27] provided a sample with $[\alpha]_D^{25}$ +30.8° (*c* 0.5, EtOH), providing further confirmation of absolute configuration.

**(1*S*,2*S*)-1,2-diphenyl-1,2-di(piperidin-1-yl)ethane ((*S*,*S*)-2.48)**

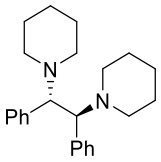


1,5-dibromopentane (0.50 mL, 3.69 mmol, 1.10 equiv) was added to a suspension of (1*S*,2*S*)-1,2-diphenyl-2-(piperidin-1-yl)ethan-1-amine (935 mg, 3.33 mmol, 1.00 equiv, 93.5:6.5 e.r.) and $K_2CO_3$ (1.15 mg, 8.38 mmol, 2.50 equiv) in MeCN (26.8 mL). The reaction mixture was

heated under reflux for 24 h. The reaction mixture was filtered through celite and concentrated to afford crude product. The crude product was purified by flash silica chromatography (elution gradient 0 to 100% $Et_2O$ in pentane) to afford the title compound as a white solid (1.09 g, 3.13 mmol, 94%).

**mp** 164-165 °C; **$\nu_{max}$** (thin film) /$cm^{-1}$ 2928, 1451, 1161, 874, 696; **$^1$H NMR** (400 MHz, $CDCl_3$) δ 7.15 – 7.09 (m, 4H), 7.09 – 7.00 (m, 6H), 4.18 (s, 2H), 2.69 – 2.52 (m, 4H), 2.46 – 2.26 (m, 4H), 1.67 – 1.56 (m, 8H), 1.38 – 1.20 (m, 4H); **$^{13}$C NMR** (101 MHz, $CDCl_3$) δ 137.2, 129.4, 127.5, 126.5, 69.2, 50.3, 27.1, 25.2; **HRMS** ($ESI^+$) calc. for $C_{24}H_{33}N_2$ ($[M+H]^+$): 349.2638; found: 349.2638; $[\alpha]_D^{25}$ -13.8° (*c* 1.0, $CHCl_3$).

**NB**: Enantiomeric ratio was determined by $^1$H NMR analysis with (*R*)-(−)-1,1′-binaphthyl-2,2′-diyl hydrogenphosphate as chiral shift reagent.[28] (*S*,*S*)-**2.48** (3.5 mg) and (*R*)-(−)-1,1′-binaphthyl-2,2′-diyl hydrogenphosphate (3.5 mg) was dissolved in $CDCl_3$ (1 mL). 0.1 mL of this solution was diluted 10-fold to 1 mM. Sample analysis was conducted on a Bruker AVANCE III 500 MHz spectrometer cooled to 233 K. $^1$H NMR spectra were collected with 512 scans. Data was processed with MestReNova 12.0.0. qGSD (quantitative global spectrum deconvolution) of the signals at 5.02 (minor) and 4.97 (major) provided the enantiomeric ratio.

### 4.4.5 Mechanistic studies of HB-PTC with sodium azide

#### $^1$H NMR titration of 2.41a and tetrabutylammonium chloride

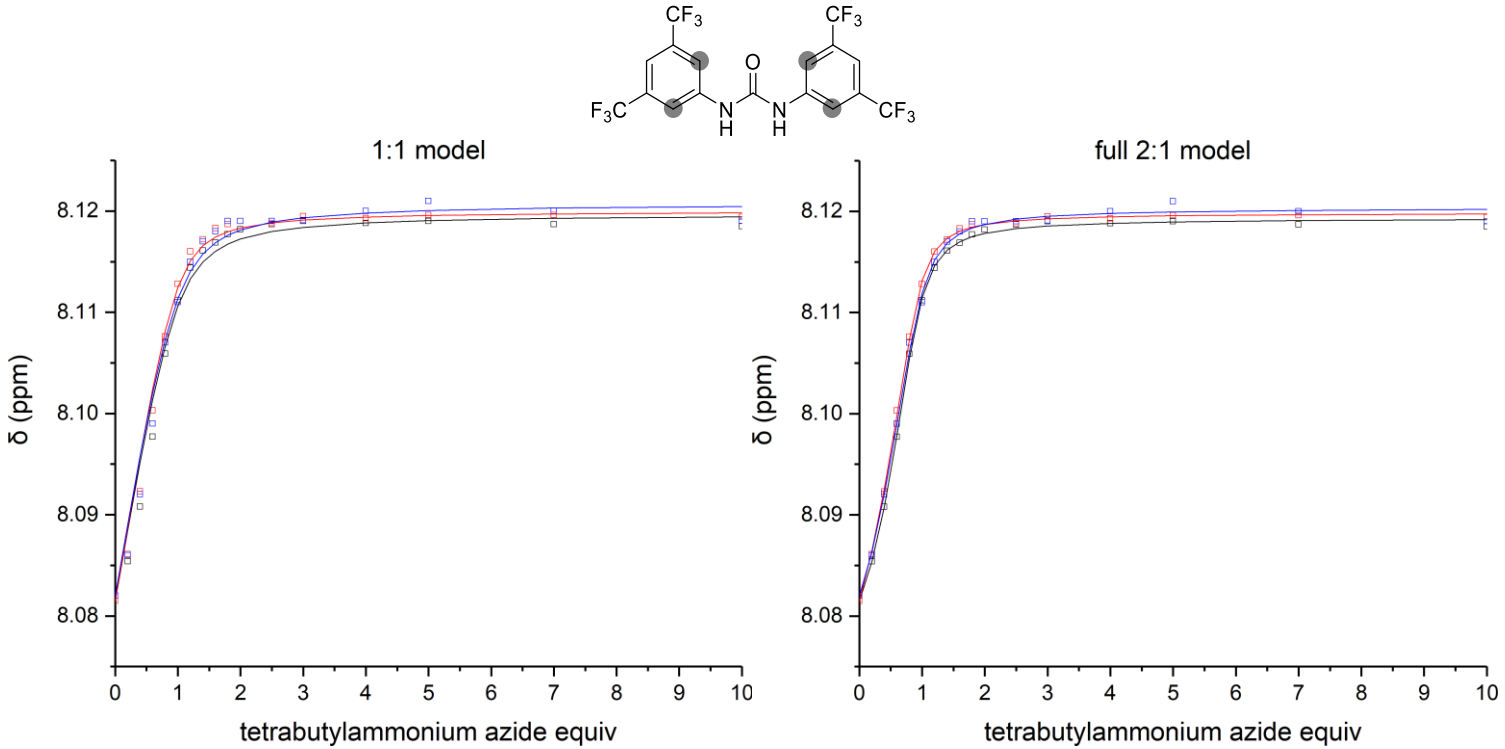


**Figure 4.9** $^1$H NMR titration data of **2.41a** with tetrabutylammonium chloride. One set of symbols (□, ○, △) refers to experimental data from one set of measurements. Lines are the calculated isotherms of the described model. (2 mM **2.41a**, $CH_3CN/CD_3CN$ 8:2, 500 MHz, 298 K).

**Table 4.10** Comparison of binding models

| model | entry | $cov_{fit}$ ($10^{-3}$) | $cov_{fit}$ factor | $K_{a(1:1)}$ ($M^{-1}$) | $K_{a(2:1)}$ ($M^{-1}$) | $\Delta G_{(1:1)}$ (kJ $mol^{-1}$) | $\Delta G_{(2:1)}$ (kJ $mol^{-1}$) |
|---|---|---|---|---|---|---|---|
| 1:1 | 1 | 18.31 | 1 | $6.77 \times 10^3$ | - | | |
| | 2 | 10.05 | 1 | $1.06 \times 10^4$ | - | | |
| | 3 | 15.53 | 1 | $6.48 \times 10^3$ | - | | |
| | **mean** | **14.63** | **1** | **$8.0 \pm 1.9 \times 10^3$** | **-** | **-22.3 ± 0.6** | **-** |
| **full 2:1** | 1 | 0.60 | 11.0 | $5.24 \times 10^4$ | $1.02 \times 10^2$ | | |
| | 2 | 0.46 | 21.8 | $6.41 \times 10^4$ | $1.05 \times 10^2$ | | |
| | 3 | 1.95 | 8.0 | $2.54 \times 10^4$ | $3.05 \times 10^2$ | | |
| | **mean** | **1.00** | **13.6** | **$4.7 \pm 1.6 \times 10^4$** | **$1.7 \pm 0.9 \times 10^2$** | **-26.7 ± 0.8** | **-12.7 ± 1.3** |

$cov_{fit}$ factor is $cov_{fit}$ for the 1:1 model divided by the $cov_{fit}$ for the binding model under study.[7] Values calculated with BindFit v0.5,[5] error is the standard deviation from 3 independent replicas.

The mean $cov_{fit}$ for the full 2:1 model is significantly higher than the mean $cov_{fit}$ for the 1:1 model, suggesting this system is best described by the full 2:1 model.

**$^1$H NMR titration of (*S*)-2.43b and tetrabutylammonium chloride**

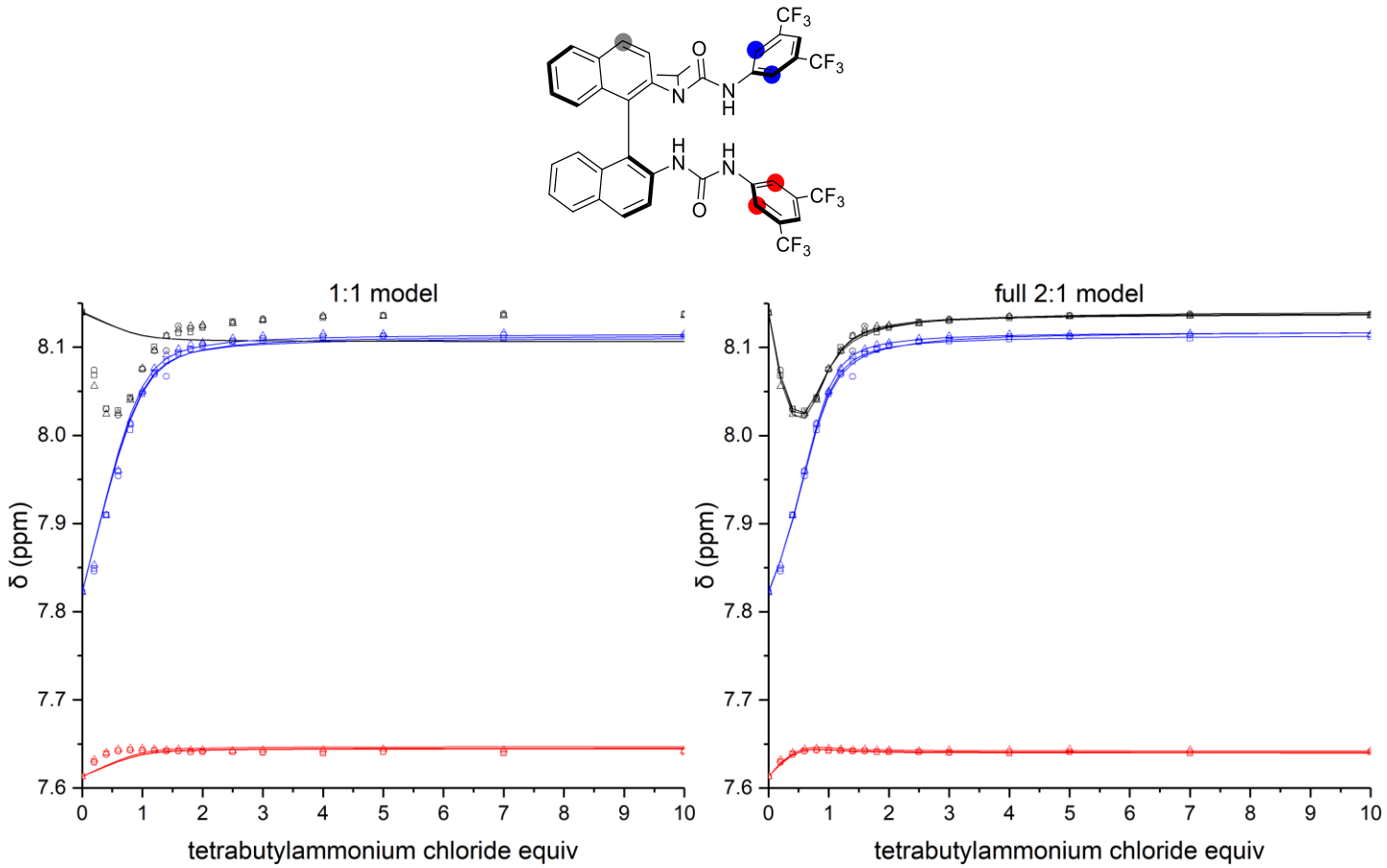


**Figure 4.10** $^1$H NMR titration data of (*S*)-**2.43b** with tetrabutylammonium chloride. One set of symbols (□, ○, △) refers to experimental data from one set of measurements. Lines are the calculated isotherms of the described model. (2 mM (*S*)-**2.43b**, $CDCl_3$ 8:2, 500 MHz, 298 K).

**Table 4.11** Comparison of binding models.

| model | entry | $cov_{fit}$ ($10^{-3}$) | $cov_{fit}$ factor | $K_{a(1:1)}$ ($M^{-1}$) | $K_{a(2:1)}$ ($M^{-1}$) | $\Delta G_{(1:1)}$ (kJ $mol^{-1}$) | $\Delta G_{(2:1)}$ (kJ $mol^{-1}$) |
|---|---|---|---|---|---|---|---|
| 1:1 | 1 | 46.11 | 1 | $9.03 \times 10^3$ | - | | |
| | 2 | 48.29 | 1 | $7.67 \times 10^3$ | - | | |
| | 3 | 49.37 | 1 | $9.44 \times 10^3$ | - | | |
| | **mean** | **47.92** | **1** | **$8.7 \pm 0.8 \times 10^3$** | **-** | **-22.5 ± 0.2** | **-** |
| **full 2:1** | 1 | 0.31 | 148.7 | $1.85 \times 10^4$ | $1.90 \times 10^2$ | | |
| | 2 | 1.11 | 43.5 | $2.66 \times 10^4$ | $9.87 \times 10^2$ | | |
| | 3 | 0.28 | 176.3 | $1.96 \times 10^4$ | $1.47 \times 10^2$ | | |
| | **mean** | **0.57** | **122.8** | **$2.2 \pm 0.4 \times 10^4$** | **$4 \pm 3 \times 10^2$** | **-24.8 ± 0.5** | **-15 ± 2** |

$cov_{fit}$ factor is $cov_{fit}$ for the 1:1 model divided by the $cov_{fit}$ for the binding model under study.[7] Values calculated with BindFit v0.5,[5] error is the standard deviation from 3 independent replicas.

The mean $cov_{fit}$ for the full 2:1 model is significantly higher than the mean $cov_{fit}$ for the 1:1 model, suggesting this system is best described by the full 2:1 model.

**Non-linear effect**

Scalemic mixtures of catalyst **2.43b** were prepared by mixing (*S*)-**2.43b** with (±)-**2.43b**, dissolving in $CH_2Cl_2$, then evaporating the mixture to dryness. Enantiopurity of each catalyst batch was determined by HPLC. **HPLC** DAICEL CHIRALPAK® IH, 2% EtOH in heptane, 1 mL $min^{-1}$, $t_{major}$ = 6.06, $t_{minor}$ = 9.16.

**Table 4.12** Non-linear effect study.

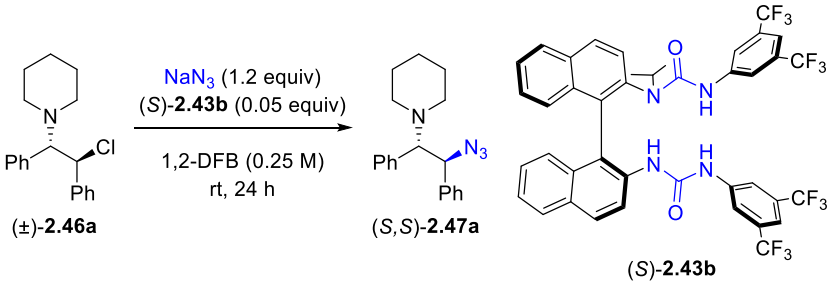


| entry | ee of **2.43b** | ee of **2.47a** |
|---|---|---|
| 1 | 100.0 | 72.8 |
| 2 | 79.4 | 61.4 |
| 3 | 56.2 | 39.2 |
| 4 | 37.8 | 27.6 |
| 5 | 19.2 | 12.8 |
| 6 | 7.6 | 4.0 |
| 7 | 0.0 | -0.2 |

Average of two runs, major enantiomer of **2.43b** in scalemic mixtures is (*S*). 1,2-DFB = 1,2-difluorobenzene. Non-linear effect investigation was conducted in collaboration with Dr. M. A. Horwitz.

**ReactIR data collection**

Reaction monitoring by *in situ* infra-red spectroscopy was conducted with a Mettler Toledo ReactIR 15 equipped with a 6.3 mm silicon composite probe. Reactions were conducted in a 5 cm tall test tube with a B12 adaptor made from medium (1.5 ± 0.25 mm) walled tubing. Reactions were stirred with an 8×3 mm magnetic stir bar.

A stock solution containing substrate and internal standard was prepared by making up a 1mL volumetric flask. Catalyst and $NaN_3$ was added to the selected reaction vessel charged with an 8×3 mm stir bar. 1,2-difluorobenzene (0.4 mL) was slowly injected. The probe as lowered, and the stirring and acquisition was started to pre-stir the reaction mixture. After 15 minutes, the substrate stock solution was carefully injected. The probe was lifted such that it was just

touching the surface of the reaction mixture. The reaction was stirred for the desired time. The reaction was quenched by filtration through a plug of silica and eluted with $Et_2O$. The reaction mixture was filtered through silica, eluted with $Et_2O$ and concentrated. Full conversion was confirmed by $^1H$ NMR. Enantiomeric excessed was determined on a sample purified by pTLC.

## 4.4 Supporting Information for Chapter 3

### 4.4.1 General procedures

**General procedure 3.1 (GP3.1, synthesis of bis-urea catalysts)**
Dry $CH_2Cl_2$ (0.4 M) was added to a flame dry Schlenk tube charged with the terphenyl aniline (2.00 equiv) and (*S*)-BINAM derivative (1.00 equiv) under $N_2$. The reaction mixture was sealed and stirred at 40 °C for 36 h. The reaction mixture was cooled to rt and diluted with MeOH. The reaction mixture was stirred at rt for 1 h. The reaction mixture was concentrated to afford crude product. The crude product was purified as indicated.

**General procedure 3.2 (GP3.2, synthesis of racemic products)**
THF (0.2 mL, 0.25 M) was added to tetrabutylammonium cyanide (16.1 mg, 0.6 mmol, 1.20 equiv) and substrate **3.39a-d** (0.05 mmol, 1 equiv) in a 1.75 mL vial. The reaction mixture was stirred at rt for 12 h. The reaction mixture was purified by flash silica chromatography.

**General procedure 3.3 (GP3.3, reaction optimisation)**
**Room temperature or 4 °C**: (Precooled) solvent was added to a 1.75 mL vial charged sequentially with substrate (0.05 mmol, 1.00 equiv), catalyst, and cyanide salt. The reaction mixture was stirred at the indicated temperature and *ca*. 600 rpm for the indicated time. The reaction mixture was filtered through a silica plug, eluted with EtOAc, and concentrated to afford crude product. The NMRy was determined by $^1H$ NMR with $Ph_3CH$ (12.2 mg, 1 equiv) internal standard. The enantiomeric ratio was determined with HPLC on a sample purified by pTLC.

**Below 4 °C**: Precooled solvent was added to a 2 mL Schlenk tube (7 mm internal diameter) charged sequentially with substrate (0.05 mmol, 1 equiv), catalyst, and potassium cyanide under air. The reaction mixture was stirred at the indicated temperature and *ca*. 600 rpm for the indicated time. The NMRy was determined by $^1$H NMR with $Ph_3CH$ (12.2 mg, 1 equiv) internal standard. The enantiomeric ratio was determined with HPLC on a sample purified by pTLC.

**General procedure 3.4 (GP3.4, synthesis of enantioenriched products)**
Precooled α,α,α-trifluorotoluene (0.2 mL, 0.25 M) was added to a 1.75 mL vial charged sequentially with substrate (0.05 mmol, 1.00 equiv), (*S*)-**3.49h** (3.9 mg, 0.0025 mmol, 0.05 equiv), and potassium cyanide (7.8 mg, 0.12 mmol, 2.40 equiv). The reaction mixture was stirred at 4 °C and *ca*. 600 rpm for 24 h. The NMRy was determined by $^1$H NMR with $Ph_3CH$ (12.2 mg, 1 equiv) internal standard. The enantiomeric ratio was determined with HPLC on a sample purified by pTLC.

### 4.4.2 Solid state studies of a urea-cyanide complex

**Tetrabutylammonium cyanide(1,3-bis(3,5-bis(trifluoromethyl)phenyl)urea) (3.35·CN·Bu$_4$N)**

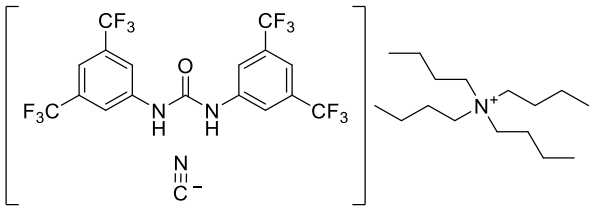

A suspension of tetrabutylammonium cyanide (134 mg, 0.5 mmol, 1.00 equiv) and 1,3-bis(3,5-bis(trifluoromethyl)phenyl)urea (242 mg, 0.5 mmol, 1.00 equiv) in hexane (31.25 mL) was heated to reflux for 0.5 h. The reaction mixture was cooled to rt. The solids were collected by filtration, washed with hexane, and dried to afford the title compound (331 mg, 0.44 mmol, 88%) as an off-white solid. The solid obtained was used without further purification.

Single crystals suitable for X-ray crystallography were grown by layering cyclohexane onto a saturated solution of the title compound in $Et_2O$.

**mp** 101-102 °C; **$\nu_{max}$** (neat) /$cm^{-1}$ 1714, 1626, 1578, 1471, 1374, 1272, 1167, 1123, 929, 899, 681; **$^{1}$H NMR** (500 MHz, $CD_3CN$) δ 8.12 (s, 4H), 7.46 (s, 2H), 3.10 – 3.03 (m, 8H), 1.67 – 1.53 (m, 8H), 1.34 (h, *J* = 7.5 Hz, 8H), 0.95 (t, *J* = 7.5 Hz, 12H); **$^{19}$F NMR** (470 MHz, $CD_3CN$) δ -63.65; **$^{13}$C NMR** (126 MHz, $CD_3CN$) δ 165.6, 155.5, 144.4, 132.3 (q, *J* = 33.0 Hz), 124.7 (q, *J* = 272.0 Hz), 119.0 (q, *J* = 3.5 Hz), 114.8 (dt, *J* = 7.0, 3.0 Hz), 59.3 (d, *J* = 3.0 Hz), 24.3, 20.3 (t, *J* = 1.5 Hz), 13.8.

### 4.4.3 Solution studies of urea-cyanide complexes

#### $^1$H NMR titration of 3.35 and tetrabutylammonium cyanide

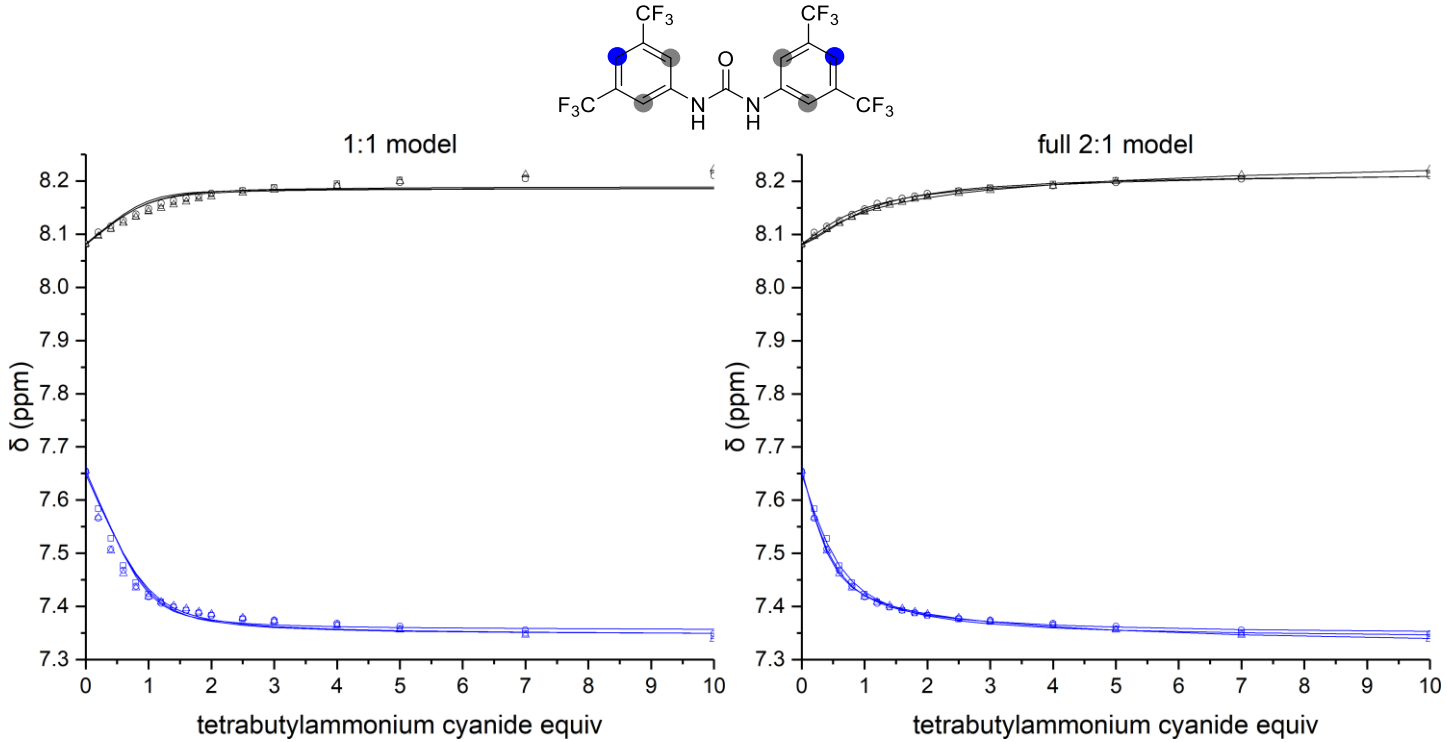


**Figure 4.11** $^1$H NMR titration data of **3.35** with tetrabutylammonium cyanide. One set of symbols (□, ○, △) refers to experimental data from one set of measurements. Lines are the calculated isotherms of the described model. (2 mM **3.35**, $CH_3CN/CD_3CN$ 8:2, 500 MHz, 298 K).

**Table 4.13** Comparison of binding models.

| model | entry | $cov_{fit}$ ($10^{-3}$) | $cov_{fit}$ factor | $K_{a(1:1)}$ ($M^{-1}$) | $K_{a(2:1)}$ ($M^{-1}$) | $\Delta G_{(1:1)}$ (kJ $mol^{-1}$) | $\Delta G_{(2:1)}$ (kJ $mol^{-1}$) |
|---|---|---|---|---|---|---|---|
| 1:1 | 1 | 4.49 | 1 | $4.34 \times 10^3$ | - | | |
| | 2 | 6.82 | 1 | $7.19 \times 10^3$ | - | | |
| | 3 | 10.40 | 1 | $5.11 \times 10^3$ | - | | |
| | **mean** | **7.24** | **1** | **$5.5 \pm 1.2 \times 10^3$** | **-** | **-21.3 ± 0.5** | **-** |
| **full 2:1** | 1 | 0.37 | 19.9 | $2.53 \times 10^3$ | $5.73 \times 10^2$ | | |
| | 2 | 0.15 | 45.5 | $1.92 \times 10^3$ | $9.96 \times 10^2$ | | |
| | 3 | 0.073 | 142.5 | $1.80 \times 10^3$ | $2.76 \times 10^3$ | | |
| | **mean** | **0.20** | **36.2** | **$2.1 \pm 0.3 \times 10^3$** | **$1.4 \pm 0.9 \times 10^3$** | **-19.0 ± 0.3** | **-17.9 ± 1.6** |

$cov_{fit}$ factor is $cov_{fit}$ for the 1:1 model divided by the $cov_{fit}$ for the binding model under study.[7] Association constants calculated with BindFit v0.5,[5] error is standard deviation from 3 independent replicas.

The mean $cov_{fit}$ for the full 2:1 model is significantly higher than the mean $cov_{fit}$ for the 1:1 model, suggesting this system is best described by the full 2:1 model.

**$^1$H NMR assignment of (*S*)-3.36a ($CD_3CN$)**

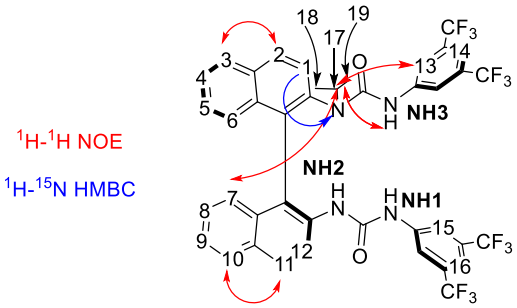


**$^1$H NMR** (500 MHz, $CD_3CN$) δ 8.36 – 8.30 (m, 2H, **H12, H2**), 8.17 (d, *J* = 8.5 Hz, 1H, **H3**), 8.08 (d, *J* = 9.0 Hz, 1H, **H11**), 7.96 (d, *J* = 8.0 Hz, 1H, **H10**), 7.74 (s, 2H, **H13**), 7.73 (d, *J* = 9.0 Hz, 1H, **H1**), 7.66 – 7.61 (m, 1H, **H4**), 7.54 – 7.34 (m, 5H, **H5, H9, H15, NH1/2**), 7.24 (d, *J* = 8.5 Hz, 1H, **H6**), 7.23 – 7.10 (m, 4H, **H8, H14, H16, NH1/2**), 6.98 (s, 1H, **NH3**), 6.83 (s, 1H, **H7**), 3.19 (br s, 1H, **H17**), 1.10 (s, 3H, **H18/19**), 0.43 (s, 3H, **H18/19**).

**$^1$H NMR titration of (*S*)-3.36a and tetrabutylammonium cyanide**

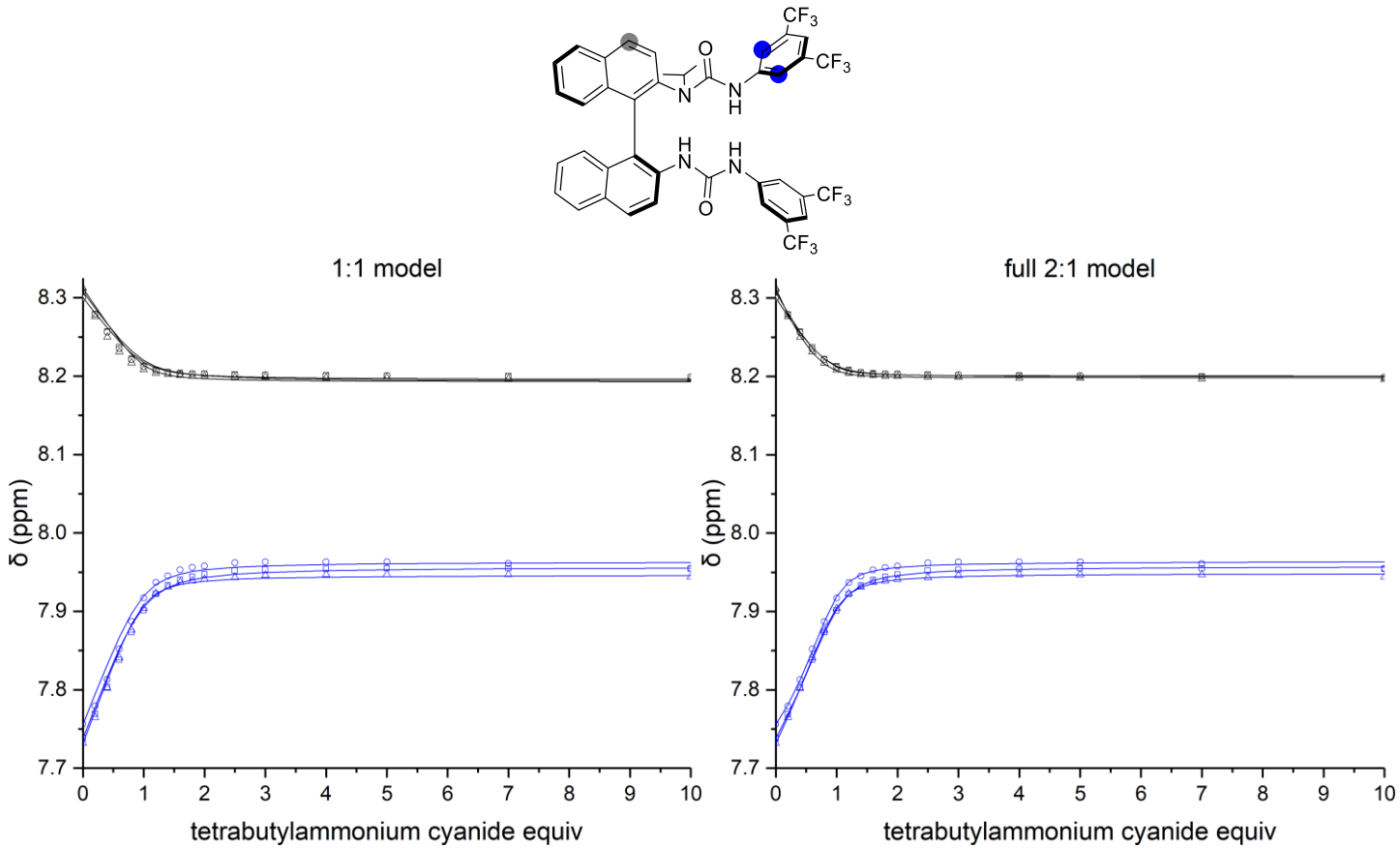


**Figure 4.12** $^1$H NMR titration data of (*S*)-**3.36a** with tetrabutylammonium cyanide. One set of symbols (□, ○, △) refers to experimental data from one set of measurements. Lines are the calculated isotherms of the described model. (2 mM (*S*)-**3.36a**, $CH_3CN/CD_3CN$ 8:2, 500 MHz, 298 K).

**Table 4.14** Comparison of binding models.

| model | entry | $cov_{fit}$ ($10^{-3}$) | $cov_{fit}$ factor | $K_{a(1:1)}$ ($M^{-1}$) | $K_{a(2:1)}$ ($M^{-1}$) | $\Delta G_{(1:1)}$ (kJ $mol^{-1}$) | $\Delta G_{(2:1)}$ (kJ $mol^{-1}$) |
|---|---|---|---|---|---|---|---|
| **1:1** | 1 | 1.89 | 1 | $7.06 \times 10^3$ | - | | |
| | 2 | 2.49 | 1 | $8.95 \times 10^3$ | - | | |
| | 3 | 1.87 | 1 | $1.31 \times 10^4$ | - | | |
| | **mean** | **2.08** | **1** | **$1.0 \pm 0.3 \times 10^4$** | **-** | **-22.8 ± 0.7** | **-** |
| full 2:1 | 1 | 0.41 | 4.6 | $6.47 \times 10^3$ | $-2.04 \times 10^2$ | | |
| | 2 | 0.24 | 10.4 | $1.45 \times 10^4$ | $-1.04 \times 10^2$ | | |
| | 3 | 0.068 | 27.5 | $1.28 \times 10^4$ | $-8.30 \times 10^1$ | | |
| | **mean** | **0.24** | **14.2** | **$1.1 \pm 0.3 \times 10^4$** | **$-1.3 \pm 0.5 \times 10^2$** | **-23.1 ± 0.7** | **n/a** |

$cov_{fit}$ factor is $cov_{fit}$ for the 1:1 model divided by the $cov_{fit}$ for the binding model under study.[7] Association constants calculated with BindFit v0.5,[5] error is standard deviation from 3 independent replicas.

The mean $cov_{fit}$ for the full 2:1 model is significantly higher than the mean $cov_{fit}$ for the 1:1 model. However as the values obtained for $K_{a(2:1)}$ were all negative, this system is likely best described by the 1:1 model.

**Variable temperature studies of (*S*)-3.36a and tetrabutylammonium cyanide**

Tetrabutylammonium cyanide (3.0 mg, 11.17 µmol, 1.00 equiv) was placed in an NMR tube. A solution of (*S*)-**3.36a** in $CD_2Cl_2$ (0.45 mL, 0.25 M, 1.00 equiv) was added, and the mixture was shaken until all solids were dissolved. This sample was immediately used for analysis.

### 4.4.4 Synthesis of chiral catalysts

(*S*)-**3.36a-e**,[14] **3.47**,[29] (*S*)-**3.48**,[30] (*S*)-**3.49a**,[17] and (*S*)-**3.49f-g**[31] were prepared according to the reported procedures.

**1,1'-((1*R*,2*R*)-1,2-bis(2-hydroxyphenyl)ethane-1,2-diyl)bis(3-(3,5-bis(trifluoromethyl)phenyl)urea) ((*R*,*R*)-3.46)**

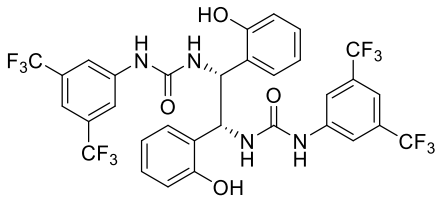

3,5-Bis(trifluoromethyl)phenyl isocyanate (1.42 mL, 8.18 mmol, 2.00 equiv) was added to a solution of (1*R*,2*R*)-1,2-bis(2-hydroxyphenyl)ethylenediamine (1.00 g, 4.09 mmol, 1.00 equiv) was in dry $CH_2Cl_2$ (8.2 mL) under $N_2$. The reaction mixture was stirred at rt for 16 h. The reaction mixture was diluted with $CH_2Cl_2$ (50 mL) and washed with 1 M HCl (50 mL). The organic layer was dried with $MgSO_4$, filtered, and concentrated to afford crude product. The crude product was purified by flash silica chromatography (elution gradient 0 to 30% EtOAc in pentane) to afford the title compound as an off-white solid (1.26 g, 1.68 mmol, 41%).

**mp** 174-176 °C; $\boldsymbol{\nu_{max}}$ (neat) /cm$^{-1}$ 3388, 1671, 1544, 1276, 1176, 1126; **$^1$H NMR** (500 MHz, DMSO-$d_6$) 9.82 (s, 1H), 9.74 (s, 1H), 7.86 (d, *J* = 1.5 Hz, 2H), 7.29 (t, *J* = 1.5 Hz, 1H), 6.93 (td, *J* = 7.5, 1.5 Hz, 1H), 6.82 – 6.72 (m, 2H), 6.69 – 6.60 (m, 1H), 6.49 (t, *J* = 7.5 Hz, 1H), 5.55 (dt, *J* = 10.5, 5.0 Hz, 1H); **$^{19}$F NMR** (471 MHz, DMSO-$d_6$) δ -62.03; **$^{13}$C NMR** (126 MHz, DMSO-$d_6$) δ 155.1, 155.0, 142.5, 130.3 (q, *J* = 32.5 Hz) , 129.7, 128.2, 125.4, 123.2 (q, *J* = 272.5 Hz), 118.6, 116.3, 115.3, 112.9, 56.4; **HRMS** (ESI$^+$) calc. for $C_{32}H_{23}O_4N_4F_{12}$ ([M+H]$^+$): 755.1522; found: 755.1515; $[\boldsymbol{\alpha}]_{\boldsymbol{D}}^{\mathbf{25}}$ -32.1° (*c* 1.00, MeOH).

**(*S*)-6,6'-dibromo-*N*$^2$-isopropyl-[1,1'-binaphthalene]-2,2'-diamine**

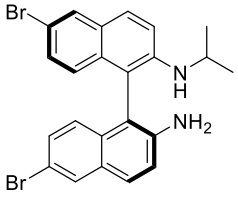


$H_2SO_4$ (20% in $H_2O$, 18 mL) was added to acetone (0.93 mL, 12.54 mmol, 1.40 equiv) in THF (36 mL). The reaction mixture was stirred at rt for 30 min. (*S*)-6,6'-dibromo-[1,1'-binaphthalene]-2,2'-diamine[32] (3.96 g, 8.96 mmol, 1.00 equiv) was added in one portion, and the reaction mixture was stirred at rt for 5 min. The reaction mixture was cooled to 0 °C. $NaBH_4$ (3.39 g, 89.61 mmol, 10.00 equiv) was added carefully portionwise. The reaction mixture was stirred at rt for 1 h. The reaction mixture was diluted with 1 M KOH (50 mL), extracted with EtOAc (50 mL), dried with $MgSO_4$, filtered, and concentrated to afford crude product. The crude product was purified by flash silica chromatography (elution gradient 5 to 10% EtOAc in pentane) to afford the title compound (1.38 g, 2.87 mmol, 32%) as a pale-yellow solid.

**mp** 83-85 °C; **$\nu_{max}$** (neat) /cm$^{-1}$ 3378, 2963, 1612, 1588, 1493, 1333, 1151, 875, 808; **$^1$H NMR** (400 MHz, $CDCl_3$) δ 7.94 (d, *J* = 2.0 Hz, 1H), 7.91 (d, *J* = 2.0 Hz, 1H), 7.77 (d, *J* = 9.0 Hz, 1H), 7.72 (d, *J* = 9.0 Hz, 1H), 7.27 (d, *J* = 9.0 Hz, 1H), 7.24 (dd, *J* = 9.0, 2.0 Hz, 1H), 7.21 (dd, *J* = 9.0, 2.0 Hz, 1H), 7.15 (d, *J* = 9.0 Hz, 1H), 6.85 (d, *J* = 9.0 Hz, 1H), 6.78 (d, *J* = 9.0 Hz, 1H), 3.78 (dp, *J* = 13.0, 6.0Hz, 1H), 3.69 (br s, 2H), 3.41 (br s, 1H), 1.07 (d, *J* = 6.0 Hz, 3H), 0.99 (d, *J* = 6.0 Hz, 3H); **$^{13}$C NMR** (101 MHz, $CDCl_3$) δ 144.4, 143.4, 132.5, 132.3, 130.2×3, 130.1, 129.7, 129.0×2, 128.8, 125.8, 125.6, 119.4, 116.2, 116.1, 115.5, 112.0, 111.7, 44.7, 23.4, 23.3; **HRMS** (ESI$^+$) calc. for $C_{23}H_{21}N_2{}^{79}Br_2$ ([M+H]$^+$): 483.0066; found: 483.0065; $[\boldsymbol{\alpha}]_{\boldsymbol{D}}^{\mathbf{25}}$ -62.4° (*c* 1.00, $CHCl_3$).

**1-isopropyl-3-(3,3'',5,5''-tetrakis(trifluoromethyl)-[1,1':3',1''-terphenyl]-5'-yl)-1-(2'-(3-(3,3'',5,5''-tetrakis(trifluoromethyl)-[1,1':3',1''-terphenyl]-5'-yl)ureido)-[1,1'-binaphthalen]-2-yl)urea ((*S*)-3.49b)**

Characterisation data from A. C. Vicini.

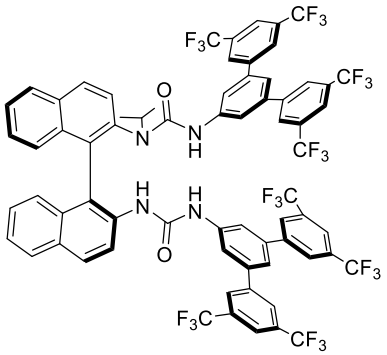

Prepared according to GP4.1 with 5'-isocyanato-3,3'',5,5''-tetrakis(trifluoromethyl)-1,1':3',1''-terphenyl[33] (869 mg, 1.60 mmol, 2.00 equiv) and (*S*)-*N*$^2$-isopropyl-[1,1'-binaphthalene]-2,2'-diamine[14] (261 mg, 0.80 mmol, 1.00 equiv). The crude product was purified by flash silica chromatography (elution gradient 0 to 10% EtOAc in pentane) to afford the title compound as a white solid (423 mg, 0.30 mmol, 37%).

**mp** 196-198 °C; **$\nu_{max}$** (thin film) /cm$^{-1}$ 3327, 365, 2936, 1680, 1623, 1599, 1546, 1508, 1469, 1428, 1367, 1276,1174, 1127, 901, 844, 734, 705, 683, 639; **$^1$H NMR** (500 MHz, $CDCl_3$) δ 8.40 (br s, 1H), 8.15 (d, *J* = 8.5 Hz, 1H), 8.10 (d, *J* = 9.0 Hz, 1H), 8.03 (d, *J* = 8.0 Hz, 1H), 7.96 (d, *J* = 8.2 Hz, 1H), 7.81 (d, *J* = 1.5 Hz, 4H), 7.75 (s, 2H), 7.73 (s, 6H), 7.63 (d, *J* = 8.5 Hz, 1H), 7.59 (ddd, *J* = 8.0, 7.0, 1.0 Hz, 1H), 7.54 (s, 2H), 7.46 (ddd, *J* = 8.0, 7.0, 1.0 Hz, 1H), 7.36 (ddd, *J* = 8.5, 7.0, 1.5 Hz, 1H), 7.32 – 7.27 (m, 4H), 7.23 (d, *J* = 8.5 Hz, 1H), 7.16 (br s, 1H), 7.13 (s, 1H), 7.00 (s, 1H), 6.96 (d, *J* = 8.5 Hz, 1H), 6.62 (s, 1H), 3.55 (br s, 1H), 1.19 (d, *J* = 7.0 Hz, 3H), 0.74 – 0.61 (m, 3H); **$^{19}$F NMR** (471 MHz, $CDCl_3$) δ -63.00, -63.02; 2.82, -63.02; **$^{13}$C NMR** (126 MHz, $CDCl_3$) δ 155.6 (br), 152.7, 142.1, 141.6, 139.9, 139.8, 139.7, 139.6, 139.5, 134.9 (br), 133.9, 133.4, 133.0, 132.2 (q, *J* = 33.5 Hz), 132.2, 132.1 (q, *J* = 33.5 Hz), 131.0 (br), 130.7, 130.4, 128.8 (br), 128.6, 128.4, 128.0, 127.7, 127.3, 127.1–127.0 (m), 126.9–126.8 (m), 126.7, 125.6, 125.3 (br), 123.1 (q, *J* = 273.0 Hz), 123.0 (q, *J* = 273.0 Hz), 121.6–121.4 (m), 121.4–121.2 (m), 120.8 (br),

120.3 (br), 120.1, 118.3, 54.5 (br), 20.9, 20.0 (br); **HRMS** (ESI$^+$) calc. for $C_{69}H_{41}O_2N_4F_{24}^+$ ([M+H]$^+$): 1413.2841, found 1413.2780; $[\boldsymbol{\alpha}]_{\boldsymbol{D}}^{\mathbf{25}}$ -133.0° (*c* 0.50, $CHCl_3$).

**NB**: $^{13}C$ spectra contained overlapping signals.

**1-(6,6'-dibromo-2'-(3-(3,3'',5,5''-tetrakis(trifluoromethyl)-[1,1':3',1''-terphenyl]-5'-yl)ureido)-[1,1'-binaphthalen]-2-yl)-1-isopropyl-3-(3,3'',5,5''-tetrakis(trifluoromethyl)-[1,1':3',1''-terphenyl]-5'-yl)urea ((*S*)-3.49c)**

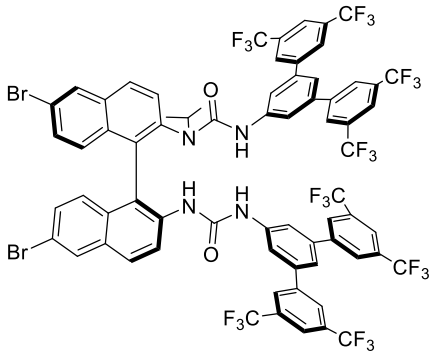

Prepared according to GP4.1 with 5'-isocyanato-3,3'',5,5''-tetrakis(trifluoromethyl)-1,1':3',1''-terphenyl[33] (224 mg, 0.42 mmol, 2.00 equiv) and (*S*)-6,6'-dibromo-*N*$^2$-isopropyl-[1,1'-binaphthalene]-2,2'-diamine (100 mg, 0.21 mmol, 1.00 equiv). The crude product was purified by flash silica chromatography (elution gradient 0 to 10% EtOAc in pentane), then recrystallised from $Et_2O$/pentane, and washed with pentane to afford the title compound as a white solid (116 mg, 0.07 mmol, 36%).

**mp** 173-175 °C; **$\nu_{max}$** (thin film) /cm$^{-1}$ 1548, 1397, 1367, 1279, 1133, 706, 683; **$^1$H NMR** (500 MHz, $CDCl_3$) δ 8.68 (d, *J* = 8.0 Hz, 1H), 8.17 (d, *J* = 2.0 Hz, 1H), 8.10 (d, *J* = 2.0 Hz, 1H), 8.07 (d, *J* = 9.0 Hz, 1H), 7.99 (d, *J* = 9.0 Hz, 1H), 7.82 (s, 4H), 7.77 (s, 2H), 7.75 (s, 2H), 7.70 (s, 4H), 7.64 (d, *J* = 8.5 Hz, 1H), 7.57 (s, 2H), 7.45 (br s, 1H), 7.40 (dd, *J* = 9.0, 2.0 Hz, 1H), 7.33 (dd, *J* = 9.0, 2.0 Hz, 1H), 7.30 (br s, 1H), 7.25 (d, *J* = 1.5 Hz, 2H), 7.22 (s, 1H), 7.04 (d, *J* = 1.5 Hz, 1H), 7.02 (d, *J* = 9.0 Hz, 1H), 6.78 – 6.65 (m, 2H), 3.74 – 3.61 (m, 1H), 1.09 (d, *J* = 7.0 Hz, 3H), 0.80 (d, *J* = 7.0 Hz, 3H); **$^{19}$F NMR** (471 MHz, $CDCl_3$) δ -62.95, -62.99; **$^{13}$C NMR** (126 MHz, $CDCl_3$) δ 156.7, 152.4, 142.3, 141.4, 140.3, 140.1, 140.1, 139.8, 139.5, 136.6, 134.3, 132.5, 132.4 (q, *J* = 33.5 Hz), 132.2 (q, *J* = 33.5 Hz), 131.9, 131.5, 131.2, 130.8, 130.7, 130.5, 130.0, 129.7, 129.5, 128.7, 127.1 (q, *J* = 3.0 Hz), 127.0, 127.0 (q, *J* = 4.0 Hz), 123.1 (q, *J* = 273.0 Hz), 122.9 (q, *J* = 272.5 Hz),

122.0, 121.9 – 121.8 (m), 121.8, 121.5 (p, *J* = 4.0 Hz), 121.3, 120.5, 118.9, 118.0, 53.4, 21.4, 20.9; **HRMS** ($ESI^+$) calc. for $C_{69}H_{39}O_2N_4{}^{79}Br_2F_{24}^+$ ($[M+H]^+$): 1569.1051, found 1569.1041; $[\boldsymbol{\alpha}]_{\boldsymbol{D}}^{\mathbf{25}}$ -85.6° (*c* 1.00, $CHCl_3$).

**NB**: $^{13}C$ spectra contained overlapping signals.

**2'-fluoro-3,3'',5,5''-tetrakis(trifluoromethyl)-[1,1':3',1''-terphenyl]-5'-amine**

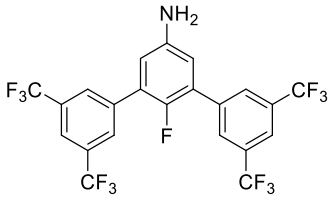


Palladium acetate (42 mg, 0.19 mmol, 0.05 equiv) was added to a mixture of 3,5-dibromo-4-fluoroaniline (1.00 g, 3.72 mmol, 1.00 equiv), 3,5-bis(trifluoromethyl)phenylboronic acid (3.34 g, 1.02 mmol, 3.50 equiv), SPhos (0.15 g, 0.37 mmol, 0.10 equiv), and potassium carbonate (1.40 g, 37.19 mmol, 5 equiv) in degassed THF (50 mL)) and degassed $H_2O$ (10 mL) under $N_2$. The reaction mixture was heated to reflux overnight. The reaction mixture was cooled to rt, diluted with $H_2O$ (50 mL), extracted with $CH_2Cl_2$ (50 mL), washed with sat. brine (25 mL), dried with $MgSO_4$, filtered, and concentrated to afford crude product. The crude product was purified by flash silica chromatography (elution gradient 0% to 50% $CH_2Cl_2$ in pentane) to afford the title compound as an off-white solid (1.66 mg, 3.10 mmol, 83%).

**mp** 178-180 °C; $\boldsymbol{\nu_{max}}$ (thin film) /$cm^{-1}$ 1621, 1370, 1280, 1122, 904, 684; **$^1$H NMR** (500 MHz, $CDCl_3$) δ 8.00 (s, 4H), 7.91 (s, 2H), 6.79 (d, *J* = 6.0 Hz, 2H), 3.83 (s, 2H); **$^{19}$F NMR** (377 MHz, $CDCl_3$) δ -62.84, -137.41 (tt, *J* = 6.0, 1.5 Hz).; **$^{13}$C NMR** (126 MHz, $CDCl_3$) δ 149.7 (d, *J* = 242.0 Hz), 143.6 (d, *J* = 3.0 Hz), 137.8, 132.1 (q, *J* = 33.5 Hz), 129.3 (t, *J* = 3.5 Hz), 128.0 (d, *J* = 15.5 Hz), 123.4 (q, *J* = 273.0 Hz), 121.9 (p, *J* = 4.0 Hz), 116.9 (d, *J* = 2.0 Hz); **HRMS** ($ESI^+$) calc. for $C_{22}H_9F_{13}^+$ ($[M+H]^+$): 534.0533, found 534.0531.

**2'-fluoro-5'-isocyanato-3,3'',5,5''-tetrakis(trifluoromethyl)-1,1':3',1''-terphenyl**

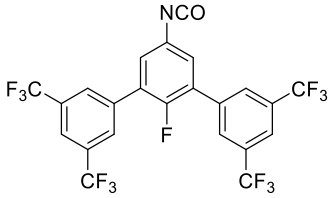


A solution of 2'-fluoro-3,3'',5,5''-tetrakis(trifluoromethyl)-[1,1':3',1''-terphenyl]-5'-amine (1.64 g, 3.06 mmol, 1.00 equiv) in $CH_2Cl_2$ (30 mL) was added to a solution of triphosgene (0.34 g, 1.13 mmol, 0.37 equiv) in $CH_2Cl_2$ (20 mL) at 0 °C. A solution of sat. $NaHCO_3$ (30 mL) was added to the reaction mixture. The reaction mixture was stirred at 0 °C for 45 min. The organic layer was separated, dried with $MgSO_4$, filtered, and concentrated to afford crude product. The crude solid was recrystallised from hot hexane with a minimal quantity of THF to afford the title compound (0.91 g, 1.62 mmol, 53%) as a white solid.

**mp** 147-149 °C; $\boldsymbol{\nu_{max}}$ (thin film) /$cm^{-1}$ 2275, 1366, 1278, 1163, 1122, 684; **$^1$H NMR** (500 MHz, $CDCl_3$) δ 8.00 (s, 4H), 7.91 (s, 2H), 6.79 (d, *J* = 6.0 Hz, 2H), 3.83 (s, 2H); **$^{19}$F NMR** (377 MHz, $CDCl_3$) δ -62.85, -125.76 (t, *J* = 6.0 Hz); **$^{13}$C NMR** (126 MHz, $CDCl_3$) δ 153.9 (d, *J* = 251.5 Hz), 136.3, 132.5 (q, *J* = 33.5 Hz), 131.1 (d, *J* = 4.0 Hz), 129.4 (t, *J* = 3.5 Hz), 128.9 (d, *J* = 16.0 Hz), 127.1 (d, *J* = 3.0 Hz), 125.4, 123.2 (q, *J* = 273.0 Hz), 122.6 (p, *J* = 3.5 Hz); **HRMS** ($ESI^-$) calc. for $C_{23}H_7F_{13}NO^-$ ($[M-H]^-$): 560.0326, found 560.0312.

**3-(2'-fluoro-3,3'',5,5''-tetrakis(trifluoromethyl)-[1,1':3',1''-terphenyl]-5'-yl)-1-(2'-(3-(2'-fluoro-3,3'',5,5''-tetrakis(trifluoromethyl)-[1,1':3',1''-terphenyl]-5'-yl)ureido)-[1,1'-binaphthalen]-2-yl)-1-isopropylurea ((*S*)-3.49d)**

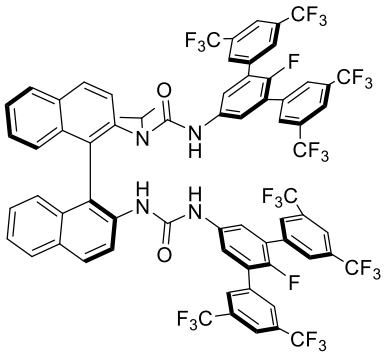


Prepared according to GP4.1 with 2'-fluoro-5'-isocyanato-3,3'',5,5''-tetrakis(trifluoromethyl)-1,1':3',1''-terphenyl (172 mg, 0.31 mmol, 2.00 equiv) and (*S*)-*N*$^2$-isopropyl-[1,1'-binaphthalene]-2,2'-diamine[14] (50 mg, 0.15 mmol, 1.00 equiv). The crude product was purified

by flash silica chromatography (elution gradient 0 to 10% EtOAc in pentane) to afford the title compound as a white solid (156 mg, 0.11 mmol, 70%).

**mp** 163-165 °C; $\nu_{max}$ (thin film) /cm$^{-1}$ 1680, 1529, 1398, 1279, 1186, 1162, 1133, 902, 683; **$^{1}$H NMR** (500 MHz, $CDCl_3$) δ 8.25 (br s, 1H), 8.13 (d, *J* = 8.5 Hz, 1H), 8.11 (d, *J* = 9.0 Hz, 1H), 8.02 (d, *J* = 8.0 Hz, 1H), 7.96 (d, *J* = 8.0 Hz, 1H), 7.82 (s, 4H), 7.77 (s, 4H), 7.75 (s, 2H), 7.72 (s, 2H), 7.62 (d, *J* = 8.5 Hz, 1H), 7.59 (ddd, *J* = 8.0, 7.0, 1.0 Hz, 1H), 7.48 (t, *J* = 8.0 Hz, 1H), 7.42 – 7.34 (m, 3H), 7.31 (t, *J* = 7.5 Hz, 1H), 7.25 (s, 1H), 7.24 (s, 1H), 7.21 (d, *J* = 8.5 Hz, 1H), 6.97 (s, 1H), 6.95 (s, 1H), 6.66 (br s, 1H), 6.45 (s, 1H), 3.42 (br s, 1H), 1.20 (d, *J* = 6.5 Hz, 3H), 0.56 (br s, 3H); **$^{19}$F NMR** (377 MHz, $CDCl_3$) δ -63.10, -63.12, -129.75, -130.68; **$^{13}$C NMR** (126 MHz, $CDCl_3$) δ 155.2, 153.1, 152.1 (d, *J* = 241.0 Hz), 151.7 (d, *J* = 248.5 Hz), 139.7, 136.7, 136.6, 135.3 (d, *J* = 3.5 Hz), 135.2 (d, *J* = 2.5 Hz), 134.2, 134.0, 133.6, 133.1, 132.2, 132.0×2 (q, *J* = 33.7 Hz), 130.9, 130.7, 129.0, 128.9, 128.7, 128.6, 128.0×2 (d, *J* = 15.0 Hz), 127.7, 127.5, 127.1 (d, *J* = 2.0 Hz), 126.9 (d, *J* = 2.0 Hz), 126.6, 125.9, 125.8, 123.7, 123.1 (q, *J* = 273.0 Hz), 123.1 (q, *J* = 273.0 Hz), 121.9, 55.4, 20.9, 19.7; **HRMS** (ESI$^+$) calc. for $C_{69}H_{39}O_2N_4F_{26}^+$ ([M+H]$^+$): 1449.2652, found 1449.2628; $[\alpha]_D^{25}$ -172.3° (*c* 1.00, $CHCl_3$).

**NB**: $^{13}$C spectra contained overlapping signals.

**1-(6,6'-dibromo-2'-(3-(2'-fluoro-3,3'',5,5''-tetrakis(trifluoromethyl)-[1,1':3',1''-terphenyl]-5'-yl)ureido)-[1,1'-binaphthalen]-2-yl)-3-(2'-fluoro-3,3'',5,5''-tetrakis(trifluoromethyl)-[1,1':3',1''-terphenyl]-5'-yl)-1-isopropylurea ((*S*)-3.49e)**

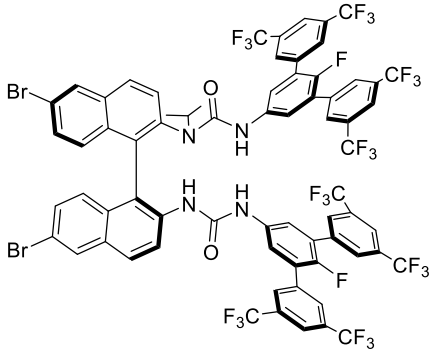


Prepared according to GP4.1 with 2'-fluoro-5'-isocyanato-3,3'',5,5''-tetrakis(trifluoromethyl)-1,1':3',1''-terphenyl (225 mg, 0.40 mmol, 2.00 equiv) and (*S*)-6,6'-dibromo-*N*$^2$-isopropyl-[1,1'-binaphthalene]-2,2'-diamine (97 mg, 0.20 mmol, 1.00 equiv). The crude product was purified

by flash silica chromatography (elution gradient 0 to 10% EtOAc in pentane), then triturated with pentane to afford the title compound as a white solid (157 mg, 0.10 mmol, 49%).

**mp** 166-168 °C; **$\nu_{max}$** (thin film) /$cm^{-1}$ 1539, 1363, 1278, 1133, 902; **$^{1}$H NMR** (500 MHz, $CDCl_3$) δ 8.58 (br s, 1H), 8.17 (d, *J* = 2.0 Hz, 1H), 8.10 (d, *J* = 2.0 Hz, 1H), 8.05 (d, *J* = 8.5 Hz, 1H), 7.99 (d, *J* = 9.0 Hz, 1H), 7.83 (s, 4H), 7.77 (s, 4H), 7.70 (s, 4H), 7.63 (d, *J* = 8.5 Hz, 1H), 7.42 – 7.37 (m, 3H), 7.34 (dd, *J* = 9.0, 2.0 Hz, 1H), 7.21 (s, 1H), 7.20 (s, 1H), 7.07 (br s, 2H), 7.00 (d, *J* = 9.0 Hz, 1H), 6.73 (d, *J* = 9.0 Hz, 1H), 6.54 (s, 1H), 3.57 (br s, 1H), 1.07 (d, *J* = 7.0 Hz, 3H), 0.72 (d, *J* = 7.0 Hz, 3H); $^{19}$F NMR (377 MHz, $CDCl_3$) δ -63.04, -63.06, -130.40 (br); **$^{13}$C NMR** (126 MHz, $CDCl_3$) δ 156.3, 152.7 (d, *J* = 250.0 Hz), 152.4, 151.5 (d, *J* = 248.0 Hz), 139.9, 136.6, 136.2, 135.9, 135.3 (d, *J* = 3.0 Hz), 134.6 (d, *J* = 3.0 Hz), 134.1, 132.3, 132.0 (q, *J* = 33.5 Hz), 131.9 (q, *J* = 33.5 Hz), 131.8, 131.7, 131.2, 130.8, 130.6, 130.4, 129.8, 129.5, 128.8, 128.7, 128.3, 127.4 (d, *J* = 15.0 Hz), 127.1 (d, *J* = 15.0 Hz), 126.9, 124.6, 123.0 (d, *J* = 273.0 Hz), 122.9 (d, *J* = 273.0 Hz), 122.0, 121.8, 121.1, 119.1, 53.8, 21.2, 20.5; **HRMS** ($ESI^+$) calc. for $C_{69}H_{35}O_2N_4{}^{79}Br_2F_{26}^+$ ($[M-H]^-$): 1603.0703, found 1603.0713; $[\alpha]_D^{25}$ -85.5° (*c* 1.00, $CHCl_3$).

**NB**: $^{13}$C spectra contained overlapping signals.

**1,3-dibromo-2-(difluoromethoxy)-5-nitrobenzene**

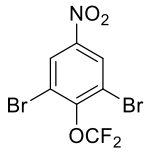


Diethyl (bromodifluoromethyl)phosphonate (1.78 mL, 20.00 mmol, 2.00 equiv) was added to a mixture of 2,6-dibromo-4-nitrophenol (2.97 g, 10.00 mmol, 1.00 equiv) in KOH (11.22 g, 200.00 mmol, 20.00 equiv), $H_2O$ (50 mL), and MeCN (50 mL). The reaction mixture was stirred at rt overnight. The reaction mixture was diluted with $H_2O$ (50 mL), extracted with EtOAc (3×100 mL), washed with sat. brine (50 mL), dried with $MgSO_4$, filtered, and concentrated to afford crude product. The crude product was purified by flash silica chromatography (elution

gradient 0 to 100% $CH_2Cl_2$ in pentane) to afford the title compound as a yellow oil that solidified on standing (1.40 g, 4.05 mmol, 40%).

**mp** 43-45 °C; **$\nu_{max}$** (thin film) /$cm^{-1}$ 1527, 1386, 1344, 1137, 1060, 738; **$^{1}$H NMR** (400 MHz, $CDCl_3$) δ 8.47 (s, 2H), 6.71 (t, *J* = 73.0 Hz, 1H); **$^{19}$F NMR** (377 MHz, $CDCl_3$) δ -80.53 (d, *J* = 73.5 Hz); **$^{13}$C NMR** (101 MHz, $CDCl_3$) δ 151.1 (t, *J* = 4.0 Hz), 145.9, 128.4, 115.9 (t, *J* = 267.5 Hz).

**3,5-dibromo-4-(difluoromethoxy)aniline**

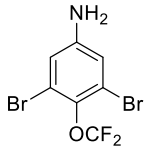


Fe powder (0.68 g, 12.15 mmol, 3.00 equiv) was added to a solution of 1,3-dibromo-2-(difluoromethoxy)-5-nitrobenzene (1.40 g, 4.05 mmol, 1.00 equiv) in AcOH (13 mL). The reaction mixture was stirred at 100 °C for 3 h. The reaction mixture was cooled to rt, basified with 5 M NaOH (100 mL), extracted with EtOAc (2×100 mL), washed with sat. brine, dried with $MgSO_4$, filtered, and concentrated to afford crude product. The crude product was purified by flash silica chromatography (elution gradient 0 to 50% $Et_2O$ in pentane) to afford the title compound as a white solid (0.64 g, 2.03 mmol, 50%).

**mp** 100-102 °C; **$\nu_{max}$** (thin film) /$cm^{-1}$ 1625, 1594, 1554, 1471, 1426, 1093; **$^{1}$H NMR** (400 MHz, $CDCl_3$) δ 6.85 (s, 2H), 6.49 (t, *J* = 74.5 Hz, 1H), 3.76 (s, 3H); **$^{19}$F NMR** (377 MHz, $CDCl_3$) δ -81.03 (d, *J* = 74.5 Hz); **$^{13}$C NMR** (101 MHz, $CDCl_3$) δ 146.3, 137.8 (br), 118.7, 118.6, 117.3 (t, *J* = 263.0 Hz).

**(2'-(difluoro-λ$^3$-methoxy)-3,3'',5,5''-tetrakis(trifluoromethyl)-[1,1':3',1''-terphenyl]-5'-yl)azane**

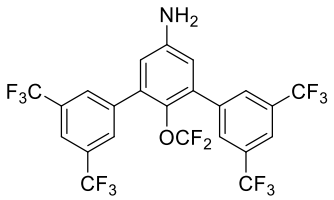


Palladium acetate (23 mg, 0.10 mmol, 0.05 equiv) was added to a mixture of 3,5-dibromo-4-(difluoromethoxy)aniline (642 mg, 2.03 mmol, 1.00 equiv), 3,5-bis(trifluoromethyl)phenylboronic acid (1.83 g, 7.11 mmol, 3.50 equiv), SPhos (83 mg, 0.20

mmol, 0.10 equiv), and potassium carbonate (1.40 g, 10.15 mmol, 5.00 equiv) in degassed THF (20 mL)) and degassed $H_2O$ (8 mL) under $N_2$. The reaction mixture was stirred at 60 °C for 48 h. The reaction mixture was cooled to rt, filtered through celite, and eluted with $Et_2O$ (50 mL). The filtrate was washed with $H_2O$ (25 mL), sat. brine (25 mL), dried with $MgSO_4$, filtered, and concentrated to afford crude product. The crude product was purified by flash silica chromatography (elution gradient 0% to 50% $Et_2O$ in pentane) to afford the title compound as an off-white solid (730 mg, 1.26 mmol, 62%).

**mp** 143-145 °C; **$\nu_{max}$** (thin film) /$cm^{-1}$ 2981, 1370, 1278, 1128, 683; **$^1$H NMR** (500 MHz, $CDCl_3$) δ 8.01 (d, *J* = 1.5 Hz, 4H), 7.90 (s, 2H), 6.75 (s, 2H), 5.71 (t, *J* = 73.5 Hz, 1H), 3.95 (s, 2H); **$^{19}$F NMR** (471 MHz, $CDCl_3$) δ -62.80, -81.39 (d, *J* = 73.5 Hz); **$^{13}$C NMR** (126 MHz, $CDCl_3$) δ 145.7, 139.6, 136.2 (t, *J* = 3.0 Hz), 135.6, 131.9 (q, *J* = 33.5 Hz), 129.7 (d, *J* = 4.0 Hz), 123.4 (q, *J* = 273.0 Hz), 121.8 (dt, *J* = 7.5, 3.5 Hz), 117.1, 116.2 (t, *J* = 264.0 Hz); **HRMS** ($ESI^+$) calc. for $C_{23}H_{10}ONF_{14}^+$ ($[M+H]^+$): 582.0544, found 582.0536.

**2'-(difluoro-λ$^3$-methoxy)-5'-isocyanato-3,3'',5,5''-tetrakis(trifluoromethyl)-1,1':3',1''-terphenyl**

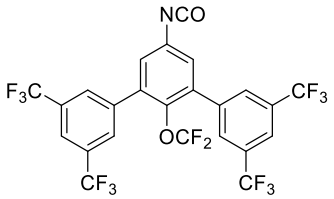


A solution of (2'-(difluoro-λ$^3$-methoxy)-3,3'',5,5''-tetrakis(trifluoromethyl)-[1,1':3',1''-terphenyl]-5'-yl)azane (715 mg, 1.23 mmol, 1.00 equiv) in $CH_2Cl_2$ (4.9 mL) was added to a solution of triphosgene (135 mg, 0.46 mmol, 0.37 equiv) in $CH_2Cl_2$ (7.4 mL) at 0 °C. A solution of sat. $NaHCO_3$ (12.3 mL) was added to the reaction mixture. The reaction mixture was stirred at 0 °C for 45 min. The reaction mixture was extracted with $CH_2Cl_2$ (25 mL). The organic layer was dried with $MgSO_4$, filtered, and concentrated to afford crude product. The crude solid was washed with pentane, then dried to afford the title compound (548 mg, 0.90 mmol, 73%) as a yellow solid.

**mp** 112-114 °C; **$\nu_{max}$** (thin film) /cm$^{-1}$ 2269, 1365, 1278, 1132; **$^{1}$H NMR** (600 MHz, $CDCl_3$) δ 8.00 (d, *J* = 1.5 Hz, 2H), 7.96 (s, 1H), 7.25 (s, 1H), 5.79 (t, *J* = 72.5 Hz, 1H); **$^{19}$F NMR** (565 MHz, $CDCl_3$) δ -62.86, -81.33 (d, *J* = 74.0 Hz); **$^{13}$C NMR** (151 MHz, $CDCl_3$) δ 141.9 (t, *J* = 3.0 Hz), 138.3, 136.5, 133.4, 132.4 (q, *J* = 33.5 Hz), 129.7 (d, *J* = 4.0 Hz), 127.5, 126.0, 123.2 (q, *J* = 124.0 Hz), 122.5 (dt, *J* = 7.5, 3.5 Hz), 115.6 (t, *J* = 266.5 Hz).

**3-(2'-(difluoromethoxy)-3,3'',5,5''-tetrakis(trifluoromethyl)-[1,1':3',1''-terphenyl]-5'-yl)-1-(2'-(3-(2'-(difluoromethoxy)-3,3'',5,5''-tetrakis(trifluoromethyl)-[1,1':3',1''-terphenyl]-5'-yl)ureido)-[1,1'-binaphthalen]-2-yl)-1-isopropylurea ((*S*)-3.49h)**

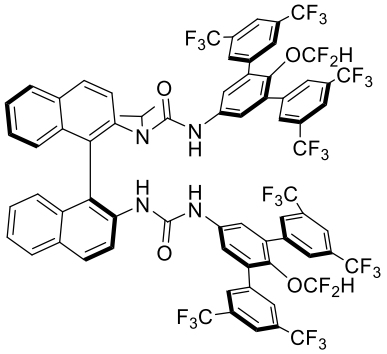

Prepared according to GP4.1 with (2'-(difluoro-λ$^3$-methoxy)-3,3'',5,5''-tetrakis(trifluoromethyl)-[1,1':3',1''-terphenyl]-5'-yl)azane (183 mg, 0.30 mmol, 2.00 equiv) and (*S*)-*N*$^2$-isopropyl-[1,1'-binaphthalene]-2,2'-diamine[14] (49 mg, 0.15 mmol, 1.00 equiv). The crude product was purified by flash silica chromatography (elution gradient 0 to 20% EtOAc in pentane) to afford the title compound as a white solid (65 mg, 0.04 mmol, 28%).

**mp** 148-150 °C; **$\nu_{max}$** (neat) /cm$^{-1}$ 2059, 2028, 1977, 1363, 1278, 1131, 682; **$^{1}$H NMR** (600 MHz, $CDCl_3$) δ 8.14 (br s, 1H), 8.03 (d, *J* = 8.5 Hz, 1H), 8.00 (d, *J* = 9.0 Hz, 1H), 7.89 – 7.87 (m, 2H), 7.83 (s, 4H), 7.80 (s, 2H), 7.77 (s, 4H), 7.72 (s, 2H), 7.48 (d, *J* = 8.5 Hz, 1H), 7.44 – 7.35 (m, 2H), 7.16 – 7.12 (m, 4H), 6.90 (d, *J* = 8.5 Hz, 1H), 6.68 (br s, 1H), 6.56 (s, 1H), 5.55 (t, *J* = 73.0 Hz, 1H), 5.54 (t, *J* = 73.0 Hz, 1H), 3.40 (br s, 1H), 1.09 (d, *J* = 7.0 Hz, 3H), 0.52 (br s, 3H); **$^{19}$F NMR** (565 MHz, $CDCl_3$) δ -62.94, -62.98, -81.30 (dd, *J* = 73.0, 5.0 Hz), -81.50 (dd, *J* = 73.5, 6.0 Hz); **$^{13}$C NMR** (151 MHz, $CDCl_3$) δ 155.3, 152.8, 140.2, 139.8, 139.4, 138.8, 138.7, 137.5, 137.4, 135.2, 134.8, 134.6, 133.7, 133.2, 132.9, 132.0, 131.8×2 (q, *J* = 33.5 Hz), 130.7, 130.3, 129.4×2, 128.6, 128.3, 127.7, 127.5, 127.4, 127.2, 126.6, 125.6, 125.5, 123.1 (q, *J* = 273.0 Hz), 123.0 (q, *J* =

272.5 Hz), 123.0, 121.8, 121.5, 115.6 (t, *J* = 265.5 Hz), 115.5 (t, *J* = 265.5 Hz), 54.7, 20.6, 20.1; **HRMS** (ESI$^+$) calc. for $C_{71}H_{41}O_4N_4F_{28}^+$ ([M+H]$^+$): 1545.2675, found 1545.2607; $[\alpha]_D^{25}$ -460.0° (*c* 0.50, $CHCl_3$).

**NB**: $^{13}C$ spectra contained overlapping signals.

**1-(6,6'-dibromo-2'-(3-(2'-(difluoromethoxy)-3,3'',5,5''-tetrakis(trifluoromethyl)-[1,1':3',1''-terphenyl]-5'-yl)ureido)-[1,1'-binaphthalen]-2-yl)-3-(2'-(difluoromethoxy)-3,3'',5,5''-tetrakis(trifluoromethyl)-[1,1':3',1''-terphenyl]-5'-yl)-1-isopropylurea ((*S*)-3.49i)**

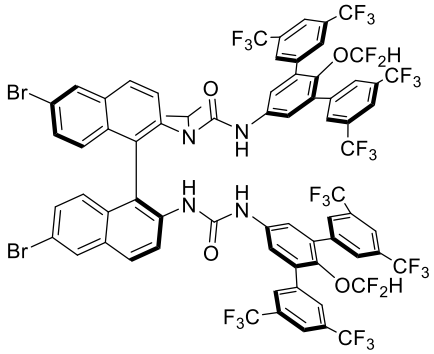

Prepared according to GP4.1 with (2'-(difluoro-λ$^3$-methoxy)-3,3'',5,5''-tetrakis(trifluoromethyl)-[1,1':3',1''-terphenyl]-5'-yl)azane (183 mg, 0.30 mmol, 2.00 equiv) and (*S*)-6,6'-dibromo-*N*$^2$-isopropyl-[1,1'-binaphthalene]-2,2'-diamine (73 mg, 0.15 mmol, 1.00 equiv). The crude product was purified by flash silica chromatography (elution gradient 0 to 20% EtOAc in pentane) to afford the title compound as a white solid (65 mg, 0.04 mmol, 25%). **mp** 169-171 °C; **$\nu_{max}$** (neat) /cm$^{-1}$ 2160, 2026, 1364, 1278, 1134, 683; **$^1$H NMR** (600 MHz, $CDCl_3$) δ 8.40 (d, *J* = 9.0 Hz, 1H), 8.11 (d, *J* = 11.5 Hz, 1H), 8.10 (d, *J* = 11.5 Hz, 1H), 8.01 (d, *J* = 8.5 Hz, 1H), 7.96 (d, *J* = 9.0 Hz, 1H), 7.89 (s, 4H), 7.87 (s, 2H), 7.85 (s, 4H), 7.80 (s, 2H), 7.55 (d, *J* = 8.5 Hz, 1H), 7.52 (br s, 1H), 7.47 (s, 2H), 7.37 – 7.30 (m, 2H), 7.26 (s, 2H), 7.00 (d, *J* = 9.0 Hz, 1H), 6.80 – 6.68 (m, 3H), 5.62 (t, *J* = 73.0 Hz, 2H), 3.57 (s, 1H), 1.13 (d, *J* = 7.0 Hz, 3H), 0.69 (br s, 3H); **$^{19}$F NMR** (565 MHz, $CDCl_3$) δ -62.95, -62.97, -81.25 (d, *J* = 72.5 Hz), -81.47 (dd, *J* = 73.0, 6.0 Hz); **$^{13}$C NMR** (151 MHz, $CDCl_3$) δ 156.0, 152.4, 140.8, 140.3, 139.5, 138.9, 138.8, 137.7, 137.2, 136.1, 135.6, 135.1, 134.2, 132.2, 132.0 (q, *J* = 33.5 Hz), 132.0, 132.0 (q, *J* = 33.5 Hz), 131.8, 131.3, 130.8, 130.4, 130.0, 129.6, 129.5, 129.3, 129.1, 128.5, 126.9, 123.5, 123.3 (q, *J* = 272.5 Hz), 123.1 (q, *J* = 272.5 Hz), 122.0, 121.9, 121.2, 119.3, 115.8 (t, *J* = 265.0 Hz), 115.6 (t, *J* = 266.5

Hz), 53.9, 21.2, 20.8; **HRMS** (ESI$^+$) calc. for $C_{71}H_{39}O_4N_4{}^{79}Br_2F_{28}{}^+$ ([M+H]$^+$): 1701.0885, found 1701.0854 ; $[\alpha]_D^{25}$ -264.4° (*c* 0.50, $CHCl_3$).

**NB**: $^{13}C$ spectra contained overlapping signals.

### 4.4.5 Additional reaction optimisation data

All reaction optimization used GP3.3.

**Table 4.15** Optimisation of reaction concentration.

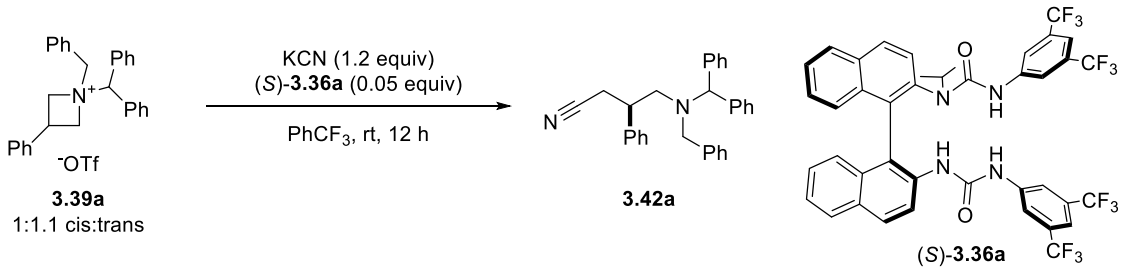


| entry | concentration | NMRy | e.r. |
|---|---|---|---|
| **1** | **0.25 M** | **74%** | **65:35** |
| 2 | 0.10 M | 60% | 64:36 |

NMRy determined with $Ph_3CH$ (1 equiv) internal standard. Absolute configuration of **3.42a** not determined. Reaction development was conducted in collaboration with G. Roagna.

**Table 4.16** Investigation of alternative cyanide sources.

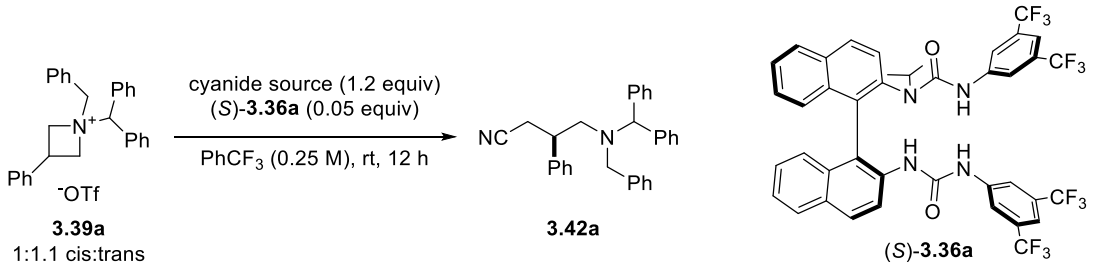


| entry | cyanide source | NMRy | e.r. |
|---|---|---|---|
| **1** | **KCN** | **74%** | **65:35** |
| 2 | NaCN | 32% | 62:38 |
| 3 | CuCN | nd | - |
| 4 | ZnCN | nd | - |

NMRy determined with $Ph_3CH$ (1 equiv) internal standard. Absolute configuration of **3.42a** not determined. Reaction development was conducted in collaboration with G. Roagna.

### 4.4.6 Synthesis of substrates and products

Substrates **3.39a-d** were prepared according to the reported literature procedures.[34,35]

**4-(benzhydryl(benzyl)amino)-3-phenylbutanenitrile (3.42a)**
Characterisation data from G. Roagna.

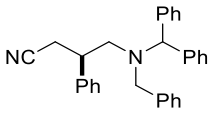


**Racemic product**: Prepared according to GP3.1 from **3.39a** to afford a clear oil.

**Enantioenriched product**: Prepared according to GP3.4 from **3.39a** to afford the title compound (40% NMRy, 62:38 e.r.).

**$\nu_{max}$** (thin film) /cm$^{-1}$ 3062, 3028, 2826, 2358, 1955, 1601, 1494, 1452, 1261, 1079, 1028, 912, 800, 761, 745, 699; **$^{1}$H NMR** (400 MHz, $CDCl_3$) δ 7.44 – 7.10 (m, 18H), 6.93 – 6.68 (m, 2H), 4.83 (s, 1H), 3.65 (d, *J* = 13.5 Hz, 1H), 3.51 (d, *J* = 13.5 Hz, 1H), 2.83 – 2.63 (m, 4H), 2.12 (dd, *J* = 16.5, 8.5 Hz, 1H); **$^{13}$C NMR** (101 MHz, $CDCl_3$) δ 140.9, 140.6×2, 139.1, 129.3×2, 129.2, 128.9, 128.6×2, 128.5, 127.6×2, 127.5×2, 127.4, 119.1, 70.3, 56.5, 56.4, 41.3, 22.0; **HRMS** (ESI$^+$) calc. for $C_{30}H_{29}N_2^+$ ([M+H]$^+$): 417.2325; found 417.2324; **HPLC** DAICEL CHIRALPAK® OJ-3, 10% EtOH in heptane, 1 mL min$^{-1}$, $t_{major}$ = 15.49, $t_{minor}$ = 10.68.

**NB**: Characterisation of racemic product provided.

**4-(benzhydryl(benzyl)amino)-3-(benzyloxy)butanenitrile (3.42b)**
Characterisation data from G. Roagna.

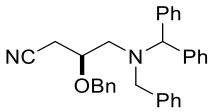


**Racemic product**: Prepared according to GP3.1 from **3.39b** to afford a clear oil.

**Enantioenriched product**: Prepared according to GP3.4 from **3.39b** to afford the title compound (95% NMRy, 79:21 e.r.).

**$\nu_{max}$** (thin film) /cm$^{-1}$ 3028, 1600, 1493, 1453, 1353, 1074, 1027, 910, 764, 735, 698; **$^{1}$H NMR** (400 MHz, $CDCl_3$) δ 7.37 – 7.08 (m, 20H), 4.81 (s, 1H), 4.34 (q, *J* = 11.5 Hz, 2H), 3.69 – 3.48 (m, 2H), 3.37 – 3.24 (m, 1H), 2.71 (dd, *J* = 14.0, 5.0 Hz, 1H), 2.55 (dd, *J* = 14.0, 8.0 Hz, 1H), 2.49 (dd, *J* = 17.0, 4.0 Hz, 1H), 2.10 (dd, *J* = 17.0, 7.5 Hz, 1H); **$^{13}$C NMR** (101 MHz, $CDCl_3$) δ 141.1, 140.8, 139.0, 137.6, 129.3, 129.2, 129.1, 128.7, 128.6×3, 128.1×2, 127.6, 127.5×2, 118.4, 74.2, 72.6,

71.6, 57.3, 54.6, 21.8; **HRMS** ($ESI^+$) calc. for $C_{31}H_{31}ON_2^+$ ($[M+H]^+$): 447.2440; found 447.2431; **HPLC** DAICEL CHIRALPAK® IB-3, 1% IPA in heptane, 1 mL $min^{-1}$, $t_{major}$ = 18.69, $t_{minor}$ = 13.99.

**NB**: Characterisation of racemic product provided.

**4-(benzhydryl(benzyl)amino)-3-methoxybutanenitrile (3.42c)**
Characterisation data from G. Roagna.

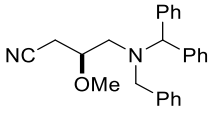


**Racemic product**: Prepared according to GP3.1 from **3.39c** to afford a clear oil.

**Enantioenriched product**: Prepared according to GP3.4 from **3.39c** to afford the title compound (89% NMRy, 73:27 e.r.).

**$\nu_{max}$** (thin film) /$cm^{-1}$ 3028, 1600, 1493, 1452, 1078, 1028, 911, 699; **$^1$H NMR** (400 MHz, $CDCl_3$) δ 7.39 – 7.13 (m, 15H), 4.85 (s, 1H), 3.65 (d, *J* = 13.5 Hz, 1H), 3.55 (d, *J* = 13.5 Hz, 1H), 3.18 (s, 3H), 3.11 – 2.98 (m, 1H), 2.69 (dd, *J* = 14.0, 5.0 Hz, 1H), 2.52 (dd, *J* = 14.0, 8.0 Hz, 1H), 2.45 (dd, *J* = 17.0, 4.0 Hz, 1H), 2.06 (dd, *J* = 17.0, 7.5 Hz, 1H); **$^{13}$C NMR** (101 MHz, $CDCl_3$) δ 141.1, 140.8, 139.1, 129.3×2, 129.1, 128.6×3, 127.6×2, 127.5, 118.3, 76.6 71.6, 58.2, 57.4, 54.0, 21.4; **HRMS** ($ESI^+$) calc. for $C_{25}H_{27}ON_2^+$ ($[M+H]^+$): 371.2118; found 371.2118. **HPLC** DAICEL CHIRALPAK® IB-3, 1% IPA in heptane, 1 mL $min^{-1}$, $t_{major}$ = 14.51, $t_{minor}$ = 10.25.

**NB**: Characterisation of racemic product provided.

**4-(benzhydryl(ethyl)amino)-3-(benzyloxy)butanenitrile (3.42d)**
Characterisation data from G. Roagna.

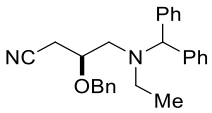


**Racemic product**: Prepared according to GP3.1 from **3.39d** to afford a clear oil.

**Enantioenriched product**: Prepared according to GP3.4 from **3.39d** to afford the title compound (91% NMRy, 87:13 e.r.). An additional sample was prepared according to GP4.2 from α,α,α-trifluorotoluene (0.2 mL, 0.25 M), potassium cyanide (7.8 mg, 0.12 mmol, 2.40

equiv), (*S*)-**3.49i** (4.3 mg, 0.0025 mmol, 0.05 equiv), and **3.39d** (25.4 mg, 0.05 mmol, 1 equiv) at -5 °C to afford the title compound (90% NMRy, 89:11 e.r.).

**$\nu_{max}$** (thin film) /$cm^{-1}$ 3028, 2967, 1599, 1493, 1451, 1179, 1077, 1027, 914, 745, 699, 621; **$^{1}$H NMR** (400 MHz, $CDCl_3$) δ 7.40 – 6.99 (m, 15H), 4.71 (s, 1H), 4.51 – 4.37 (m, 2H), 3.44 (dddd, *J* = 8.0, 7.0, 5.0, 4.0 Hz, 1H), 2.75 – 2.35 (m, 6H), 0.91 (t, *J* = 7.0 Hz, 3H); **$^{13}$C NMR** (101 MHz, $CDCl_3$) δ 142.0, 141.7, 137.7, 128.8, 128.7, 128.6×2, 128.5, 128.1, 128.0, 127.4, 127.3, 118.4, 53.5, 45.9, 21.9, 11.2; **HRMS** ($ESI^+$) calc. for $C_{26}H_{29}ON_2^+$ ($[M+H]^+$): 385.2274, found 385.2274; **HPLC** DAICEL CHIRALPAK® ID-3, 1% IPA in heptane, 1 mL $min^{-1}$, $t_{major}$ = 11.51, $t_{minor}$ = 10.20.

**NB**: Characterisation of racemic product provided.

## 4.5 References


1 H. E. Gottlieb, V. Kotlyar and A. Nudelman, *J. Org. Chem.*, 1997, **62**, 7512–7515.

2 *Prudent Practices for Disposal of Chemicals From Laboratories*, National Acadamy Press, Washington, D.C., 1983.

3 G. Stedman, *J. Chem. Soc.*, 1959, 2943–2949.

4 G. E. Eden, B. L. Hampson and A. B. Wheatland, *J. Soc. Chem. Ind.*, 1950, **69**, 244–249.

5 supramolecular.org, http://supramolecular.org, (accessed 18 September 2019).

6 P. Thordarson, *Chem. Soc. Rev.*, 2011, **40**, 1305–1323.

7 E. N. W. Howe, M. Bhadbhade and P. Thordarson, *J. Am. Chem. Soc.*, 2014, **136**, 7505–7516.

8 D. Brynn Hibbert and P. Thordarson, *Chem. Commun.*, 2016, **52**, 12792–12805.

9 D. J. Maher and S. J. Connon, *Tetrahedron Lett.*, 2004, **45**, 1301–1305.

10 S. Perveen, S. M. Abdul Hai, R. A. Khan, K. M. Khan, N. Afza and T. B. Sarfaraz, *Synth. Commun.*, 2005, **35**, 1663–1674.

11 G. Jakab, C. Tancon, Z. Zhang, K. M. Lippert and P. R. Schreiner, *Org. Lett.*, 2012, **14**, 1724–1727.

12 L. Pfeifer, K. M. Engle, G. W. Pidgeon, H. A. Sparkes, A. L. Thompson, J. M. Brown and V. Gouverneur, *J. Am. Chem. Soc.*, 2016, **138**, 13314–13325.

13 B. Sauer, T. S. Skinner-Adams, A. Bouchut, M. J. Chua, C. Pierrot, F. Erdmann, D. Robaa, M. Schmidt, J. Khalife, K. T. Andrews and W. Sippl, *Eur. J. Med. Chem.*, 2017, **127**, 22–40.

14 G. Pupo, F. Ibba, D. M. H. Ascough, A. C. Vicini, P. Ricci, K. E. Christensen, L. Pfeifer, J. R. Morphy, J. M. Brown, R. S. Paton and V. Gouverneur, *Science*, 2018, **360**, 638–642.

15 F. Ibba, G. Pupo, A. L. Thompson, J. M. Brown, T. D. W. Claridge and V. Gouverneur, *J. Am. Chem. Soc.*, 2020, **142**, 19731–19744.

16 J. B. Hendrickson, D. A. Judelson and T. Chancellor, *Synthesis (Stuttg).*, 1984, **1984**, 320–322.

17 G. Pupo, A. C. Vicini, D. M. H. Ascough, F. Ibba, K. E. Christensen, A. L. Thompson, J. M. Brown, R. S. Paton and V. Gouverneur, *J. Am. Chem. Soc.*, 2019, **141**, 2878–2883.

18 F. Broghammer, D. Brodbeck, T. Junge and R. Peters, *Chem. Commun.*, 2017, **53**, 1156–1159.

19 X. Pu, X. Qi and J. M. Ready, *J. Am. Chem. Soc.*, 2009, **131**, 10364–10365.

20 M. Kokubo, T. Naito and S. Kobayashi, *Tetrahedron*, 2010, **66**, 1111–1118.

21 E. Ramesh, T. Guntreddi and A. K. Sahoo, *European J. Org. Chem.*, 2017, **2017**, 4405–4413.

22 M. J. Mio, L. C. Kopel, J. B. Braun, T. L. Gadzikwa, K. L. Hull, R. G. Brisbois, C. J. Markworth and P. A. Grieco, *Org. Lett.*, 2002, **4**, 3199–3202.

23 S. Hong, S. Tian, M. V Metz and T. J. Marks, *J. Am. Chem. Soc.*, 2003, **125**, 14768–14783.

24 S. Wang, N. Lokesh, J. Hioe, R. M. Gschwind and B. König, *Chem. Sci.*, 2019, **10**, 4580–4587.

25 J. Kajanus, T. Antonsson, L. Carlsson, U. Jurva, A. Pettersen, J. Sundell and T. Inghardt,

*Bioorg. Med. Chem. Lett.*, 2019, **29**, 1241–1245.

26 J. González-Sabín, V. Gotor and F. Rebolledo, *Tetrahedron: Asymmetry*, 2004, **15**, 1335–1341.

27 J. Li, N. Fu, L. Zhang, P. Zhou, S. Luo and J.-P. Cheng, *European J. Org. Chem.*, 2010, **2010**, 6840–6849.

28 G. L. Hamilton, T. Kanai and F. D. Toste, *J. Am. Chem. Soc.*, 2008, **130**, 14984–14986.

29 C. Cassani, R. Martín-Rapún, E. Arceo, F. Bravo and P. Melchiorre, *Nat. Protoc.*, 2013, **8**, 325–344.

30 Y. Sudo, D. Shirasaki, S. Harada and A. Nishida, *J. Am. Chem. Soc.*, 2008, **130**, 12588–12589.

31 G. Roagna, PhD thesis, University of Oxford, 2021.

32 A. Sakakura, K. Suzuki and K. Ishihara, *Adv. Synth. Catal.*, 2006, **348**, 2457–2465.

33 A. C. Vicini, PhD thesis, University of Oxford, 2020.

34 G. Roagna, D. M. H. Ascough, F. Ibba, A. C. Vicini, A. Fontana, K. E. Christensen, A. Peschiulli, D. Oehlrich, A. Misale, A. A. Trabanco, R. S. Paton, G. Pupo and V. Gouverneur, *J. Am. Chem. Soc.*, 2020, **142**, 14045–14051.

35 D. Qian, M. Chen, A. C. Bissember and J. Sun, *Angew. Chem. Int. Ed.*, 2018, **57**, 3763–3766.

# Appendix

## Additional crystal structures

### 1,1'-((1R,2R)-1,2-bis(2-hydroxyphenyl)ethane-1,2-diyl)bis(3-(3,5-bis(trifluoromethyl)phenyl)urea)·tetrabutylammonium azide

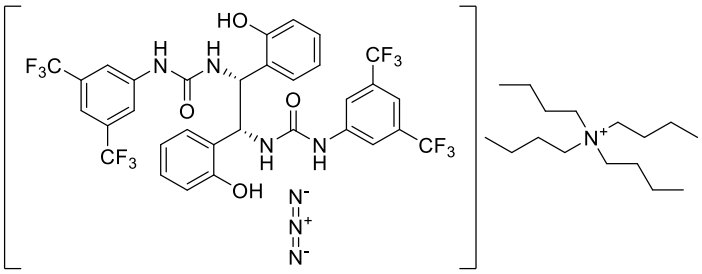

Dry MeCN (2 mL) was added to tetrabutylammonium azide (57 mg, 0.20 mmol, 1.00 equiv) and 1,1'-((1*R*,2*R*)-1,2-bis(2-hydroxyphenyl)ethane-1,2-diyl)bis(3-(3,5-bis(trifluoromethyl)phenyl)urea) (148 mg, 0.20 mmol, 1.00 equiv). The reaction mixture stirred at rt for 48 h. The reaction mixture was evaporated to dryness to afford the title compound (179 mg, 0.17 mmol, 87%) as an off-white solid. The solid obtained was used without further purification.

Single crystals suitable for X-ray crystallography were grown by layering cyclohexane onto a saturated solution of the title compound in THF.

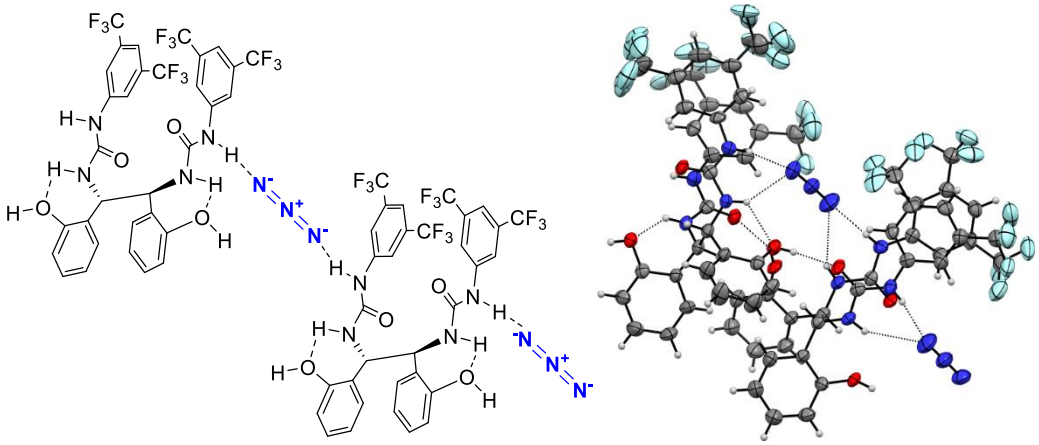

**Figure A.1** Crystal structure of 1,1'-((1*R*,2*R*)-1,2-bis(2-hydroxyphenyl)ethane-1,2-diyl)bis(3-(3,5-bis(trifluoromethyl)phenyl)urea)·tetrabutylammonium azide. Tetrabutylammonium cation omitted for clarity, displacement ellipsoid plots drawn at 50% probability level. X-ray crystallography data collection and analysis by Dr. K. E. Christensen.

**1,1'-((1*R*,2*R*)-1,2-bis(2-hydroxyphenyl)ethane-1,2-diyl)bis(3-(3,5-bis(trifluoromethyl)phenyl)urea)·(tetrabutylammonium azide)$_2$**

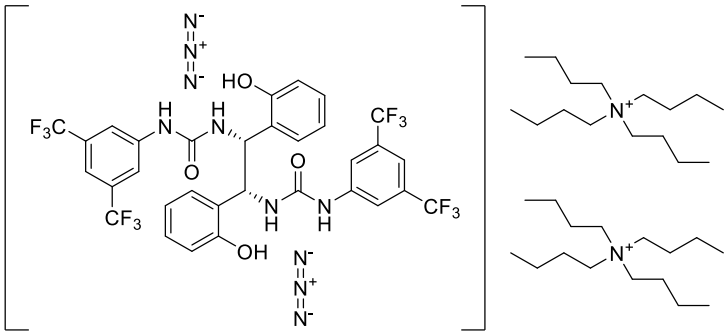

Dry MeCN (5 mL) was added to tetrabutylammonium azide (142 mg, 0.25 mmol, 1.00 equiv) and 1,1'-((1*R*,2*R*)-1,2-bis(2-hydroxyphenyl)ethane-1,2-diyl)bis(3-(3,5-bis(trifluoromethyl)phenyl)urea) (185 mg, 0.50 mmol, 2.00 equiv). The reaction mixture stirred at rt for 24 h. The reaction mixture was evaporated to dryness to afford the title compound (327 mg, 0.25 mmol, *quant*.) as an off-white solid. The solid obtained was used without further purification.

Single crystals suitable for X-ray crystallography were grown by layering cyclohexane onto a saturated solution of the title compound in MeCN.

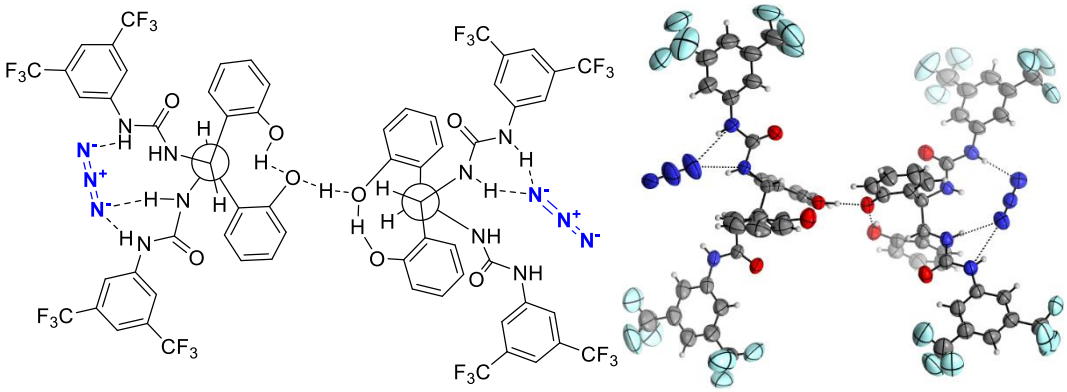

**Figure A.2** Crystal structure of 1,1'-((1*R*,2*R*)-1,2-bis(2-hydroxyphenyl)ethane-1,2-diyl)bis(3-(3,5-bis(trifluoromethyl)phenyl)urea)·(tetrabutylammonium azide)$_2$. Tetrabutylammonium cation omitted for clarity, displacement ellipsoid plots drawn at 50% probability level. X-ray crystallography data collection and analysis by Dr. K. E. Christensen.

**(1,3-bis(3,5-bis(trifluoromethyl)phenyl)urea)$_2$·tetrabutylammonium fluoride**

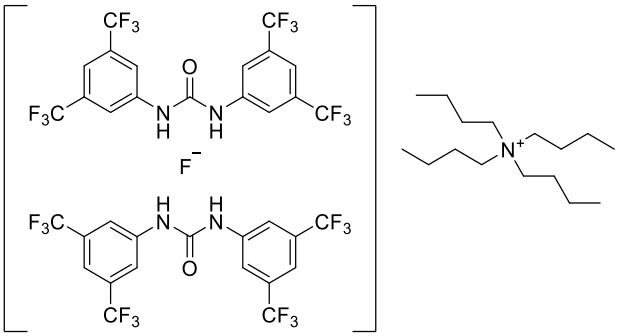

A suspension of tetrabutylammonium fluoride trihydrate (0.32 g, 1.00 mmol, 1.00 equiv) and 1,3-bis(3,5-bis(trifluoromethyl)phenyl)urea (0.97 g, 2.00 mmol, 2.00 equiv) in hexane (31.25 mL) was heated to vigorous reflux for 2 h. During the reaction, droplets of water collected on the sides of the reflux condenser. The reaction mixture was cooled to rt. The solids were collected by filtration, washed with hexane, and dried to afford the title compound (1.13 g, 0.92 mmol, 92%) as a white solid. The solid obtained was used without further purification.

Single crystals suitable for X-ray crystallography were grown by slow evaporation of a saturated solution of the title compound in hot hexane with a minimal quantity of EtOAc.

**mp** 138-140 °C; **$\nu_{max}$** (neat) /cm$^{-1}$ 2967, 1713, 1571, 1472, 1378, 1272, 1172, 1123, 1000, 931, 702; **$^1$H NMR** (400 MHz, MeCN-$d_3$) δ 11.83 (s, 4H), 8.09 (s, 8H), 7.39 (s, 4H), 3.31 – 2.75 (m, 8H), 1.68 – 1.41 (m, 8H), 1.33 (h, *J* = 7.5 Hz, 8H), 0.95 (t, *J* = 7.5 Hz, 12H); **$^{19}$F NMR** (377 MHz, MeCN-$d_3$) δ -63.85, -83.81; **$^{13}$C NMR** (101 MHz, MeCN-$d_3$) δ 154.7, 143.3, 132.3 (q, *J* = 33.0 Hz), 124.5 (q, *J* = 272.0 Hz), 119.0, 115.3 (d, *J* = 3.8 Hz), 59.4 (t, *J* = 3.0 Hz), 24.33, 20.33, 13.75.

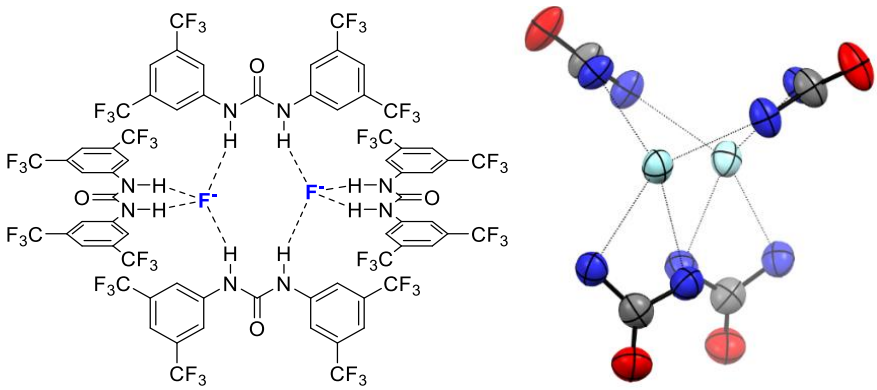

**Figure A.3** Crystal structure of (1,3-bis(3,5-bis(trifluoromethyl)phenyl)urea)$_2$·tetrabutylammonium fluoride. Selected atoms omitted for clarity, displacement ellipsoid plots drawn at 50% probability level. X-ray crystallography data collection and analysis by Dr. K. E. Christensen.

**(±)-3-(3,5-bis(trifluoromethyl)phenyl)-1-(2'-(3-(3,5-bis(trifluoromethyl)phenyl)ureido)-[1,1'-binaphthalen]-2-yl)-1-isopropylurea·tetraethylammonium cyanide**

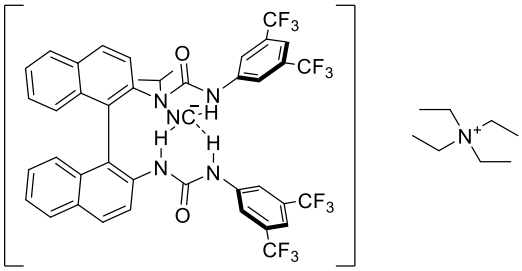

A suspension of tetraethylammonium cyanide (31 mg, 0.20 mmol, 1.00 equiv) and (±)-3-(3,5-bis(trifluoromethyl)phenyl)-1-(2'-(3-(3,5-bis(trifluoromethyl)phenyl)ureido)-[1,1'-binaphthalen]-2-yl)-1-isopropylurea (167 mg, 0.20 mmol, 1.00 equiv) in hexane (6.25 mL) was heated to vigorous reflux for 1 h. The reaction mixture was cooled to rt. The solids were collected by filtration, washed with hexane, and dried to afford the title compound (173 mg, 0.17 mmol, 87%) as a white solid. The solid obtained was used without further purification.

Single crystals of (±)-3-(3,5-bis(trifluoromethyl)phenyl)-1-(2'-(3-(3,5-bis(trifluoromethyl)phenyl)ureido)-[1,1'-binaphthalen]-2-yl)-1-isopropylurea·tetraethylammonium bicarbonate suitable for X-ray crystallography were grown by slow evaporation of a saturated solution of the title compound in hot hexane with a minimal quantity of THF.

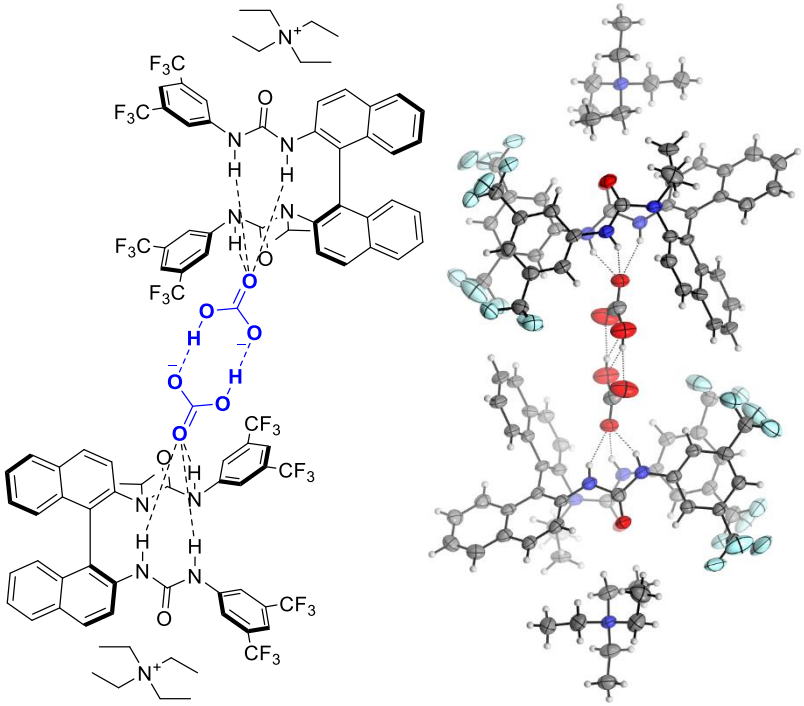

**Figure A.4** Crystal structure of (±)-3-(3,5-bis(trifluoromethyl)phenyl)-1-(2'-(3-(3,5-bis(trifluoromethyl)phenyl)ureido)-[1,1'-binaphthalen]-2-yl)-1-isopropylurea·tetraethylammonium bicarbonate. Displacement ellipsoid plots drawn at 50% probability level. X-ray crystallography data collection and analysis by Dr. K. E. Christensen.